University of Technology, Sydney

Faculty of Engineering and Information Technology

"A numerical investigation of air flow and temperature distribution in a ventilated room"

A Thesis submitted for the Degree of Master of Engineering (Research)

Tatiana Kivva

March , 2011

Certificate of authorship

I certify that the work in this thesis has not previously been submitted for a degree nor has it been submitted as part of requirements for a degree except as fully acknowledged within the text.

I also certify that the thesis has been written by me. Any help that I have received in my research work and the preparation of the thesis itself has been acknowledged. In addition, I certify that all information sources and literature used are indicated in the thesis.

Production Note:
Signature removed prior to publication.

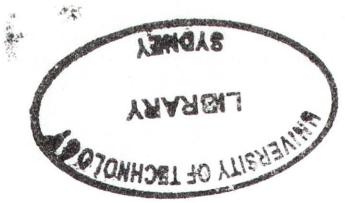

Acknowledgment

I would like to express my gratitude to all those who gave me the opportunity to complete this thesis. I am extremely grateful to my supervisors Phuoc Huynh and Matthew Gatson. I also would like to express my deep and sincere gratitude to John Reizes whose academic experience as well patience and kindness have been invaluable to me. The completion of this thesis would not have been possible without the support of my industrial supervisor Derek Munn and my colleague Tarek Alfakhrany.

Finally, I am thankful to my family for all their support and encouragement.

Table of contents

List of illustrations and tables

Nomenclature

A	area $[m^2]$
Ar	Archimedes number
C	coefficient
CN	contaminant concentration
Cp	specific heat capacity [*J/(kg·K)*]
d	diameter [*m*]
D	draught rating [*%*]
E	wall roughness
f	the ratio between the covered and exposed surface of a body,
FC	clothing function,
h	heat transfer coefficient $[Wm^{-2}/°C]$
H	height [m]
k′	is the von-Karman constant
g	is the gravitational acceleration $[m^2/s]$
Gr	Grashof number
L	length scale [*m*]
m	metabolic energy $[Wm^{-2}]$
Nu	Nusslet number
p	pressure $[Pa]$
Re	Reynolds number

Ri	Richardson number
Q	volumetric flow rate of air [m^3/s]
$\vec{s}$	intermediate parametric function between the computational and physical spaces
t	time [s]
T	temperature [$°C$]
u	velocity component [m/s]
V	velocity [m/s]
v	velocity component [m/s]
W	free energy production (external work) [Wm^{-2}]
w	velocity component [m/s]
$\vec{x}$	grid coordinate [m]
y	distance from the neutral plane [m]
Z	coordinate [m]

Greek symbols

β	incidence angle [$^{\circ}$]
Γ_t	turbulent or eddy diffusivity
δ	stretching factor

δ_{ij}	Kronecker delta
ε	turbulent energy dissipation
λ	is the conductivity air [*W/m K*]
κ	kinetic turbulent energy
μ	viscosity [*Pa s*]
ρ	density [kg/m3]
σ_t	Prandtl/Schmidt number
τ	Taylor's jet entrainment constant
υ	is the kinematic viscosity [m^2/s]
Φ	dissipation function
$\vec{\xi}$	computational domain vector

Subscripts

a	air
amb	ambient
b	bulk
bjo	free buoyant jet
cl	the absolute surface of cloths

com	combined effect
d	discharge
e	extracted
fc	forced convection
in	inside
i	tensor notation $i = 1,2,3$
L	local
m	mean
n	nozzle
nc	natural convection
0	nominal
oc	occupied
out	outside
p	pressure
ref	reference
s	supplied
sf	stratified
t	turbulent
v	vertical direction
w	wind

wl	walls
$+$	dimensionless
υ	viscous
$'$	fluctuations

Abstract

A numerical investigation of ventilation enhancement by a roof-mounted fan has been performed. The commercial code CFD-ACE is used for the quantitative and qualitative analysis of velocity and temperature distributions in a ventilated room.

The parametric study is based on the results of flow and thermal fields obtained from the numerical simulations of three-dimensional models to optimise the location and through flows of a roof-mounted fan to minimise the cooling time of a space once the fan is switched on. The four ventilator locations have been modelled and the environmental indoor conditions analysed for different speeds of extracted and injected air and temperature of walls. For all cases, Reynolds Average Navier-Stokes, continuity, energy and k-ε equations were defined for steady state and transient, incompressible, turbulent air flows. The second order upwind differential scheme was used and Boussinesq approximation was applied. The equations were solved by using a commercial code based on the finite volume method in a staggered grid system.

Chapter 1

Introduction

Ventilation is the movement of air between the internal spaces of a building and an outside area. The main purposes of ventilation are the dilution of airborne pollutants and the maintenance of thermal comfort. Thermal comfort can be defined by the range of air temperature, humidity and air velocity in which human beings feel comfortable. The perception of people to environmental conditions depends on a number of parameters, including their activity, nutrition and clothing.

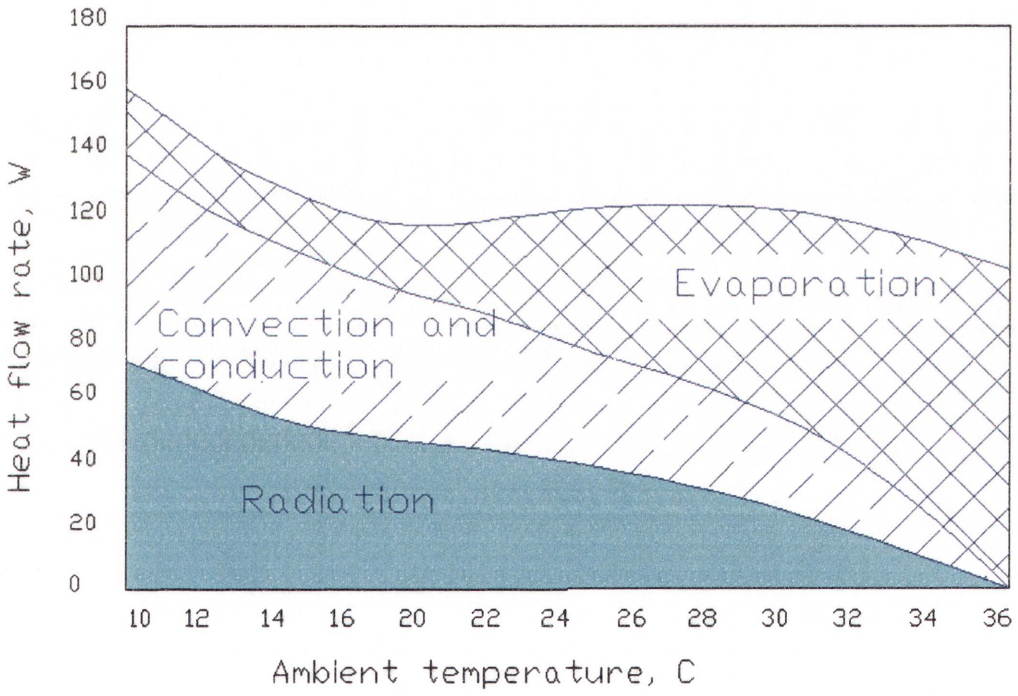

Figure 1 – The dependence of heat transfer mechanism for human body temperature reduction as a function of ambient temperature and required heat flux for a sitting person (Reproduced from Hebgen and Heck, 1973)

The body heat transfer mechanism changes as a function of ambient conditions, such as temperature, air velocity and the level of solar radiation. Above 20 ºC, a human body increases sweating in response to demands for greater cooling as is shown in the increased region of

evaporation in Figure 1. Above 36 ºC, evaporation becomes the only mechanism of heat dissipation and a person may be under significant physiological strain as the body attempts to reduce its core temperature.

Fanger, Banhidi, Olesen and Langkilde (1980) developed a relationship between comfortable room temperatures and a person's level of activity and clothing, as is shown in Figure 2.

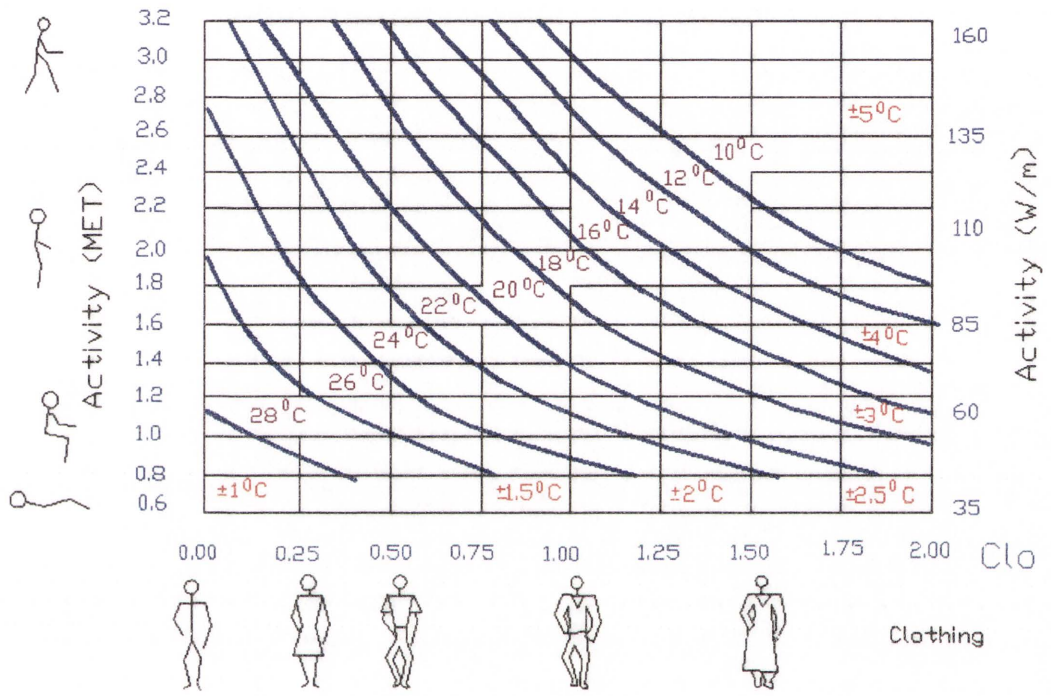

Figure 2 – Comfortable indoor temperature as a function of clothing and activity level (Reproduced from Fanger et al, 1980)

Fanger (1982) performed a survey and developed a correlation between the predicted mean vote (PMV) of occupants and metabolic activity, mechanical work, the clothing fraction and thermal resistance of clothing which he expresses as

$$PMV = (0.303e^{-0.036m} + 0.028)[m - w - 0.00305(5733 - 6.99(m - w) - p)$$

$$- 0.42(m - w - 58.15) - 0.000017m(5787 - p) - 0.0014m(3307 - T_a D) - F], \qquad (1.1)$$

Where m is metabolic energy produced, $[Wm^{-2}]$,

w is the free energy production (external work), $[Wm^{-2}]$,

p is water vapour partial pressure, $[Pa]$,

T_a is the air temperature, $[°C]$,

D is draught rating [%],

and FC is the clothing function defined as

$$FC = (3.96 \times 10^8 f(T_{cl}^4 + 273) + fh(T_{cl} - T_a), \quad (1.2)$$

f is the ratio between the covered and exposed surface of a body,

h is the convective heat transfer coefficient $[Wm^{-2} / °C]$ and

T_{cl} is the absolute surface temperature of cloths, $[°C]$.

The predicted mean vote (PMV) is the statistical estimate of people who are not satisfied with the indoor environment and is shown in Figure 3. PMV values in terms of thermal comfort mean -3=cold, -2=cool, -1=slightly cool, 0=comfort, +1=slightly warm, +2=warm, +3=hot (Awbi and Hazim , 2003).

A classification scheme is accepted by the International Organization for Standardization (ISO 7730 2005). The ISO standard recommends that the limit of PMV be between -0.5 and 0.5. In a practical design situation, the graph can be used for prediction of the performance of a ventilation system. A PMV value of zero is therefore the optimal value to minimise the number of uncomfortable people and which designers of ventilation systems should aim for.

The PMV is calculated on the assumption of a uniform ambient temperature but it has been reported that non-uniform temperature distributions also affect thermal comfort. For example, a difference in temperature of 4 K between the head and the ankles is stated as uncomfortable by 10 % of occupants, while 45 % find a difference of 6 K unpleasant (Figure 4).

Analysis of studies conducted by Duell (2006) shows that indoor temperatures often exceed the recommended comfort level during hot Australian summer nights. In fact, the thermal environment is often more comfortable outside a building than inside because the internal building temperature tends to drop at a significantly lower rate than the ambient temperature.

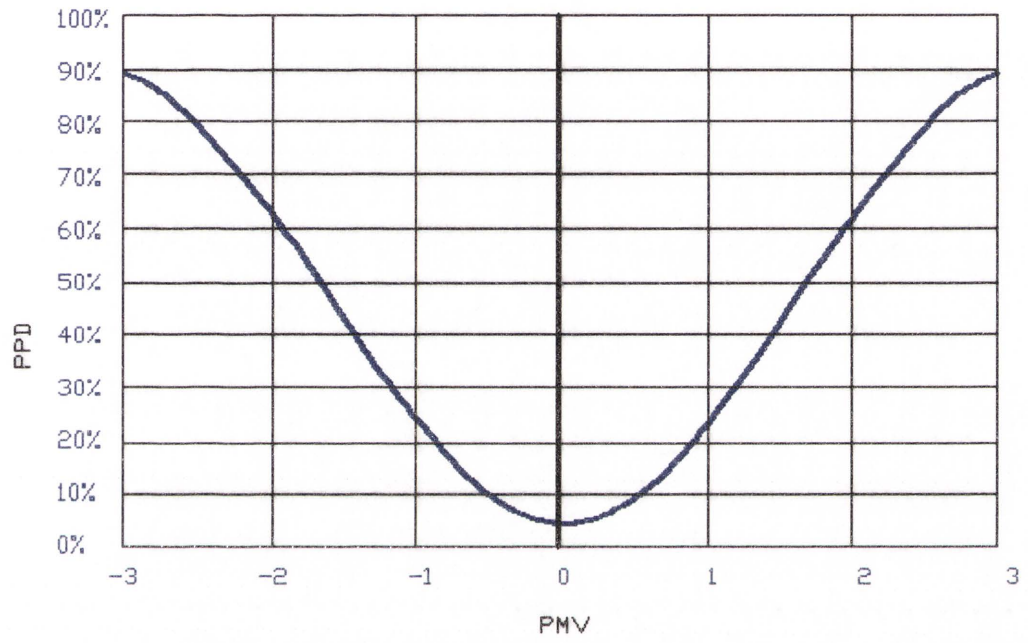

Figure 3 – The predicted distributions between predicted mean vote (PMV) and the percentage of people unsatisfied (PPD) with indoor environmental conditions (ISO 7730 2005)

The hot temperatures as well as non-uniform temperature distributions can affect human well-being (ASHRAE).

During a typical Australian summer day, thermal stratification takes place in a building. Thermal stratification occurs when buoyancy driven flows form horizontal layers of differing temperatures at different heights (Gao, Zhao and Gao, 2006). The formed lineal fluid layers may be stable. What is more, the hot layer near the ceiling and the cold layer just above the floor can augment temperature stratification in a room.

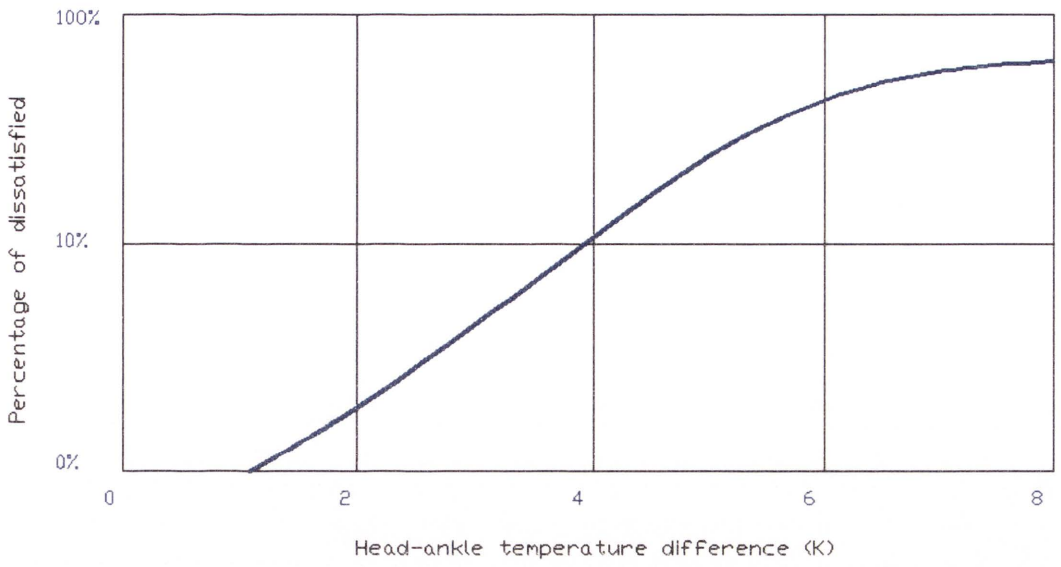

Figure 4 – The percentage of dissatisfied people as a function of temperature gradient (Awbi and Hazim, 2003)

In order to provide comfortable indoor conditions, the excess heat should be removed from a house to outside areas. Heat exchange is a complicated process and can be described by several mechanisms operating simultaneously. In general, heat transfer can be divided into convection, conduction and radiation modes (Kreith and Bohn, 1986). Convection is the main source of passive ventilation. Passive ventilation occurs when hot, light air rises up from within the building to the outside environment and cold air moves in to replace it. Density differential fluid transport is called natural convection. When natural convection is insufficient to provide the required comfort levels, forced ventilation can be used to augment natural convection. Forced ventilation can provide additional force to the air circulation generated by natural convection by creating pressure differentials between outside spaces and the effective area of a ventilation system. The effectiveness of ventilation strategies can be evaluated by how quickly the hot air in an interior space is replaced by cold outside air.

Forced ventilation in this context is defined as the process of exchanging air between an enclosure and an outside area with any mechanical aid. Alternatively, natural ventilation

is based on pressure and temperature differences without mechanical assistance; however, a limitation to the efficacy of natural ventilation systems is a lack of wind and favourable ambient conditions to achieve the desired air flow rates. Other critical issues in the design and installation of a ventilation system are limited capacity and excessive noise created by the ventilator.

Forced ventilation and air-conditioning systems require energy to maintain comfortable environmental conditions. Ventilation consumes 30-60 % of energy used in the building (Awbi and Hazim, 2003), thus the major limitation of forced ventilation is its energy requirement. Despite the energy inputs, however, an air conditioning system provides the required range of temperature and humidity level, and can be adapted to heat a ventilated room.

An additional problem with an air conditioning system is the transmission of diseases such as Legionnaires' Disease, Pontiac Fever, and Hypersensitivity Pneumonitis (Godish, 1995). What is more, Horan and Finn (2005) state that a sick building syndrome occurs when people spend significant time in a mechanically ventilated room.

Although natural ventilation cannot be seen as a stand alone alternative to an air conditioning system, the combination of natural and mechanically driven ventilation may reduce energy consumption and provide better environmental conditions. New design methods could increase the efficacy of a mechanical ventilation system; for example, the cooling performance of ventilation systems can be improved by expelling heat to the outside area and obtaining a supply of fresh air during the night.

The performance of a ventilation system can be classified by using the twin concepts of thermal and ventilation efficiency (Xue and Shu, 1999).

Thermal efficiency can be calculated as

$$\eta_t = \frac{T_e - T_s}{T_m - T_s} \tag{1.3}$$

Where T_s = supplied air temperature,

T_e = extracted air temperature,

T_m =mean air temperature.

Ventilation efficiency can also be thought of

$$\eta_c = \frac{CN_e - CN_s}{CN_{oc} - CN_s},$$

(1.4)

Where CN_s = contaminant concentration of supply air,

CN_e = contaminant concentration of extracted air,

CN_{oc} = contaminant concentration in an occupied area.

These formulae do not take into account the effect of temperature and velocity distribution in a ventilated room and the implementation of these formulae to assess a ventilation system seems questionable. For example, increasing ventilation rates can cause drafts and lead to discomfort for occupants, while low ventilation rates may result in high concentration levels of contaminants in stagnant zones, as is shown in Figure 5 (Larsen, 2007).

Firstly, a forced ventilation system has to break down the spatial gradients of temperature stratification formed during the day. Secondly, the ventilation system has to provide uniform comfortable temperature distribution, and flow generated by a fan may promote the mixing of air in a ventilated room. Natural, mixed and forced convection are the three main transport regimes of air in a ventilated room. Mixed convection depends on the ratio between the buoyancy and fan-driven flows, and possibly the angle of resultant action.

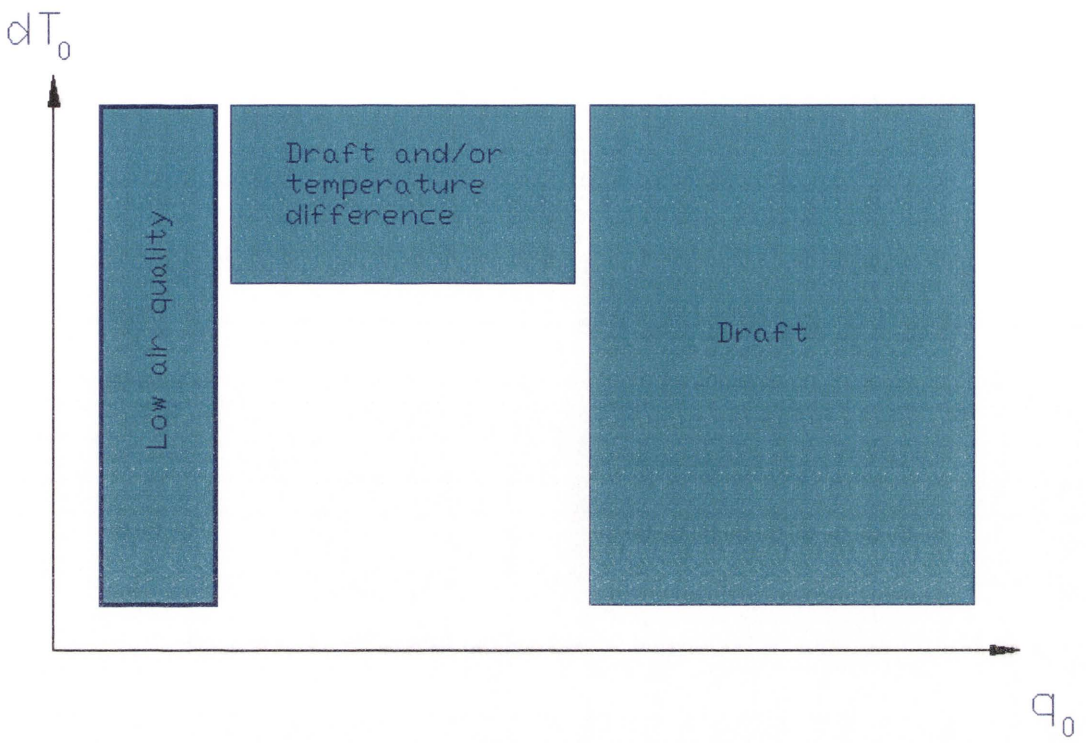

Figure 5– Design graph for a ventilated system (Source Xue and Shu, 1999)

The performance of different types of ventilation systems is hard to predict. It is difficult to determine the best ventilation to achieve the desired level of thermal comfort, even in simple buildings.

Thus the question arises as to how to estimate the effectiveness of different ventilation options to provide a healthy and safe building environment.

The measurement results can provide valuable information about the performance of a ventilation system but this investigation is usually time consuming and expensive and may only be conducted after the system is installed. On the other hand, Computational Fluid Dynamics (CFD) is a powerful and effective tool for assisting in the design and optimisation of ventilation systems.

Investigations of fluid flow and heat transfer can be conducted using CFD techniques, which will be used for the assessment of a ventilation system in this thesis. The main aim of this thesis is to analyse different ventilation strategies under natural, mixed and forced convection and to assess their impact on thermal comfort requirements. This is achieved by conducting a study of the effect on human comfort of various locations and speeds of a fan, the temperature of walls and the air transportation method.

Chapter 2

Literature review

Passive and mechanically driven ventilation is often used in an attempt to provide acceptable comfort conditions in houses during hot weather. The efficacy of these techniques is usually not evaluated once the installation has been completed, so that historically poorly validated 'rules of thumb' are used, often leading to poor results. The indoor environment of a building depends on many interacting parameters, such as the geometry of the house, the thermal properties of walls, the performance of the ventilation system and the local weather conditions.

Because of this complexity and the lack of validated information, the flow rates of mechanical ventilation for providing the required thermal comfort needs are often difficult to predict. Existing computational packages, such as Accurate software (Hearne Scientific Software, 2008) can be used to obtain a rough estimation of the energy efficiency of a building; however, ventilation solutions for a particular zone and used building materials in the zone are not well presented and cannot provide any recommendations or suggestions.

Ventilation is a dynamic process and estimation of the air flow rate with constant environmental and indoor conditions can lead to poor indoor air quality and thermal discomfort. The use of 'factors of safety' to increase the air flow rate to ensure that adequate cooling is provided may cause drafts and lead to unnecessary energy consumption.

Evaluations of existing roof fan ventilation systems are usually carried out when a client complains, and some companies also perform experimental work to determine the effect of

ventilation. CSR Edmonds,[1] for example, is conducting tests in a number of residential houses to assess the performance of roof mounted fans as a function of weather conditions. Spindler and Norford (2008) have also carried out an experimental study to evaluate different ventilation strategies for various environmental and indoor conditions. The different parameters and their impact on inside temperature were analysed and all variables were adjusted in the 'multi-mode thermal' model by using correlation factors.

Despite the fact that experimental results can provide valuable information about ventilation, the usefulness of the results to design solutions appears to be problematic due to the many types of houses and the range of climatic zones. Furthermore, an examination of all types of residential houses, the materials used in their construction and conditions in an experimental approach is a very expensive and extremely time-consuming task.

An analysis of a whole house with all the interactions between rooms and the outside environment is rather ambitious. The problem needs to be simplified, particularly as it is difficult, perhaps impossible, to fully assess the effectiveness of any ventilation strategy. The performance of such a ventilation system can be investigated through the use of a combination of simplified theoretical approaches, experimental studies and CFD predictions.

From this perspective, natural ventilation as a solution requiring less energy has been intensively analysed.

An experimental investigation of buoyancy driven flows through a big opening was carried out by Heiselberg et al (2003) and CFD simulations were conducted by Favarolo and Manz (2005).

Buoyancy driven ventilation occurs when the temperature difference inside and outside is more than 10 K (Heiselberg et al., 2003). The air flow rate through a big opening can be

---

[1] CSR Edmonds, PO Box 511, Brookvale, NSW 2100, Australia

calculated by the Bernoulli equation with an adjusted correlation coefficient. The main assumption used in this correlation is that the middle of an opening is in the neutral pressure level, as shown in Figure 6. By further assuming that streamlines are parallel, there is no heat transfer between layers of fluid, and pressure levels inside and outside of an enclosure are equivalent in the middle plane, the velocity profile can be presented as a parabolic law function and the pressure by a linear law above a neutral level. Substituting ideal gas law into the Bernoulli equation leads to the following velocity distribution equation:

$$v(y) = \sqrt{2gy\frac{T_i - T_0}{T_i}} \tag{2.1}$$

Where T_i is inside average temperature and T_0 is outside temperature, [K],

y is the distance from the neutral plane, [m],

g is the gravitational acceleration,[m^2/s].

The effects of viscosity, swirling and compressibility of flow can be included in the velocity coefficient C_v

$$v(y) = C_v\sqrt{2gy\frac{T_i - T_0}{T_i}} \tag{2.2}$$

The velocity profile has a parabolic shape and integration of velocity within the height of the opening in the vertical direction can lead to the following expression:

$$Q = \frac{1}{3}C_d A\sqrt{gH\frac{T_i - T_0}{T_i}}, \tag{2.3}$$

In which C_d is the discharge coefficient,

A is the area of the opening, [m^2],

H is the height of the opening, [m].

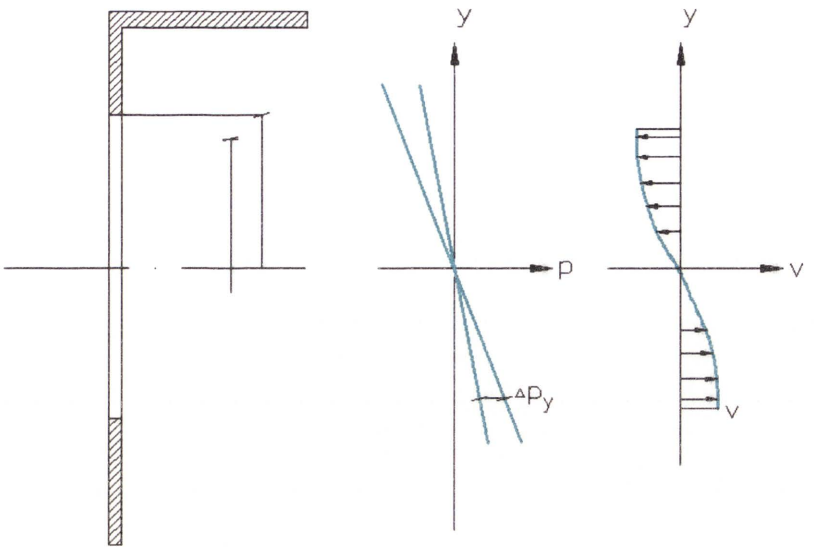

Figure 6 – Pressure and velocity profiles for buoyancy driven flows through the big opening (Source: Heiselberg et al, 2003)

A number of studies have attempted to establish the quantitative value of the discharge coefficient for different design buildings and weather conditions.

Heiselberg et al (2003) used $C_d = 0.61$ in their calculations, Shaw and Whyte (1974) suggested that C_d is equal 0.80, Maas et al. (1989) proposed C_d was 0.75, while Mahajaan (1987) suggested that C_d = 0.45, and Limam et al (1991) stated that C_d was in the range r0.6< C_d <0.75.

Riffat (1989) proposed that C_d can be found from the formula

$$C_d = 0.0835(\Delta T / T)^{-0..3} \qquad (2.4)$$

Kiel and Wilson (1989) determined the expression given by the discharge coefficient in steady buoyancy-driven flows as the function of the temperature difference:

$$C_d = (0.4 + 0.0075\Delta T) \tag{2.5}$$

Ghiaus and Allard (2005) claimed that the discharge coefficient is significantly influenced by the window height and the temperature difference; but it was found that the air velocity does not affect the value of the discharge coefficient. Pelletret (1991) determined the correlation $C_d = 0.21H$ for opening heights in the range $1.5m < H < 2.5m$.

Favaralo and Manz (2005) proposed that the numerical value of C_d varied from 0.48 to 0.73 for different sizes and positions of openings. The discharge coefficient was calculated from the formula

$$C_d = \frac{3Q}{\sqrt{gH\frac{T_{in} - T_{out}}{T_{in}}}}\frac{1}{A} \tag{2.6}$$

in which values of outside T_{out} and inside average temperatures T_{in} and the volumetric flow rate of air *Q* was calculated using a CFD code.

The computational domain used by Favaralo and Manz consisted of a room 4.9 m long, 2.6 m high and 3.9 m wide with a rectangular opening and outdoor space, as shown in Figure 7.

The numerical investigations were conducted for different types of openings. The impact of different parameters, such as room depth and wall thickness on the air rate discharge was also examined. Favaralo and Manz (2005) found that with an increase in wall thickness the discharge coefficient decreases until a critical value is reached. This phenomenon can be explained by the fact that flow separates by the edge of the wall, as shown in Figure 8. The critical value of wall thickness was found to be between 0.1 m and 0.14 m.

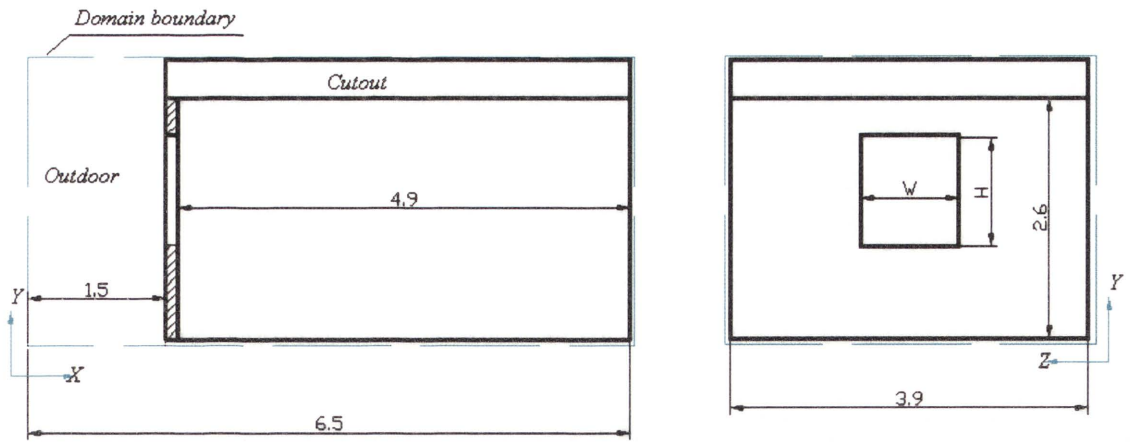

Figure 7 – Geometrical dimensions of the simulated model (Source: Favaralo and Manz, 2005)

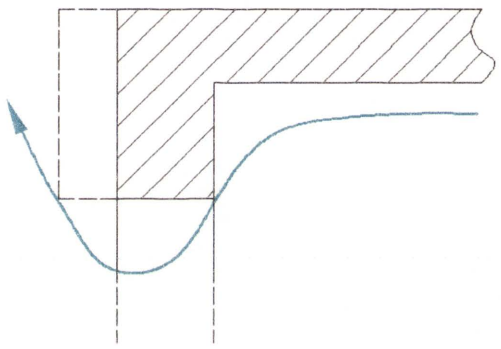

Figure 8 – Flow separation near the opening's edge (Source: Favaralo and Manz, 2005)

Favaralo and Manz (2005) also found that the value of the discharge coefficient was slightly affected by the room width and length. The following range was investigated: 3.4 m<length<6.4 m and 3.9 m<width<5.9 m.

The horizontal position of an opening was also found to have little influence on the discharge coefficient, and a significant change could be noticed only when the window was very close (near 0.2 m) to the side wall.

The vertical position of an opening was recognised as a major parameter which influenced the discharge coefficient. The air flow increased considerably when an opening was located close

to the ceiling and decreased when the opening was located close to the floor. The values of discharge coefficients at different temperature differences between the outside and inside areas and three opening locations are shown in Figure 9. As can be seen from Figure 9, less flow occurs when the opening is in the bottom position and the value of the discharge coefficient falls to 0.55. The maximum flow rate was found to be for an opening located near the ceiling; the discharge coefficient was equal to 0.7. The change to the discharge coefficient with the position of the opening can be explained by the fact that moving hot air flow patterns can be affected by the thickness of the wall, and as a result the changing recirculation of air in a room appears to be, which can reduce the efficiency of ventilation (Figure 10).

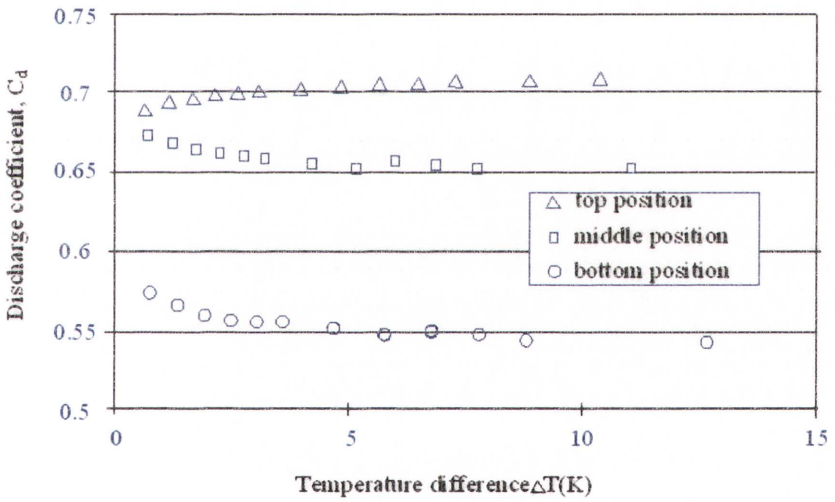

Figure 9 – The discharge coefficient as a function of the difference between outside and inside average temperatures for different position of an opening (Source: Favaralo and Manz, 2005)

It was also observed that once the difference between the outside and inside average temperatures exceeded 6 K, the value of the discharge coefficient remained near constant for all positions of the opening, as shown in Figure 9.

This literature survey shows that the numerical values of the discharge coefficient differ for each published work, and information on the calculation or estimation of the approximate

value of the discharge coefficient is contradictory and mutually exclusive. As a result, the implementation of Equation 2.4 for a practical ventilation design solution seems to be problematic.

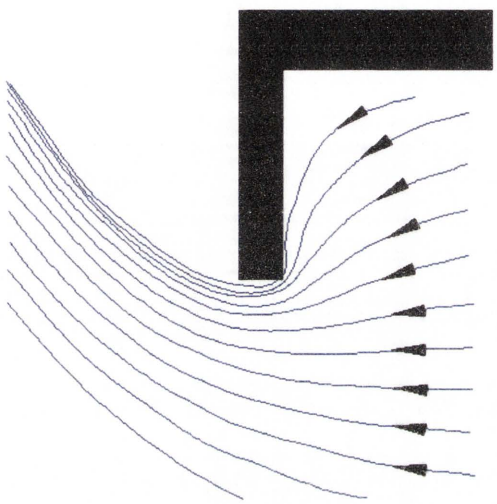

Figure 10 – Constriction of airflow streamlines near the opening edge (Source: Favaralo and Manz, 2005)

Favarolo and Manz (2005) demonstrated that the vertical position of an opening significantly affects the magnitude and direction of buoyancy driven flows. The separation of an opening and its effect on cooling performance were experimentally investigated by Tanny et al (2008). The upper opening height was kept constant and the lower opening varied in height from 0 m to 0.3 m. The heat source of 500 W was placed in the middle of the compartment and 0.3 m from the rear wall.

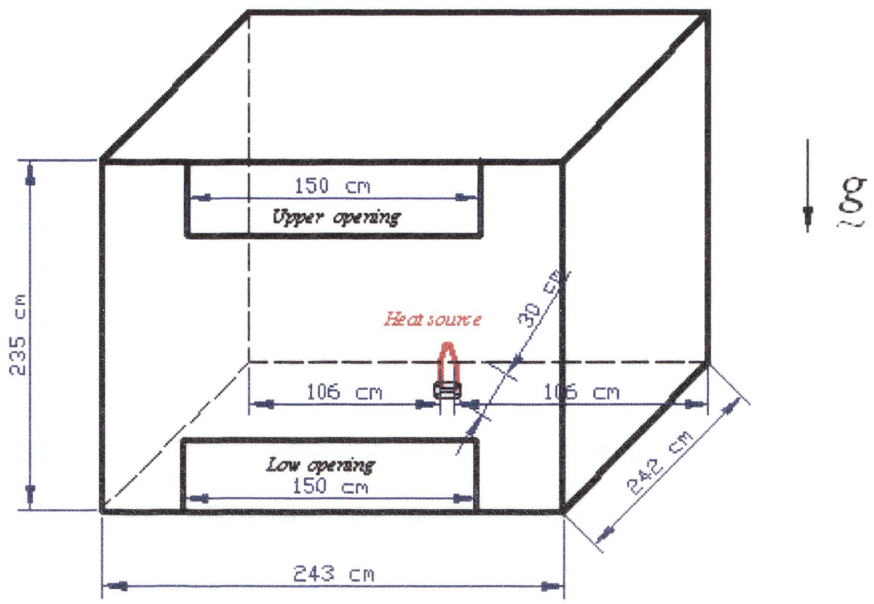

Figure 11 – The experimental setup (Source: Tanny, Haslavsky and Teitel, 2008)

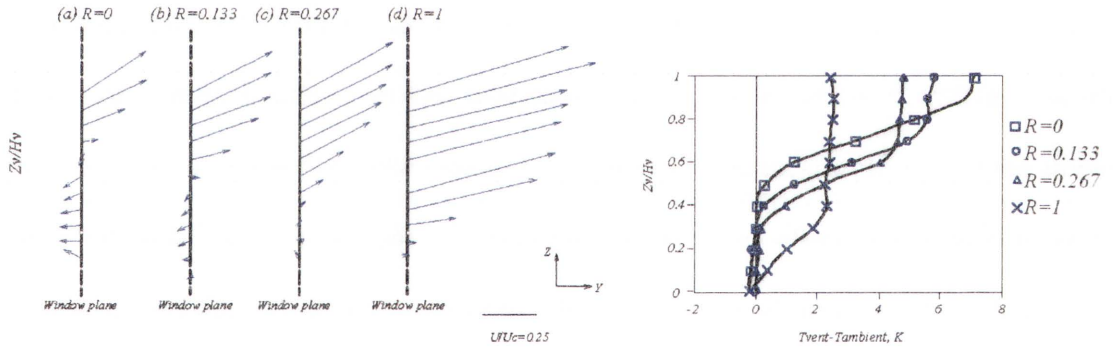

12a) 12b)

Figure 12 – Velocity and temperature distributions through the higher opening (Source: Tanny, Haslavsky and Teitel, 2008)

Figure 12a) illustrates the velocity distributions through the upper opening for four different heights of the lower opening. R is the ratio between opening heights $R_{actual} / R_{\max}$. R equals 0 when the lower opening is completely closed and R=1 for the fully opened lower opening. It was observed that airflows tend to incline upon increasing the height of lower opening.

Figure 12b) shows the differences between ambient air temperatures and temperatures through the height of the upper openings for four different heights of the lower opening, where Zv/Hv is a ratio of Zv coordinate in the vertical direction of the upper opening on Hv height of the upper opening. As it can be seen from Figure 12b), the temperature gradient through the high opening is significantly lower when the low vent is closed.

It was also observed that a high level of turbulence occurs when incoming cold air intersects with the boundary of outgoing hot airflows. Tanny et al (2008) proposed that in the case of an opening being vertically divided into two parts, inflow and outflow are separated and a higher air exchange rate can be provided due to smooth, undisturbed airflows through the openings.

The literature survey shows that the natural ventilation rate can be influenced by a number of architectural building features. Ventilation is a dynamic process and changing indoor and environmental conditions need to be taken into consideration; in other words, evaluation of a design ventilation solution requires information about the influence of transient weather dynamics such as the level of solar radiation, the direction and speed of wind, and the ambient temperature on indoor conditions. For example, the combined effect of wind velocity and air turbulence on buoyancy driven air flow rates through a single side opening can be found in the experimental work of Phaff et al (1980) and Larsen and Heiselberg (2008).

Phaff et al (1980) conducted an experimental investigation in the lowest-floor apartments of three level buildings at different locations. The measurements were gathered by tracer gas techniques. The velocity of air through half of the opening was expressed as

$$v_{eff} = \frac{V_{total}}{A/2} = \sqrt{\frac{2}{g}(\Delta p_{wind} + \Delta p_{stack} + \Delta p_{turbulence})} = \left(c_1 V_{mw}^2 + c_2 H \cdot \Delta T + c_3\right)^{1/2} \qquad (2.6)$$

V_{mw} =is the mean wind speed, [m/s]

H =is the height of the opening, [m].

The following correlation coefficients were found to fit the data with reasonable accuracy:

$c_1 \approx 0.001$ is the opening constant,

$c_2 \approx 0.0035$ is the buoyancy constant,

$c_3 = 0.01$ is the turbulent constant.

It would seem likely that the wind direction would have a significant effect on the flow rate of air through the window, so Larsen and Heiselberg (2008) included the direction of the wind in the correlation. They performed experiments in a ventilated room in a wind tunnel at the Japanese Building Research Institute. The dimensions of the ventilated room were 5.56 m x 5.56 m x 3 m and the opening was 0.86 m x 1.4 m. The internal room height was 2.4 m and wall thickness was 0.1 m. These experiments were conducted at different wind velocities from 0.3 m/s to 5 m/s, temperature differences from 0.5 ºC to 10 ºC and with the wind at different incidence angles. The volume flow rate was determined as

$$Q_v = \pm C_D \cdot \frac{1}{2} A \sqrt{\frac{2\left|P_{wind} + \Delta P_{thermal} + \Delta P_{fluct}\right|}{\rho}} =$$

$$= A \sqrt{C_1 \cdot f(\beta)^2 \cdot \left|C_P\right| \cdot U_{ref}^2 + C_2 \Delta T \cdot H + C_3 \frac{\Delta C_{p,opening} \cdot \Delta T}{U_{ref}^2}} \qquad (2.7)$$

in which U_{ref} is the reference wind speed, [m/s]

$f(\beta)$ is the incidence angle coefficient of the wind,

and Cp is pressure coefficient.

Warren and Parkins (1985) determined the values of the pressure coefficient as a function of the ratio between local velocity in front of the window (m/s) U_L and the reference wind velocity (m/s) U_{ref} as shown in Figure 13.

Larsen and Heiselberg (2008) found that the function $(U_L / U_{ref}) / \sqrt{|C_p|}$ can be correlated by the fourth order curve, as shown in Figure 14.

The correlation constants C_1, C_2 and C_3 are given in Table 2.1.

Table 2.1 - Values for constants C_1, C_2 and C_3 (Source: Larsen and Heiselberg, 2008)

Direction	Incidence angle (ß)	C_1	C_2	C_3
Windward	$\beta = 285 - 360°, \beta = 0 - 75°$	0.0015	0.0009	-0.0005
Leeward	$\beta = 105 - 255°$	0.00500	0.0009	0.0160
Parallel flow	$\beta = 90°, \beta = 270°$	0.0010	0.0005	0.0111

Neither equation 2.6 nor equation 2.7 has been validated for the different types of building and weather conditions. The practical implementation of these correlations for calculating the air flow rate for ventilation of residual houses is therefore questionable.

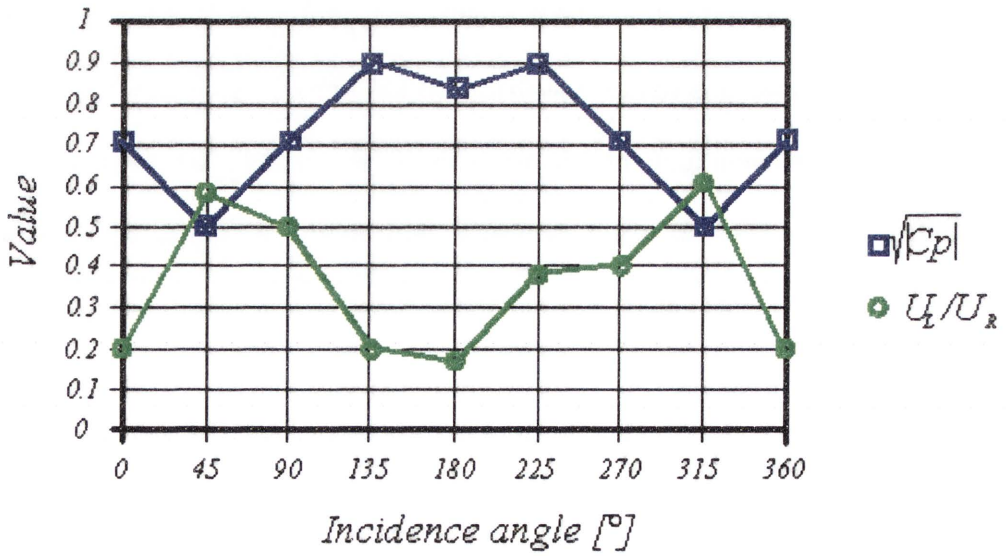

Figure 13 – The dependence of the pressure coefficient and the ratio of local velocity and reference velocity (Source : Warren and Parkins, 1985)

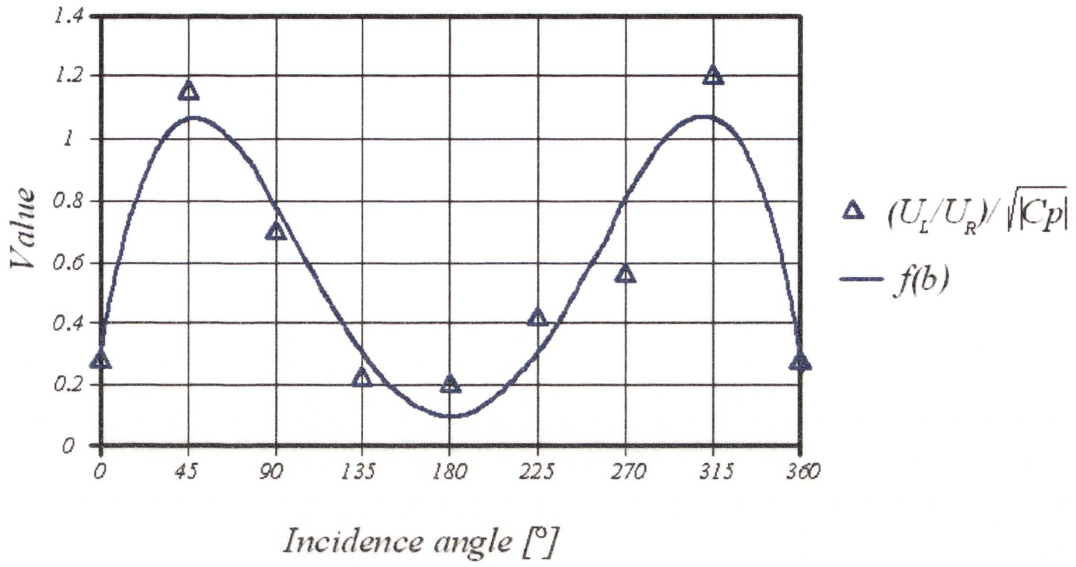

Figure 14 – The value of $f(\beta)$ as a function of incidence angles and $(U_L/U_R)/\sqrt{|C_p|}$ (Source: Larsen and Heiselberg, 2008)

As can been seen, natural ventilation systems can be improved or augmented by a variety of strategies, including building shapes, opening orientations and the building materials used. Despite intensive research into aspects of natural ventilation and efficient building design, a purely naturally ventilated solution cannot always provide the occupants with a desirable degree of control of environmental conditions. It follows that forced ventilation is usually used in addition to natural convection. Mechanical devices can be employed in order to increase the rate of heat removal and provide higher air circulation. Roof mounted ventilators, as well as other ventilation systems, may be used to maintain the indoor environment within acceptable thermal comfort limits at most times during hot Australian nights (Alfakhrany, 19 May 2009, Sydney).

The need for high performance of mechanical devices used in ventilation has led researchers to investigate the augmentation of heat and mass transfer induced by forced convection. Jambunathan (1992) collated a large number of published experimental data in order to

identify the main parameters which influence heat transfer behaviour for an orthogonally impinged circular jet. A number of geometrical and flow conditions were analysed.

He proposed that the heat transfer dimensionless ***Nusslet number*** $Nu = \frac{hD}{\lambda}$,

where

h is the heat transfer coefficient [W/m^2 K],

D is the nozzle exit diameter [m],

λ is the conductivity air [W/m K]

and ***Reynolds number*** $\mathrm{Re} = \frac{DU_n}{\upsilon}$,

where U_n velocity of air through the nozzle exit [m/s],

υ is the kinematic viscosity [m^2/s].

can be correlated by exponential function as

$$Nu = k\,\mathrm{Re}^a \qquad (2.8)$$

in which ***k*** is a constant and exponential value ***a*** varies with the distance from the stagnation point ***x*** and with the distance ***z*** from the jet to the surface A, as shown in Figure 15.

Jambunathan (1992) also found that nozzle geometry may influence the field flow behaviour; in particular, the nozzle configuration may change the level of turbulence produced and the sizes and formations of vortices, which in turn may change the process of air mixing and heat transfer.

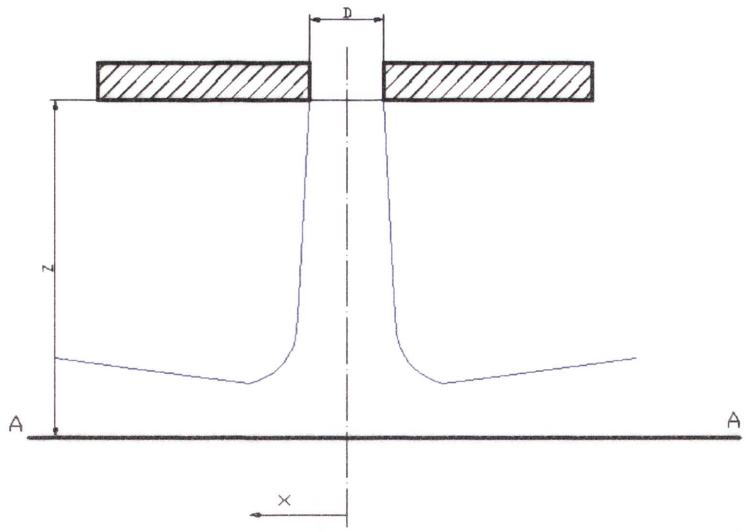

Figure 15 – Geometrical characteristics of an impinging jet and enclosure (Source: Jambunathan, 1992)

Determination of the sufficient entrainment velocity and the criteria for breaking down the stratification layers by a round injected free buoyant jet in two dimensional volumes can be found in the work by Peterson (1994).

The characteristic horizontal entrainment velocity of a turbulent forced jet was defined as

$$u_e = U_o \left(\frac{d_{bjo}}{4H_{sf}} \right) \left(1 + \frac{d_{bjo}}{4\sqrt{2\tau H_{sf}}} \right)^{-1} \tag{2.9}$$

in which U_0 is the nominal velocity of a penetrated flow jet (m/s),

H_{sf} -the height of stratified fluid (m),

d_{bjo} -the diameter of an entranced free buoyant jet (m^2),

τ -Taylor's jet entrainment constant, this value is approximately equal 0.05.

The schematic representations of geometrical parameters of penetrating jets in a large enclosure are given in Figure 16.

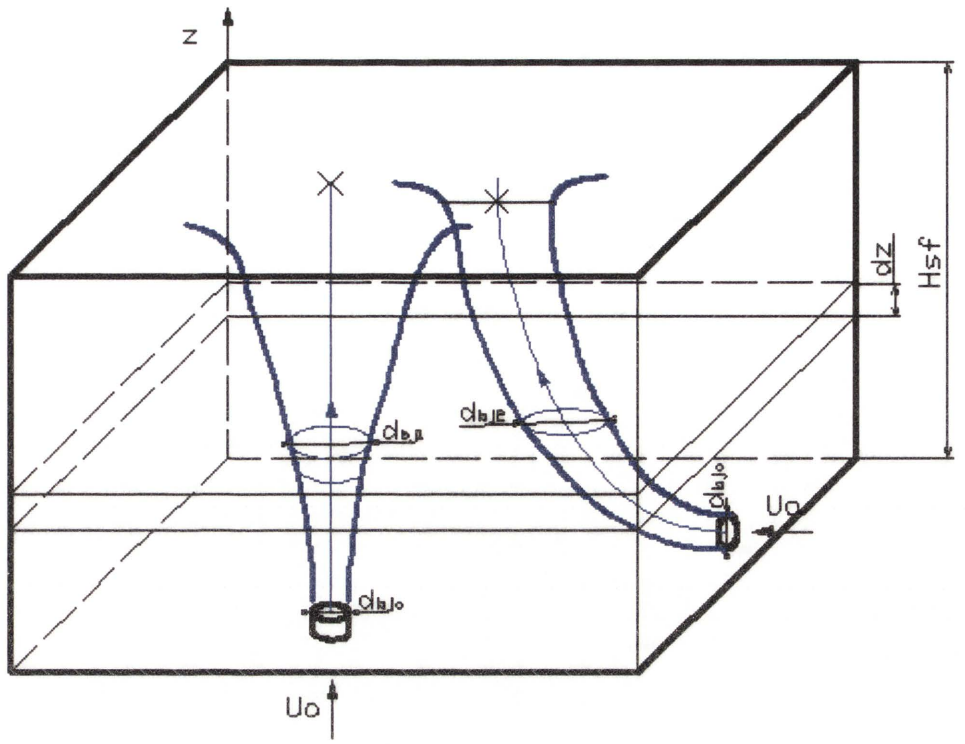

Figure 16 – Geometrical parameters of impinging round free buoyant jets (Source: Peterson, 1994)

The derivation of criteria for the breakdown of ambient stratification by buoyancy driven flows is based on the ratio

$$\left(\frac{H_{sf}}{d_{bjo}}\right) = CRi_{dbjo}^{1/3}\left(1+\frac{d_{bjo}}{4\sqrt{2\lambda_t H_{sf}}}\right)^{2/3}, \tag{2.10}$$

in which ***C*** is a correlated coefficient and

Ri is a jet Richardson number which can be defined as

$$Ri_{d_{jo}} = \frac{(\rho_{amb}-\rho_0)gd_{bjo}}{\rho_a U_0^2}, \tag{2.11}$$

and ρ_{amb} is the ambient density (kg/m^3),

ρ_0 is the entrance or nominal density(kg/m^3).

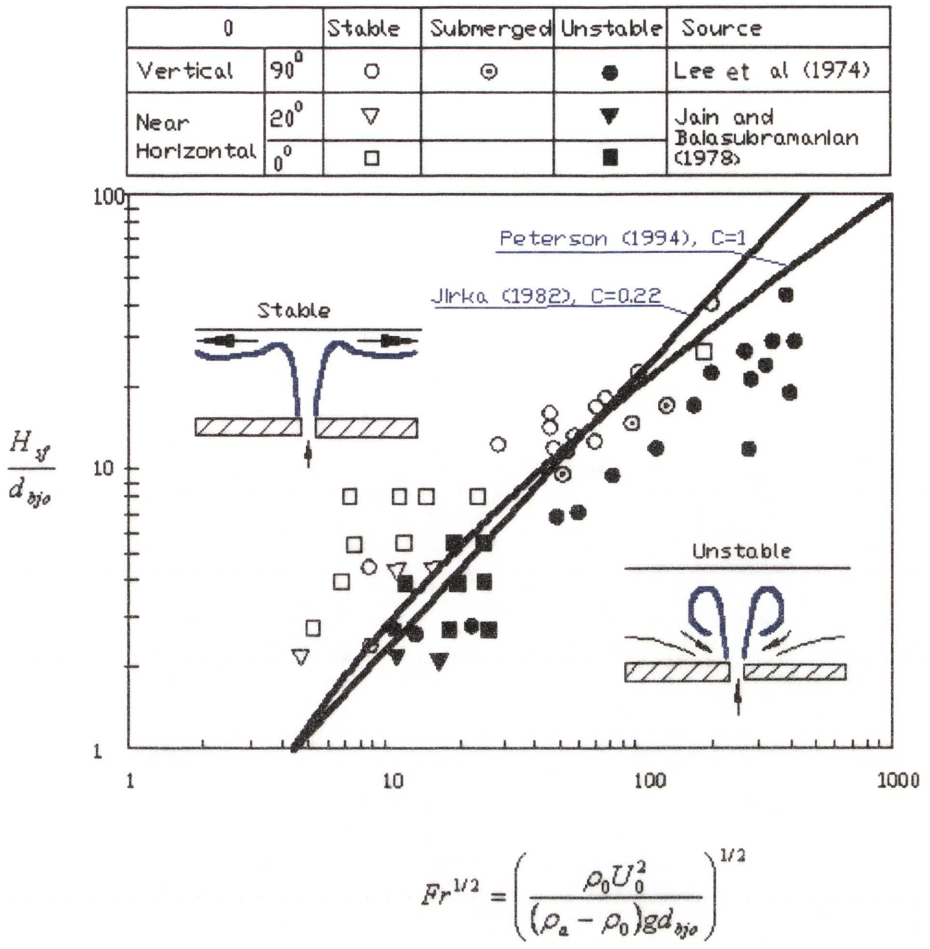

Figure 17 – Experimental data and correlation results for stability criterion (Source: Peterson, 1982)

This concept was evaluated by experimental studies, as shown in Figure 17. The top right corner of the graph relates to the cases in which the jet has sufficient energy to break down thermal stratification and the bottom left corner presents the unstable condition of jet penetration. The curves with two correlation coefficients C=0.22 (Jirka, 1982) and C=1 (Peterson, 1994) were plotted. As can be seen from Figure 17, correlation coefficient C =1 performs better at higher values of the ratio $\frac{H_{sf}}{d_{bjo}}$. According to Peterson (1994), this criterion can be used for vertical and nonvertical jet injections.

The effect of jet orientations and the influence of buoyancy driven flows on the rate of heat removal and the development of flow mixing in ventilated enclosures was studied experimentally by Kuhn et al (2002). The experimental assembly consisted of a cylindrical container with a diameter of 2.29 m, and the heights of the enclosure were 0. 42 m, 0.61 m, 0. 80 m and 0.9 m. There were two 53 mm diameter outlet openings on the top of the enclosure and the bottom of the cylinder was made from a copper plate which was heated or cooled with warm and cold water representing the destabilising or stabilising effects on buoyancy driven flows.

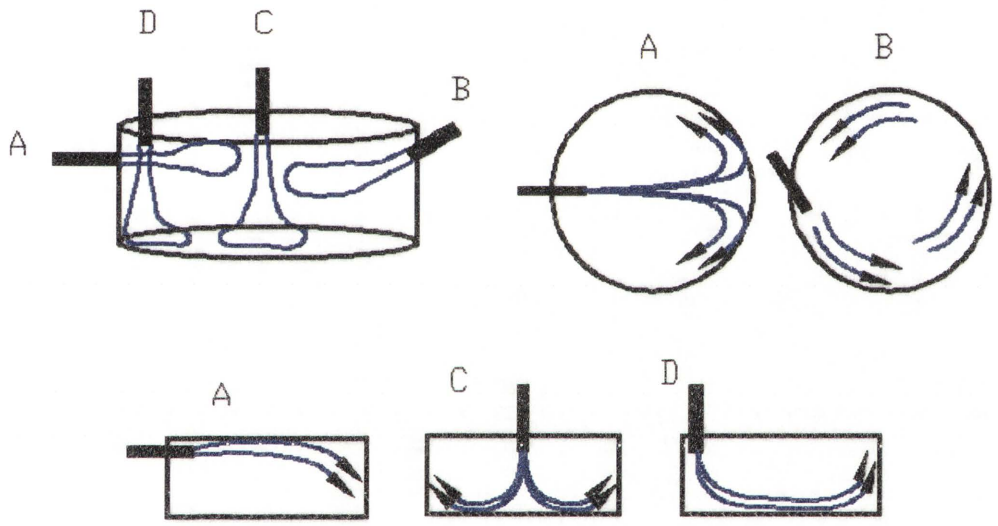

Figure 18 – Orientation of jets (Source: Kuhn et al, 2002)

An investigation into combining the effects of natural and forced convection on heat transfer augmentation for three jet diameters 15 mm, 26 mm and 53 mm and four different jet injections locations radial (A), azimuthal (B), vertical near centre (C) and vertical near wall (D) was conducted (Figure 18).

The ratio between dimensionless heat transfer coefficients Nu_{com} / Nu_{nc} versus Archimedes number (Ar) was plotted for stabilising density gradient (Figure 19a):

$$Nu_{com} = Nu_{fc} + Nu_{nc} \tag{2.12}$$

in which Nu_{fc} is Nusslet number for natural convection, Nu_{nc} for forced convection

and Nu_{com} defines their combined effect

and destabilising effect (Figure 19b)

$$Nu_{com} = Nu_{fc} - Nu_{nc} \tag{2.13}$$

Ar is the Archimedes number $Ar = \dfrac{\mathrm{Re}_j^{\,2}}{Gr_D}$ (2.14)

can be written as the ratio between the Reynolds number $\mathrm{Re} = \dfrac{\rho u d_j}{\mu}$ (2.15)

and enclosure Grashof number $Gr = \dfrac{g\beta(T_{wl} - T_h)D^3}{v^2}$, (2.16)

where T_{wl} is the walls temperature and T_b is the bulk temperature,

and D is the diameter of the enclosure.

Experimental data was found to be fit in the following correlation

$$\frac{Nu_D}{Nu_{nc}} = \left\{ \left(C_2 Ar^{1/3} \left(\frac{\mu_b}{\mu_w} \right)^{0.14} \right)^3 \pm 1 \right\}^{1/3}, \tag{2.17}$$

in which C_2 is the correlation coefficient.

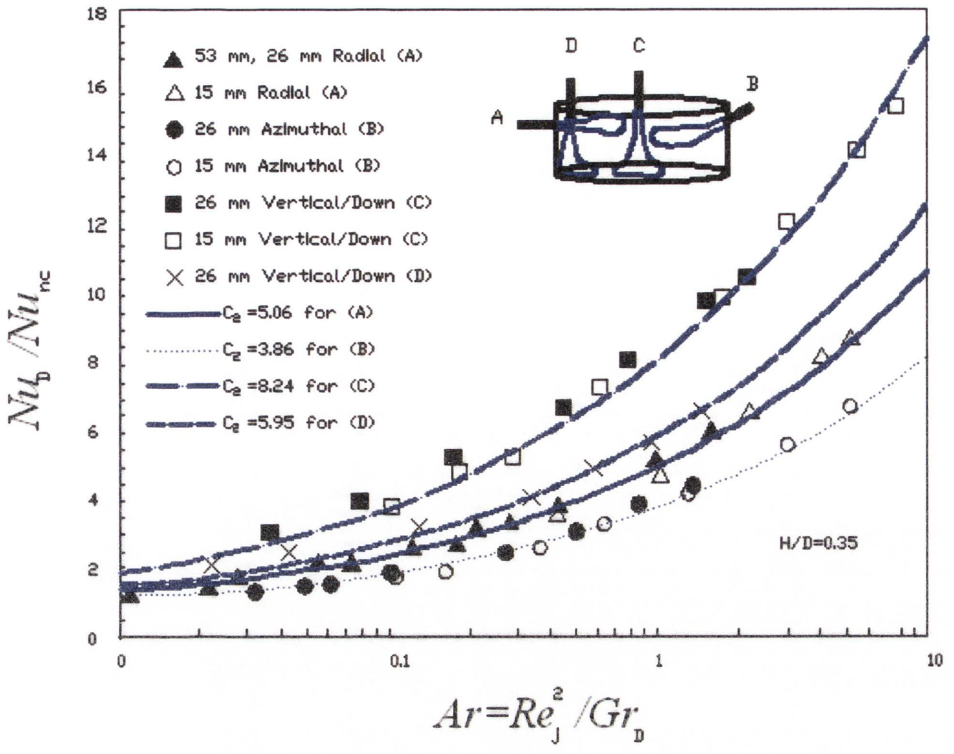

a)

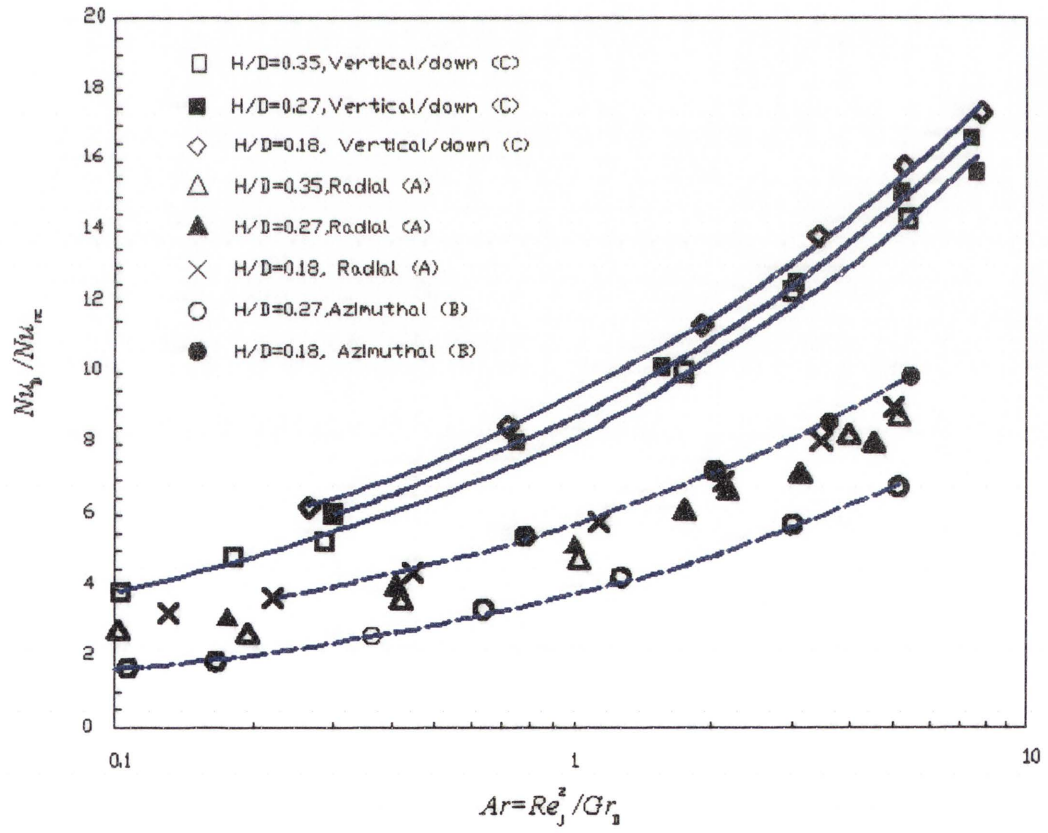

b)

Figure 19 – Natural and forced heat transfer for different jet orientations

The height of an enclosure slightly affected the heat removal rate and air mixing in a cylinder. It was found that the most effective jet orientation was the radial injection. This injection orientation generated a sufficient air circulating flow field and provided a good air mixing.

Kuhn et al (2002) also found that obstacles may significantly reduce the momentum of flow when a jet was directly impinged through the obstacles; as a result, the efficiency of heat transfer and air mixing was also decreased due to momentum drag losses.

The performance of a mechanical ventilation system which draws cold air from an outside space and expels hot air from an inside space can be determined in a similar manner. The cooler ambient airflows need to provide sufficient circulations to create a good air mixing; however, thermal comfort considerations place a limitation on the locations and the amount of injected (extracted) air. Draft and large temperature gradients in an occupied zone cannot be tolerated by a person; for example, due to these requirements, direct radial injection (Figure 19, vertical/down C) cannot be used for the design of ventilation systems. There is limited information about the performance of mechanical ventilation systems which integrate natural and mechanical ventilation.

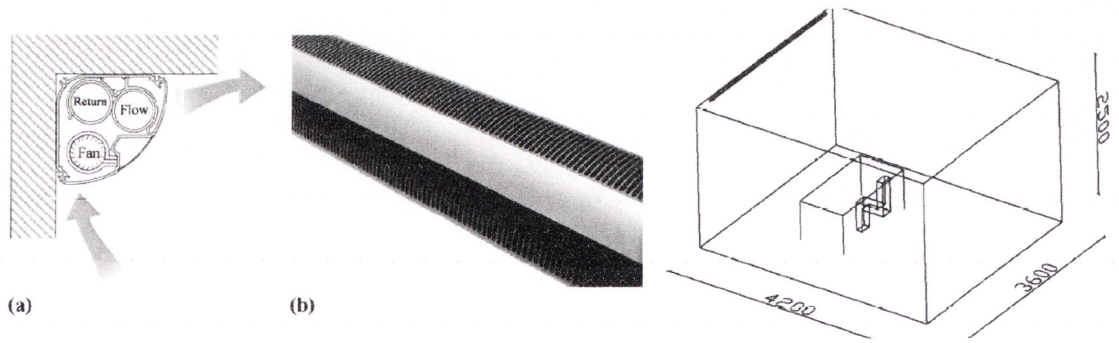

Figure 20 – Schematics of the tested room and convector (Source: Larsen et al, 2007)

A design evaluation of the 'convector' – a ceiling mounting ventilation system – can be found in Larsen et al (2007). A schematical representation of the convector and room installation layout is given in Figure 20.

The room, measuring 4.2m x 3.6 m x 2.5m, has a single person working at a desk. Heat loads included a thermal mannequin, a lamp and a computer. Measurements were conducted for a number of blowing velocities of the fan from 0.42 m/s to 1.44 m/s and different heat loads from 210 W to 350 W.The parameters of thermal comfort were investigated in terms of air quality with the minimum air ventilation rate of 10 L/s per person, sensitivity to drafts which should not normally exceed 0.35 m/s at desk level and 0.15 m/s near head and feet, and mixing of air which should provide uniform temperature distribution where the temperature gradient should be less than 2.5 K/m. Temperature differences did not exceed 1 ^{0}C in all experiments. The results presented by Larsen et al (2007) results show that air drafts were found to be a main source of discomfort. Figure 21 depicts velocity distributions in a room for two supplied air velocities 0.42 m/s and 0.77 m/s. At low velocities, airflows may directly fall down into the occupied zone and result in thermal discomfort for the person. Due to this fact, the convector should not operate at low velocities. It was also found that the cooling capacity of the convector is insufficient to remove heat in excess of 350 W created by electrical devices.

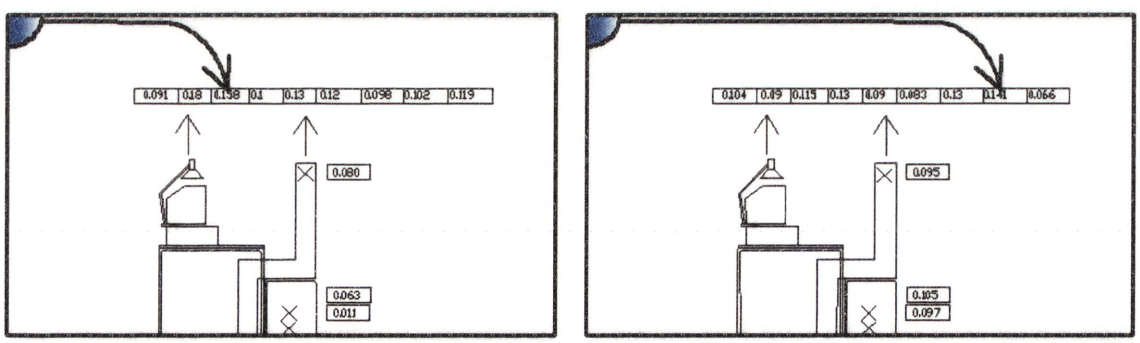

a) b)

Figure 21 – Velocity distributions a) for ventilator speed 0.42 m/s and b) for ventilated speed 0.77 m/s (Source: Larsen et al, 2007)

The investigations were conducted just for one position of the convector and just for this particular type of room and cannot be used for design ventilation solutions.

Currently, there is a lack of information about ideal airflow rates and inlet and exhaust positions of ventilation systems which are driven by buoyancy and kinetic energy, such as roof-mounted fans. Despite the attention paid to the development of low energy consumption devices, the effects on performance of this type of ventilation system are not yet well understood, but finding the optimal location for a fan may improve energy efficiency without compromising thermal comfort requirements. This numerical investigation is an attempt to develop a technique which can be used for design solution, and this research may thus also lead to a better understanding of the physics of air mixing and heat transfer generated by mixing convection.

Chapter 3

Computational methodology

3.1 Mathematical methods

3.1.1 Mass, momentum and energy conservation equations

Fluid motion and heat transfer to and from an enclosure can be modelled by solving the three conservation equations.

The conservation of mass, often termed the continuity equation

$$\frac{\partial \rho}{\partial t} + \frac{\partial (\rho u_i)}{\partial x_i} = 0, \tag{3.1}$$

is written using the tensor notation in which $i = 1,2,3$ and ρ is density, t is time, u_i are velocity components in the x_i direction.

The conservation of momentum, usually termed the Navier-Stokes equations

$$\rho\left[\frac{\partial u_i}{\partial t} + \left(u_j \frac{\partial}{\partial x_j}\right)u_i\right] = -\frac{\partial p}{\partial x_i} + \rho g_i + \frac{\partial}{\partial x_i}\left[\mu\left[\frac{\partial u_i}{\partial x_j} - \frac{\partial u_j}{\partial x_i}\right]\right] \tag{3.2}$$

in which p is the pressure and g is the acceleration due to the gravity;

and finally the conservation of energy called the energy equation

$$\frac{\partial (\rho C_p T)}{\partial t} + u_j \frac{\partial (\rho C_p T)}{\partial x_j} = \frac{\partial}{\partial x_j}\left(k\left[\frac{\partial T}{\partial x_j}\right]\right) + p\frac{\partial u_j}{\partial x_j} + \Phi \tag{3.3}$$

in which C_p is the specific heat capacity at constant pressure, k is the thermal conductivity and Φ is the dissipation function, defined

$$\Phi = \mu\left(\frac{\partial u_i}{\partial x_j} + \frac{\partial u_j}{\partial x_i}\right)\frac{\partial u_i}{\partial x_j} \tag{3.4}$$

When ventilation is modelled, the temperature differences are rarely greater than 30 K, so that the Boussinesq approximation is valid. Since the variations in density are small, the Boussinesq approximation is usually supposed to consist of two parts:

(i) the density is assumed to be constant except in the buoyancy term in the Navier-Stokes equation

(ii) all other transport properties are constant.

With these assumptions, equations (3.1) and (3.2) become

$$\frac{\partial u_i}{\partial x_i} = 0 \tag{3.5}$$

and

$$\frac{\partial u_i}{\partial t} + (u_j \frac{\partial}{\partial x_j})u_i = -\frac{1}{\rho_{ref}}\frac{\partial p}{\partial x_i} + \frac{\rho}{\rho_{ref}}g_i + \frac{\mu}{\rho_{ref}}\frac{\partial^2 u_i}{\partial x_j \partial x_j} \tag{3.6}$$

in which the subscript ***ref*** indicates a reference state.

Further it is usually assumed that as a first approximation the density in the buoyancy term may be written as

$$\rho = \rho_{ref}\left(1 - \beta\left[T - T_{ref}\right]\right) \tag{3.7}$$

In which β is the coefficient of thermal expansion defined as

$$\beta = -\frac{1}{\rho}\left(\frac{\partial \rho}{\partial T}\right)_p \tag{3.8}$$

Equation (3.6) therefore becomes

$$\frac{\partial u_i}{\partial t} + (u_j \frac{\partial}{\partial x_j})u_i = -\frac{1}{\rho_{ref}} \frac{\partial p}{\partial x_i} + (1 - \beta(T - T_{ref}))g_i + \upsilon_{ref} \frac{\partial^2 u_i}{\partial x_j \partial x_j} \quad (3.9)$$

In which υ is the kinematic viscosity.

Finally, the energy equation becomes

$$\rho_{ref} C_p \left[\frac{\partial T}{\partial t} + u_j \frac{\partial T}{\partial x_j} \right] = k \frac{\partial^2 T}{\partial x_j \partial x_j} + \Phi \quad (3.10)$$

Equations (3.5), (3.9) and (3.10) need to be solved simultaneously with the appropriate boundary conditions to permit the modelling of a ventilated room.

3.1.2.1 Turbulence equations

Unfortunately, as the air velocity is increased, the smooth laminar flows become unstable and fluid can experience transition to a turbulent state. The transition between laminar and turbulent flows typically moves closer to the ventilation system exhaust points and the smooth laminar regions can be observed in the corners of a room (Blomqvist and Sandberg, 1997).

Turbulent flows are chaotic and can be characterised by a wide range of length and time scales. Turbulence starts with big eddies with low wave numbers and frequencies. Due to the viscosity of flow and the effects of movement stretching, turbulence produces smaller and smaller eddies with higher frequencies and wave numbers (Davidson (2004)).

The latest computational techniques or DNS (direct numerical simulations), in which equations (3.5), (3.9) and (3.10) are solved directly, can capture detailed information about the turbulence but require large computational resources, making it difficult to implement these tools for the assessment of ventilation system performance (Awbi and Hazim, 2003).

In this case, it is sufficient to solve Reynolds Average equations which are based on the assumption that the average time and space of fluctuations approach zero in a relatively long time.

The instantaneous values of any flow variable can be decomposed into mean and fluctuating parts as

$$f(x,t) = F(x) + f'(x,t) \tag{3.11}$$

in which $F_i(x)$ is a time average value

$$F(x) = \lim_{\tau\to\infty} \frac{1}{\tau} \int_o^{\tau} f(x,t) \tag{3.12}$$

in practice

$$F(x) = \lim_{\tau\to\tau^*} \frac{1}{\tau} \int_o^{\tau} f(x,t), \tag{3.13}$$

in which τ^* is a sufficiently long time to obtain a reliable mean value.

It follows from equations (3.11) and (3.12) that

$$\lim_{\tau\to\tau^*} \int f'(x,t)dt = 0 \tag{3.14}$$

The above procedure is known as Reynolds averaging.

Whereas $\overline{f'(x,t)} = 0$ from equation 3.14 and similarly $\overline{g'(x,t)} = 0$ for function

$g'(x,t) > 0$ the product $\overline{f'(x,t)f'(x,t)} \neq 0$ can take any values (negative, zero or positive)..

The substitution of equation (3.14) into each of the components of the Navier-Stokes equations and then averaging leads to the production of six extra terms $\overline{u_i' u_j'}$, in which $i = 1,2,3$ and $j = 1,2,3$ known as Reynolds stresses. Similarly, the substitution of equation (3.14) for both the velocities and temperatures of equation (3.10) leads to three new terms $\overline{u_i' T'}$, called Reynolds heat fluxes.

Governing equations of Reynolds-averaged conservation of mass and momentum, and balance of energy for turbulent incompressible flow can be written as

$$\frac{\partial U_j}{\partial x_j} = 0 \tag{3.15}$$

$$\frac{\partial U_i}{\partial t} + U_j \frac{\partial U_i}{\partial x_j} = -\frac{1}{\rho_{ref}} \frac{\partial P}{\partial x_i} + \frac{\partial}{\partial x_j}[\nu(\frac{\partial U_i}{\partial x_j} + \frac{\partial U_j}{\partial x_i}) - \overline{u_i u_j}] - \beta(T - T_{ref}) g_i \tag{3.16}$$

$$\rho_{ref} C_p (\frac{\partial T}{\partial t} + U_j \frac{\partial T}{\partial x_j}) = k \frac{\partial^2 T}{\partial x_j \partial x_j} - \rho C_p \frac{\partial}{\partial x_j}(\overline{u_j T'}) + \mu \left(\frac{\partial U_i}{\partial x_j} + \frac{\partial U_j}{\partial x_i} \right) \frac{\partial U_i}{\partial x_j} +$$

$$+ \mu \left(\overline{(\frac{\partial u_i}{\partial x_j})(\frac{\partial u_i}{\partial x_j})} + \overline{(\frac{\partial u_i}{\partial x_j})(\frac{\partial u_j}{\partial x_i})} \right) \tag{3.17}$$

With these new unknown correlations, the set of mean flow Reynolds average equations cannot be solved without a knowledge of how they vary.

Whilst it is possible to set up equations for $\overline{u_i' u_j'}$ further unknown correlations such as $\overline{u_i' p'}$ and $\overline{u_i' u_j' u_k'}$ are generated so that the set of equations is not closed. No matter how far one proceeds, more and more unknown correlations are generated. This is called the closure

problem and leads directly to the need to model the effect of the Reynolds stresses and heat fluxes.

There are different levels of approximations which are used to close the system of equations. One was proposed by Boussinesq, who suggested that diffusion generated by turbulence is connected to the mean rate of strain by so-called turbulent or eddy viscosity

$$-\rho\overline{u_i'u_j'} = \mu_t\left(\frac{\partial U_i}{\partial x_j}+\frac{\partial U_j}{\partial x_i}\right)-\frac{2}{3}\rho k\delta_{ij} \tag{3.18}$$

in which k is the turbulent kinetic energy per unit mass $k=\frac{1}{2}(\overline{u'^2}+\overline{v'^2}+\overline{w'^2})$, μ_t is turbulent viscosity and δ_{ij} is the Kronecker delta $\delta_{ij}=1$ if $i=j$ and $\delta_{ij}=0$ if $i\neq j$

and Reynolds evaluated the concept of turbulent diffusivity

$$-\rho\overline{u_i'\psi'} = \Gamma_t\frac{\partial\psi}{\partial x_i} \tag{3.19}$$

in which Γ_t is the turbulent or eddy diffusivity.

ψ is a scalar quantity, such as temperature, concentration; ψ' is the fluctuating component of ψ.

The ratio between the eddy viscosity and the eddy diffusivity, the Prandtl/Schmidt number

$$\sigma_t=\frac{\mu_t}{\Gamma_t} \tag{3.20}$$

is found to be near constant from many experiments (Versteeg and Malalasekera, 2007).

A number of turbulence models are based on Boussinesq assumption, such as the mixing length model, k-ε and the Reynolds stresses. In the mixing length model, turbulent flows are

described by the positions of the turbulent viscosity. The k-ε model is a more sophisticated model which is able to portray turbulence dynamics through convection, diffusion and dissipation. The Reynolds stress model solves six equations for each of the Reynolds stresses (Versteeg and Malalasekera, 2007).

3.1.2.2 k-ε equations and wall functions

The k-ε model is a semi-empirical turbulence model in which k is turbulent kinetic energy and ε its rate of dissipation. The standard k-ε model (Launder and Spalding, 1974) is obtained from Navier-Stokes equations by multiplying all sets of equations by u'. From the physical point of view, it can be explained as the conservation of velocity fluctuations of mechanical energy. The k-ε model assumes that turbulence is isotropic.

The kinetic turbulent energy k can found as

$$\frac{\partial k}{\partial t}+U_j\frac{\partial k}{\partial x_j}=\frac{\partial}{\partial x_j}[(\nu+\frac{\nu_t}{\sigma_K})\frac{\partial k}{\partial x_j}]+\nu_t[(\frac{\partial U_i}{\partial x_j}+\frac{\partial U_j}{\partial x_i})\frac{\partial U_i}{\partial x_j}+\frac{\beta}{\sigma_t}g_j\frac{\partial T}{\partial x_j}]-\varepsilon \qquad (3.21)$$

and the equation of turbulent energy dissipation $\boldsymbol{\varepsilon}$ can be written as,

$$\frac{\partial \varepsilon}{\partial t}+U_j\frac{\partial \varepsilon}{\partial x_j}=C_{\varepsilon 1}\frac{\varepsilon}{K}\nu_t[(\frac{\partial U_i}{\partial x_j}+\frac{\partial U_j}{\partial x_i})\frac{\partial U_i}{\partial x_j}+\frac{\beta}{\sigma_t}g_j\frac{\partial T}{\partial x_j}]-C_{\varepsilon 2}\frac{\varepsilon^2}{K}+$$

$$\frac{\partial}{\partial x_j}[(\nu+\frac{\nu_t}{\sigma_\varepsilon})\frac{\partial \varepsilon}{\partial x_j}] \qquad (3.22)$$

and turbulent kinematic viscosity ν_t is

$$\nu_t=\frac{C_\mu\cdot k^2}{\varepsilon} \qquad (3.23)$$

The constants were determinated from a number of experiments and Launder and Spalding (1974) assumed that $C_{\mu} = 0.09, C_{\varepsilon 1} = 1.44\ C_{\varepsilon 2} = 1.92\ \sigma_k = 1.0$ and $\sigma_{\varepsilon} = 1.3$.

Turbulence does not usually exist or is very low near solid walls due to viscous forces (Figure 22a). These effects can be represented by applying 'the damping function' f_h in the term of turbulent viscosity or by using the wall function laws. When the damping function is used, the turbulent viscosity can be written as

$$v_t = \frac{C_{\mu} \cdot f_h\, k^2}{\varepsilon} \tag{3.24}$$

In the case, where ***k-ε*** equations are not solved in cells adjacent to walls (Figure 22b), functions are implemented.

The wall functions are usually related to the Law of the Wall which was developed by Prandtl in the 1930's (Versteeg and Malalasekera, 2007). Prandtl stated that the dimensionless velocity v^+ is a function of the dimensionless distance y^+. He performed the dimensional analysis for this given problem. The velocity near walls can be written as a function of viscosity ν, density ρ, shear stresses τ_w and distance from the wall y

$$u = f(\mu, \tau_w, \rho, y) \tag{3.25}$$

The result of the dimensional analysis can be expressed as,

$$\frac{u\rho^{1/2}}{\tau_w^{1/2}} = f\left(\frac{y\rho^{1/2}\tau_w^{1/2}}{\mu}\right) \tag{3.26}$$

Non-dimensional terms were determined as

$$u^* = \sqrt{\frac{\tau_w}{\rho}} \quad u^+ = \frac{u}{u^*} \quad y^+ = \frac{\rho y u^*}{\mu} \tag{3.27}$$

where u^* is the so-called friction velocity,

τ_w is the wall shear stress,

u^+ is a non-dimensional velocity with the friction velocity as the reference value,

y^+ is a Reynolds number within the distance from the wall as the characteristic distance and the friction velocity as the characteristic velocity.

The Law of the Wall asserts that u^+ is purely is a function of a dimensionless distance from a wall y^+.

Prandtl stated that in the viscous sub-layer, where y^+ is less than 5, the velocity profile is linear and fluid is laminar. Thus, the equation in the first near-wall node can be written as

$$u^+ = y^+ \text{ for } u^+ \leq y_v^+ \tag{3.28}$$

in which y_v is the thickness of the viscous sublayer.

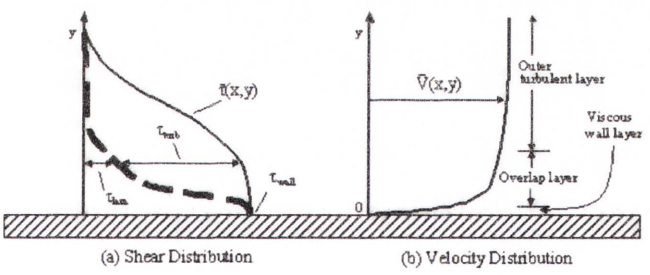

a) Typical velocities and shear distributions in turbulent flow near the wall

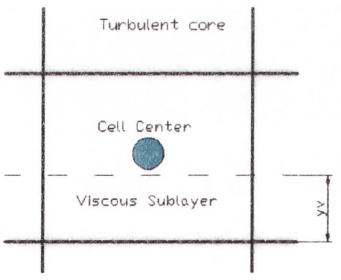

b)Schematics of the cell adjacent to walls

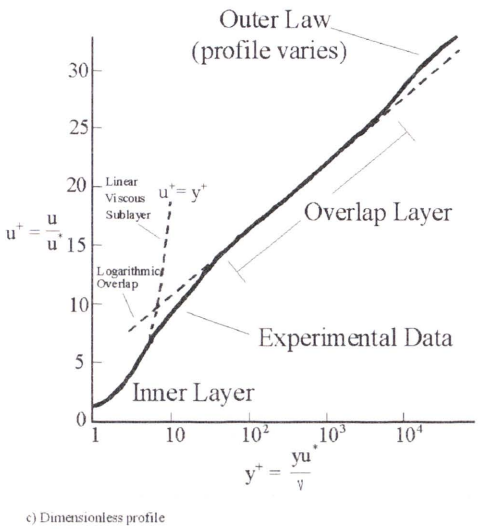

c) Dimensionless profile

Figure 22 – The turbulent boundary layers

Above $y^+ > 30$, the turbulent shear dominates and the dimensionless profile is altered by a logarithmic law

$$u^+ = \frac{1}{\kappa'} \ln(Ey^+) \text{ for } y^+ > y_v^+, \tag{3.29}$$

In which κ' is the von-Karman constant (κ' =0.4), and E is a function of wall roughness. Between two these laws an overlap mixing layer exists (Figure 22c).

The standard k-ε turbulent model with the adjusted near solid boundaries wall functions is usually used for turbulent flows with high Reynolds numbers and does not perform well for flows with low Reynolds numbers. For such fluid problems, it is usually sufficient to implement damping functions instead of using the wall functions. The main disadvantage of using damping functions in turbulent equations is the first grid point requirement which proposes that the grid point near the solid wall should be placed in a laminar region. This requirement may lead to a more computationally expensive solution in terms of the mesh distributions.

3.2 Numerical methods

Numerical methods are used to solve partial differential continuity, Navier Stokes, turbulence and energy equations. In the present work, the equations were discretised by the finite volume method. The flow field was divided into a number of cells. Each cell represents a whole control volume (Figure 23). The physical properties are assumed to be constant through each of the finite volumes. The Gauss divergence theorem was implemented and volume integrals were transformed into the surface integrals. The continuous differential equations were converted into the finite difference equations via integration over control volumes in a rectangular mesh. All fluid properties were calculated in the centre of each finite element according to the change in the mass, momentum and energy on the boundaries of this element. The finite volume spatial discretisation algorithms stores all values at the centre of each cell.

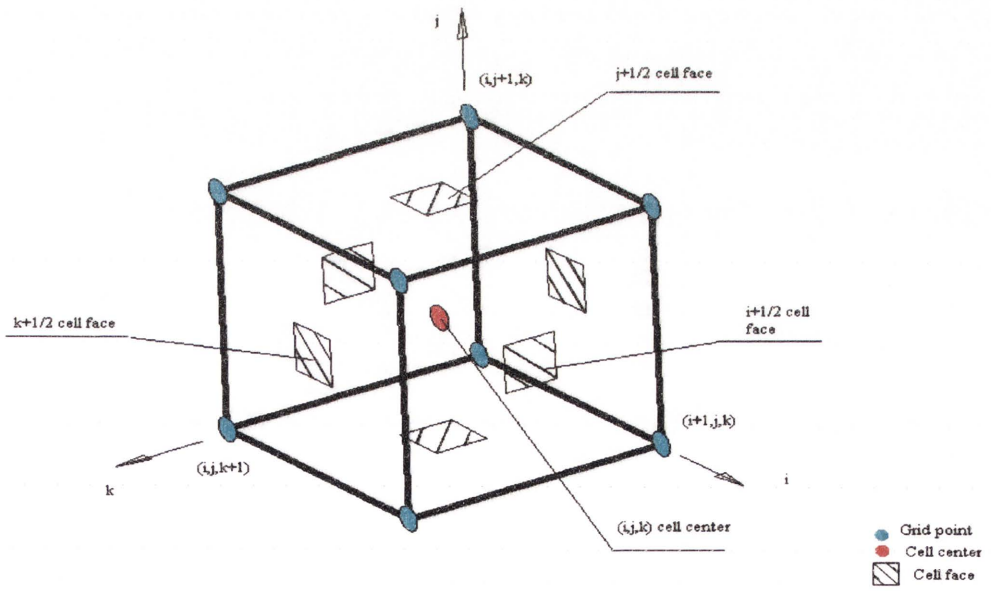

Figure 23 – The finite volume

The discretisation of a geometrical volume on finite element volumes was generated using the commercial software CFD–Geom (ESI Group). The short description of the code is given in Chapter 3.3.

The partial differential equations were broken into the set of algebraic equations for each finite volume.

The solutions of all variables were also taken in the centre of each cell.

The method of solving derivative terms of differential equations involves Taylor series expansions.

Taylor series expansion of a function $f(x)$ can be written as

$$f(x+\Delta x) = f(x) + \left(\frac{\partial f}{\partial x}\right)\frac{\Delta x}{1!} + \left(\frac{\partial^2 f}{\partial x^2}\right)_{i,j}\frac{(\Delta x)^2}{2!} + \left(\frac{\partial^3 f}{\partial x^3}\right)_{i,j}\frac{(\Delta x)^3}{3!} + \ldots\ldots$$

$$\ldots + \left(\frac{\partial^n f}{\partial x^n}\right)\frac{(\Delta x)^n}{n!} + \ldots \qquad (3.30)$$

Derivative terms of equations can be approximately defined by using the values of these functions at neighbour grid points and the grid spacing between them.

The value of a function at the neighbouring grid point $i+1$ (Figure 24) can be expressed as

$$f_{i+1,j} = f_{i,j} + \left(\frac{\partial f}{\partial x}\right)_{i,j}\frac{\Delta x}{1!} + \left(\frac{\partial^2 f}{\partial x^2}\right)\frac{(\Delta x)^2}{2!} + \left(\frac{\partial^3 f}{\partial x^3}\right)\frac{(\Delta x)^3}{3!} + \ldots \qquad (3.31)$$

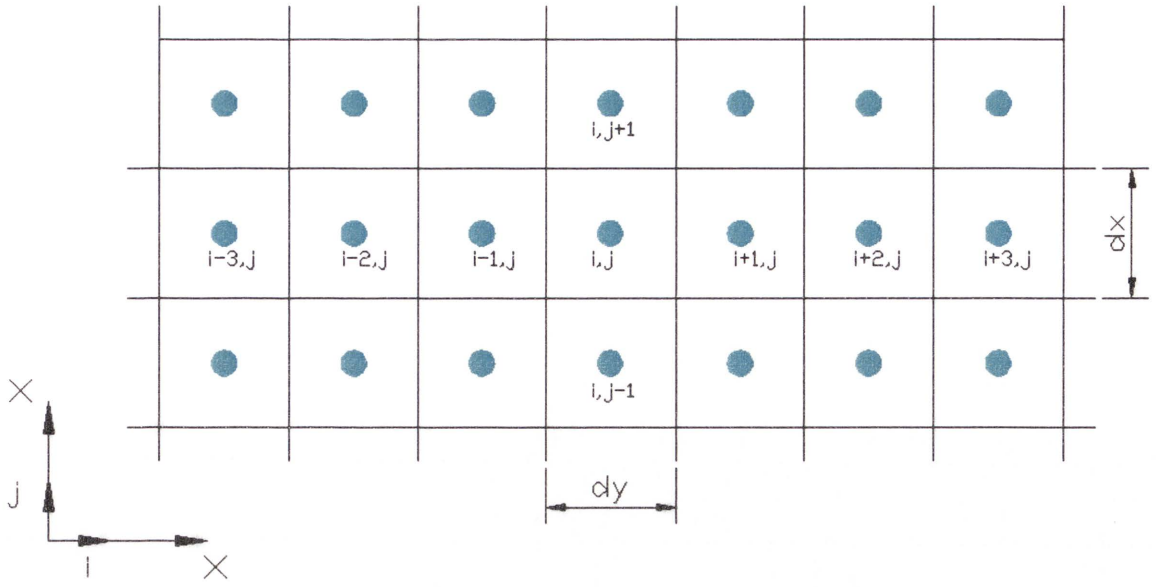

Figure 24 – The finite difference expressions

and at the neighbouring grid point $i-1$ can be written as

$$f_{i-1,j} = f_{i,j} + \left(\frac{\partial f}{\partial x}\right)_{i,j} \frac{(-\Delta x)}{1!} + \left(\frac{\partial^2 f}{\partial x^2}\right)_{i,j} \frac{(-\Delta x)^2}{2!} + \left(\frac{\partial^3 f}{\partial x^3}\right)_{i,j} \frac{(-\Delta x)^3}{3!} + \ldots \tag{3.32}$$

The first derivative of f with respect to space may be found by re-arranging Equation 3.31:

$$\left(\frac{\partial f}{\partial x}\right)_{i,j} \approx \frac{f_{i+1,j} - f_{i,j}}{\Delta x} + O(\Delta x) \tag{3.33}$$

in which $O(\Delta x)$ defines the accuracy of the finite differential approximation. The derivative given by equation (3.33) therefore is first order accurate.

A second order accurate difference scheme can be obtained by subtracting Equation 3.31 from Equation 3.32:

$$\left(\frac{\partial f}{\partial x}\right)_{i,j} \approx \frac{f_{i+1,j} - f_{i-1,j}}{2\Delta x} + O(\Delta x)^2 \tag{3.34}$$

As can be seen from Equations 3.33 and 3.34, the derivative terms of equations can be evaluated in many ways depending on the number of grid points and the spacing between them. Higher order and high accuracy schemes require more grid points or smaller grid spacing.

There are also different space stepping schemes, such as Equation 3.33 describes forward differences and backward differences can be written as

$$\left(\frac{\partial f}{\partial x}\right)_{i,j} = \frac{f_{i,j} - f_{i-1,j}}{\Delta x} + O(\Delta x) \tag{3.35}$$

and central differences

$$\left(\frac{\partial f}{\partial x}\right)_{i,j} = \frac{f_{i+1,j} - f_{i-1,j}}{2\Delta x} + O(\Delta x)^2 \tag{3.36}$$

and time stepping schemes; for example Forward Differencing (Euler method), Backward Differencing (Backward Euler) and centred differencing (Crank-Nicolson).

The discretised equations were assembled in matrix form and solved by using the pressure correction SIMPLEC algorithm. The commercial solver used ran multiple iterations until convergence was reached.

3.3 Brief description of the CFD-ACE commercial code

The commercially available software CFD-ACE has been used to simulate the flow, thereby allowing the prediction of velocity and temperature distributions in a ventilated room.

CFD ACE is a product of the ESI Group research corporation. CFD-ACE is a well known Navier Stokes equations code for general purposes. The three main modules of this software have been used in this thesis: CFD-GEOM, CFD-ACE and CFD-VIEW. The CFD-GEOM module was used to draw the analysed domain, mesh generation and transformation of the created model into the readable form files for the main solver CFD-ACE+. The CFD-ACE + software has numerically solved governing equations using an iterative method. The CFD-VIEW module was used for visualising the obtained results.

More detailed information can be found on the ESI Group Homepage www.esi-group.com .

Chapter 4

CFD modelling

4.1 Geometry and flow conditions

Computational modelling of a whole house is both a complicated and time consuming task. The results obtained from whole house simulations would also be difficult to implement for assessment of the performance of a ventilated system because ventilation is a complex phenomenon with many physical processes occurring simultaneously. For this complicated problem, it is more realistic to use a simplified model to predict specific characteristics of a ventilation system and try to develop general recommendations. Consequently, the geometric modelling of a room with a fan and indoor area has been performed in order to analyse the impacts of different parameters and conditions on ventilation effectiveness.

The flow field was modelled using a commercial computational fluid dynamics code (CFD) CFD-ACE+ (ESI CFD Inc (2007)).

The schematic representations of boundary conditions and computational domains can be seen in Figure 25. The computational domain consists of the indoor internal spaces, external wall and outside sub-domain. The dimensions and positions of the model for four fan locations are given in Figures 26 to 29.

The model divides the fluid domain into external and internal spaces filled with air.

The properties of air are given in Table 1. The flows involved in this fluid problem are governed by dynamics associated with the buoyancy force; thus, the Boussinesq approximation is implemented. The mathematical description of the Boussinesq approximation is given in Chapter 3.

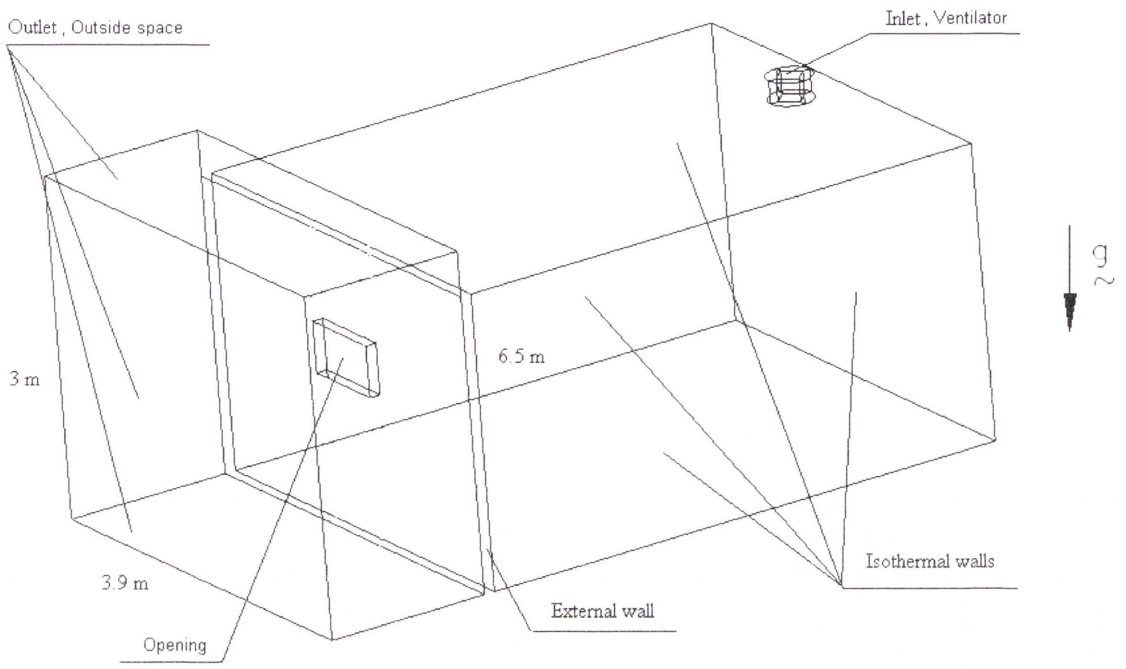

Figure 25 – Geometry and boundary conditions

The external wall which contains the opening was modelled as the solid material domain. The material properties of the wall are given in Table 2.

Table 1 - Properties of air

Density, kg/m3	Viscosity, kg/m-s	Specific heat, J/kg-K	Thermal conductivity, W/m-K
1.1614	1.84E-05	1007	0.0263

Table 2 - Properties of wall material

Density, kg/m3	Specific heat, J/kg-K	Thermal conductivity, W/m-K
1700	800	0.04

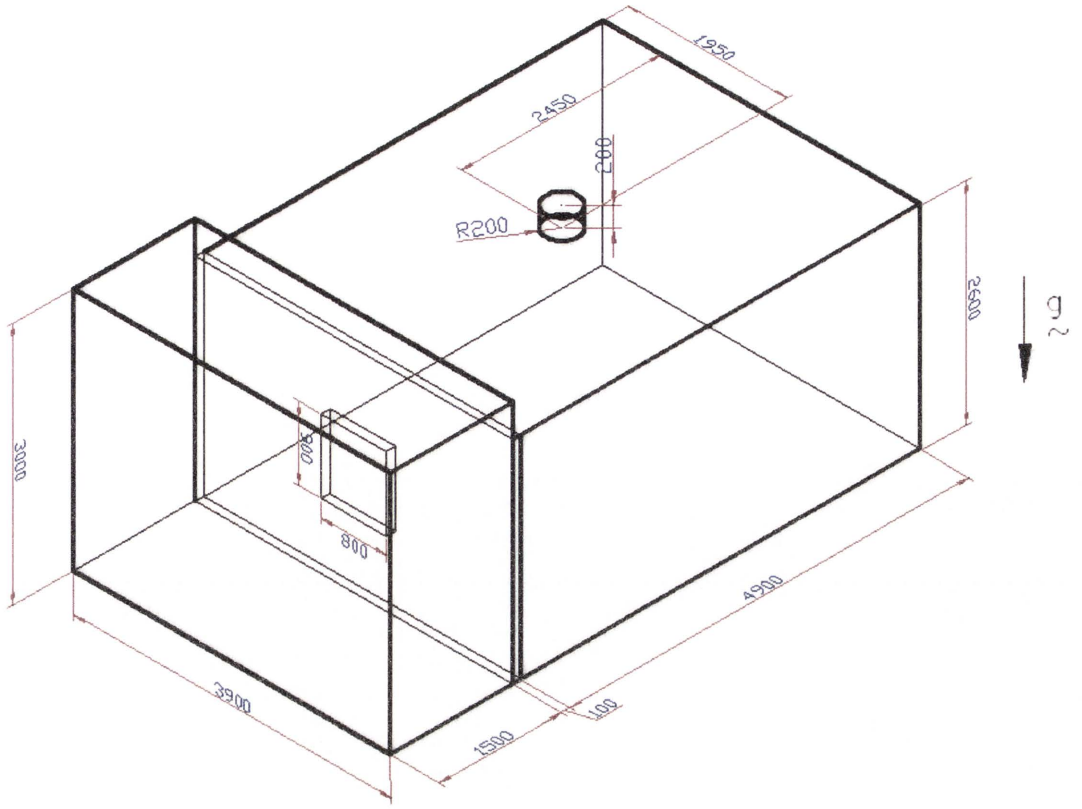

Figure 26 – CFD geometry for the room with a fan located in the middle of the ceiling (Location 1)

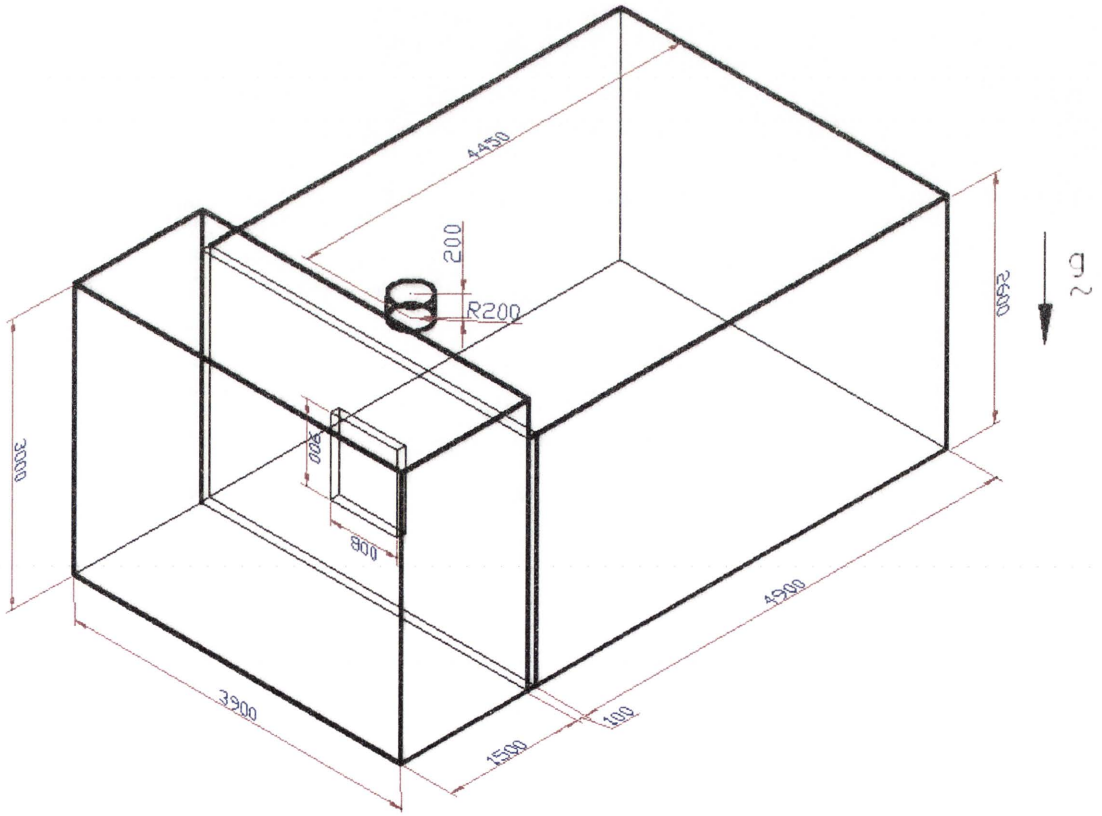

Figure 27 – CFD geometry for the room with a fan located on the ceiling near the opening (Location 2)

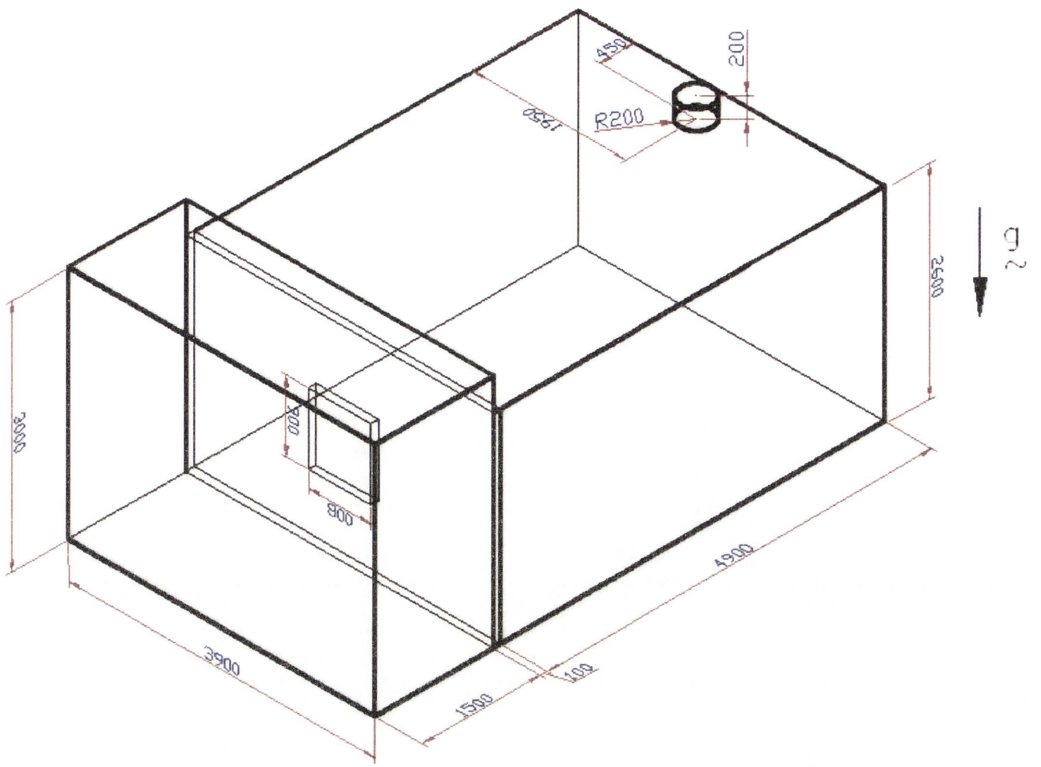

Figure 28 – CFD geometry for the room with a fan located on the ceiling near the back wall (Location 3)

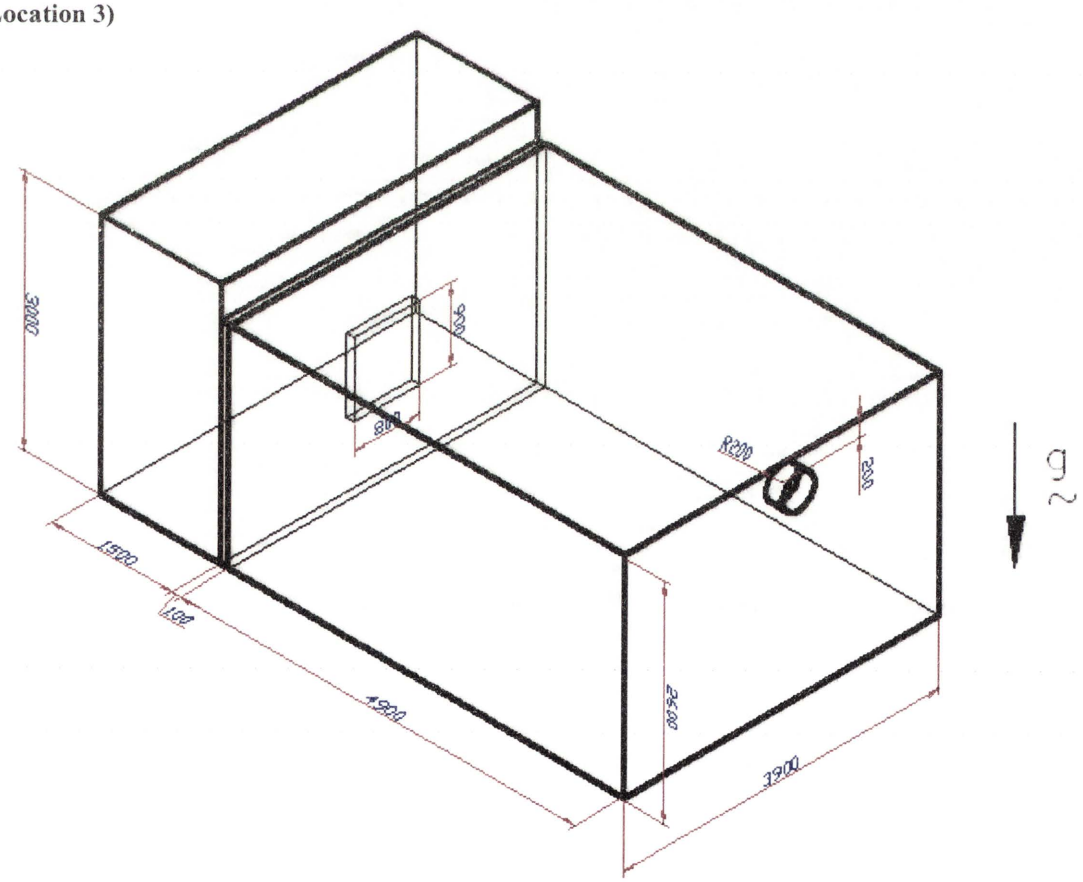

Figure 29 – CFD geometry for the room with a fan located on the back wall (Location 4)

4.2 Grid generation

A grid mesh was created manually by using the tool set provided in the pre-processor CFD–GEOM.

The mesh can be specified by the number of grid points and their distributions. A fine grid was constructed close to the surface intersections and in the areas of expected high air velocity and temperature gradients, for example the fan inlet, the opening and the corners of a room. A coarser grid was used in areas where changes in gradients are relatively smaller, for example in the middle of a room. Stretching functions were used to smoothly distribute points along the line segment from a fine to a coarse mesh. In the present work, hyperbolic tangent mesh generation technique was used to provide good smoothness and orthogonality of mesh.

The coordinate of the grid $\vec{x}$ through the computational domain vector $\vec{\xi}$ can be represented by a vector function as

$$\vec{x} = \vec{x}\left(\vec{s}\left(\vec{\xi}\right)\right) \tag{4.1}$$

in which $\vec{\xi}$ is limited by the length of the segment as $\xi \in [0, I]$ and $\vec{s}$ is a intermediate parametric function between the computational and physical spaces can be found as

$$s(\xi) = \frac{u(\xi)}{A + (1 - A)u(\xi)} \tag{4.2}$$

for a double sided stretching function $u(\xi)$ is defined as

$$u(\xi) = \frac{1}{2}\left[1 + \frac{\tanh\left[\delta\left(\xi / I - 1/2\right)\right]}{\tanh\left(\delta / 2\right)}\right], \tag{4.3}$$

in which A can be found as the ratio between the square root of the spacings at the ends of the length of the segment

$$A = \frac{\sqrt{\Delta s_2}}{\sqrt{\Delta s_1}}. \tag{4.4}$$

and δ is a stretching factor which can be found from the equation

$$\frac{\sinh(\delta)}{\delta} = B \tag{4.5}$$

in which $B = \frac{1}{I\sqrt{\Delta s_2 \Delta s_1}}$. (4.6)

Figure 30 defines the locations of the edge element and Table 3 shows the length of segments, the number of grid points and the parameters used in the hyperbolic tangent function.

The circular surface of the fan was discretised into the five structured faces by using the mesh tool 'Butterfly Faces' incorporated into the CFD-GEOM program. Figure 31 depicts the geometry and mesh distributions of the created circular tube. The radius of the circular cross section is 200 mm. The circumference is divided into the four equal arcs AB, BC, CD and AC. The position and dimensions of the core rectangular mesh can be suitably regulated by the length of BF, HC, GD and AE. In most cases, FG and EH are equal 280 mm.

The number of grid points of external circular and internal rectangular edges is 12 and the connected edges BF, HC, GD and AE consist of 5 grid points. The height of the circular tube AI (0.2 m) was discretised by five equally spaced grid points .

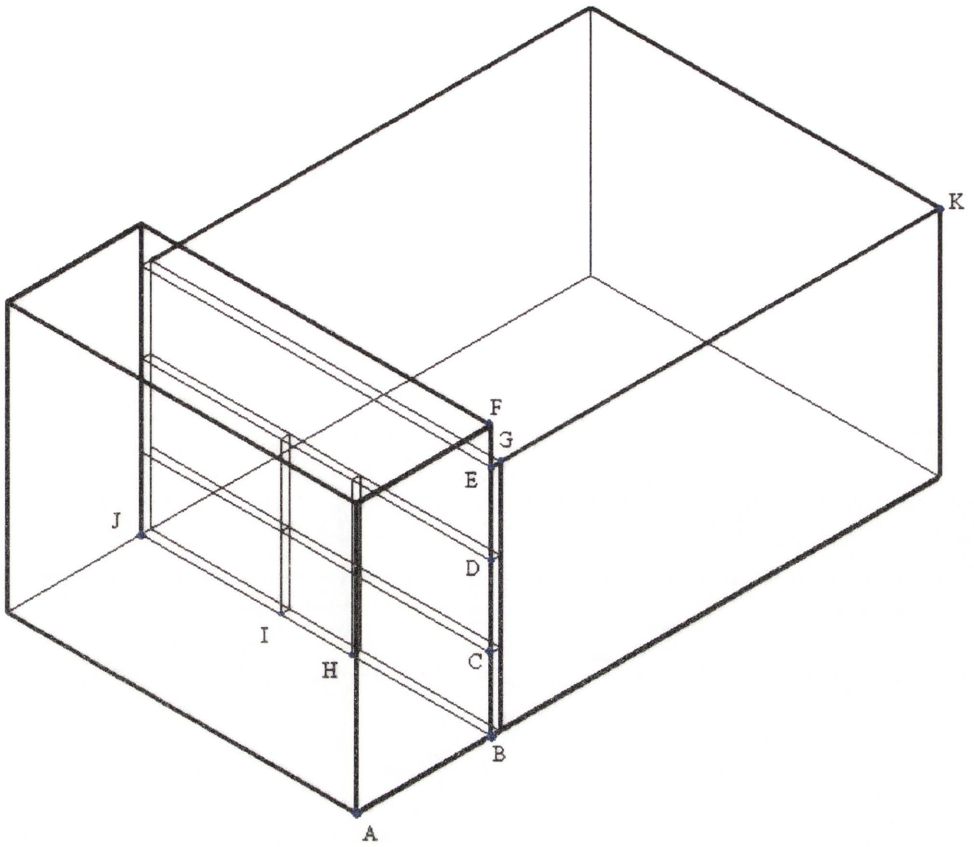

Figure 30 – Locations of the edge elements

Table 3 – The mesh parameters

Edge	Length, mm	Number of grid points	Start point spacing, mm	End point spacing, mm
AB	1500	30	10	10
BC	800	30	10	10
CD	900	30	10	10
DE	900	40	10	10
EF	400	15	10	10
FG	100	7	uniform	uniform
GK	4900	80	10	10
BH	1550	30	10	10
HI	800	35	10	10
IJ	1550	30	10	10

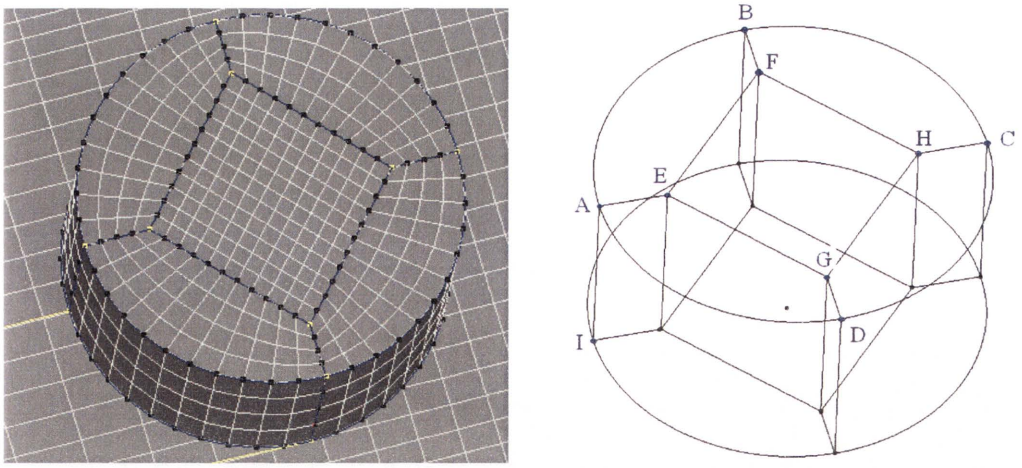

Figure 31 – Butterfly mesh distributions

The ceiling and the lower surface of the fan was connected by using the CFD-ACE (ESI CFD Inc.) built-in feature 'Arbitrary interface'. This feature allows matching of faces with different mesh distributions by dividing them into the number of polyhedrals, as shown in Figure 32.

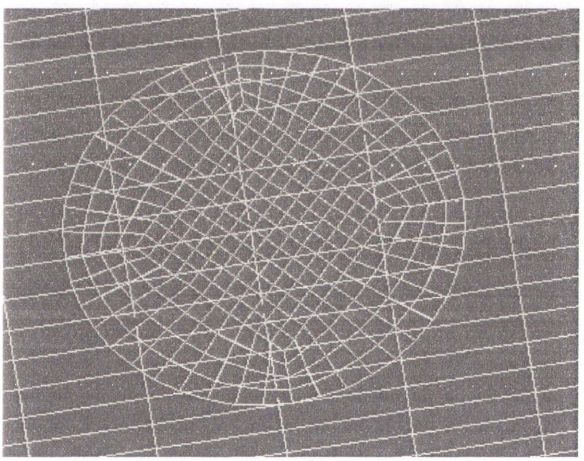

Figure 32 – Arbitrary interface

The resulting mesh is shown in Figure 33.

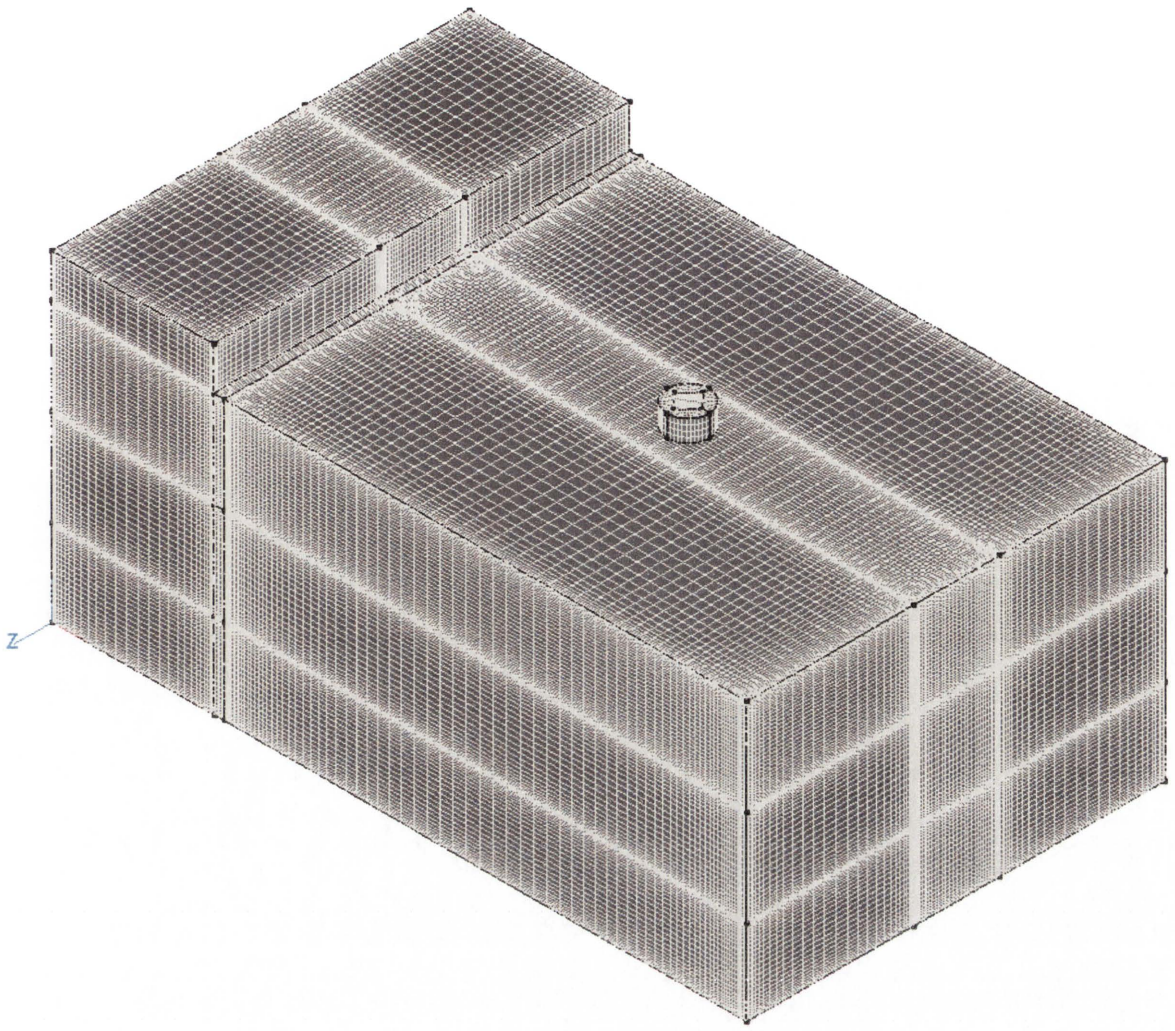

Figure 33 – Final mesh distributions

4.3 Boundary conditions

Boundary conditions give specifications of the main physical properties, such as velocity, temperature and pressure at domain boundaries. Short descriptions of boundary conditions for each sub domain are given in Table 4.

Table 4 – Boundary conditions

Variable	Walls(including ground surfaces)	Inlet	Outlet*
u	0	0	Outflow
v	0	0.0001 m/s....3.5 m/s	Outflow
w	0	0	Outflow
p	-	Calculated by software	Ambient value
k	k-equation	0	Calculated by software
ε	Wall function	0	Calculated by software
T	303 K, 305 K, 307 K	298 K	298 K

*- if flow into the computational domain is detected, an outlet boundary with prescribed conditions will be disregarded by the software and replaced by calculated velocity and temperature.

-if flow out the computational domain is detected, an inlet boundary pressure will be disregarded by the software and replaced by calculated value.

The surrounding walls are considered isothermal, having three possible temperatures of 303 K, 305 K and 307 K. For solid walls, no-slip boundary conditions were applied. Viscous effects become dominant near the solid walls and the wall functions for turbulent Navier-Stokes equations were applied to the first computational node. Ground surfaces are also taken to be isothermal walls in this work.

The fan's exhaust-flow condition is prescribed as an inlet boundary with velocity (flowing in or out of the computational domain). The velocity vector was normal to the inlet area and velocity distributions were assumed to be uniform. Extracted and injected normal velocities ranged from 0.0001 m/s to 5 m/s.

Turbulent kinetec energy ***k*** and dissipation rate ***ε*** at the inlet and the outlet was assumed to be zero. The kinetic turbulent energy is

$$k = \frac{1}{2}\left(u'^2 + v'^2 + w'^2\right), \tag{4.7}$$

where u', v', w' are fluctuations of velocity in x, y and z axes respectively, [m/s].

Backflow dissipation rate can be determined as

$$\varepsilon = \frac{C_H^{0.75} \cdot k}{\kappa^* \cdot L} \tag{4.8}$$in

which $C_H = 0.09$ and $\kappa^* = 0.4$ are constants and L is reasonable length scale, [m].

As a part of the coursework graduate project (Kivva, Graduate project, 2008), investigation of the impact of turbulence boundary conditions at the inlet and outlet on the values of discharge coefficient and the average temperature in a room was conducted. Computational simulations with smaller values of k=1E-06 m^2/s^2 and ε=2.47E-07 m^2/s^3 were performed.

A negligibly small difference between results was observed, as can be seen from Table 5 and Figure 34.

Table 5 - The temperature and air flow rate results

Value of k, [m^2/s^2]	Value of ε, [m^2/s^3]	Temperature average inside the room, [K]	Air flow rate through the window, [m^3/s]
1E-06	2.47E-07	300.971	0.2928
0	0	300.978	0.2924

a) b)

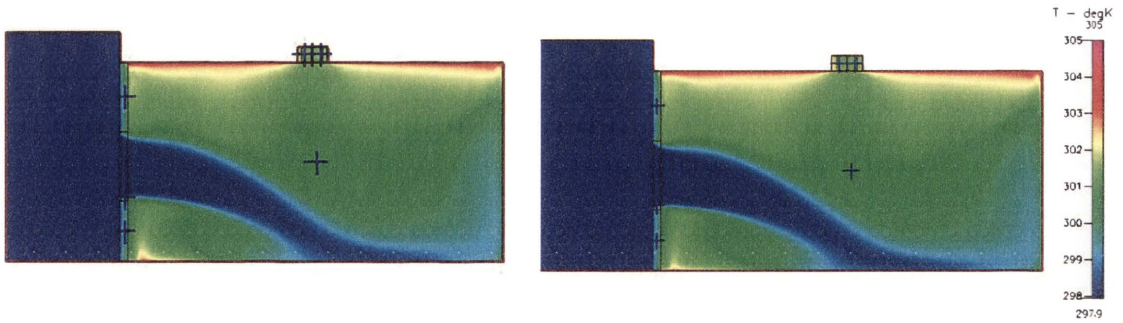

Figure 34 – Temperature contours in the middle plane for simulations with a) small values of k and ε b) with k and ε equal 0 at inlet boundary condition

4.4 Validation and verification

The CFD simulation results may contain some uncertainties and require intensive validation and verification to ensure that the right equations are solved, and solved correctly. The assessment of the computational model should be accomplished using the experimental knowledge.

The accuracy of this model was assessed with experimental data and the CFD simulations were published in Favaralo and Manz (2005).

Computational models were validated by experimental tests performed by Jepsen (2003) who measured the airflow rate through a large rectangular opening using a tracer gas and hot wire anemometers technique in a laboratory environment. The results are presented in Figure 35 and the uncertainty of each measurement is considered to be in the 10% range.

Figure 35 depicts the numerical values of the discharge coefficients for different vertical positions of the window. For the value of the dimensionless height of 1 or when the window is located just beneath the ceiling, the discharge coefficient can be found from Equation 2.6 as

$$C_d = \frac{3Q}{\sqrt{gH\frac{T_0 - T_i}{T_i}}}\frac{1}{A} = \frac{3 \cdot 0.296}{\sqrt{9.81 \cdot 1.44\frac{291.478 - 279}{279}}}\frac{1}{2.592} = 0.71 \qquad (4.9)$$

As can be seen from Figure 35, the computed discharge coefficients compared reasonably well with the experimental discharge coefficients available in the literature, which provided reasonable confidence in the accuracy of the predicted momentums of temperature driven flows.

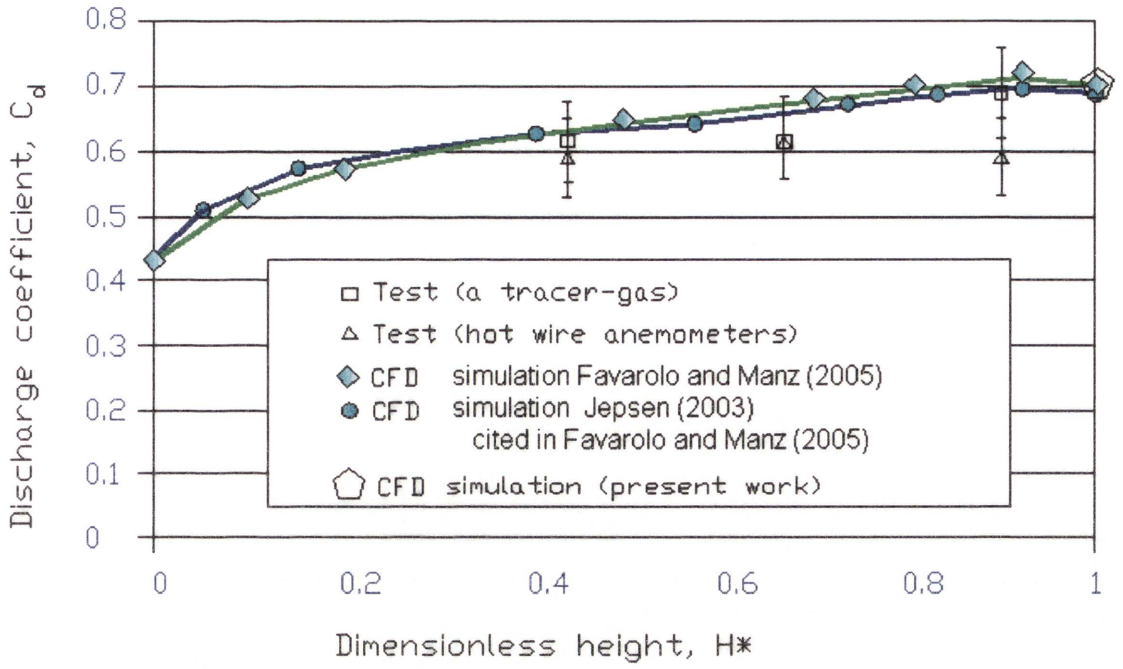

Figure 35 – A plot of discharge coefficients versus dimensionless opening heights

Further validation of this CFD model was performed by comparison with results from Favaralo and Manz (2005)'s computational model.

A brief description of the initial conditions, spatial differential schemes, number of grid points and turbulence models is given in Table 6, and Figure 36 depicts the temperature contour results in the middle section of the room for steady states simulations performed by Favarolo and Manz (2005) (a) and the present work (b).

Table 6-The description of computational models

	Walls temperature	Outside temperature	Special differencing scheme	Number of grid cells	Turbulence model
Favaralo and Manz (2005)	299.15K	279,15K	upwind	1 million	LVEL-k-ε
Present work	299 K	279 K	2 order upwind	1.23 million	Low Re Chien

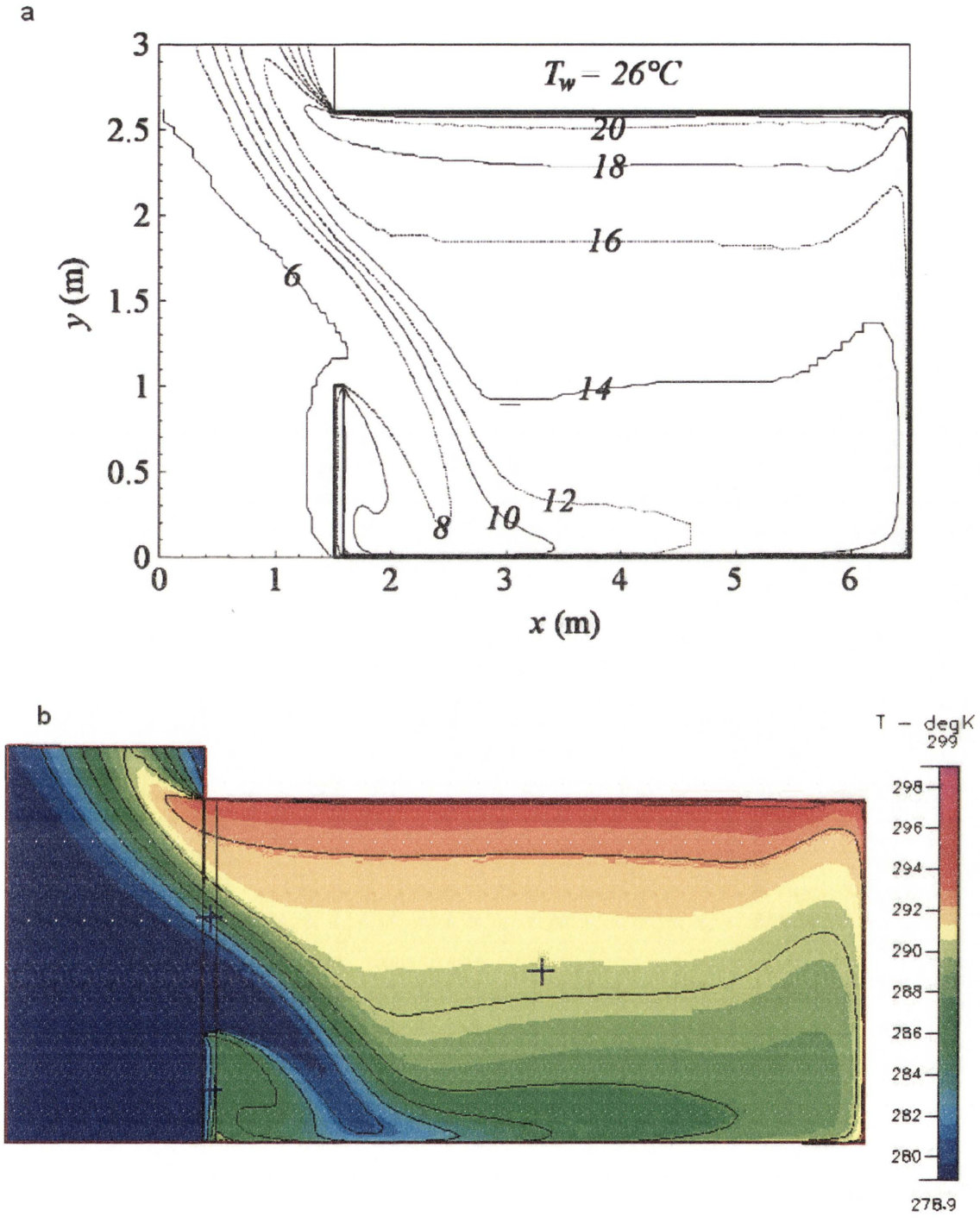

Figure 36 – The temperature contours for steady state solutions performed by a) Favaralo and Manz, 2005, b) present work

A slight difference in temperature distribution contours can be seen for the results obtained from different spatial differential schemes and turbulent models, as can be seen in Figure 36. The numerical value of the discharge coefficients also show very good agreement.

In order to verify this simulation model, a sensitivity study is carried out with different turbulent models and on different grid distributions.

The simulations have been conducted using standard k-ε and Low Re Chien turbulent models. Only small differences in results for steady state can be noticed.

The discrepancy in results for average temperatures was found to be

$$\delta T' = \frac{\delta T}{\Delta T} = \frac{T_{k\varepsilon} - T_{LRC}}{T_{walls} - T_{outside}} = \frac{291.7354 - 291.478}{299 - 279} = 0.01 \tag{4.10}$$

Table 7-The results obtained using different turbulent models

Turbulence model	Temperature average inside the room, K	Air flow rate through the lower ½ of window	Air flow rate through the upper ½ of window	Discharge coefficient Cd
Low Re Chien	297.478	0.2015	0.1993	0.7103
k-ε	297.735	0.2017	0.1994	0.7111

and for the value of the discharge coefficient

$$\delta_{Cd} = \frac{Cd_{LRC} - Cd_{ke}}{Cd_{ke}} \cdot 100\% = \frac{0.7111 - 0.7103}{0.7111} \cdot 100\% = 0.103\% \tag{4.11}$$

$$\delta_{Q} = \frac{Q_{\inf low} - Q_{outflow}}{\left(Q_{\inf low} - Q_{outflow}\right)/2} \cdot 100\% = \frac{(0.2015 - 0.1993)}{(0.2015 + 0.1993)/2} \cdot 100\% = 1.097\% \tag{4.12}$$

Figure 37 depicts the temperature contours for simulations with Low Re Chien and standard k-ε turbulent models.

As can be seen, there is only a small difference between the results of Low Re Chien and the standard k-ε models.

The Low Re Chien turbulence model was designed to handle near-wall low-Reynolds-number flows. However, the used in these turbulent equations damping functions require the high grid resolutions to be near walls. In order to satisfy y^+ constraints, the high parameters of hyperbolic tangent mesh generation function were used, the start and end point spacing were equal to 0.001.

The mesh distribution was steep and the grid spacing was not uniform through the length of an edge. In order to verify this CFD model, computational simulations with more uniform grid distributions were performed, the start and end point spacing were equal to 0.01.

The divergence in results for average temperature inside the room between CFD models using the same k-ε turbulence model but different mesh distributions is

$$\delta T_3^{'} = \frac{\delta T}{\Delta T} = \frac{T_{ke1} - T_{ke}}{T_{walls} - T_{outside}} = \frac{291.7354 - 291.478}{299 - 279} = 1.287\% \tag{4.13}$$

The discrepancy in results for the value of the discharge coefficient can be defined as

$$e_{Cd3} = \frac{Cd_{ke1} - Cd_{ke}}{Cd_{ke}} \cdot 100\% = \frac{0.7486 - 0.7103}{0.7103} \cdot 100\% = 5.38\% \tag{4.14}$$

The conducted study shows that the results rather depend on grid points distributions than on the turbulent model used and, as result, the model with more uniform mesh distributions was used for further analysis.

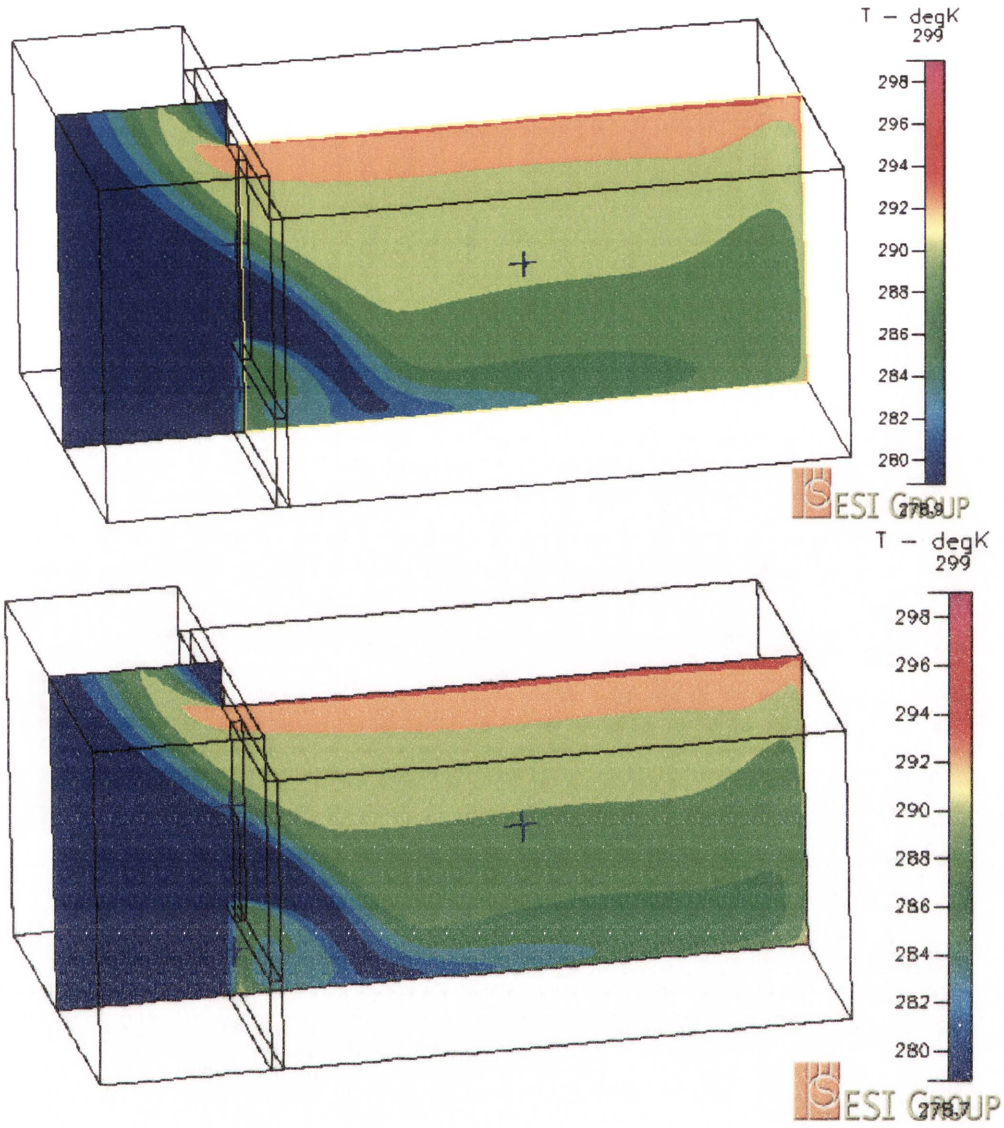

Figure 37 – The temperature contours for the computation using a) Low Re Chien, 2005, b) standard k-ε turbulence models

The influence of mesh resolution on the quality of the predicted results has been investigated as part of the coursework graduate project (Kivva, Graduate project, 2008).

The numerical results obtained from different model simulations were compared with one another and with the published work of Favaralo and Manz (2005) in terms of temperature driven flows parameters, such as average temperatures in the room, air flow rate through the lower and upper parts of the opening, and the numerical values of the discharge coefficient.

A grid resolution study is presented in Table 8 with a number of grid points being increased or decreased by approximately 20 %. A relatively small discrepancy in results has been noticed (Table 8, Formula 4.12 and Formula 4.13).

Table 8 -A grid resolution study

Name	Number grid cells	Temperature average inside the room	Air flow rate through the lower ½ of window	Air flow rate through the upper ½ of window	Discharge coefficient Cd
Low resolution	1 026 292	284.0424	0.2015	0.1993	0.7414
Medium resolution	1 238 676	284.0074	0.2017	0.1994	0.7443
High resolution	1 489 710	283.9841	0.2019	0.1996	0.7470

The divergence in results between models with different grid numbers for average temperature inside the room can be calculated as

$$\delta T_{gr} = \frac{\delta T}{\Delta T} = \frac{T_{mr} - T_{lr}}{T_{walls} - T_{outside}} = \frac{284.0074 - 284.0424}{299 - 279} = -0.175\% \text{ and} \qquad (4.15)$$

$$\delta T_{gr}' = \frac{\delta T}{\Delta T} = \frac{T_{mr} - T_{hr}}{T_{walls} - T_{outside}} = \frac{284.0074 - 283.9841}{299 - 279} = 0.116\% \qquad (4.16)$$

The grid resolution study shows that the results mildly depend on a number of grid points and the model grid resolution is adequate to provide a desirable level of accuracy.

Chapter 5

Results and Discussion

A number of simulations have been conducted in order to investigate the performance of a roof mounted ventilator. The evaluation method was based on the ability of the ventilation system to maintain good air mixing and provide comfortable indoor temperatures.

5.1 Effect of fan flow rate

To estimate the optimal amount of supplied air for sufficient ventilation, simulations have been conducted with different air flow rates and an analysis of temperature and velocity distributions has been performed. A full set of results can be found in Appendix 1.

The temperature contour results for five levels of ventilator air velocities with a wall temperature of T=305 K are presented in Figures 38-42.

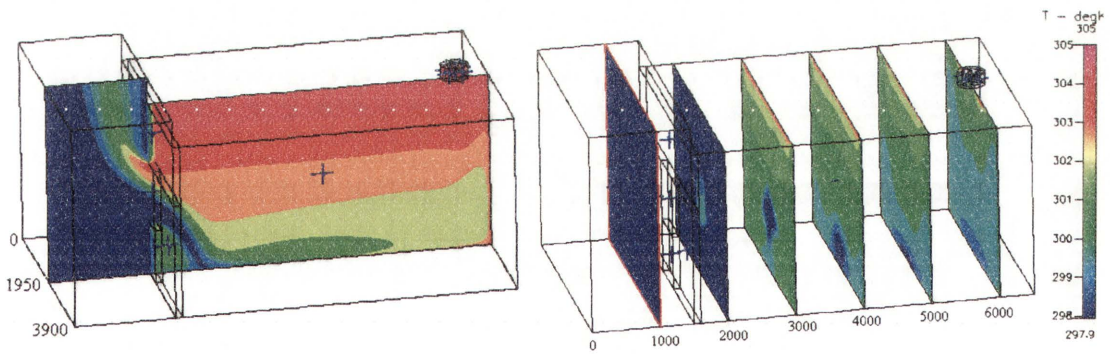

Figure 38 – Temperature contours with air flow through the fan 0.0001 m/s

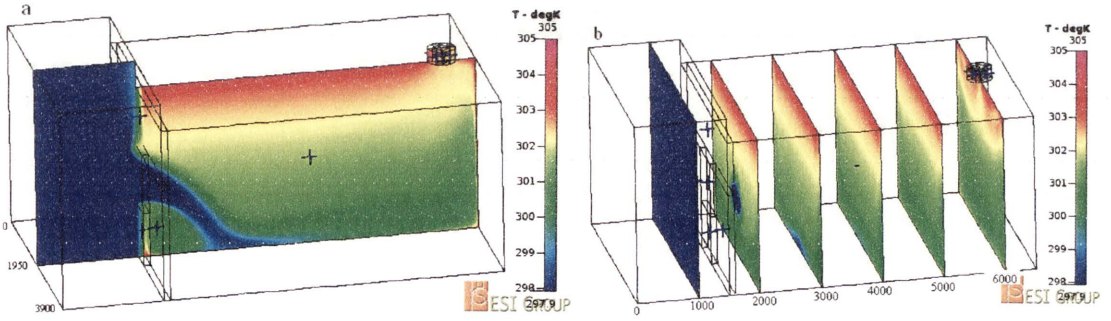

Figure 39 – Temperature contours with air flow through the fan 1 m/s

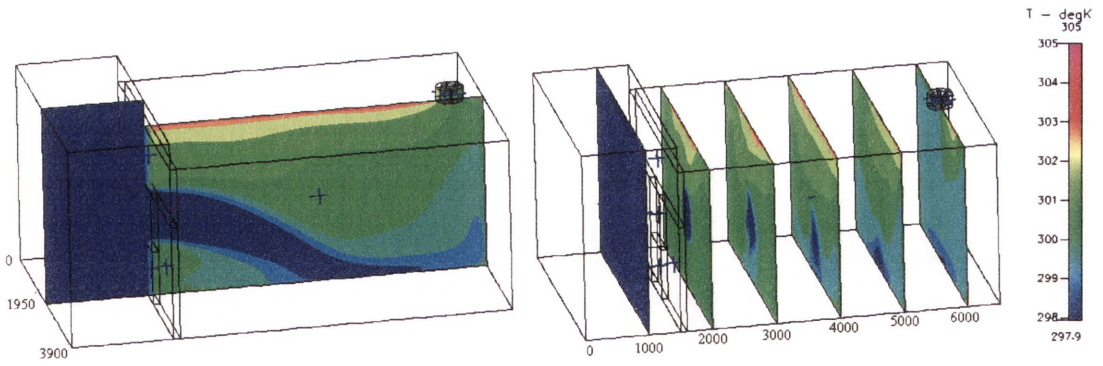

Figure 40 – Temperature contours with air flow through the fan 2 m/s

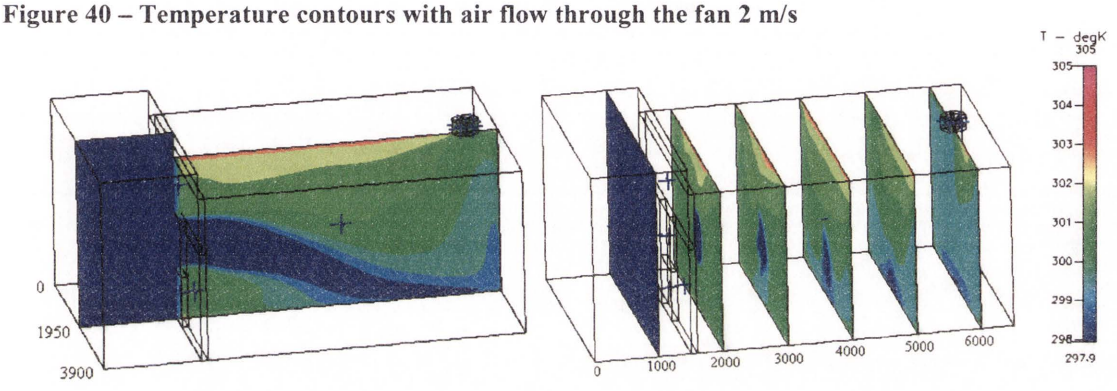

Figure 41 – Temperature contours with air flow through the fan 2.5 m/s

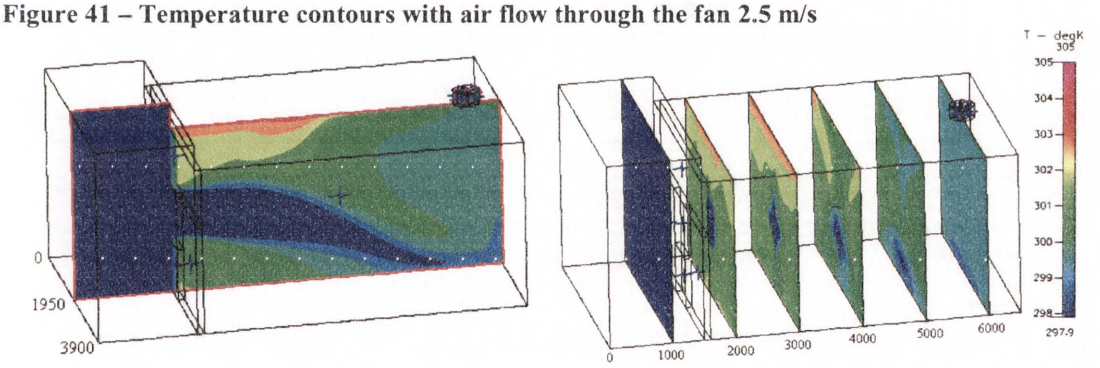

Figure 42 – Temperature contours with air flow through the fan 3.7 m/s

At a low airflow rate, the induced pressure differential is insufficient to break down thermal stratification in the room, as shown in Figure 38 . In this case, the main source of ventilation is the buoyancy driven flow. The cold air currents formed by natural convection are localised in the small area near the window, just above the floor, and the vertical structure of thermal stratified air layers remains throughout the rest of the room. When ventilation is employed, natural convection is enhanced by additional temperature differences between the ceiling and the floor. The amount of heat accumulated in the roof spaces creates hot air layers just

beneath the ceiling, while the floor maintains a relatively low constant temperature during the day (Yoshida et al. 1990/91). The steep temperature gradients would create an uncomfortable indoor environment for occupants.

A medium level of air flow rate results in a significant reduction in thermal stratification, as shown in Figure 39. The ventilator creates a low pressure region that draws air down through the opening into the lower levels of the room. The warm interior is removed from the room and air gradually mixes with the cool incoming air. The pressure differential encourages large air movements and drives a flow of air through the room.

A higher level of air fan flow rate not only overcomes the buoyancy effects of cool ambient air but also prevents the cool air currents descending into the lower parts of the room, as shown in Figure 40. The changes in the direction of the cool air injection lead to a change of air circulation patterns. Smaller scale motions of cool air result in poorer air mixing and localised areas of hot air near the ceiling and the floor.

Figure 41 and 42 show that further increasing the air flow rate leads to a shorter path of incoming cold air from the opening to the exhaust ventilator area. As a result, the imposed air circulations consist of a narrow current of cold ambient air surrounded by hotter air pockets. The hot air trapped in these pockets is then slowly removed by advection, conduction and radiation into the cooler areas (Hugo and Hens, 2008).

Forced and natural convection of air can induce very rapid heat removal compared with the rate imposed by advection, conduction and radiation. Dilution of temperature areas becomes even more difficult for the areas just below the ceiling and near the walls. Typically, the thick exterior mass of the walls absorbs heat from outside the building during the day and releases the heat by conduction and radiation in a room during the night (Binggeli, 2007). As a result, the amount of heat transferred into the convective cooler ambient currents may be replaced by the same amount of heat released from the interior walls. Consequently, the time needed to achieve comfortable environmental conditions may be increased significantly. The longer

the path of incoming cool air through the room spaces and areas near hot temperature regions, the more quickly indoor temperature decreases. thereby providing a more uniform temperature distribution.

5.2 Effect of fan location

Different ventilation strategies were investigated to determinate the best ventilation arrangements. Computations for four different locations of a fan were performed and simulations were conducted with the fan located: in the middle of the ceiling (43a), on the ceiling near the opening (43b), on the ceiling near the rear wall (43c) and at the top of the rear wall (43d).

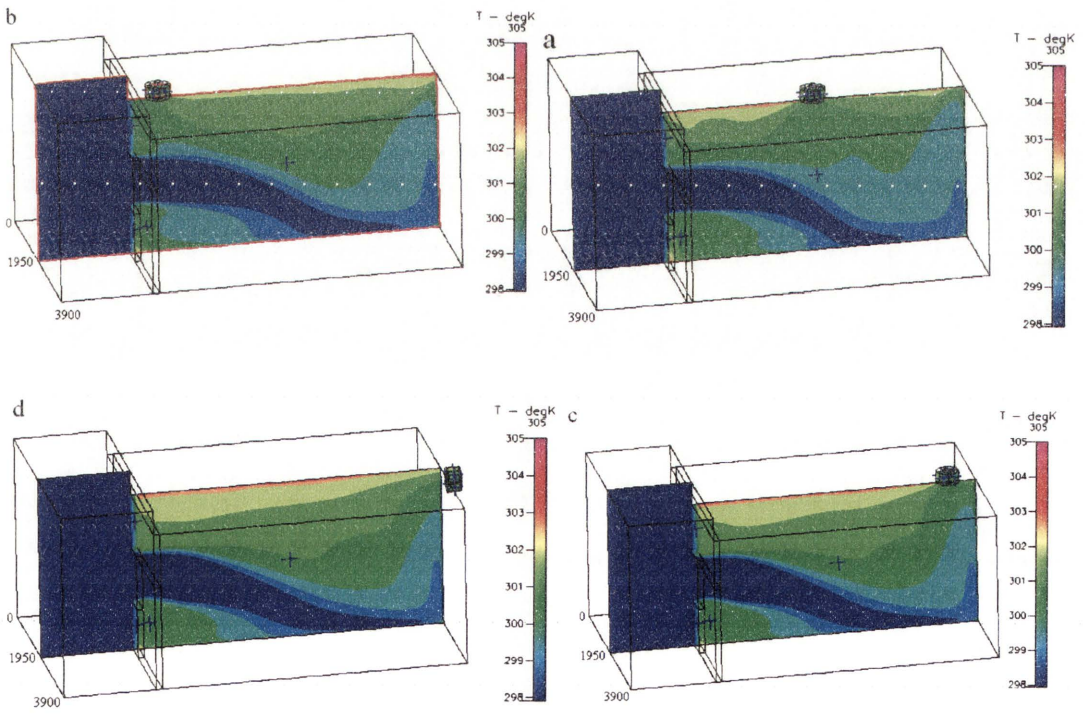

Figure 43 – Visualisation of temperature distributions for different locations of a fan

The cut planes of temperature contours on the central plane of the room with wall temperatures at 305 K and extracted air velocity of 2m/s for each of the fan location are shown in Figure 43, and it is clear that the position of a ventilator does not significantly affect the temperature distribution and ventilation efficiency in the occupied zone. There are slight differences in the temperature distributions in areas of the living space. In all models, there is a little mixing in the corner just above the floor near the opening and the area just beneath the ceiling. However, these areas are not usually part of the occupied zone. As is shown in Figure 44, the pressure differential drives a convective loop of cold air through the occupied zone in a very similar manner for all four cases of the ventilator position.

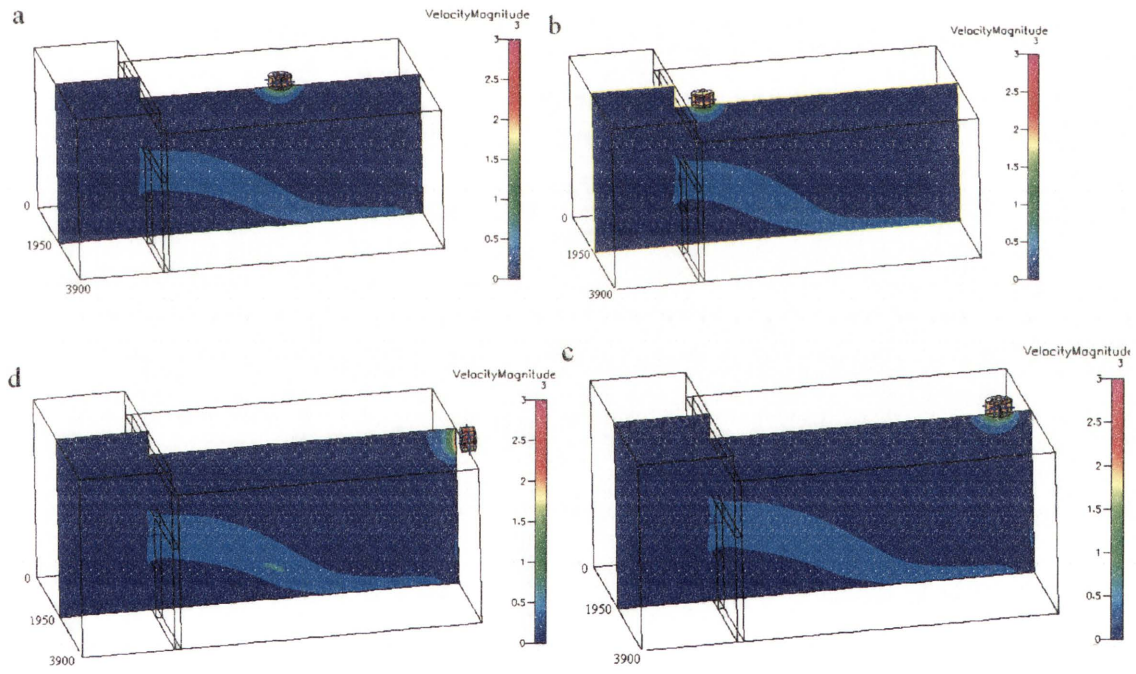

Figure 44 – Fan locations and resulting velocity distributions in a room

The best ventilation arrangement is achieved with the ventilator located near the opening (Figure 44b). In this case, the fan causes the greatest augmentation of the natural ventilation; the air flow path is at its longest with the incoming air passing through the lower levels of the room to the rear wall and then into the ceiling to the fan exhaust area, as shown in Figure 45.

The greater distance of this air flow path appears to result in the best possible opportunity for mixing the whole internal air volume.

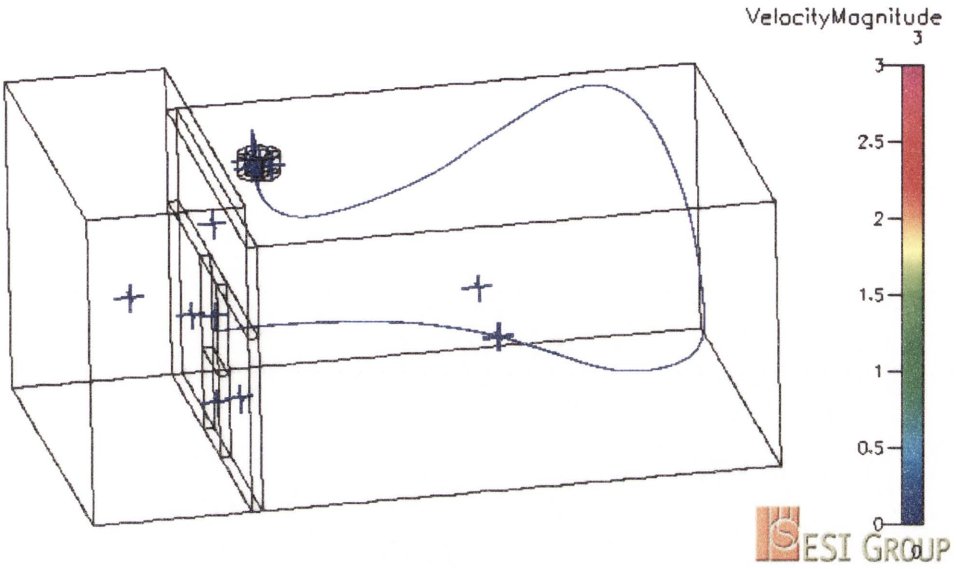

Figure 45 – The particle trace of incoming air

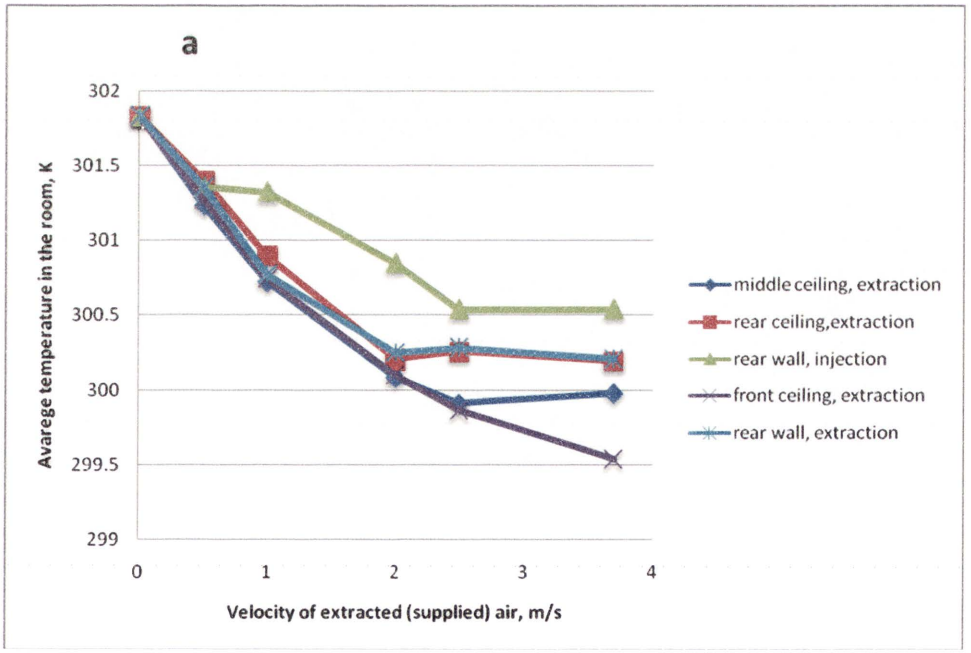

Figure 46 – The average temperature in a room with surface temperature of the walls 303 K

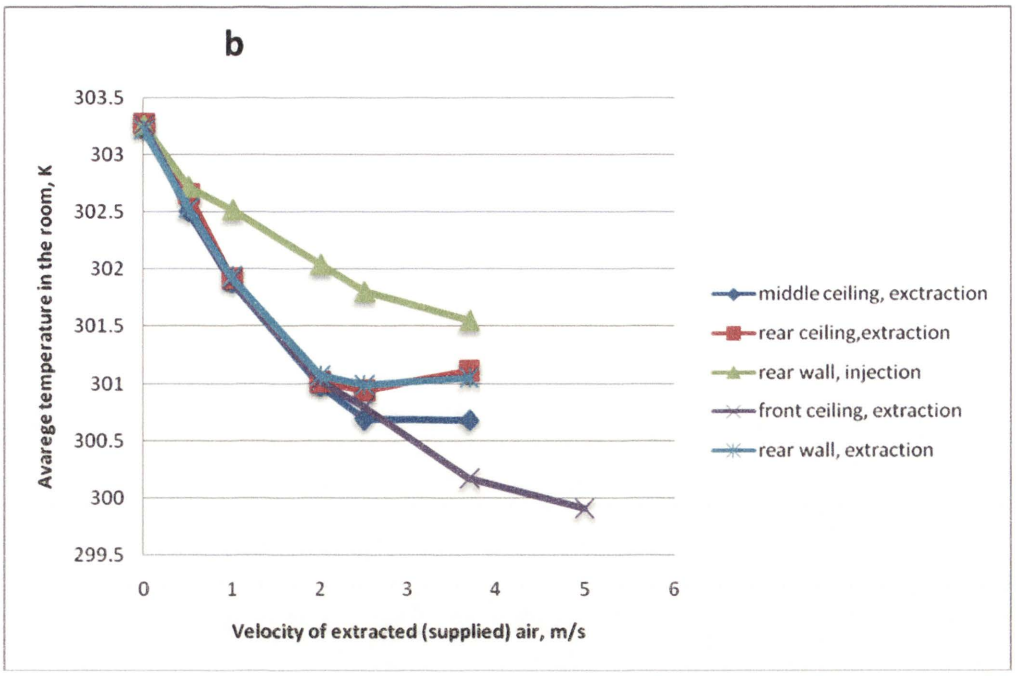

Figure 47 – The average temperature in a room with surface temperature of the walls 305 K

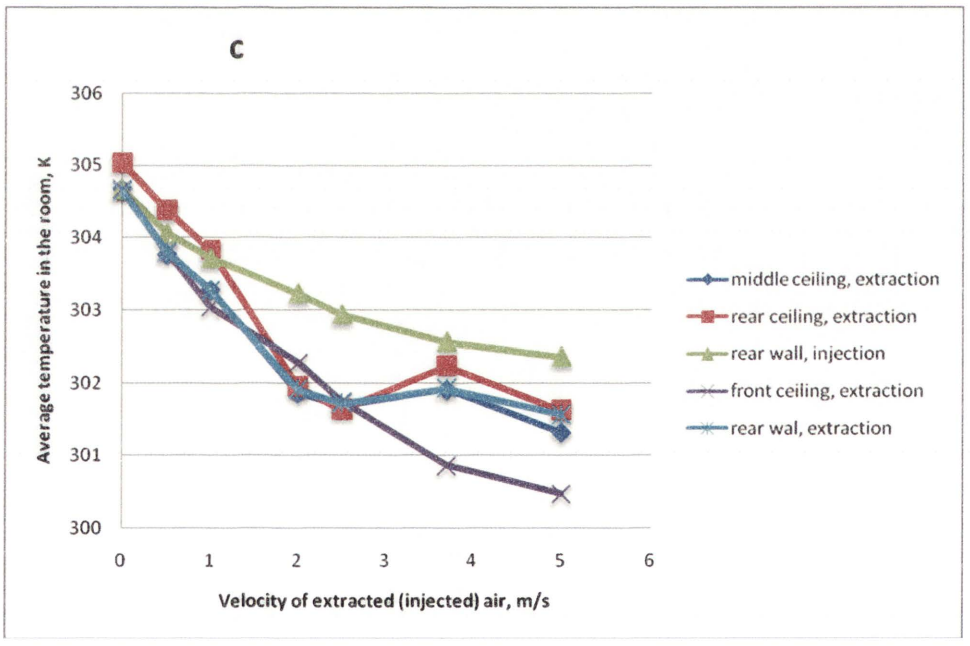

Figure 48 – The average temperature in a room with surface temperature of the walls 307

5.3 Effect of wall temperatures

A qualitative analysis of temperature distributions as well as a quantitative comparison of the average temperatures in a room for three different wall temperatures (Figures 46, 47 and 48) confirm these expectations and show that a fan positioned near the front wall is able to maintain optimum performance and maximise ventilation efficiency. Figures 46, 47 and 48 depict the dependence between the average temperature in the room and the extracted air velocities through the fan for four ventilator locations and three wall surface temperatures .

Figures 46-48 show that the average temperature increases after the supplied air velocity reaches 2.5m/s for the ventilation system with a fan located in the middle of the ceiling and near the rear wall as a direct effect of the high momentum of incoming airflows, the shorter path of cold air currents and, as a result, poor air mixing. The high velocity of extracted air at 5 m/s (Figure 48) reduces the average temperature in a room but increases the risk of high air speed and temperature gradients in an occupied zone. Thermal comfort conditions are deteriorated as a result of the remarkable reduction of temperature uniformity and poor air mixing.

Figure 49 illustrates that the surface temperature of walls is not a major parameter which influences ventilation efficiency. Figure 49 depicts the temperature contours for three different wall temperatures 303 K (Figure 49a), 305 K (Figure 49b) and 307 K (Figure 49c) with a constant outside temperature of 298 K.

Figure 49 shows that there is a slight difference in temperature distributions for the achieved steady state solutions. Although the average temperature in a room is increased with a rise in wall temperatures from 299.9 K (Figure 49a), 300.69 K (Figure 49b) to 301.68 K (Figure 49c), the temperature contours remain relatively constant. The forced convective loop transfers the same amount of cool ambient air and forms similar air flow patterns. The effect of ventilation is greatest at the higher wall temperatures due to higher temperature differences and as result of enhanced natural ventilation.

5.4 Effect of air transportation method

In an attempt to improve ventilation arrangements, an investigation of different air transportation methods was performed. Instead of extracting the hot air from the indoor environment, the ventilator was used to inject the fresh air into the room from the outside space. One drawback of the injection of fresh air into a room is that people are sensitive to the higher air velocity (Larsen et al, 2007).

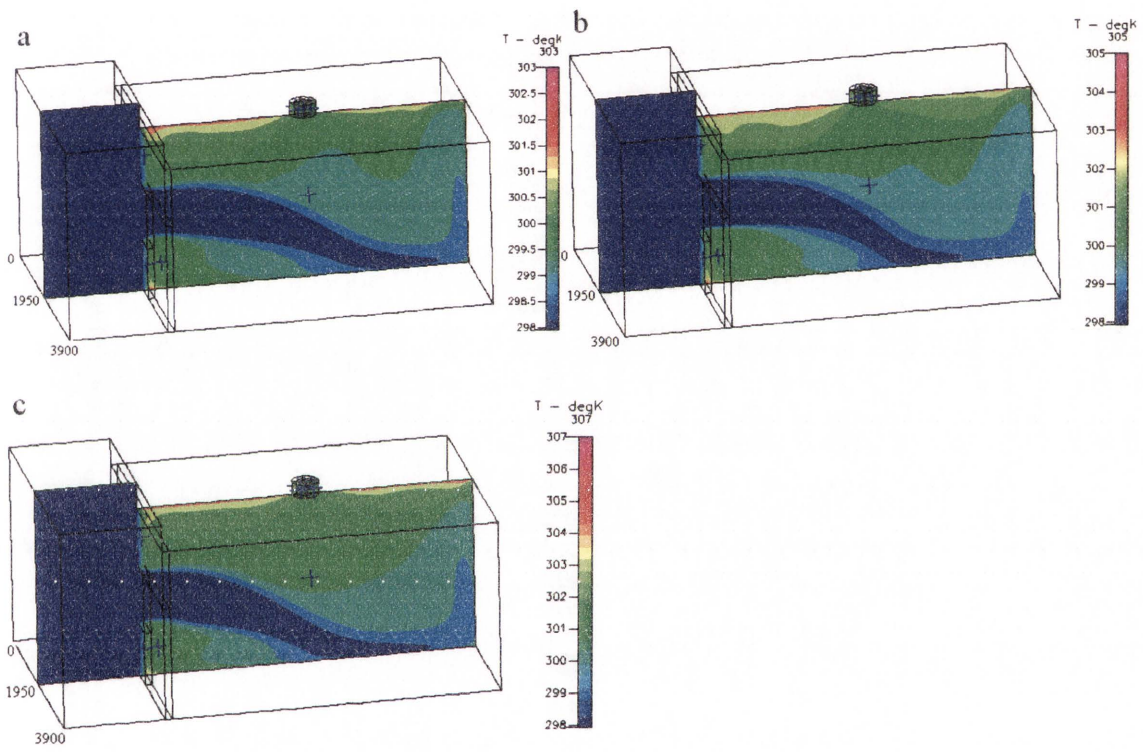

Figure 49 – Visualisation of temperature contours for different temperature of the walls

As a result of this thermal comfort requirements restraint, the position of a ventilator on the ceiling is not suitable for the evaluation of these ventilation arrangements due to the implicit reduction in local thermal comfort. Shading devices such as louvers can separate flow and reduce air speed by changing the direction and magnitude of incoming airflows, but they

reduce current air momentum due to friction losses and may lead to a higher level of energy consumption.

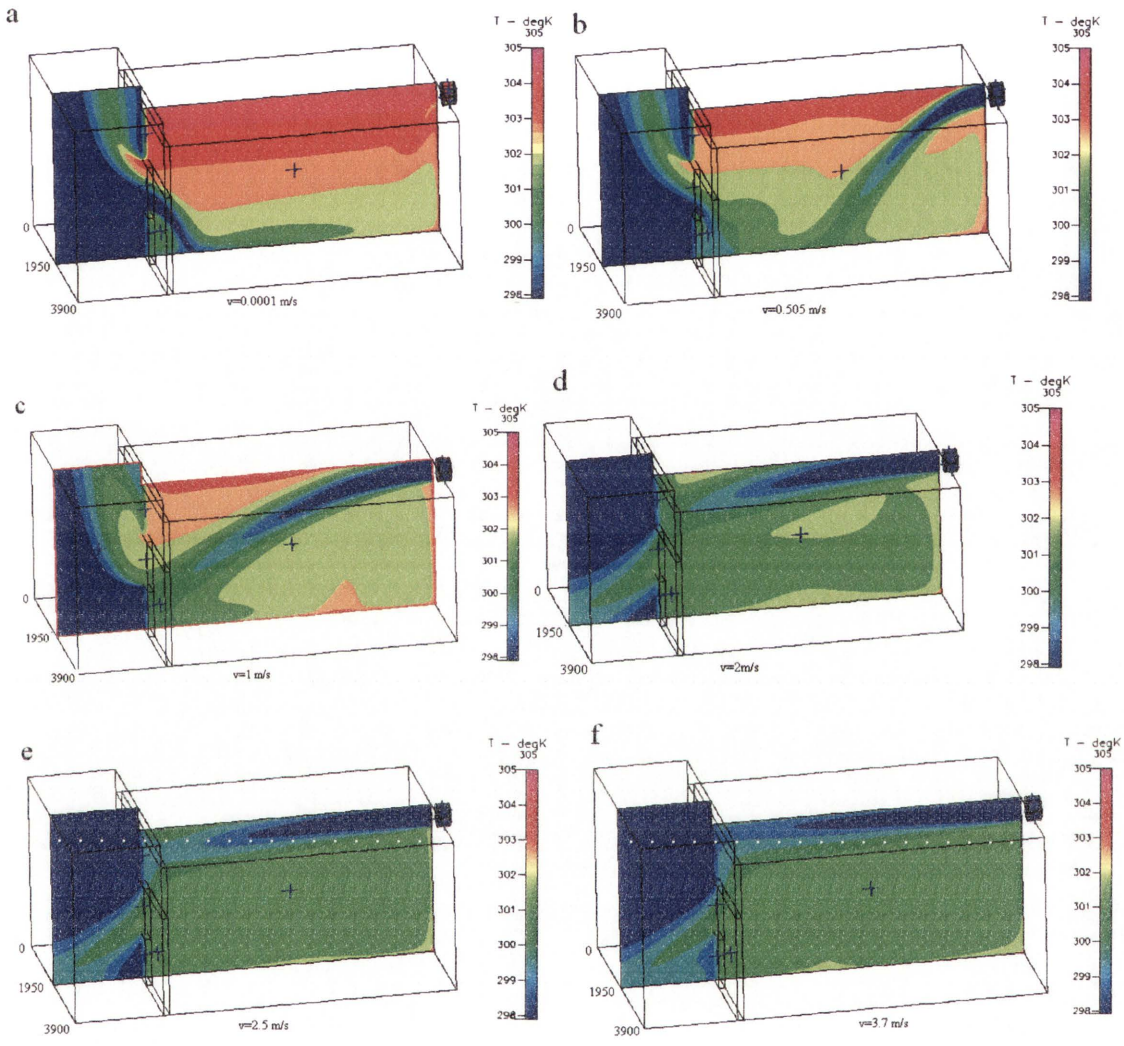

Figure 50 – Visualisation of temperature contours for different velocities of supplied air a) 0.0001 m/s, b) 0.505 m/s, c) 1 m/s, d) 2 m/s, e)2.5 m/s f)3.7 m/s

CFD simulations were therefore conducted with the ventilator adjusted on the rear wall only. As can be seen in Figure 50a, the low level of air flow rate is not able to break down the thermal stratification between the upper layer just beneath the ceiling and the lower layer just above the floor. The temperature differs in the various parts of the room and the formed temperature gradients cannot satisfy thermal comfort requirements (Gorton & Sassi 1982).

Figures 50b and 50c show that, at medium supplied air velocities, the incoming stream falls down into the occupied zone and may also result in a reduction of comfort needs.

The higher momentum of fluid is able to drive cold airflows through the area of the ceiling in the direction to the front wall (Figure 50d). The cold ambient air decreases the temperature in the region of the ceiling and the horizontal layer of the cool ambient air just beneath the ceiling breaks down thermal stratification by inducing the gravity currents of buoyancy plumes.

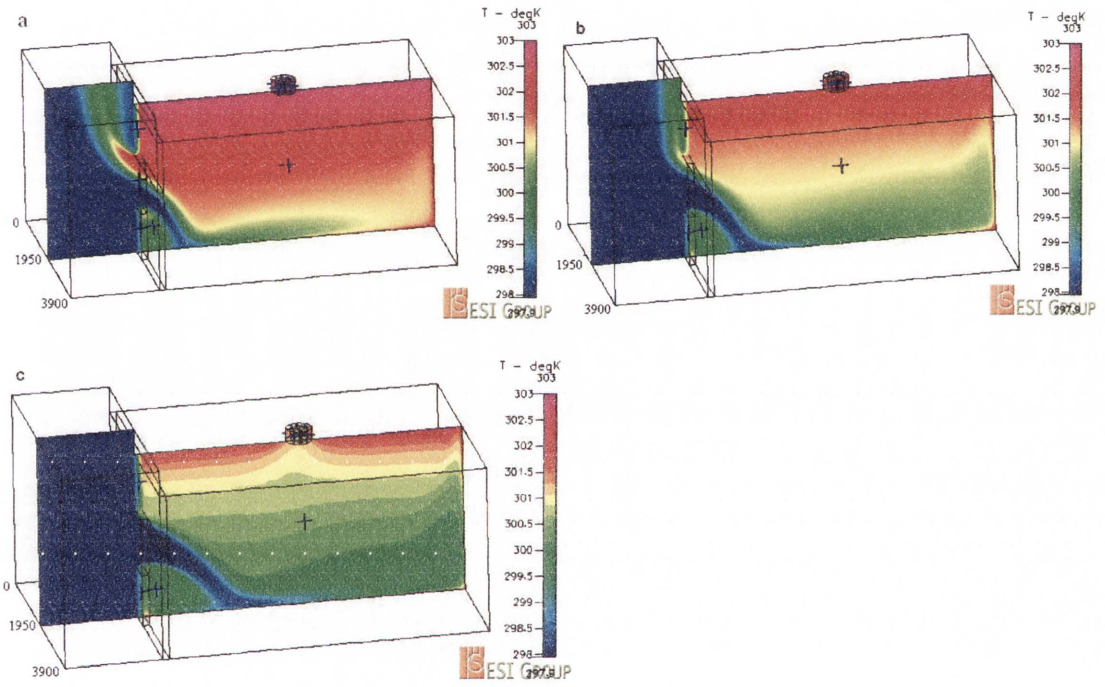

Figure 51 – Temperature contours for different velocities of extracted air a) 0.0001 m/s, b) 0.505 m/s, c) 1 m/s,

It was also observed that the air transportation method affects natural convection heat transfer through the opening. As can be seen in Figure 51, the amount of hot air through the upper part of the opening decreases with the increasing air flow rate through the fan when operated in the extraction regime. At the low fan speed (0.0001 m/s), the system of air circulation through the opening can be described in terms of natural convection. Once the air

flow rate reaches 1m/s, forced convection becomes dominant and the flow pattern through the opening is characterised by the forced convection currents of cold ambient air.

By comparison, the fan operating in the injection regime with an air flow rate of 1 m/s induces the extraction of hot air from the indoor environment into the atmosphere (Figure 51b). Figures 50d, 50e and 50f show that high values of air flow rate result in declining hot buoyancy driven downward flows.

Figures 50e and 50f also show that the high level of injected ambient air is able to provide uniform temperature and velocity distributions in the room. Compared to the 'extraction' regime of the fan, whereby comfortable indoor environment conditions are difficult to predict in advance and are not easily controlled by the amount of supplied air, the ventilation arrangements of the 'injection' regime can achieve the required comfort needs without the limitations of the high velocity supply. In other words, the higher required air flow rate may lead to a significant reduction in ventilation efficiency of the extraction regime, in contrast to the injection regime in which higher air flow rate result in a decrease in the average room temperature due to the increased magnitude of buoyancy driven forces and a large amount of cold supplied air.

Chapter 6

Conclusion and recommendations

The computational tests were designed to study the key parameters governing heat transfer and air mixing under forced convection in a mechanically ventilated room. Four fan locations and two methods of inducing air movement—injection of cold ambient air and extraction of hot indoor air—were examined to ensure that the fan met the performance criteria to provide the desired comfort needs. In order to investigate different ventilation cases, computational simulations were conducted for a range of air speeds of 0.0001-5 m/s through the fan and with three wall temperatures: 303 K, 305 K and 307 K. The influence of the changing parameters on temperature and velocity distributions were examined and different ventilation strategies were evaluated.

The following conclusions have been drawn from computational simulations. The temperature of the walls did not significantly affected ventilation efficiency. The air transportation method, the location of a fan and the value of supplied velocities were recognised as the main parameters which influenced the thermal comfort conditions. It was found that a ventilator operating in an extraction regime with adjusted low and high levels of air flow rate was not able to provide adequate ventilation. Low extracted velocities through the ventilator were not sufficient to break down thermal stratification and the high velocities of airflows formed stagnant zones of high temperatures and short-circuiting of the supply of air to the extract points. Despite the large amount of supplied air, poor air mixing produced different temperature zones within the room and high temperature gradients, which in turn may result in a sharp drop in ventilation efficiency and cause thermal discomfort for occupants.

It was also found that the level of air mixing and temperature uniformity directly related to the incoming ambient air path formed by the pressure differential. The flow pattern generated by

the fan located near the opening was found to be more productive in mixing the whole volume due to having the longest possible air path through the room space.

In comparison with extraction, the injection method performed well at high velocities but had similar operating limitations at low velocities. The fan operating in the injection regime required higher air flow rates to achieve the same level of average temperature in a room. In terms of thermal comfort requirements such as temperature and velocity distribution uniformity, the injection method gives a better performance due to the fact that cold ambient currents are driven into the area of the ceiling and do not affect occupied zones. This can be seen as another big advantage of the injection method, because the presence of solid obstacles such as furniture in the fluid path may reduce convection momentum and restrict heat transfer when cold air is transported through the room spaces. Further work needs to be carried out to examine these effects and the level of air separation and recirculation in the obstacle areas.

Further evaluation of the injection method may include an investigation of 'pulsating' effects. Cold air can be supplied at high velocity for a short time, and it is highly possible that the ventilation level may be maintained by the buoyancy effects between the operational fan time. This suggestion is based on the observation by Heiselberg et al (2003) who state that short-time airing for a single-side opening room offers strategically more effective ventilation and claim that the required air quality and thermal comfort can be provided during the first ten minutes of airing.

Further research needs to be undertaken to elucidate the influence of transient weather dynamics on the ventilation efficiency of a roof-mounted fan, such as the level of solar radiation, and the direction and speed of the wind. The impact of the dimensions and the numbers of ventilators used on cooling performance should be also investigated.

Conducting experimental tests to provide a detailed validation of this CFD model is also recommended, as is the investigation of different numerical schemes and turbulence models.

Appendix

Nomenclature of Figures

Name	Location of the fan	Temperature of walls, K	Method	Fan flow rate, m/s
1_0.0001_303	Middle ceiling	303	extraction	0.0001
1_0.505_303	Middle ceiling	303	extraction	0.505
1_1_303	Middle ceiling	303	extraction	1
1_2_303	Middle ceiling	303	extraction	2
1_25_303	Middle ceiling	303	extraction	2.5
1_37_303	Middle ceiling	303	extraction	3.7
1_0.0001_305	Middle ceiling	305	extraction	0.0001
1_0.505_305	Middle ceiling	305	extraction	0.505
1_1_305	Middle ceiling	305	extraction	1
1_2_305	Middle ceiling	305	extraction	2
1_25_305	Middle ceiling	305	extraction	2.5
1_37_305	Middle ceiling	305	extraction	3.7
1_0.0001_307	Middle ceiling	307	extraction	0.0001
1_0.505_307	Middle ceiling	307	extraction	0.505
1_1_307	Middle ceiling	307	extraction	1
1_2_307	Middle ceiling	307	extraction	2
1_25_307	Middle ceiling	307	extraction	2.5
1_37_307	Middle ceiling	307	extraction	3.7
2_0.0001_303	Front ceiling	303	extraction	0.0001
2_0.505_303	Front ceiling	303	extraction	0.505
2_1_303	Front ceiling	303	extraction	1
2_2_303	Front ceiling	303	extraction	2
2_25_303	Front ceiling	303	extraction	2.5

Name	Location of the fan	Temperature of walls, K	Method	Fan flow rate, m/s
2_37_303	Front ceiling	303	extraction	3.7
2_0.0001_305	Front ceiling	305	extraction	0.0001
2_0.505_305	Front ceiling	305	extraction	0.505
2_1_305	Front ceiling	305	extraction	1
2_2_305	Front ceiling	305	extraction	2
2_25_305	Front ceiling	305	extraction	2.5
2_37_305	Front ceiling	305	extraction	3.7
2_5_305	Front ceiling	305	extraction	5
2_0.0001_307	Front ceiling	307	extraction	0.0001
2_0.505_307	Front ceiling	307	extraction	0.505
2_1_307	Front ceiling	307	extraction	1
2_2_307	Front ceiling	307	extraction	2
2_25_307	Front ceiling	307	extraction	2.5
2_37_307	Front ceiling	307	extraction	3.7
2_5_307	Front ceiling	307	extraction	5
3_0.0001_303	Rear ceiling	303	extraction	0.0001
3_0.505_303	Rear ceiling	303	extraction	0.505
3_1_303	Rear ceiling	303	extraction	1
3_2_303	Rear ceiling	303	extraction	2
3_25_303	Rear ceiling	303	extraction	2.5
3_37_303	Rear ceiling	303	extraction	3.7
3_0.0001_305	Rear ceiling	305	extraction	0.0001
3_0.505_305	Rear ceiling	305	extraction	0.505
3_1_305	Rear ceiling	305	extraction	1
3_2_305	Rear ceiling	305	extraction	2
3_25_305	Rear ceiling	305	extraction	2.5

Name	Location of the fan	Temperature of walls, K	Method	Fan flow rate, m/s
3_37_305	Rear ceiling	305	extraction	3.7
3_0.0001_307	Rear ceiling	307	extraction	0.0001
3_0.505_307	Rear ceiling	307	extraction	0.505
3_1_307	Rear ceiling	307	extraction	1
3_2_307	Rear ceiling	307	extraction	2
3_25_307	Rear ceiling	307	extraction	2.5
3_37_307	Rear ceiling	307	extraction	3.7
3_5_307	Rear ceiling	307	extraction	5
4extraction_0.0001_303	Rear wall	303	extraction	0.0001
4extraction _0.505_303	Rear wall	303	extraction	0.505
4extraction _1_303	Rear wall	303	extraction	1
4extraction _2_303	Rear wall	303	extraction	2
4extraction _25_303	Rear wall	303	extraction	2.5
4extraction _37_303	Rear wall	303	extraction	3.7
4extraction _0.0001_305	Rear wall	305	extraction	0.0001
4extraction _0.505_305	Rear wall	305	extraction	0.505
4extraction _1_305	Rear wall	305	extraction	1
4extraction _2_305	Rear wall	305	extraction	2
4extraction _25_305	Rear wall	305	extraction	2.5
4extraction 37_305	Rear wall	305	extraction	3.7
4extraction _0.0001_307	Rear wall	307	extraction	0.0001
4extraction _0.505_307	Rear wall	307	extraction	0.505
4extraction _1_307	Rear wall	307	extraction	1
4extraction _2_307	Rear wall	307	extraction	2
4extraction _25_307	Rear wall	307	extraction	2.5
4extraction _37_307	Rear wall	307	extraction	3.7
4extraction _5_307	Rear wall	307	extraction	5

Name	Location of the fan	Temperature of walls, K	Method	Fan flow rate, m/s
4injection_0.0001_303	Rear wall	303	injection	0.0001
4 injection _0.505_303	Rear wall	303	injection	0.505
4 injection _1_303	Rear wall	303	injection	1
4 injection _2_303	Rear wall	303	injection	2
4 injection _25_303	Rear wall	303	injection	2.5
4 injection _37_303	Rear wall	303	injection	3.7
4 injection _0.0001_305	Rear wall	305	injection	0.0001
4 injection _0.505_305	Rear wall	305	injection	0.505
4 injection _1_305	Rear wall	305	injection	1
4 injection _2_305	Rear wall	305	injection	2
4 injection _25_305	Rear wall	305	injection	2.5
4 injection 37_305	Rear wall	305	injection	3.7
4 injection _0.0001_307	Rear wall	307	injection	0.0001
4 injection _0.505_307	Rear wall	307	injection	0.505
4 injection _1_307	Rear wall	307	injection	1
4 injection _2_307	Rear wall	307	injection	2
4 injection _25_307	Rear wall	307	injection	2.5
4 injection _37_307	Rear wall	307	injection	3.7
4 injection _5_307	Rear wall	307	injection	5

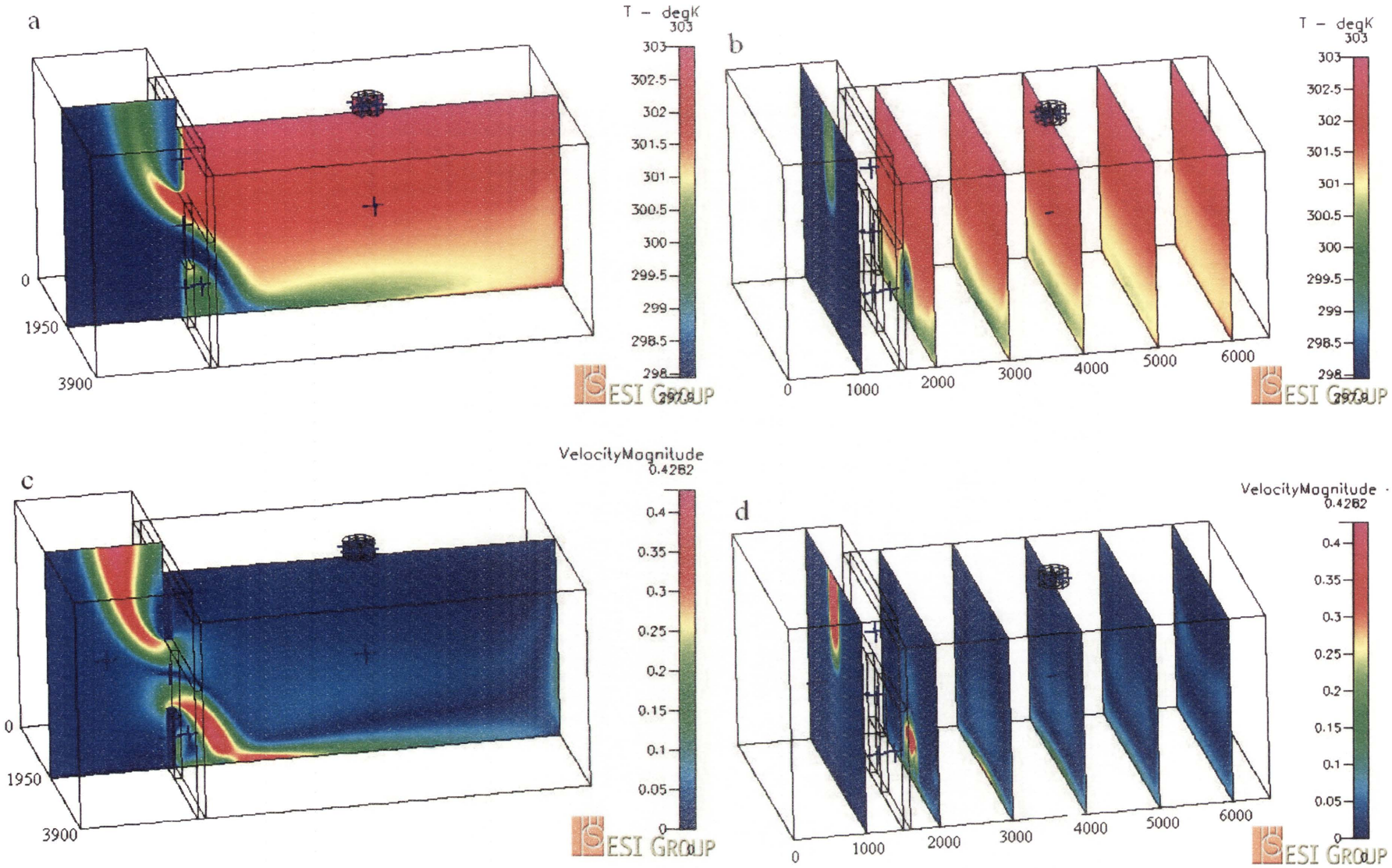

Figure 52 – 1_0.0001_303 Temperature and velocity distributions with airflows through fan of 0.0001 m/s

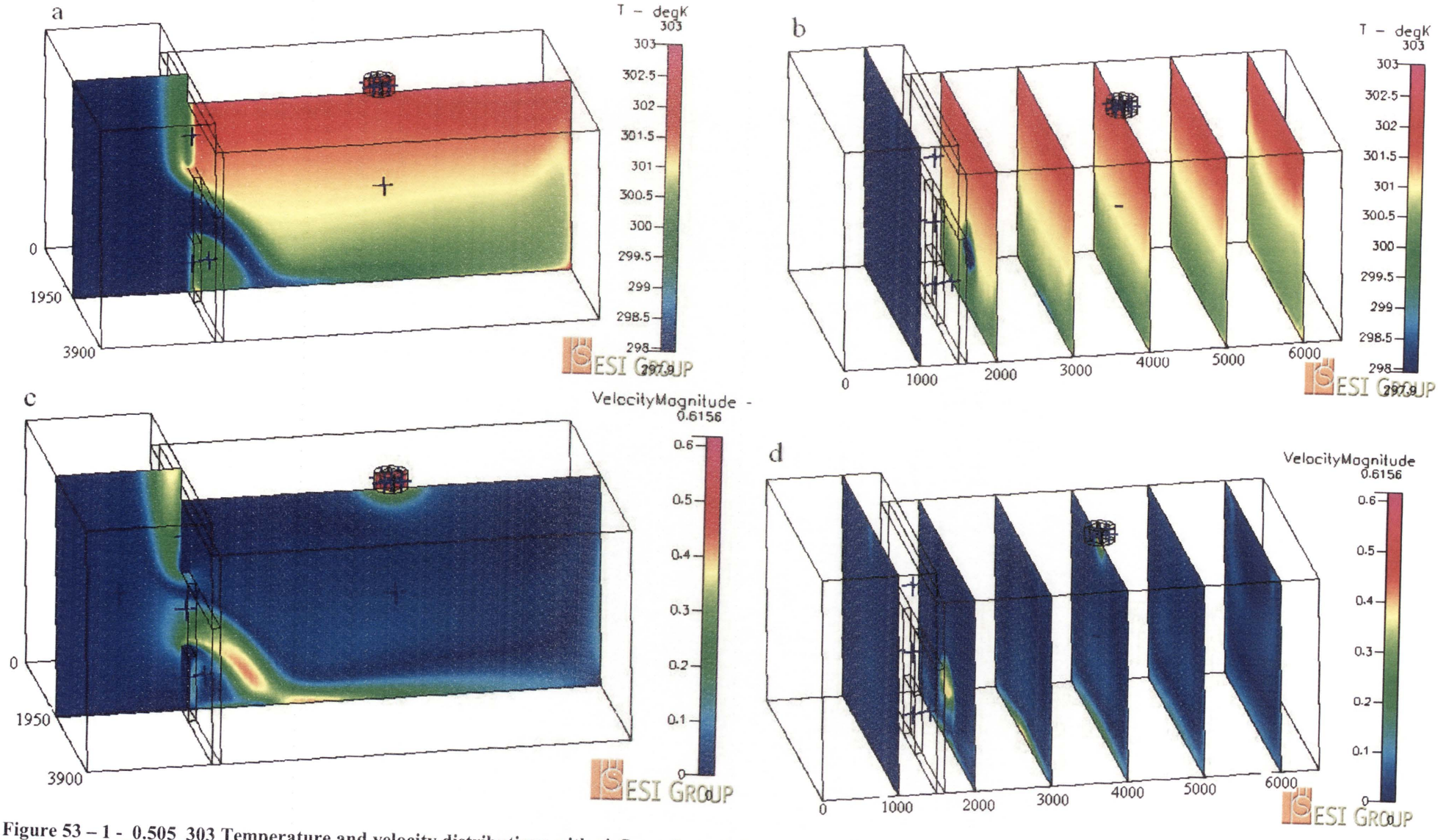

Figure 53 – 1 - _0.505_303 Temperature and velocity distributions with airflows through fan of 0.505 m/s

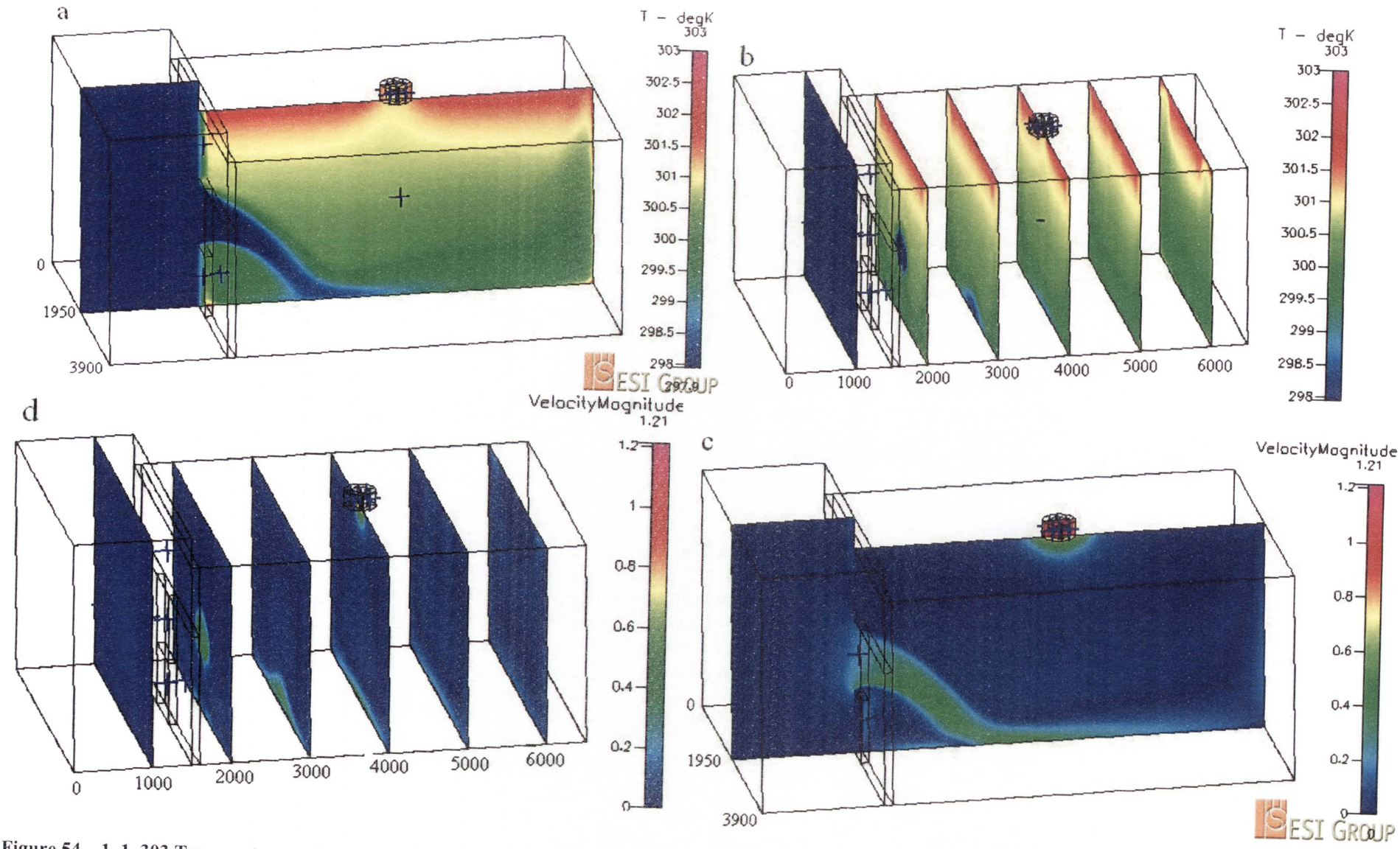

Figure 54 – 1_1_303 Temperature and velocity distributions with airflows through fan of 1 m/s

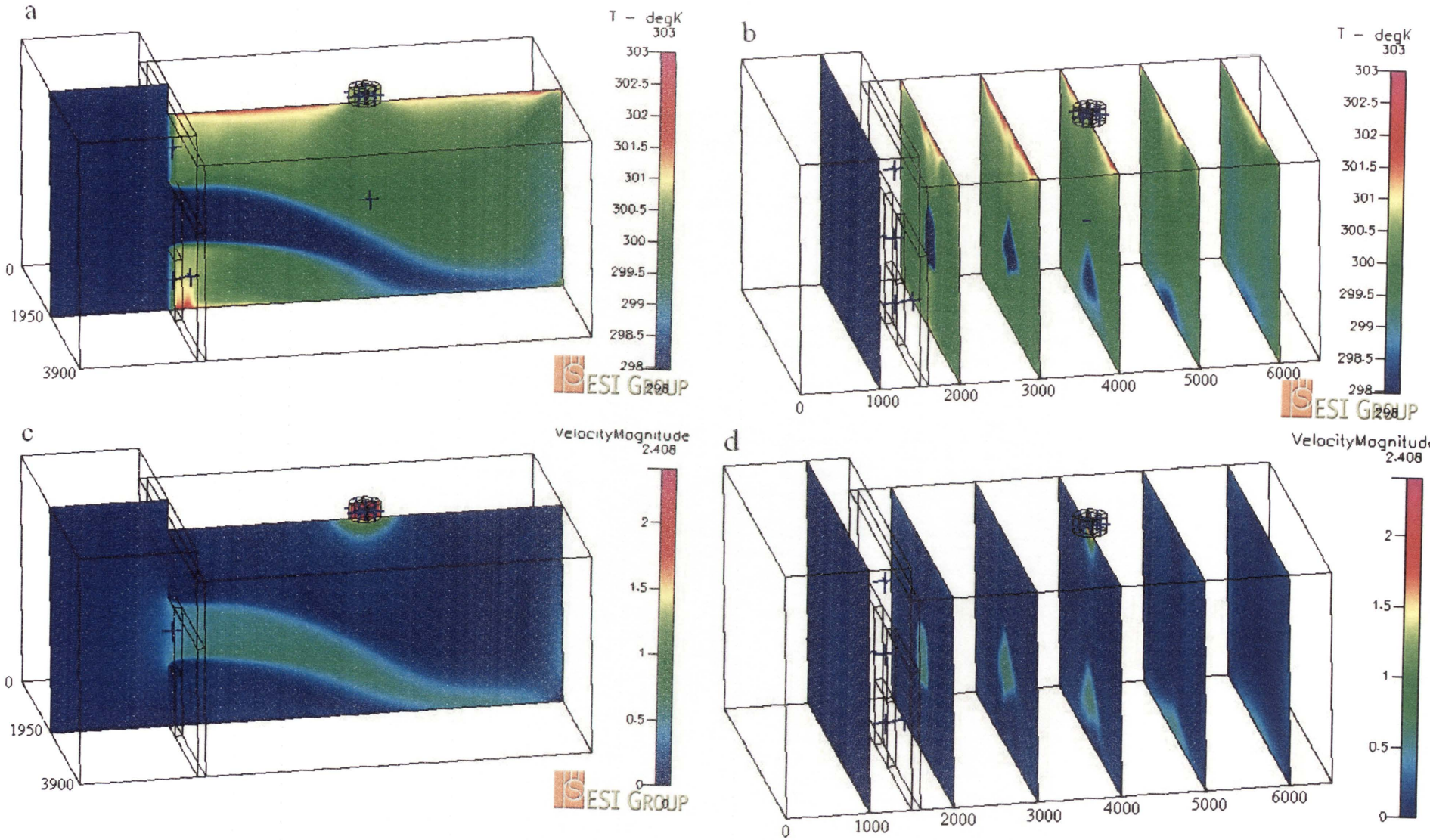

Figure 55 – 1.2_303 Temperature and velocity distributions with airflows through fan of 2 m/s

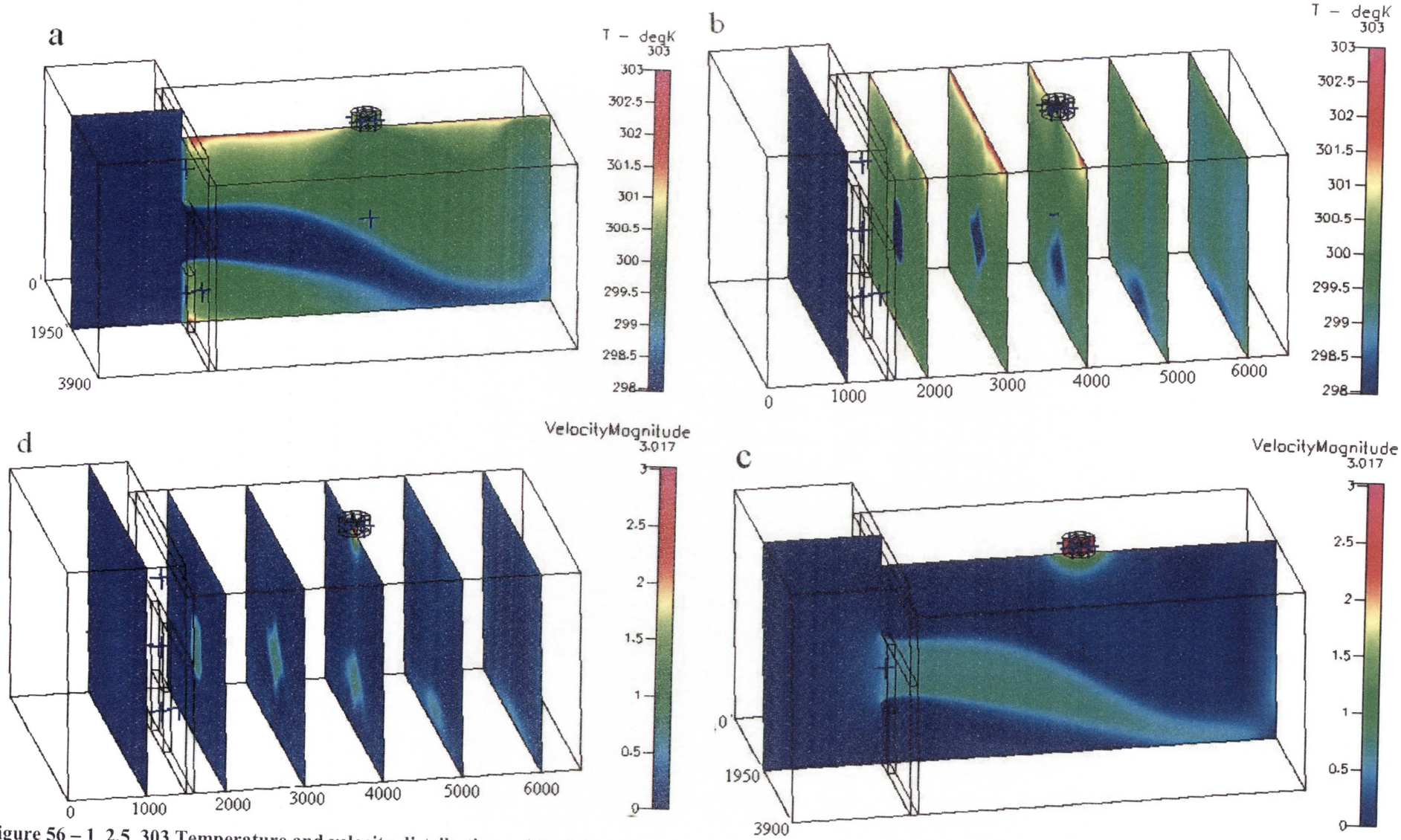

Figure 56 – 1_2.5_303 Temperature and velocity distributions with airflows through fan of 2.5 m/s

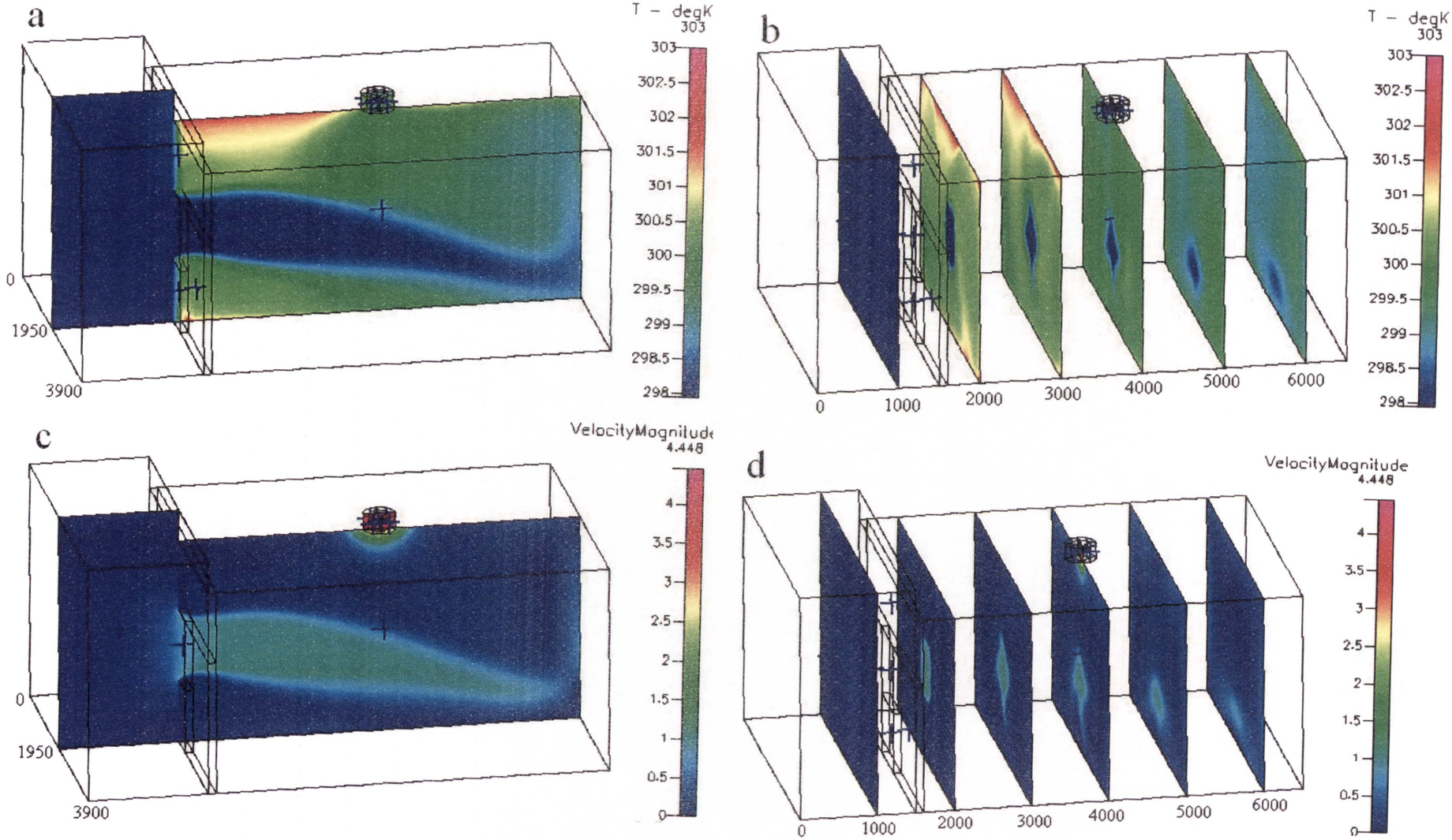

Figure 57 – 1_3.7_303 Temperature and velocity distributions with airflows through fan of 3.7 m/s

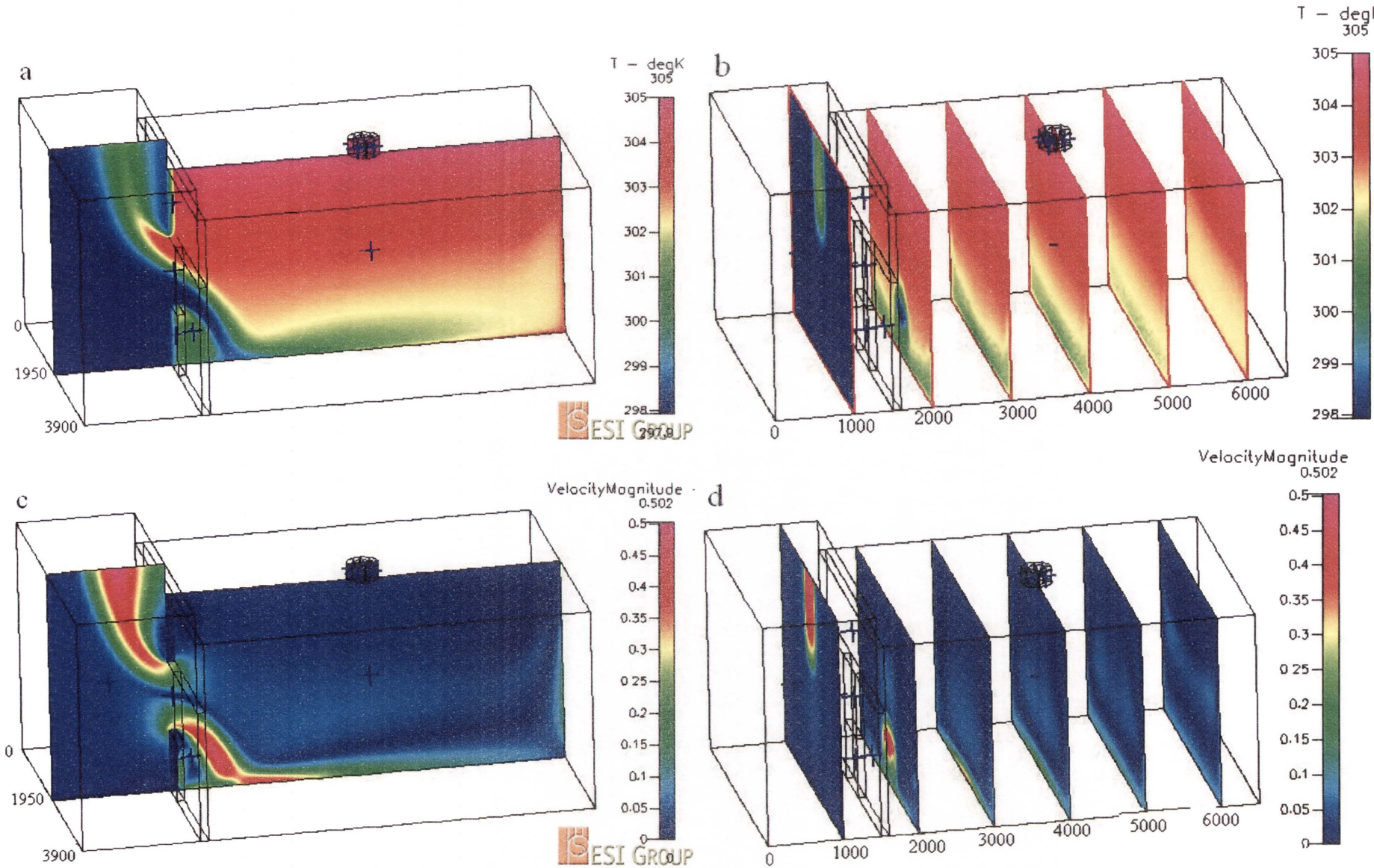

Figure 58 – 1_0.0001_305 Temperature and velocity distributions with airflows through fan of 0.0001 m/s

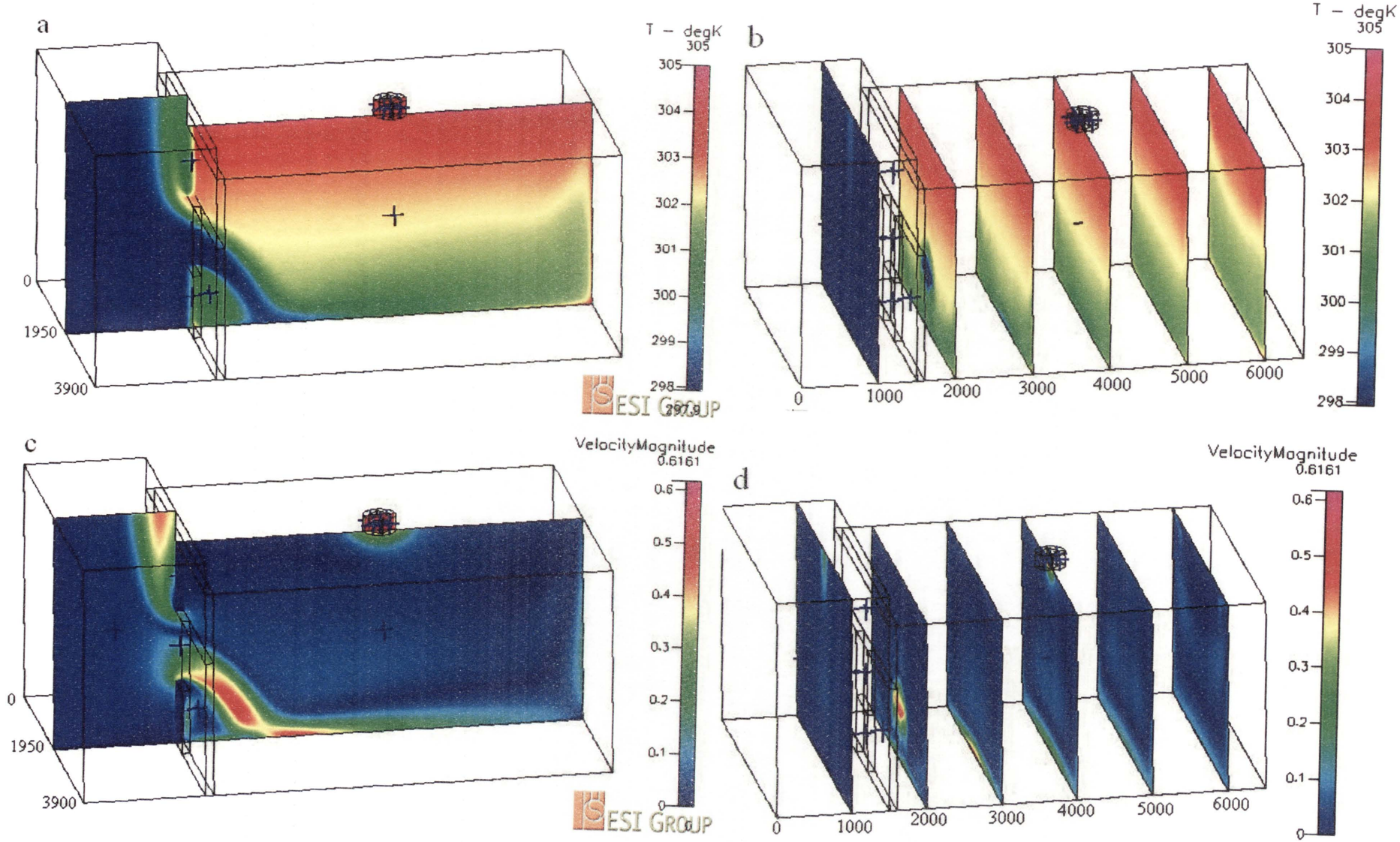

Figure 59 – 1_0.505_305 Temperature and velocity distributions with airflows through fan of 0.505 m/s

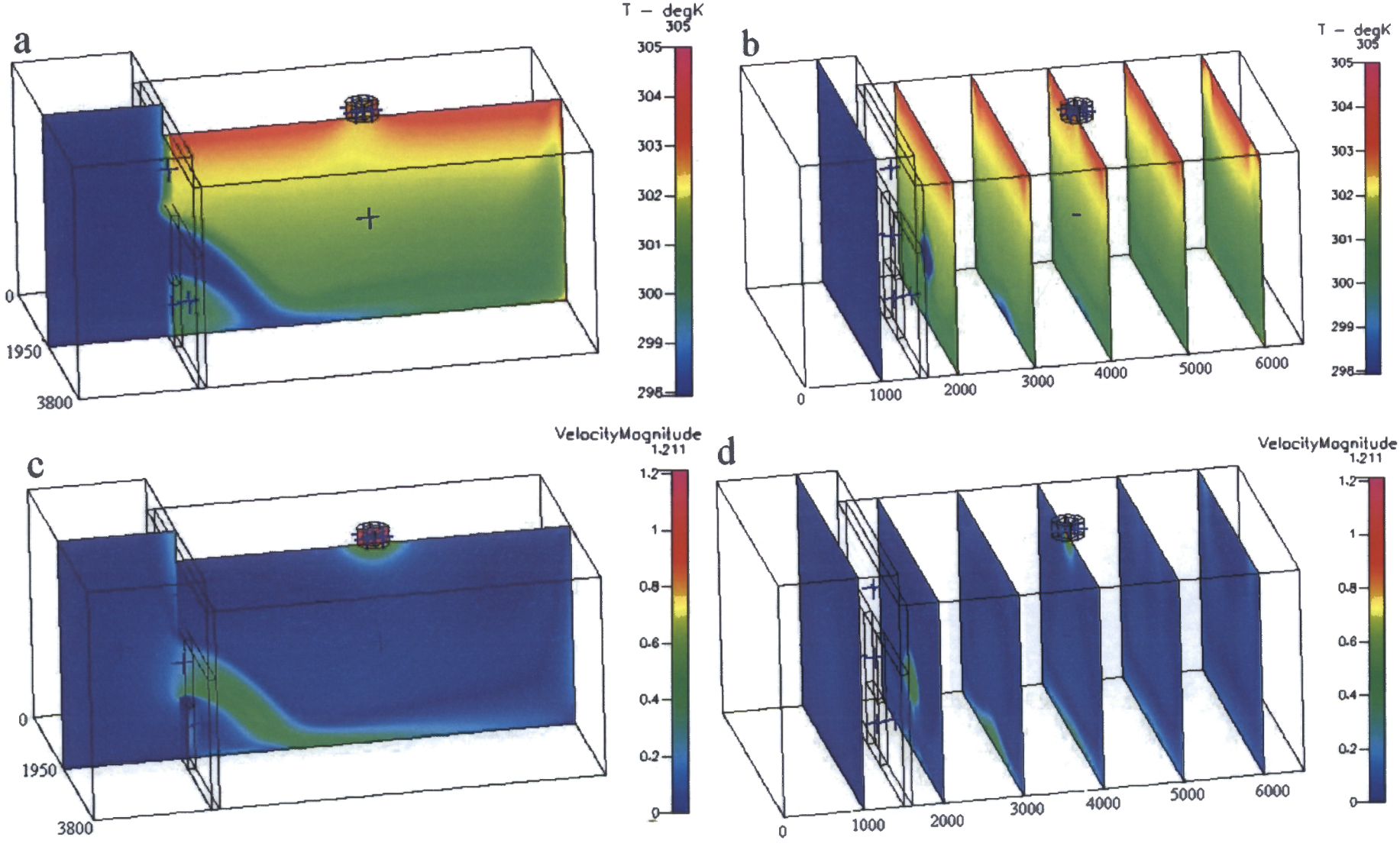

Figure 60 – 1_1_305 Temperature and velocity distributions with airflows through fan of 1 m/s

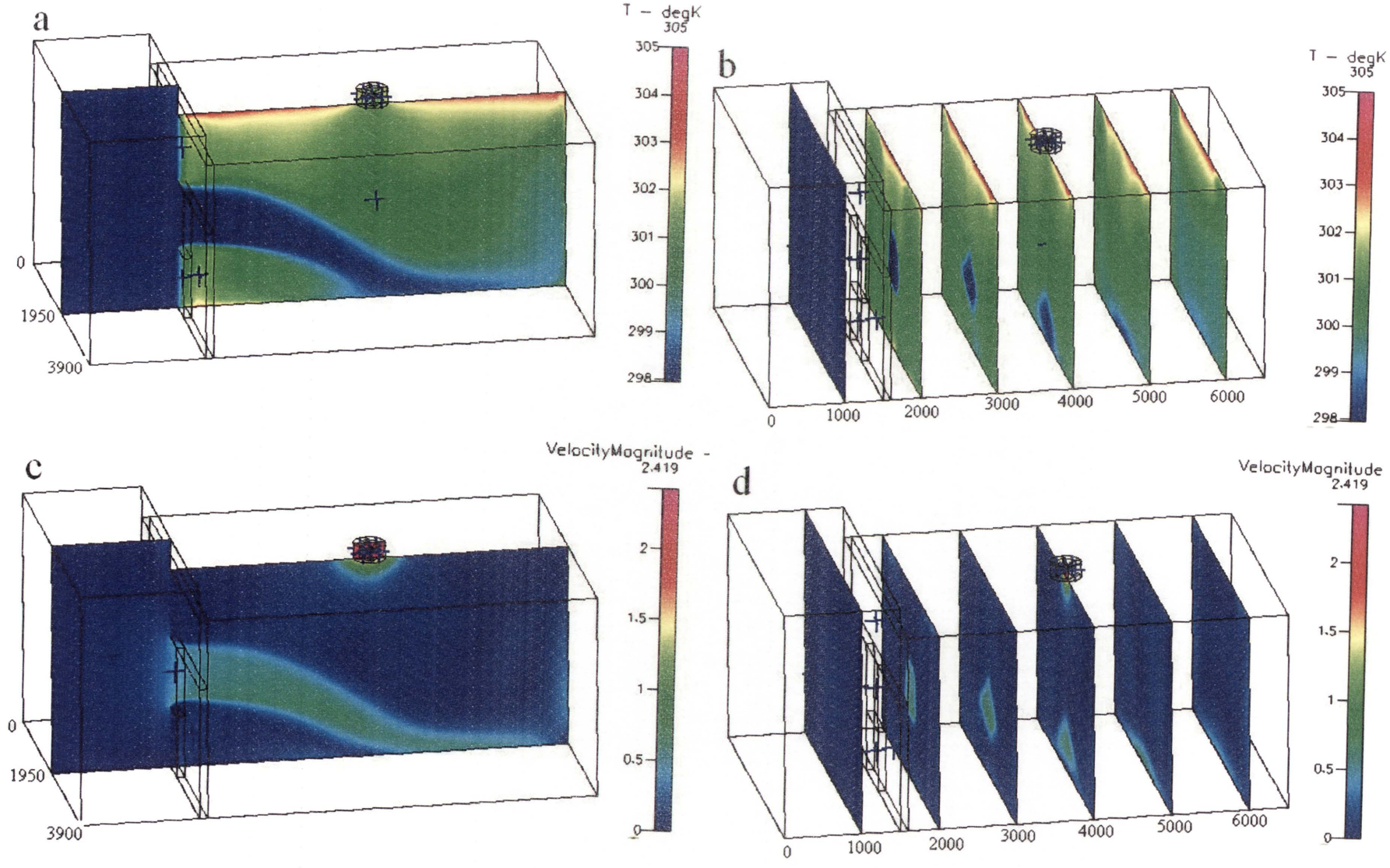

Figure 61– 1_2_305 Temperature and velocity distributions with airflows through fan of 2 m/s

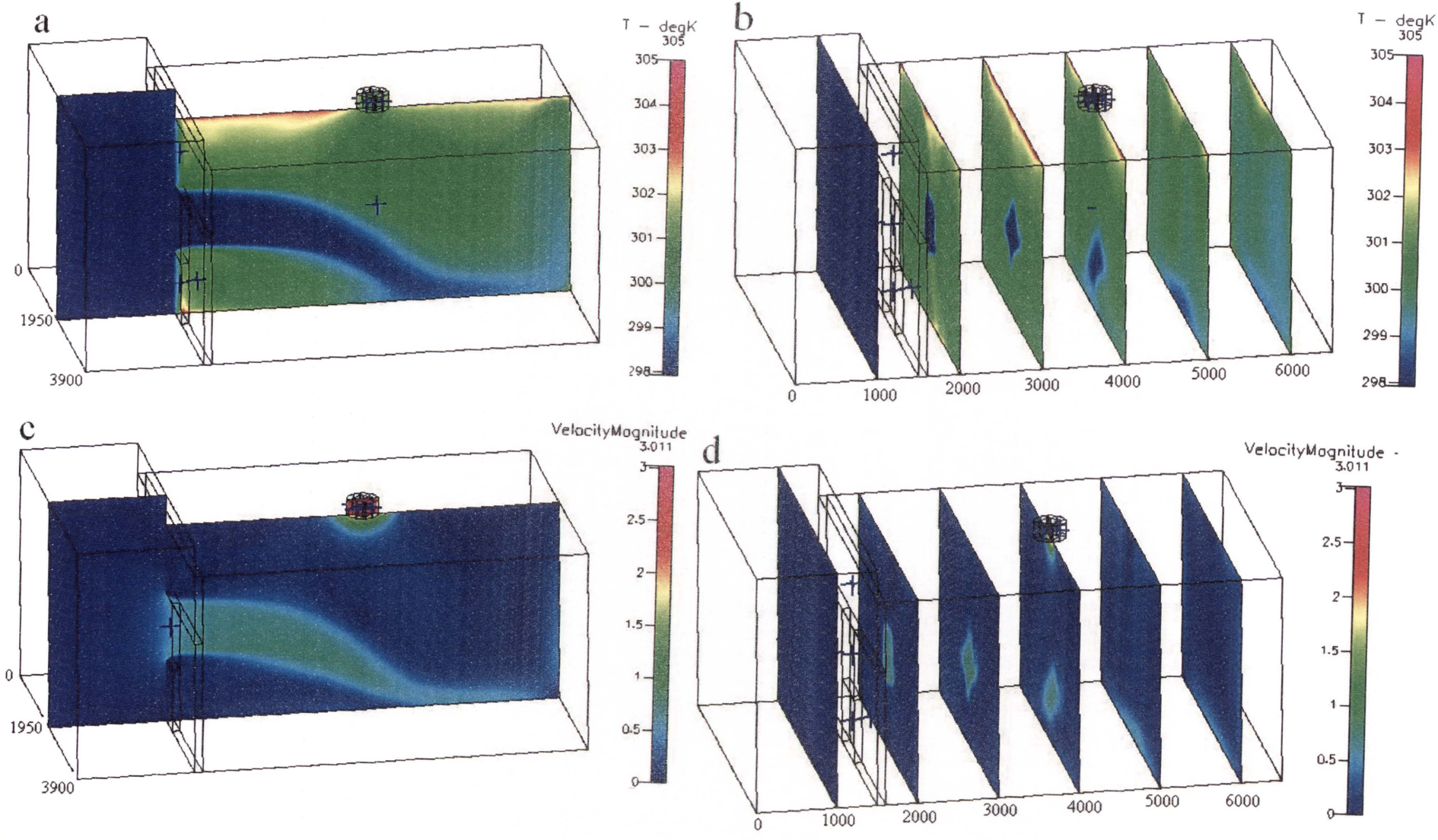

Figure 62 – 1_2.5_305 Temperature and velocity distributions with airflows through fan of 2.5 m/s

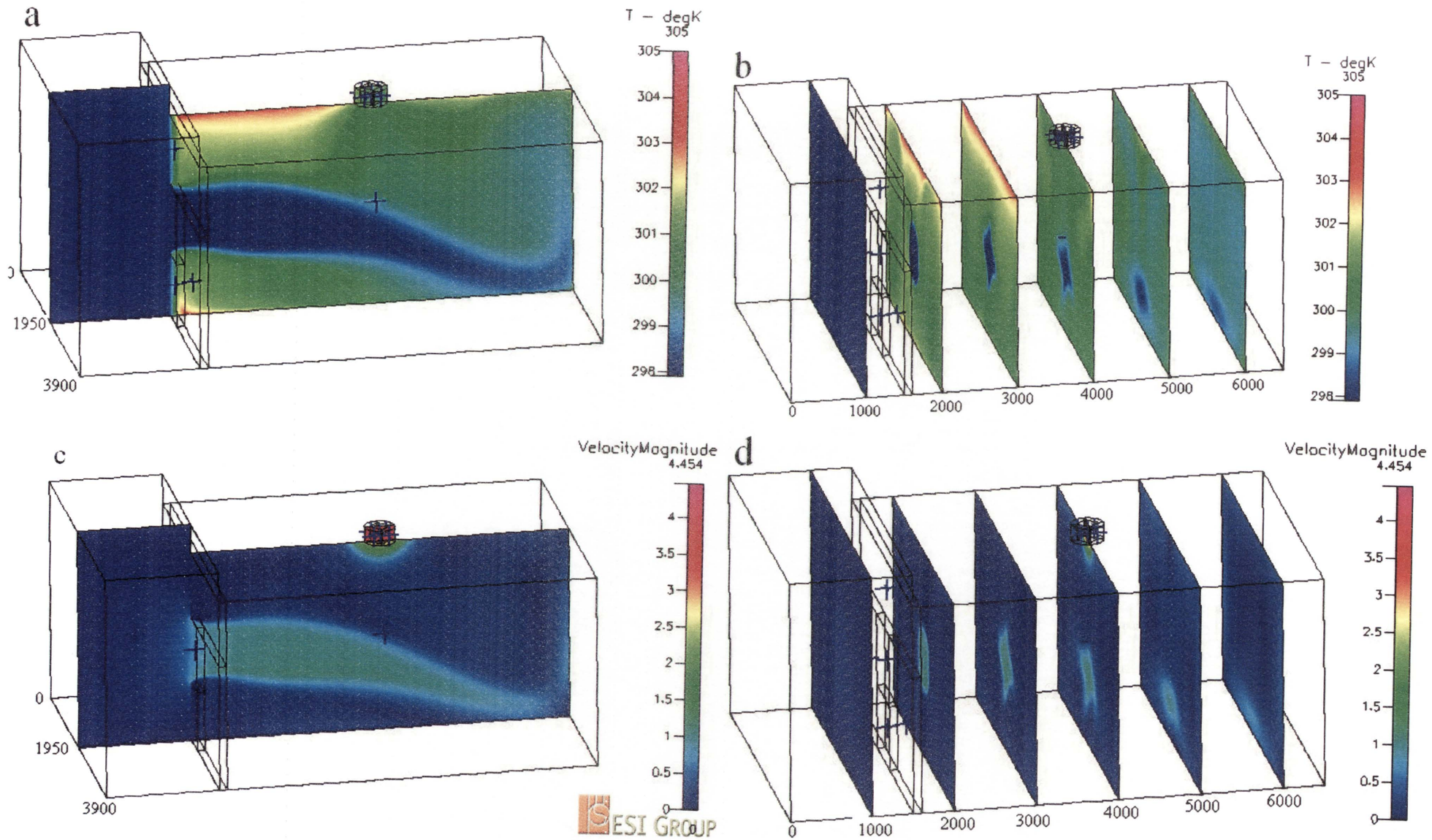

Figure 63 – 1_3.7_305 Temperature and velocity distributions with airflows through fan of 3.7 m/s

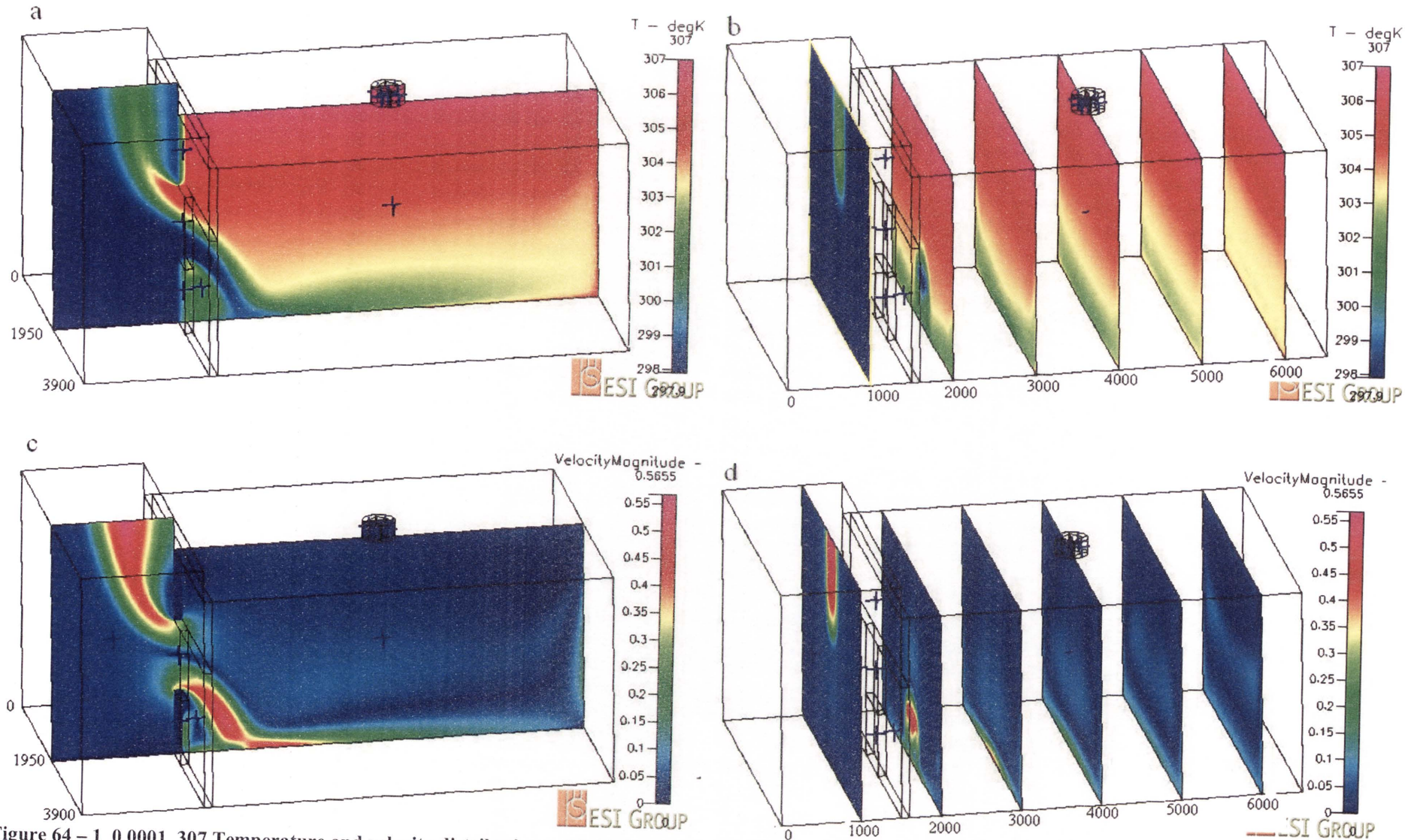

Figure 64 – 1_0.0001_307 Temperature and velocity distributions with airflows through fan of 0.0001 m/s

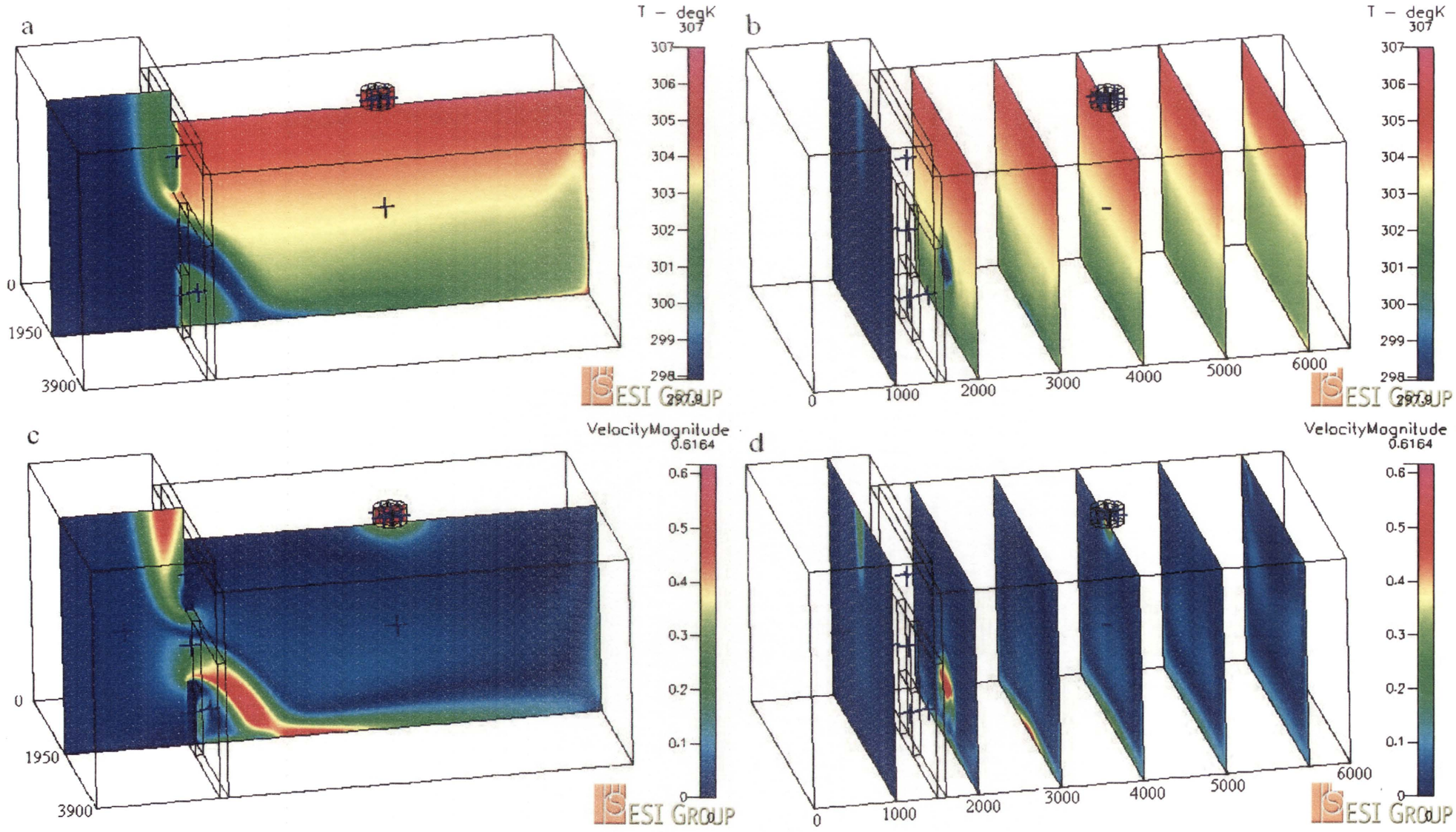

Figure 65 – 1_0.505_307 Temperature and velocity distributions with airflows through fan of 0.505 m/s

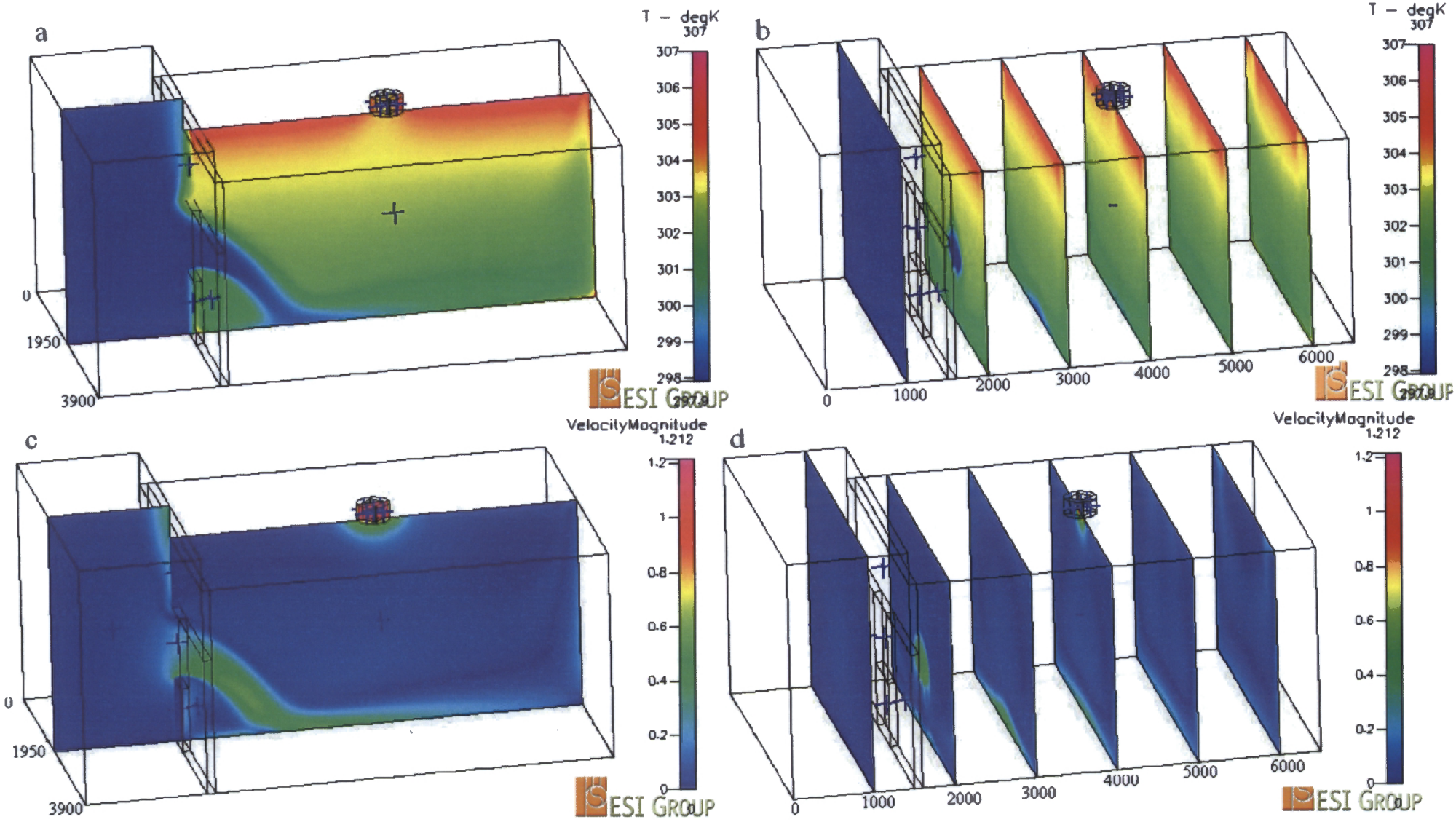

Figure 66 – 1_1_307 Temperature and velocity distributions with airflows through fan of 1 m/s

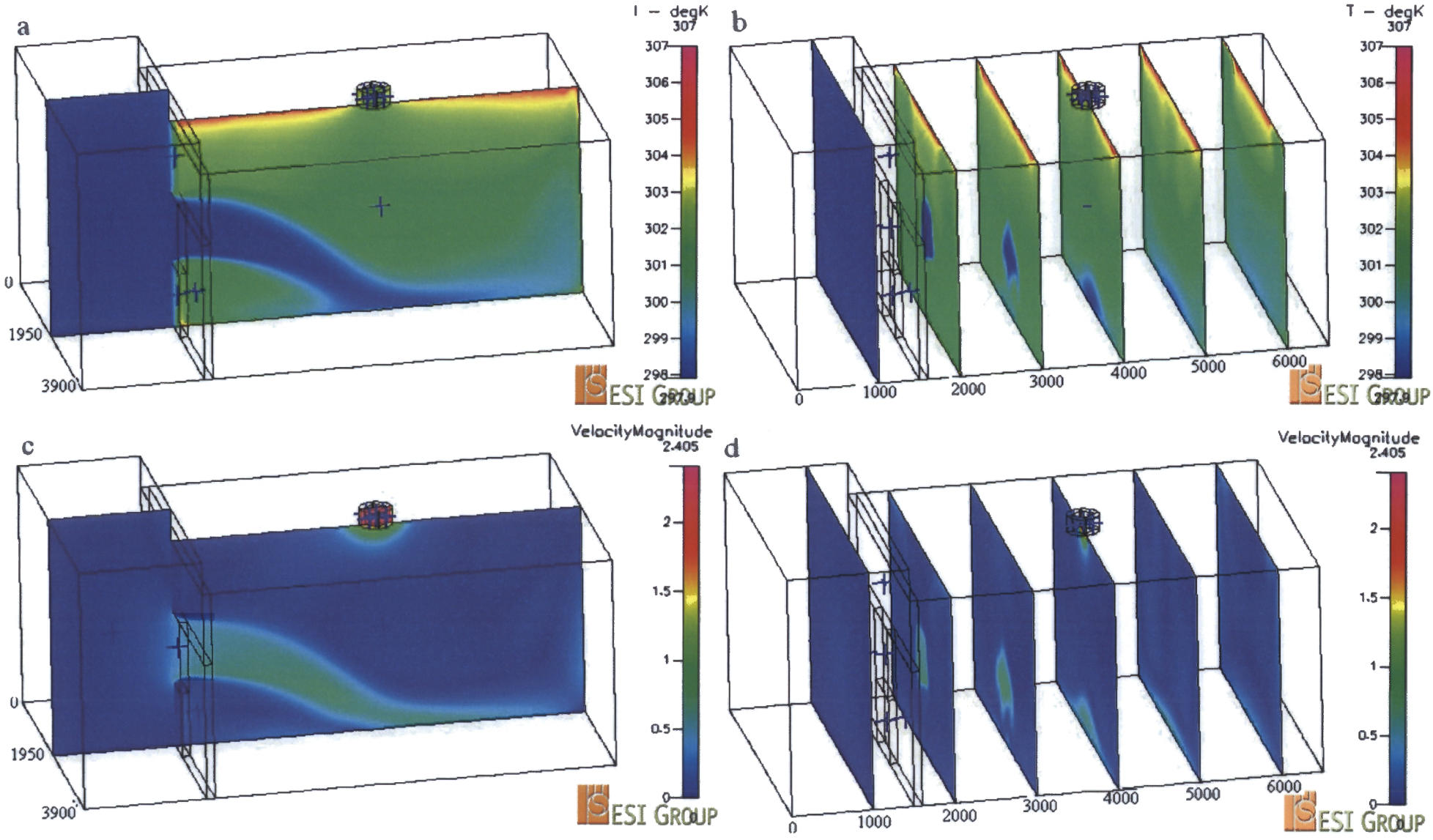

Figure 67 – 1_2_307 Temperature and velocity distributions with airflows through fan of 2m/s

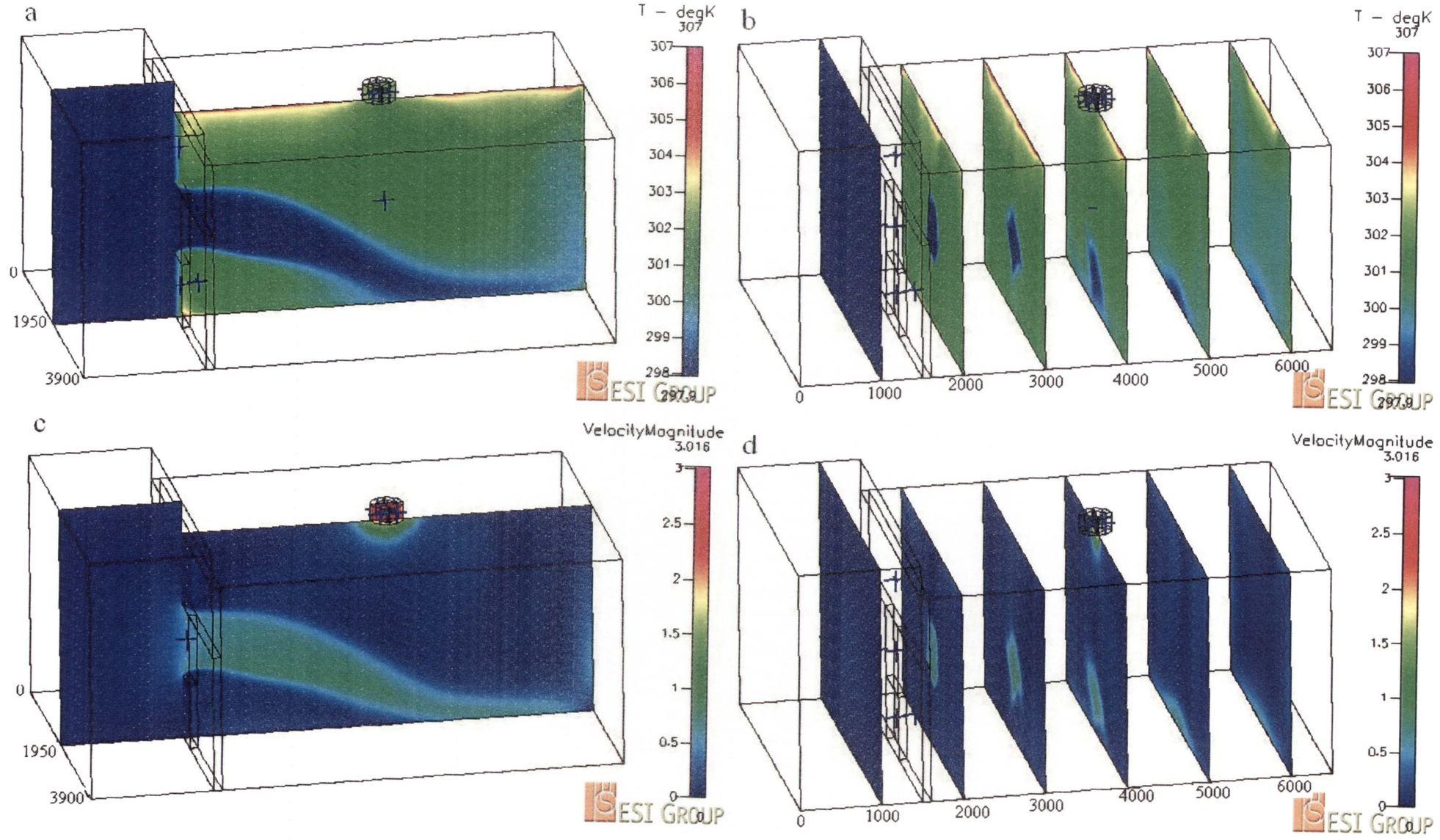

Figure 68 – 1_2.5_307 Temperature and velocity distributions with airflows through fan of 2.5m/s

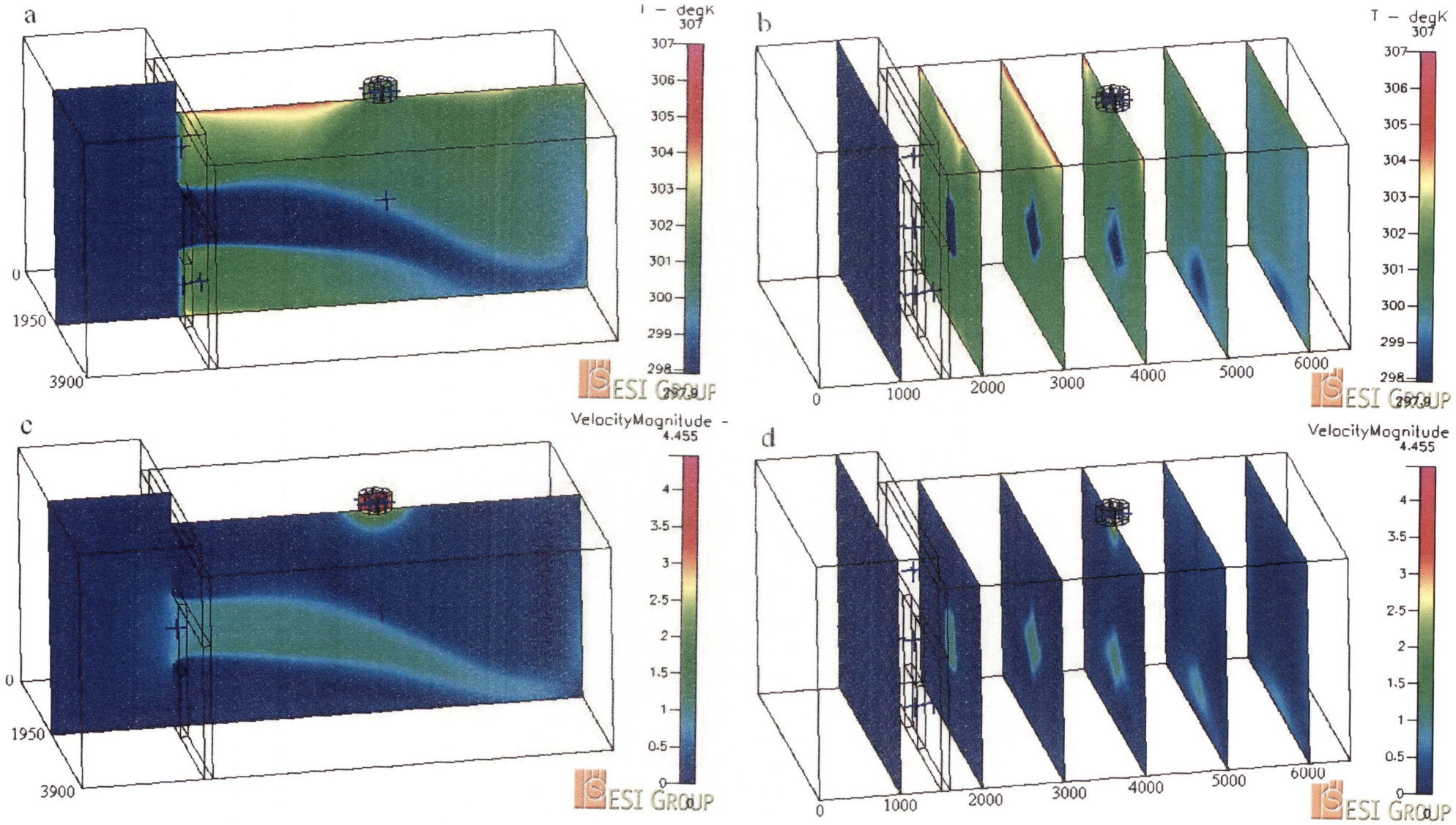

Figure 69 – 1_3.7_307 Temperature and velocity distributions with airflows through fan of 3.7m/s

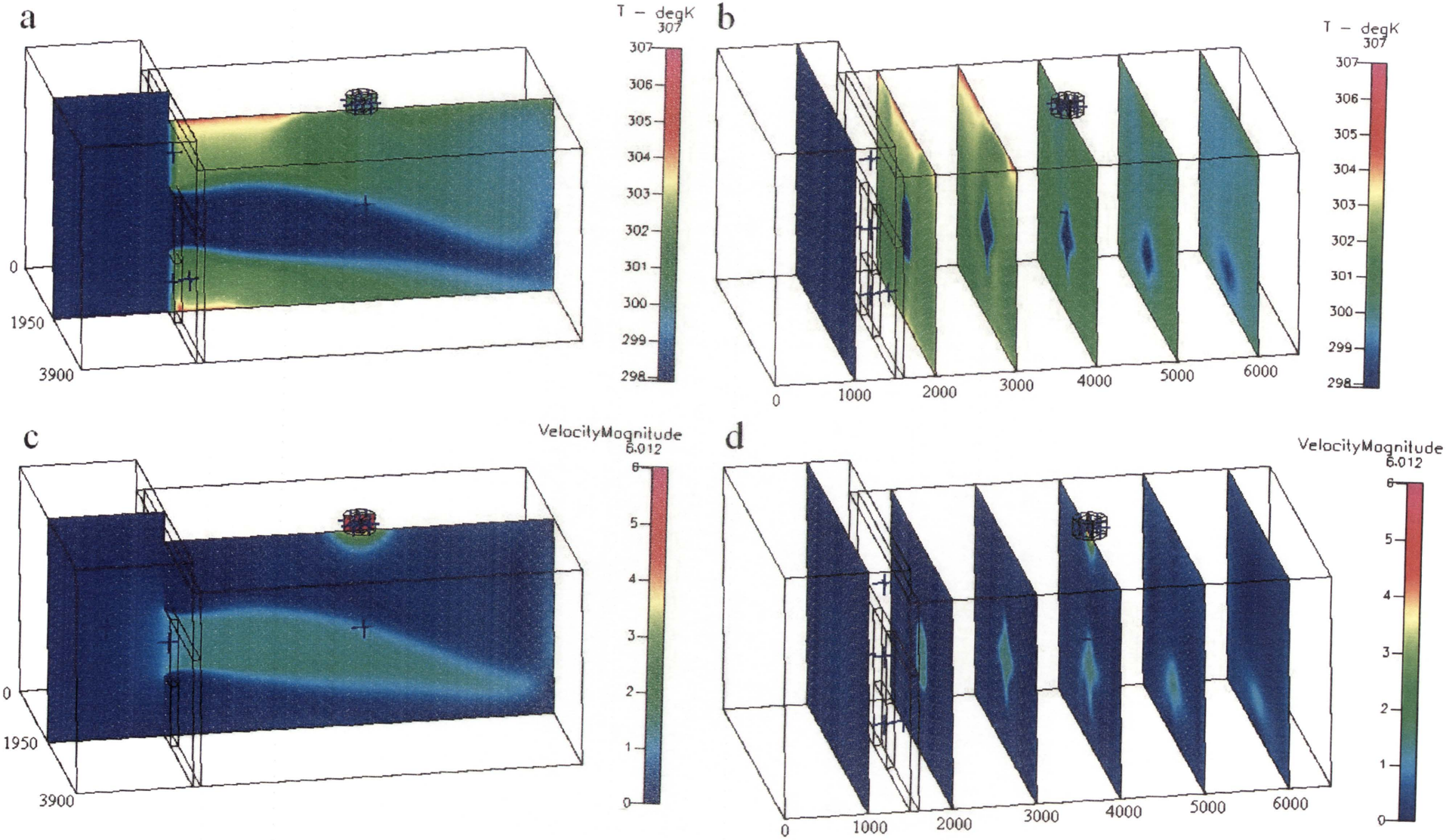

Figure 70 – 1_5_307 Temperature and velocity distributions with airflows through fan of 5 m/s

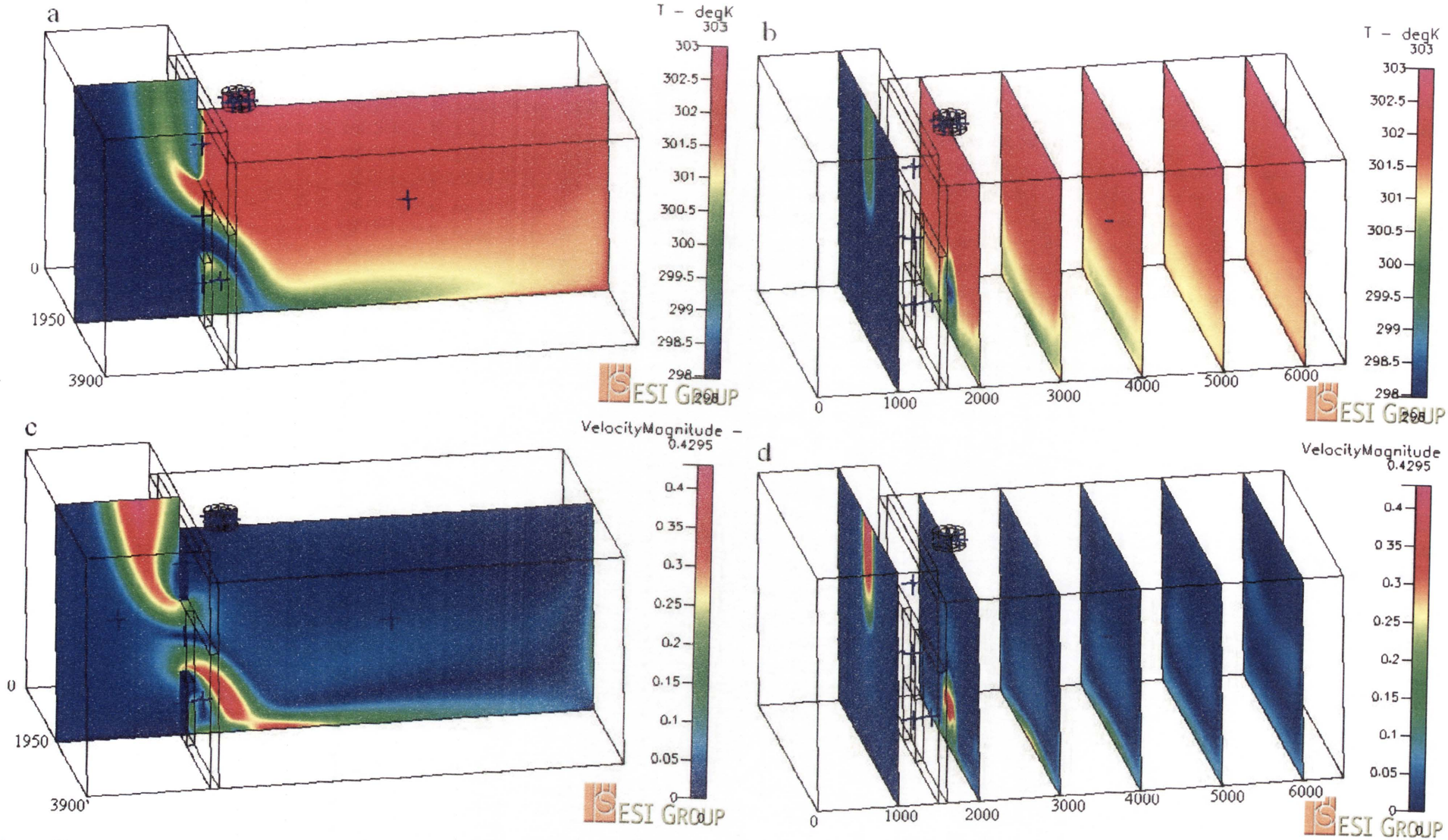

Figure 71 – 2_0.0001_303 Temperature and velocity distributions with airflows through fan of 0.0001 m/s

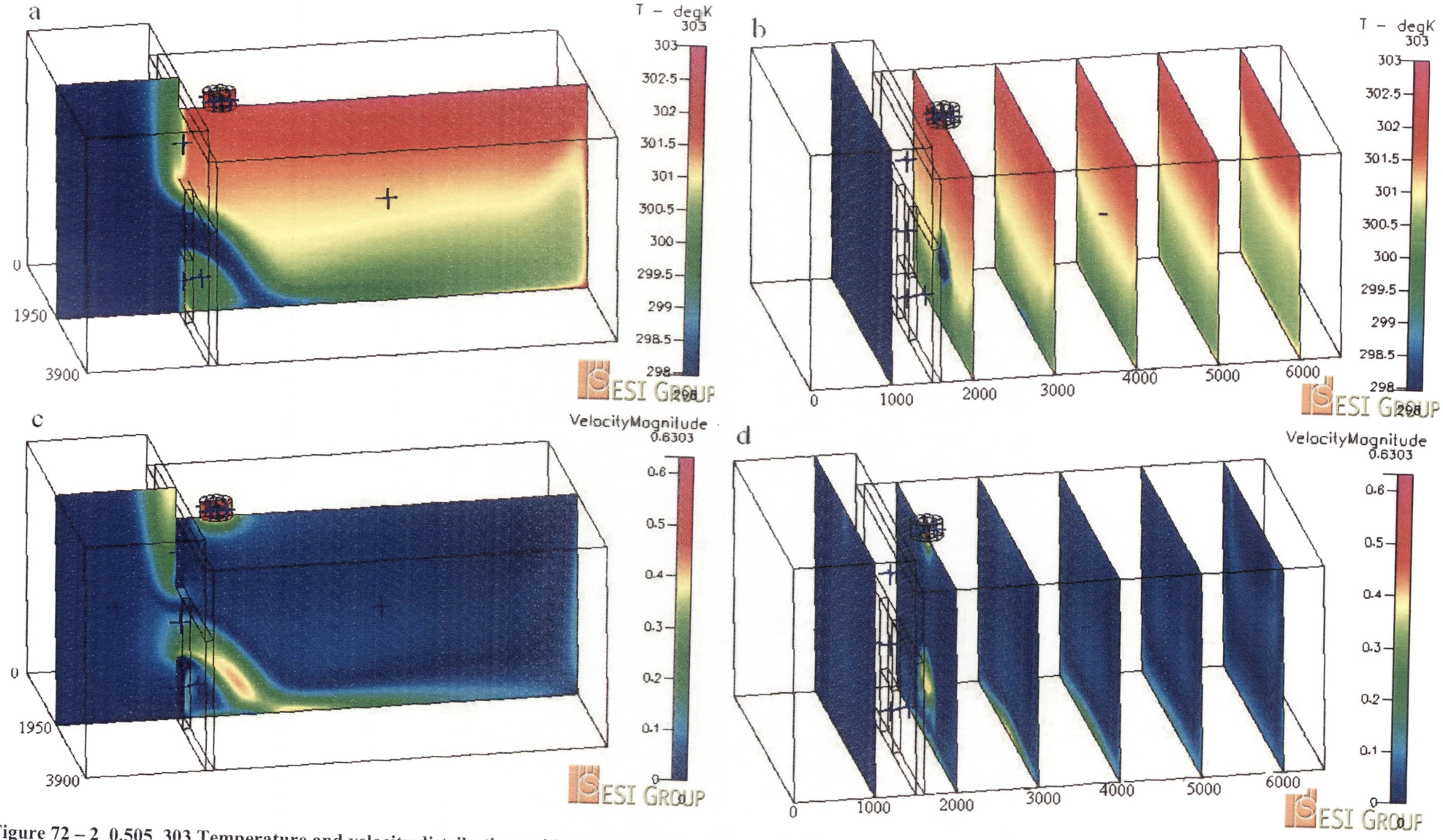

Figure 72 – 2_0.505_303 Temperature and velocity distributions with airflows through fan of 0.505 m/s

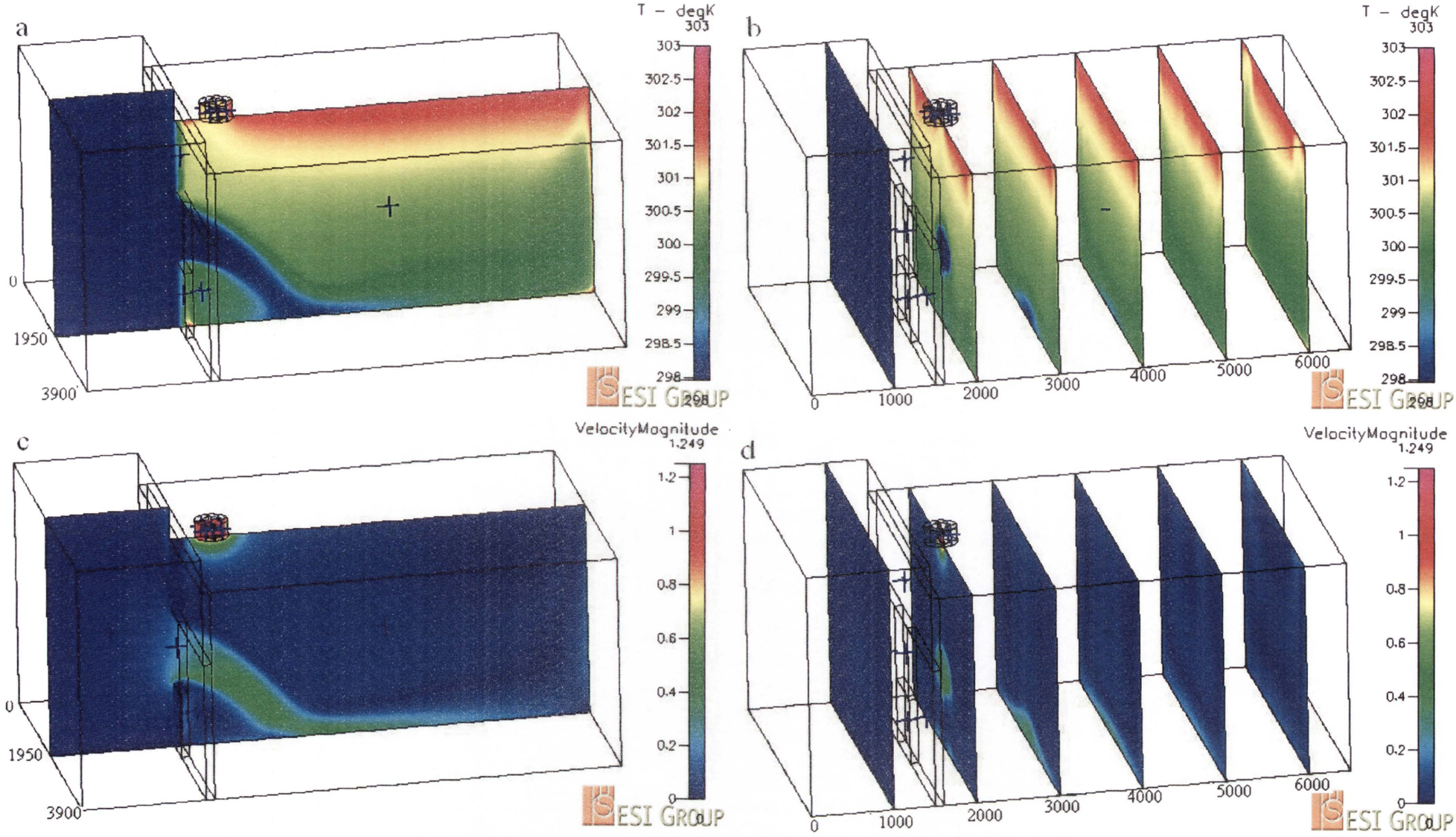

Figure 73 – 2_1_303 Temperature and velocity distributions with airflows through fan of 1 m/s

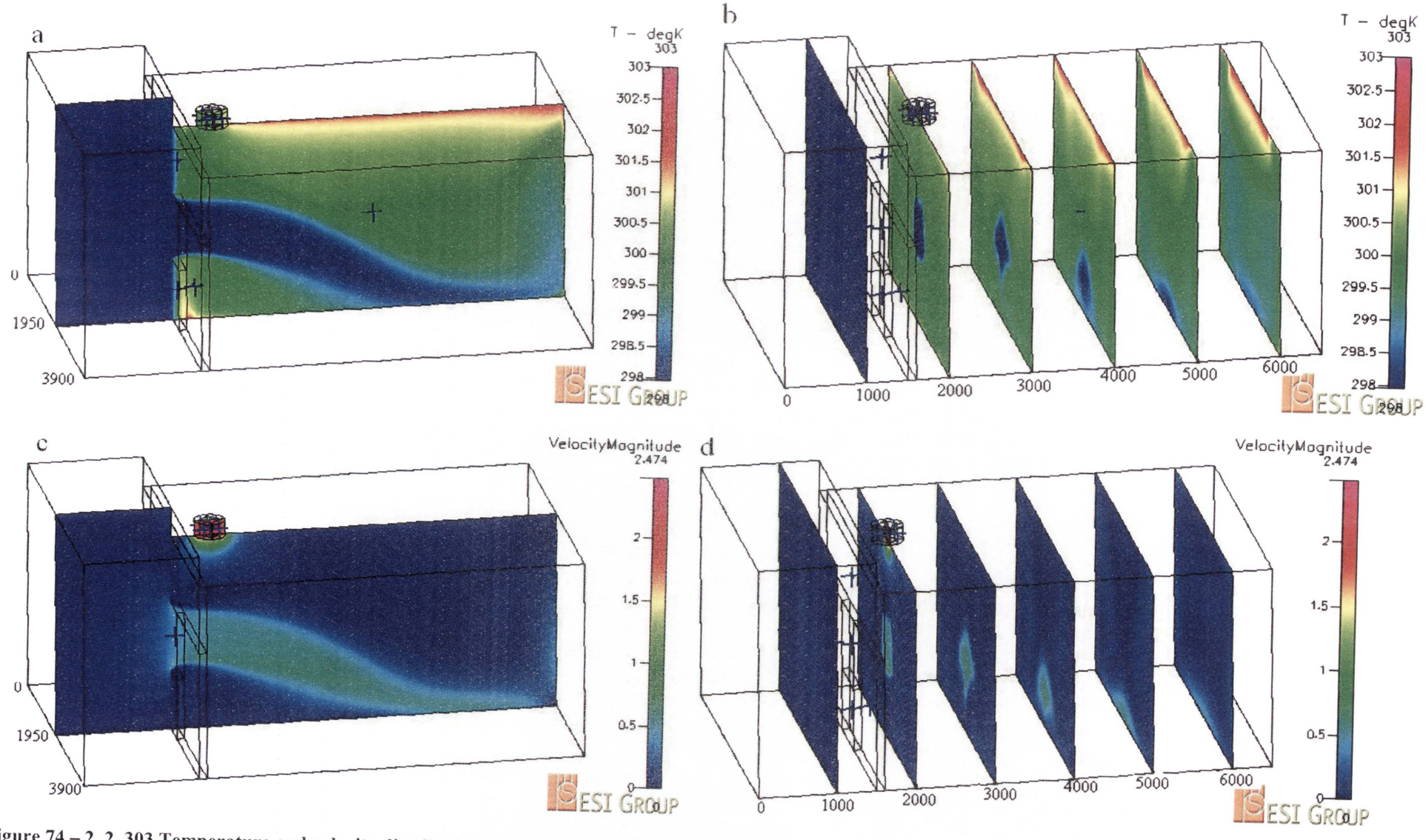

Figure 74 – 2_2_303 Temperature and velocity distributions with airflows through fan of 2 m/s

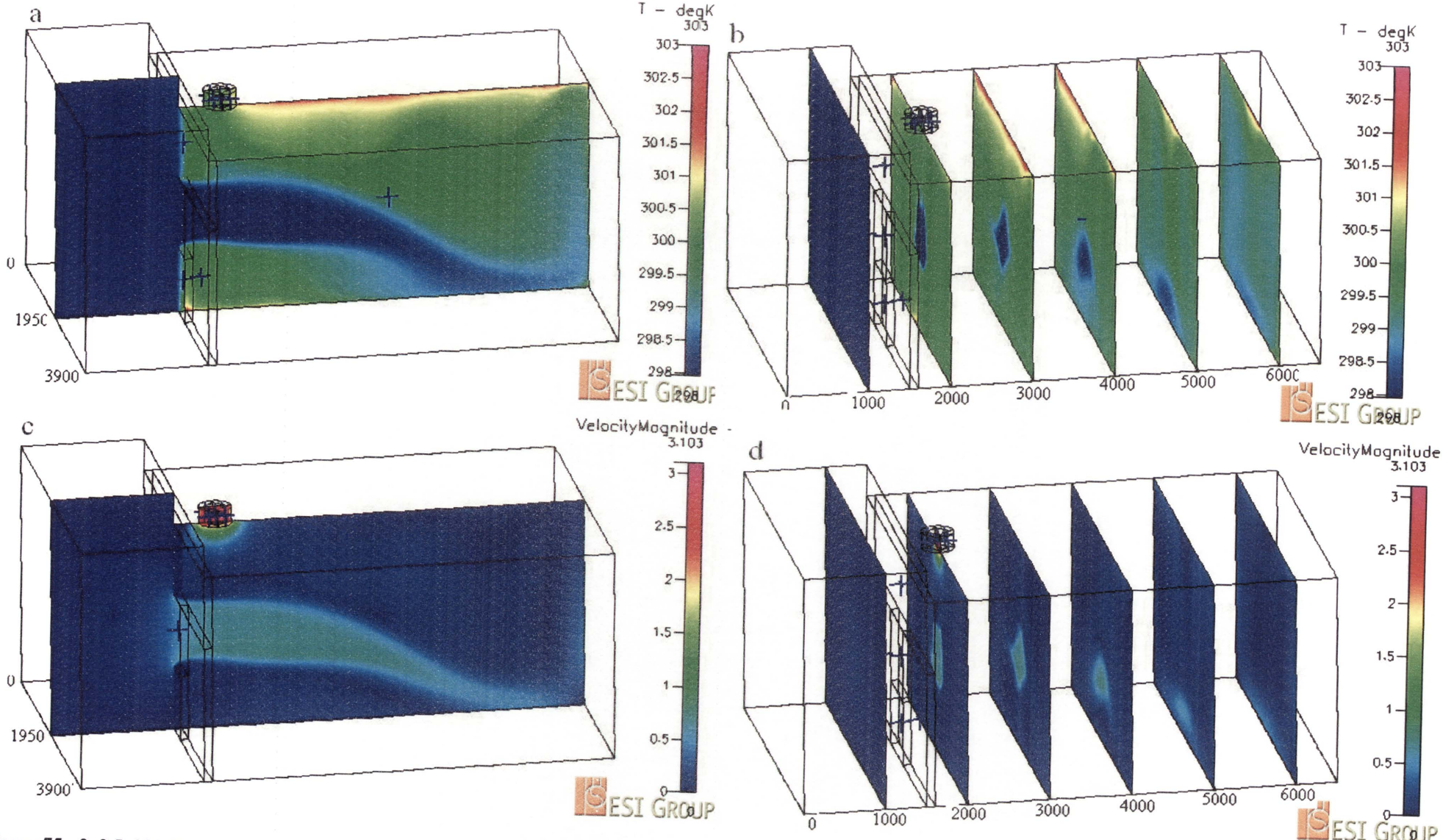

Figure 75 - 2_2.5_303 Temperature and velocity distributions with airflows through fan of 2.5 m/s

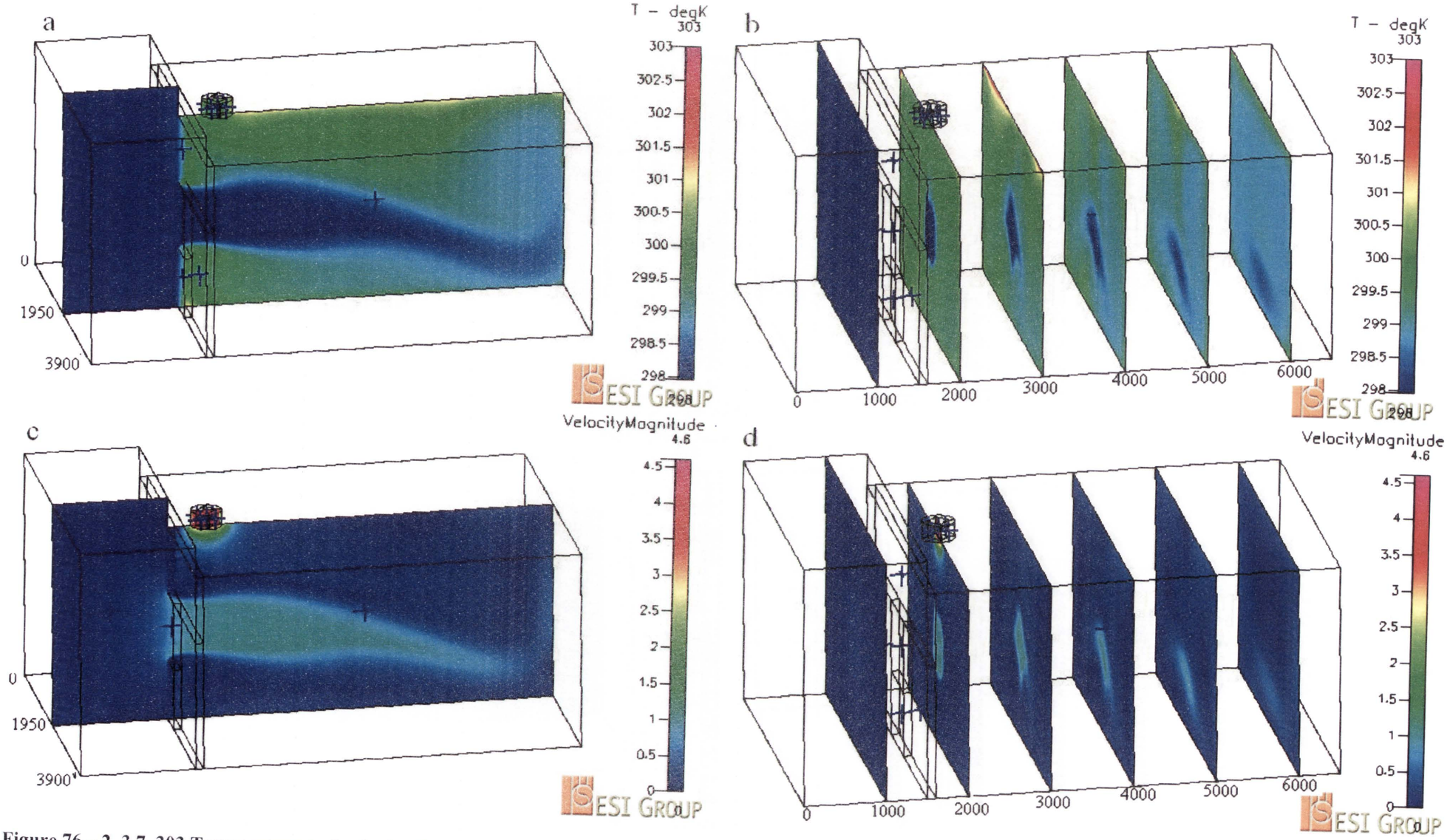

Figure 76 – 2_3.7_303 Temperature and velocity distributions with airflows through fan of 3.7 m/s

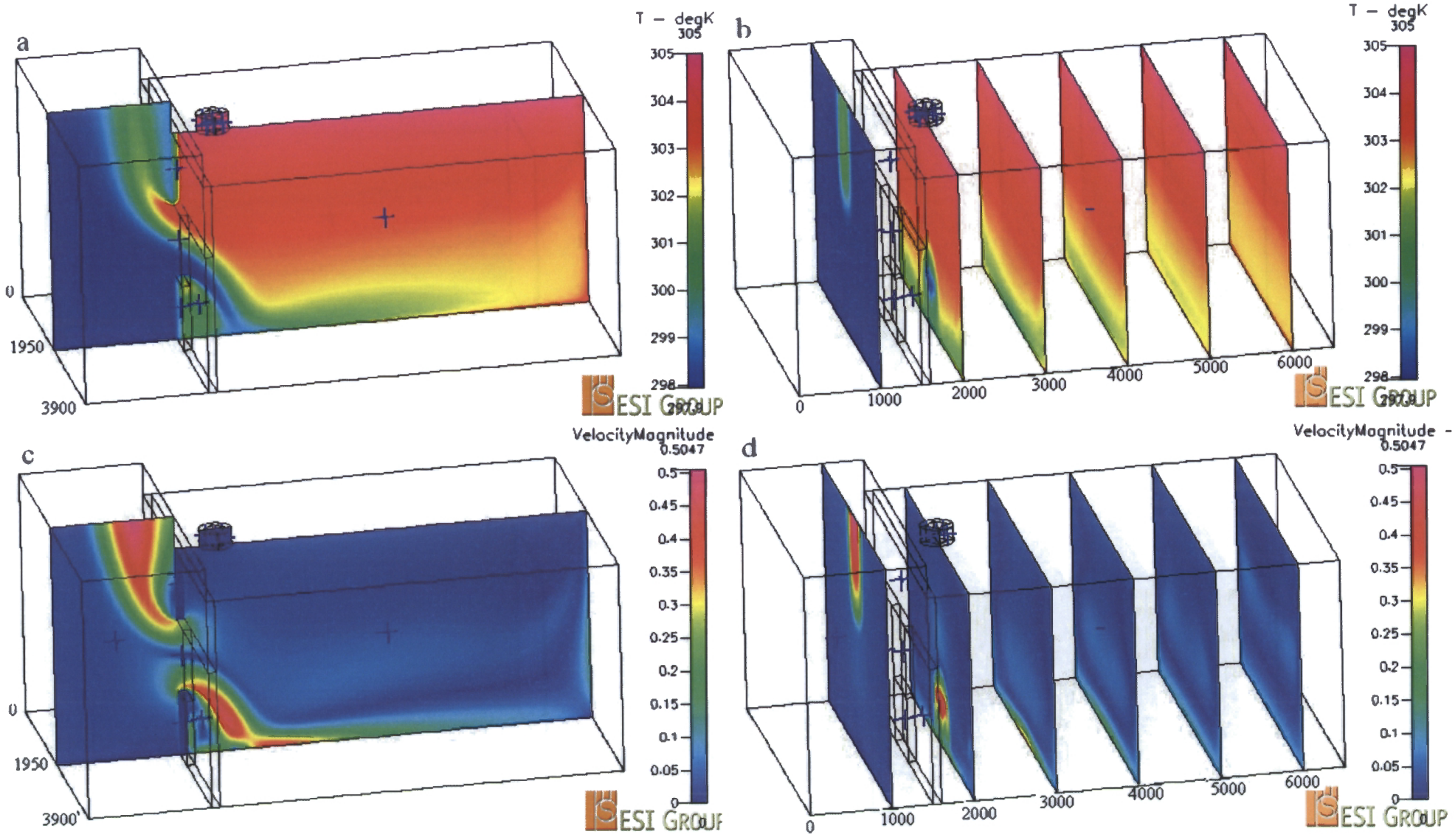

Figure 77 – 2_0.0001_305 Temperature and velocity distributions with airflows through fan of 0.0001 m/s

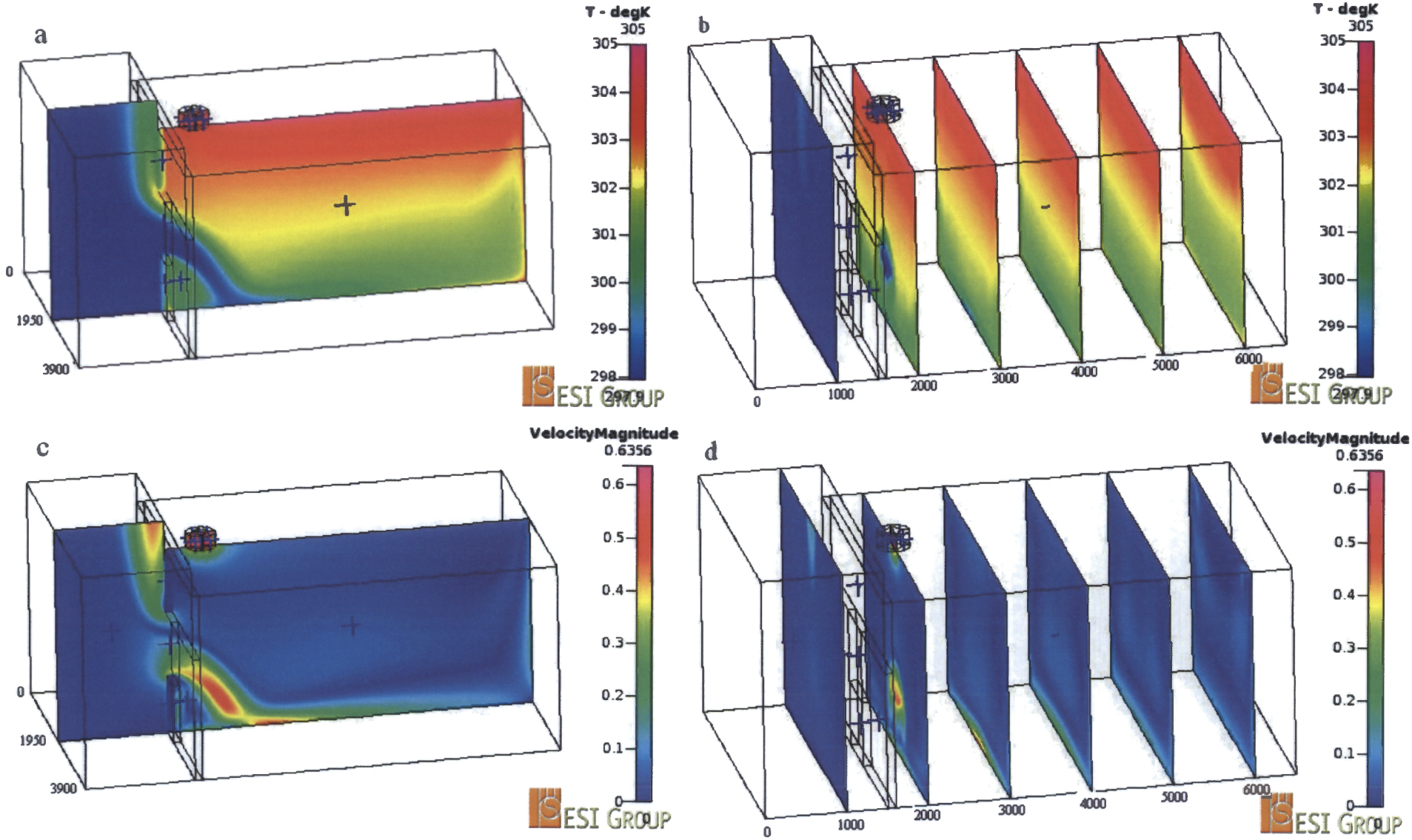

Figure 78 – 2_0.505_305 Temperature and velocity distributions with airflows through fan of 0.505 m/s

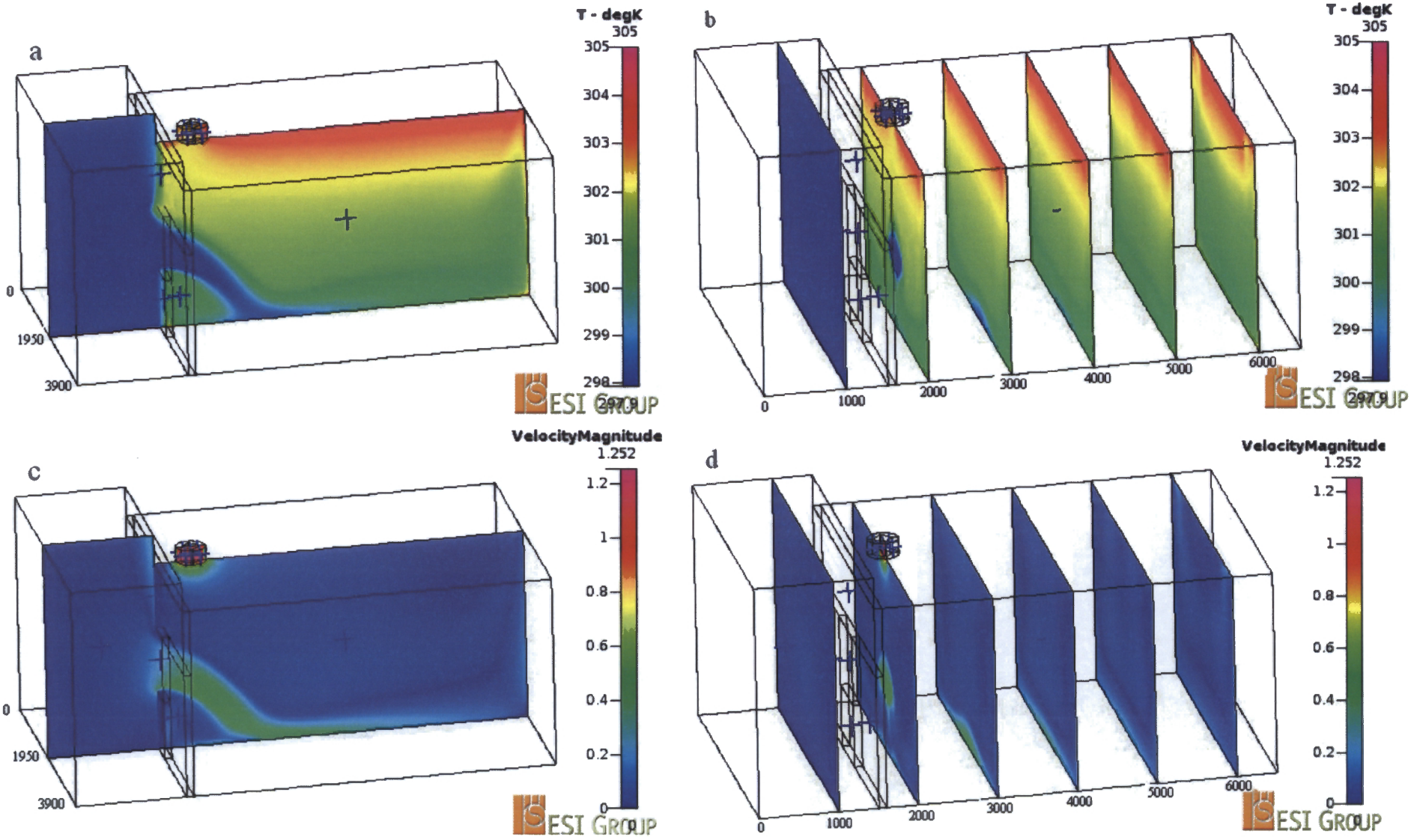

Figure 79 – 2_1_305 Temperature and velocity distributions with airflows through fan of 1 m/s

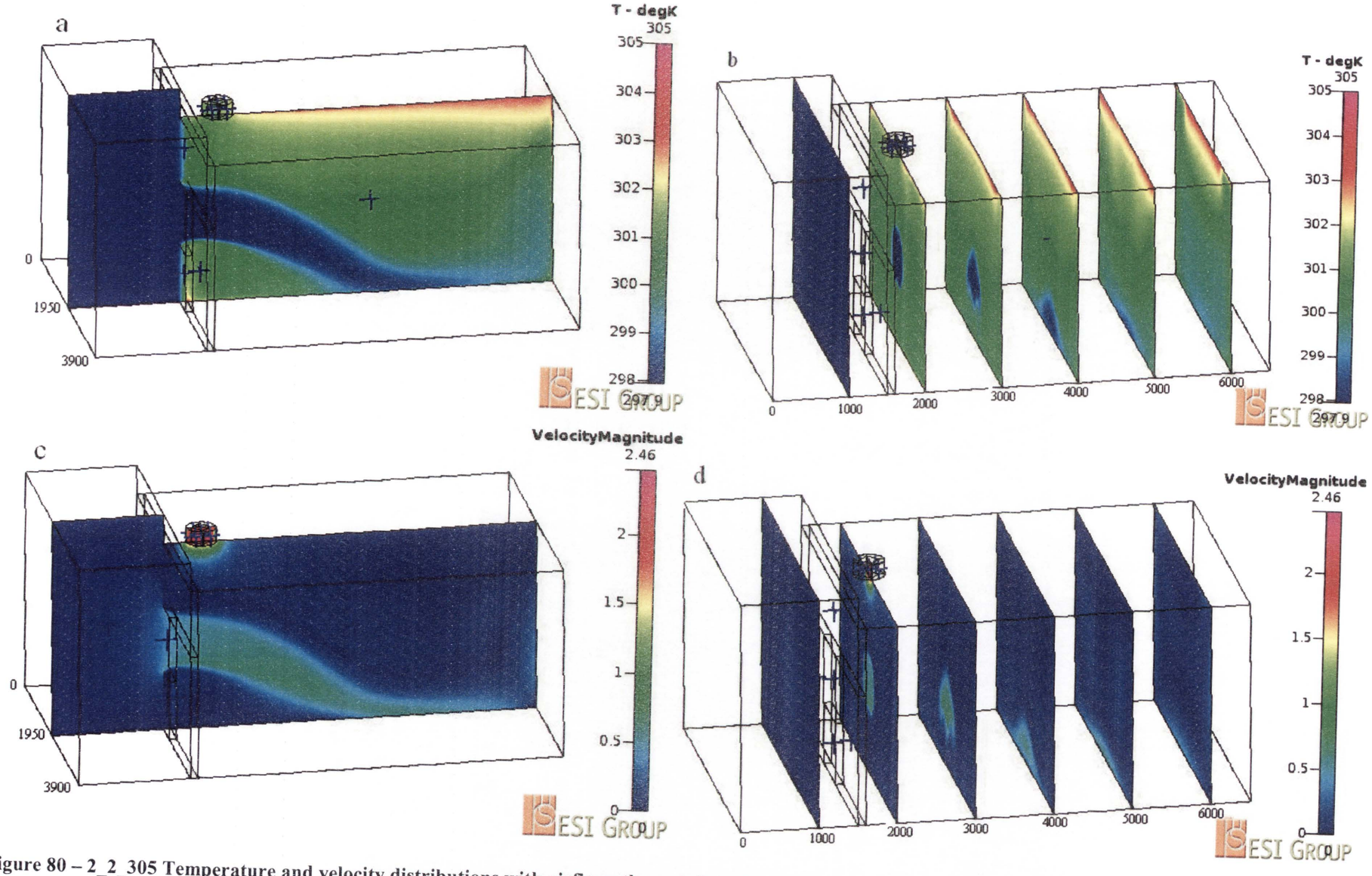

Figure 80 – 2_2_305 Temperature and velocity distributions with airflows through fan of 2 m/s

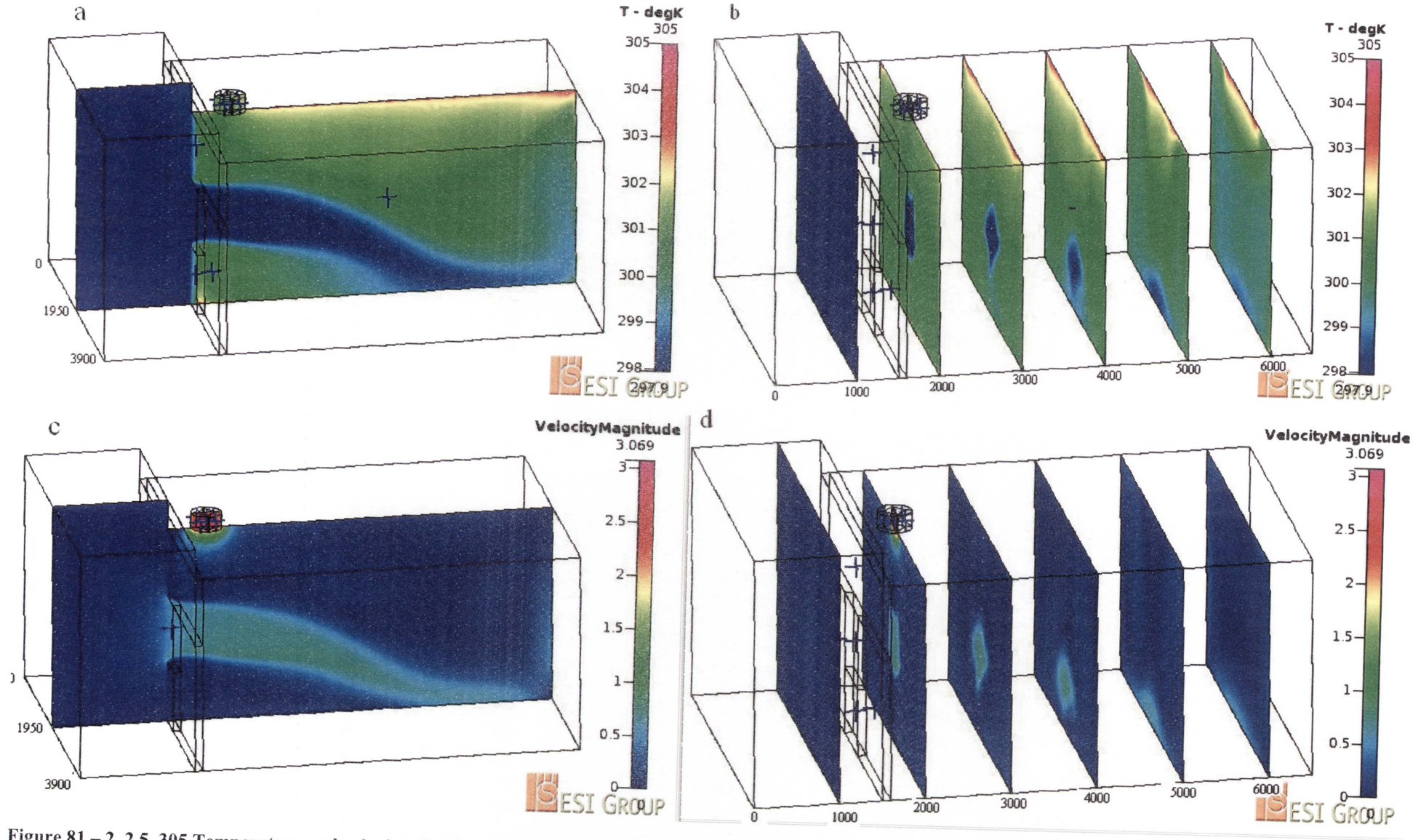

Figure 81 – 2_2.5_305 Temperature and velocity distributions with airflows through fan of 2.5 m/s

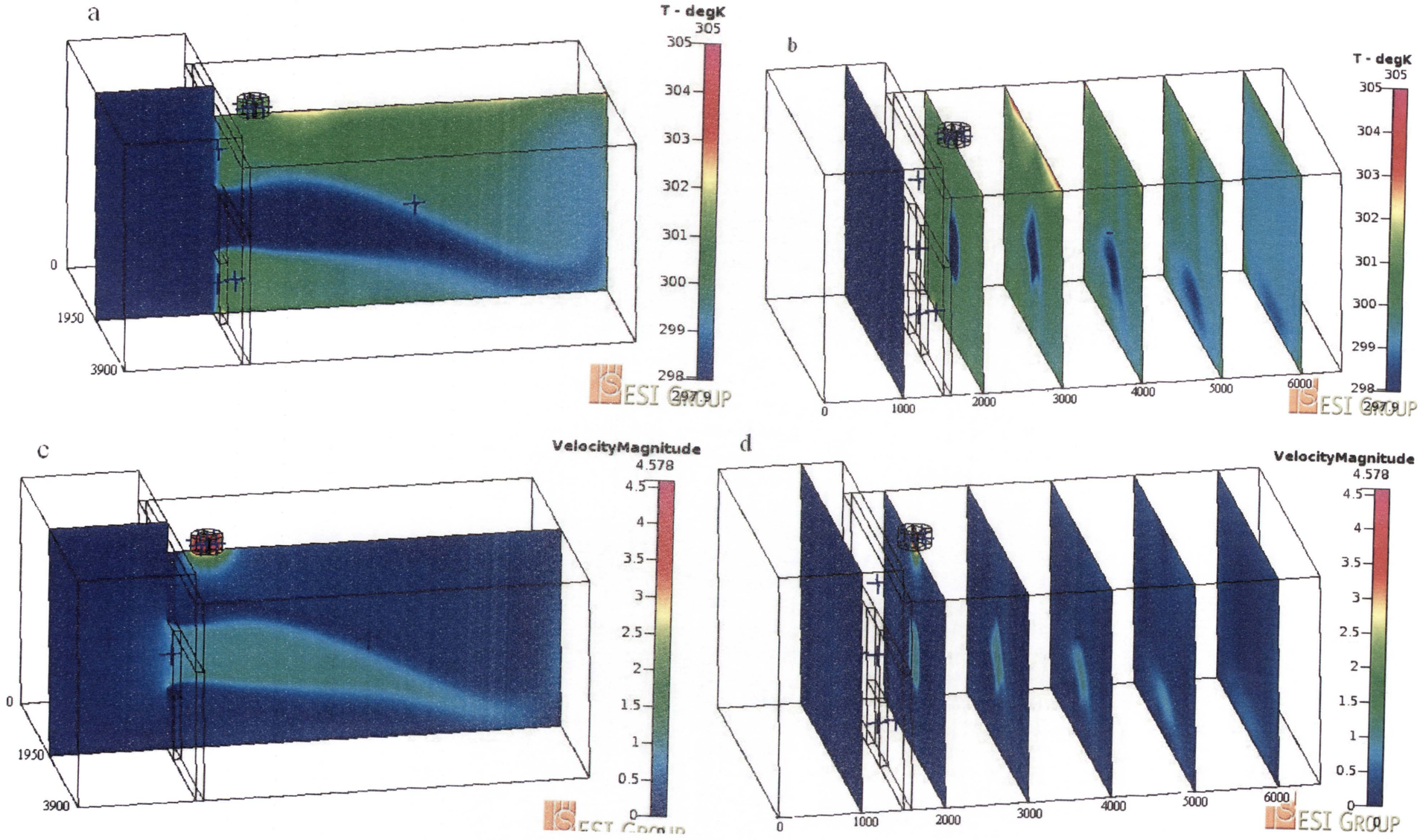

Figure 82 – 2_3.7_305 Temperature and velocity distributions with airflows through fan of 3.7 m/s

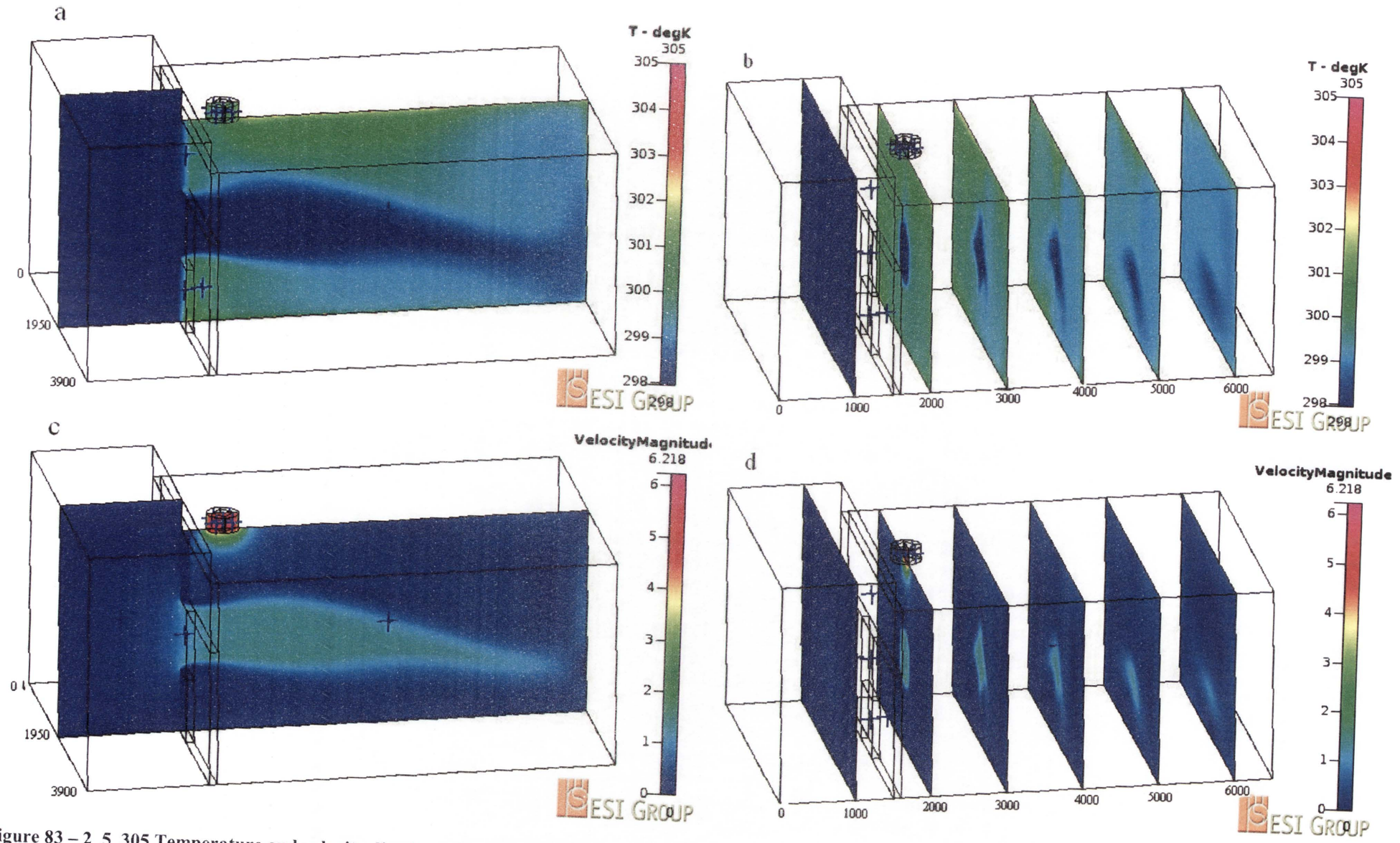

Figure 83 – 2_5_305 Temperature and velocity distributions with airflows through fan of 5 m/s

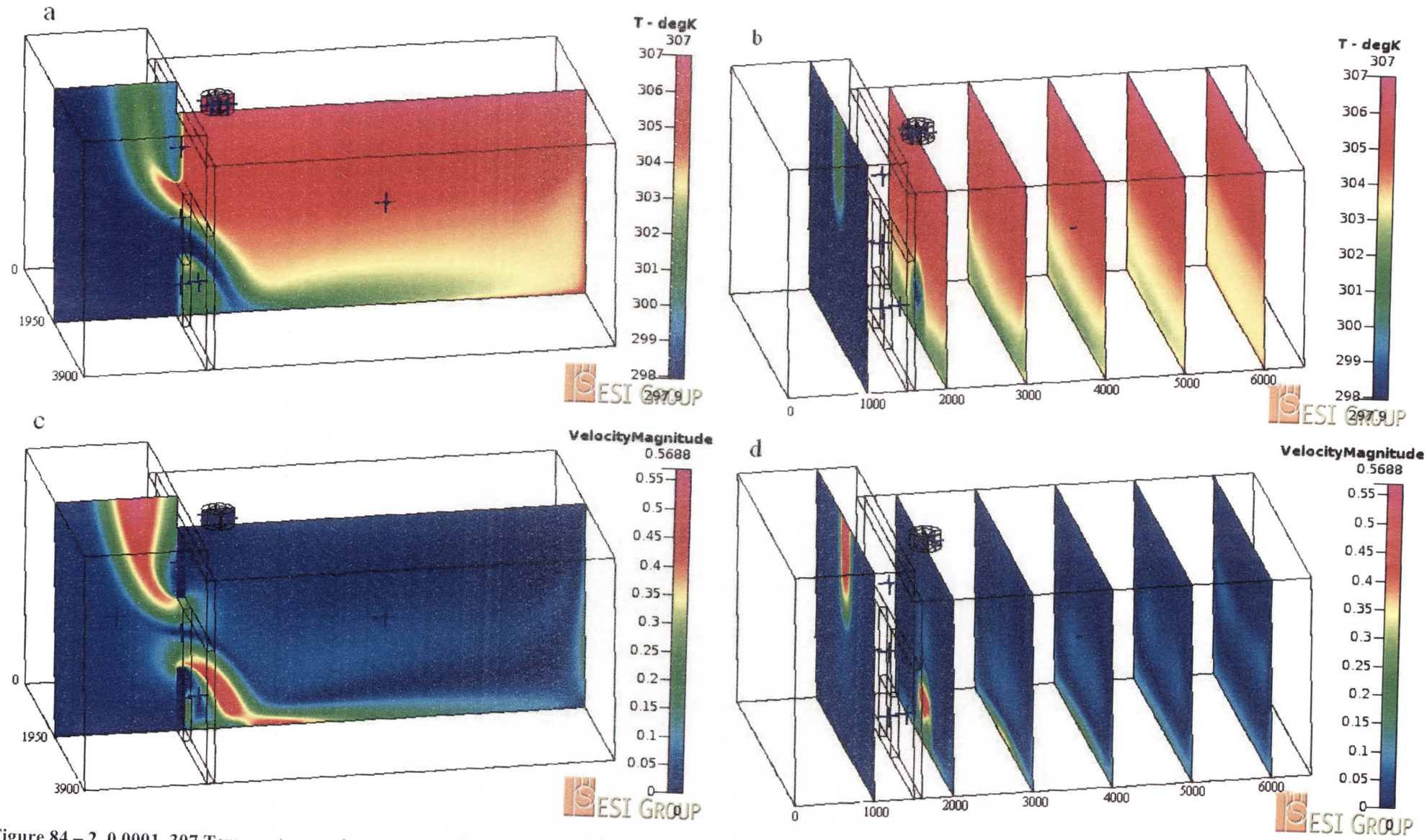

Figure 84 – 2_0.0001_307 Temperature and velocity distributions with airflows through fan of 0.0001 m/s

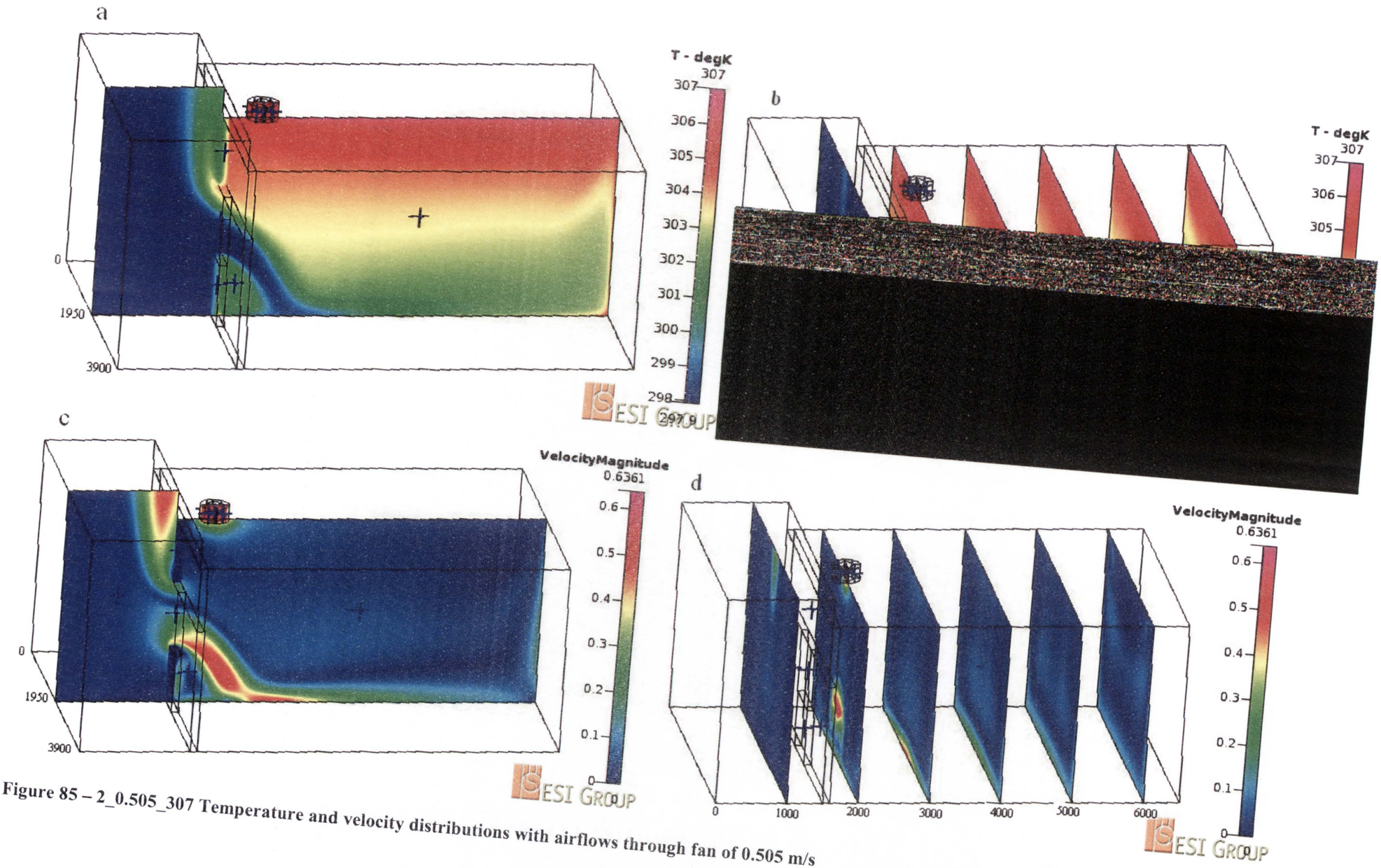

Figure 85 – 2_0.505_307 Temperature and velocity distributions with airflows through fan of 0.505 m/s

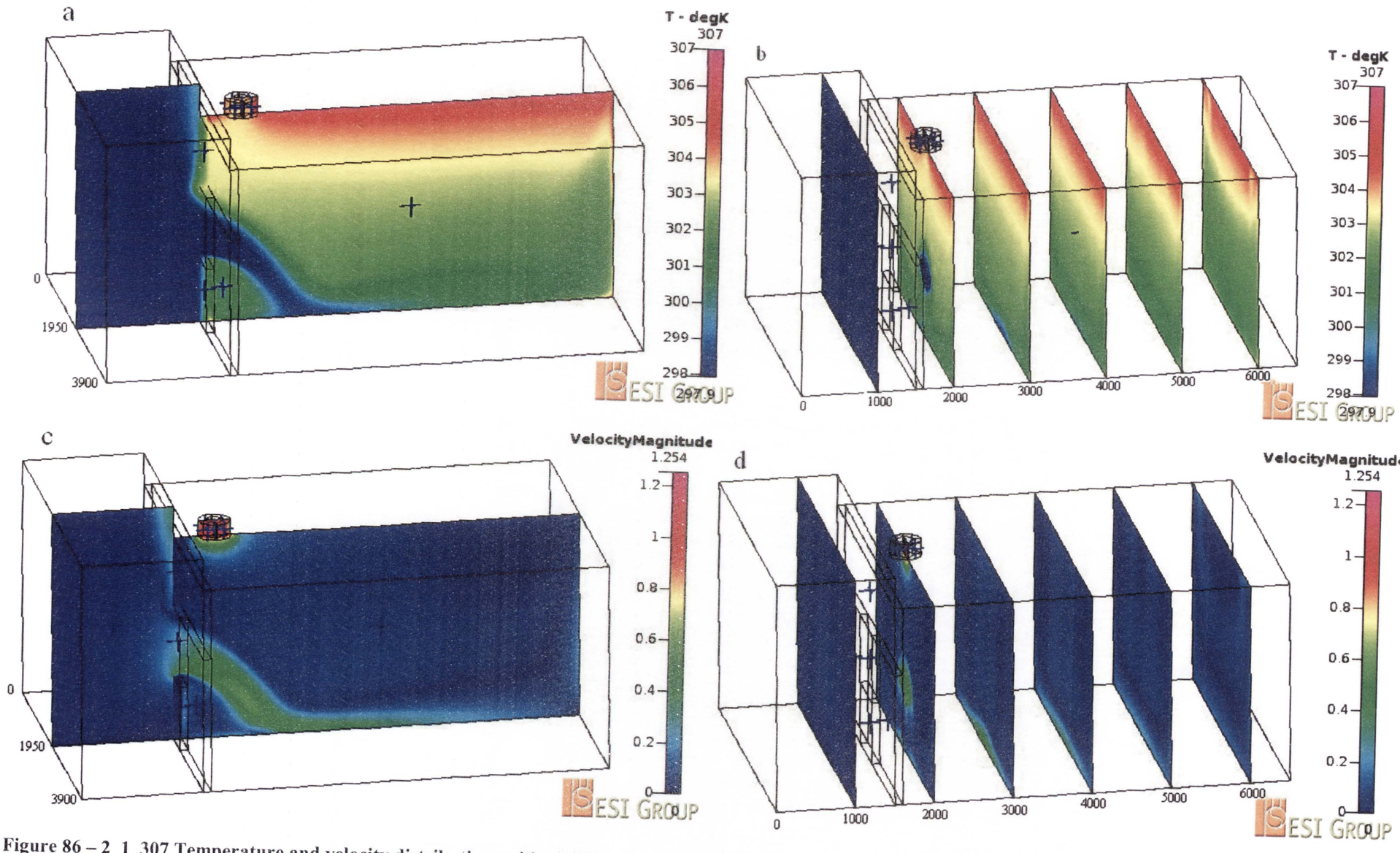

Figure 86 – 2_1_307 Temperature and velocity distributions with airflows through fan of 1 m/s

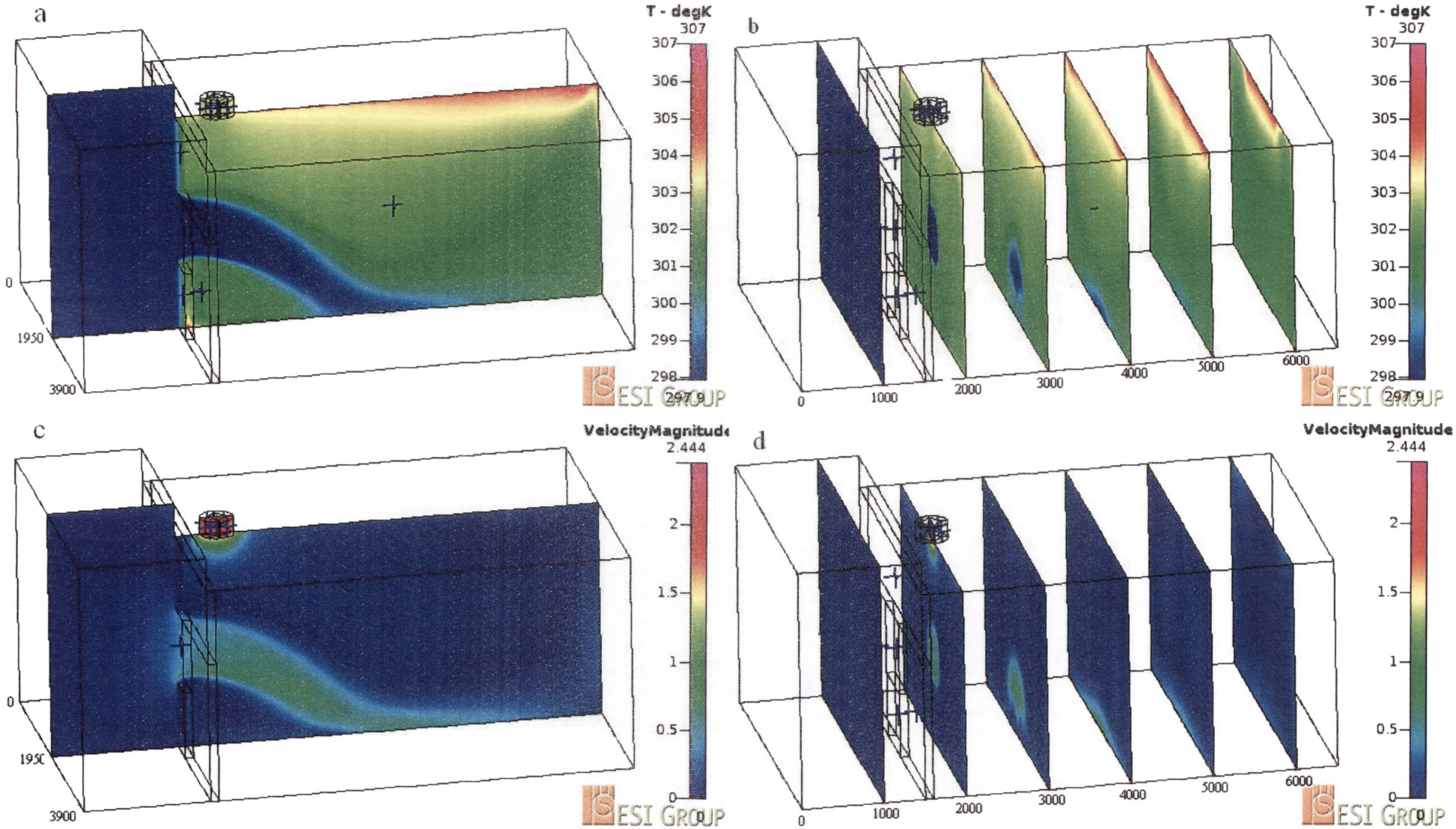

Figure 87 – 2_2_307 Temperature and velocity distributions with airflows through fan of 2 m/s

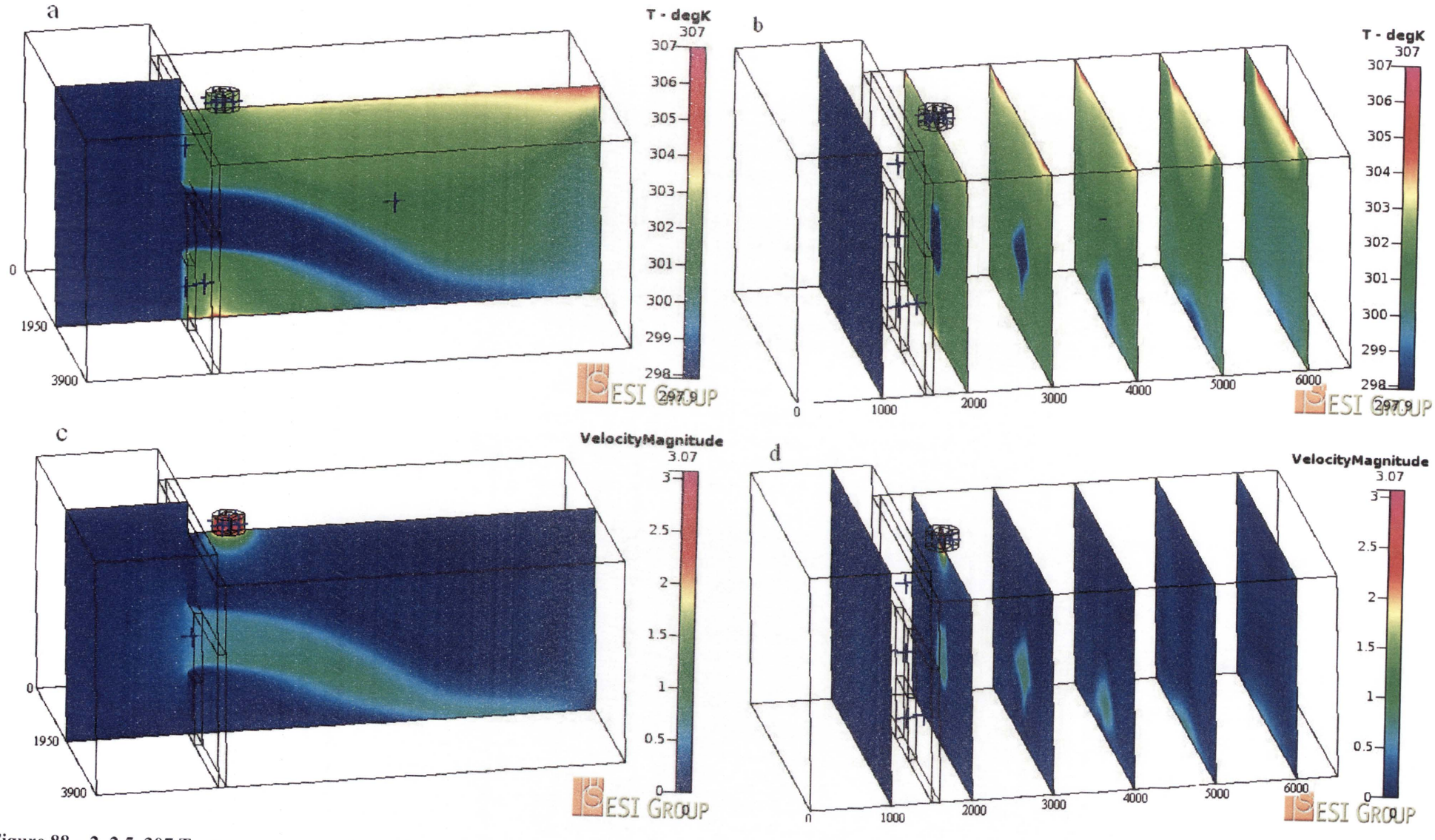

Figure 88 – 2_2.5_307 Temperature and velocity distributions with airflows through fan of 2.5 m/s

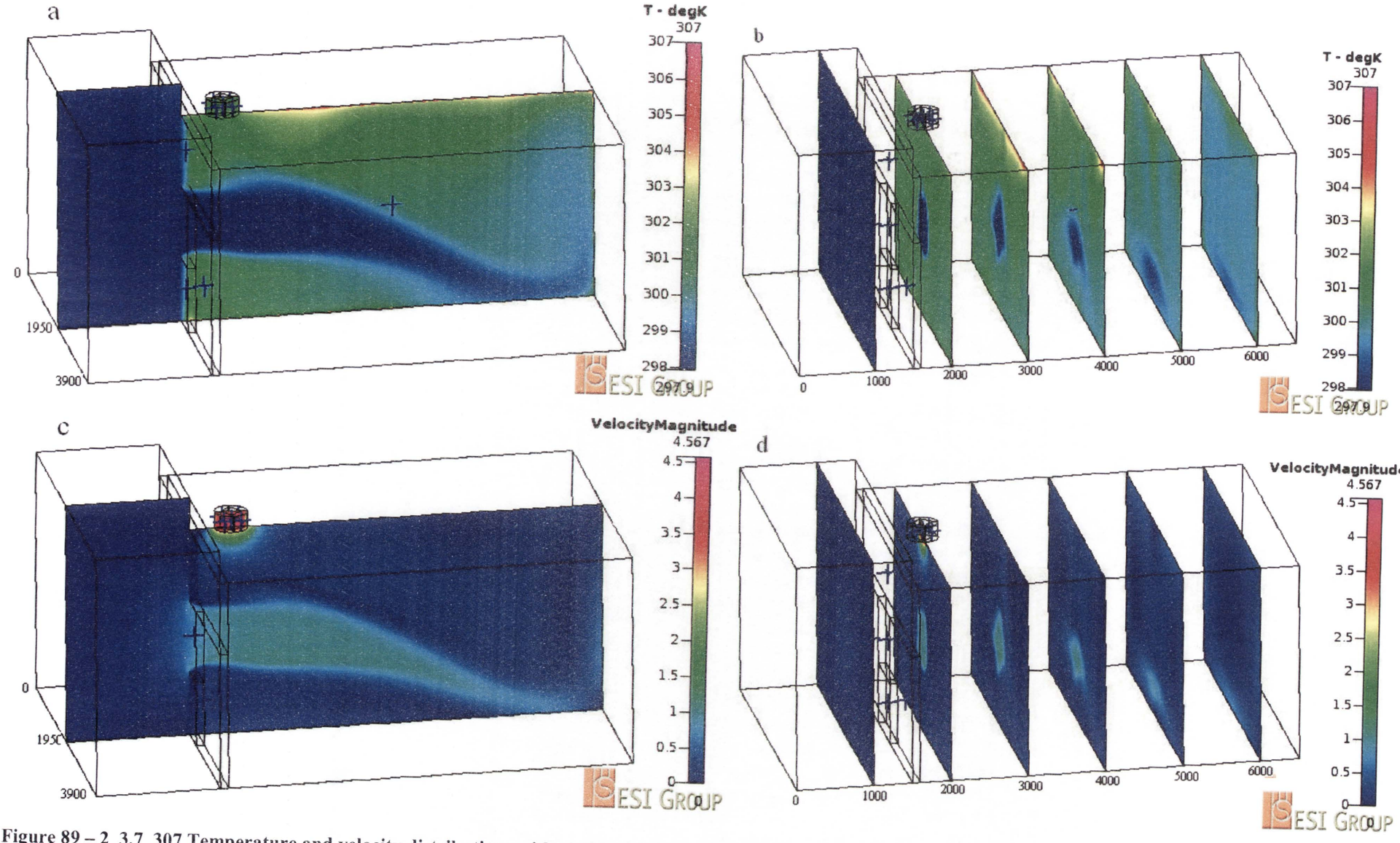

Figure 89 – 2_3.7_307 Temperature and velocity distributions with airflows through fan of 3.7 m/s

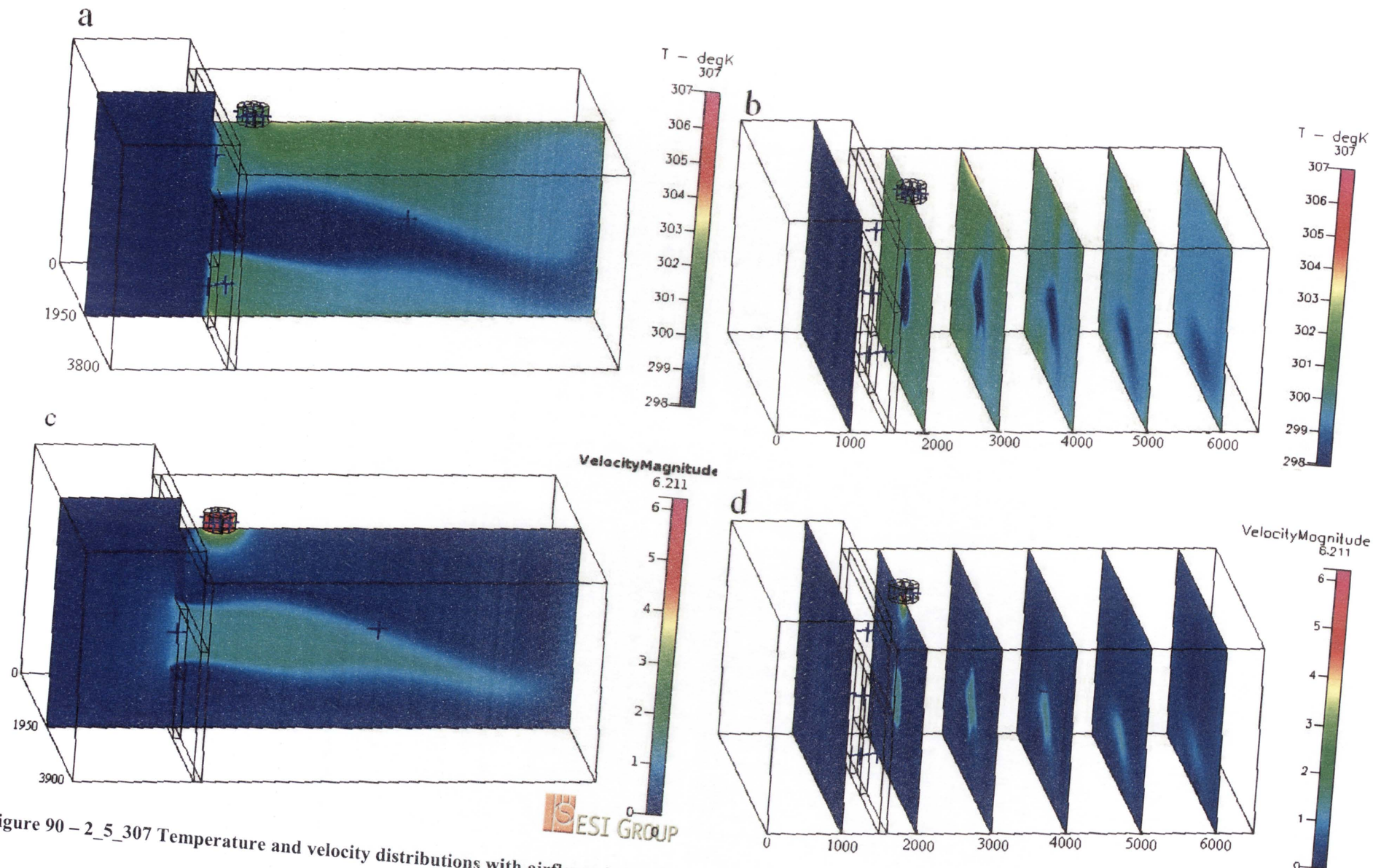

Figure 90 – 2_5_307 Temperature and velocity distributions with airflows through fan of 5 m/s

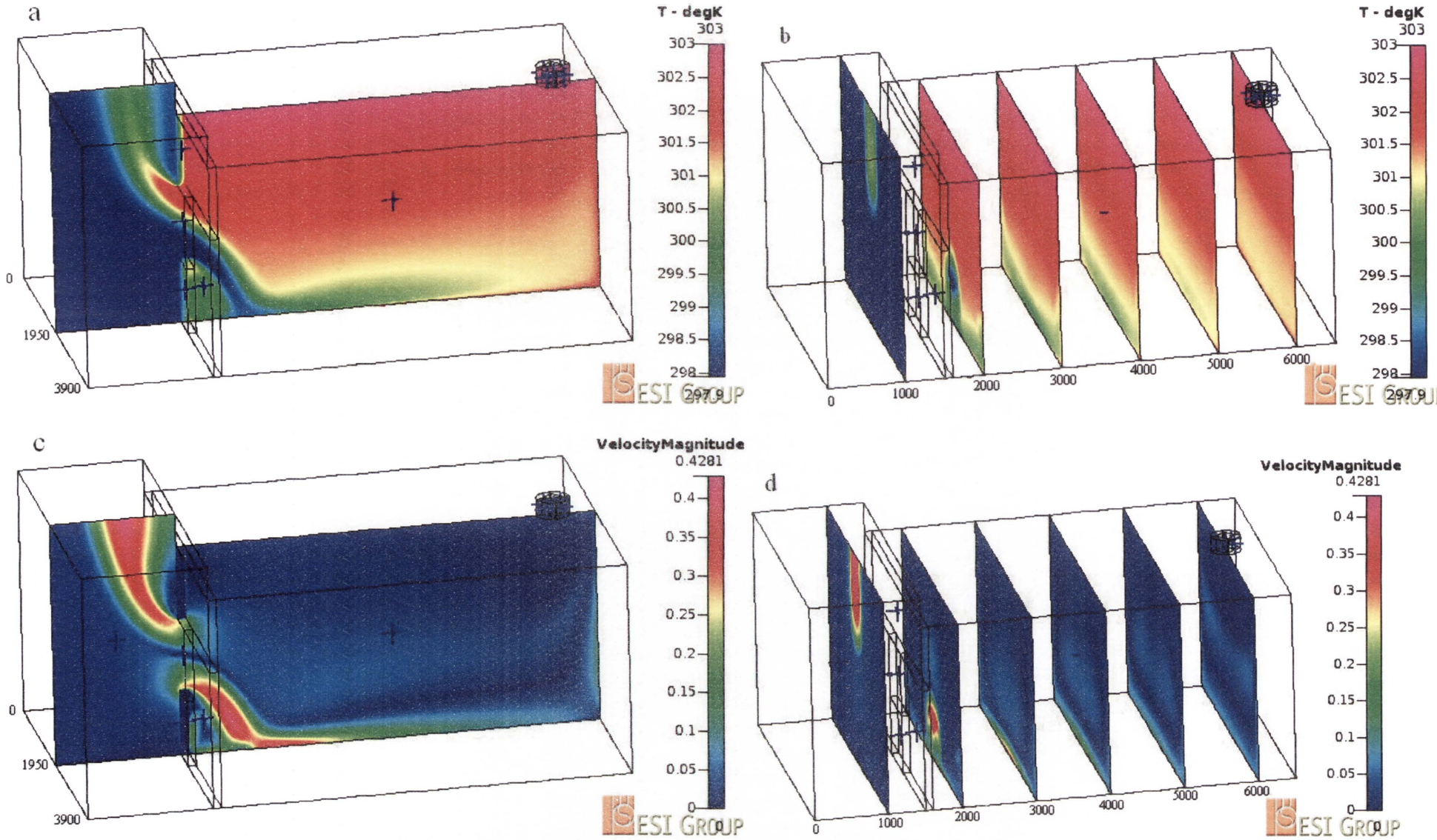

Figure 91 – 3_0.0001_303 Temperature and velocity distributions with airflows through fan of 0.0001 m/s

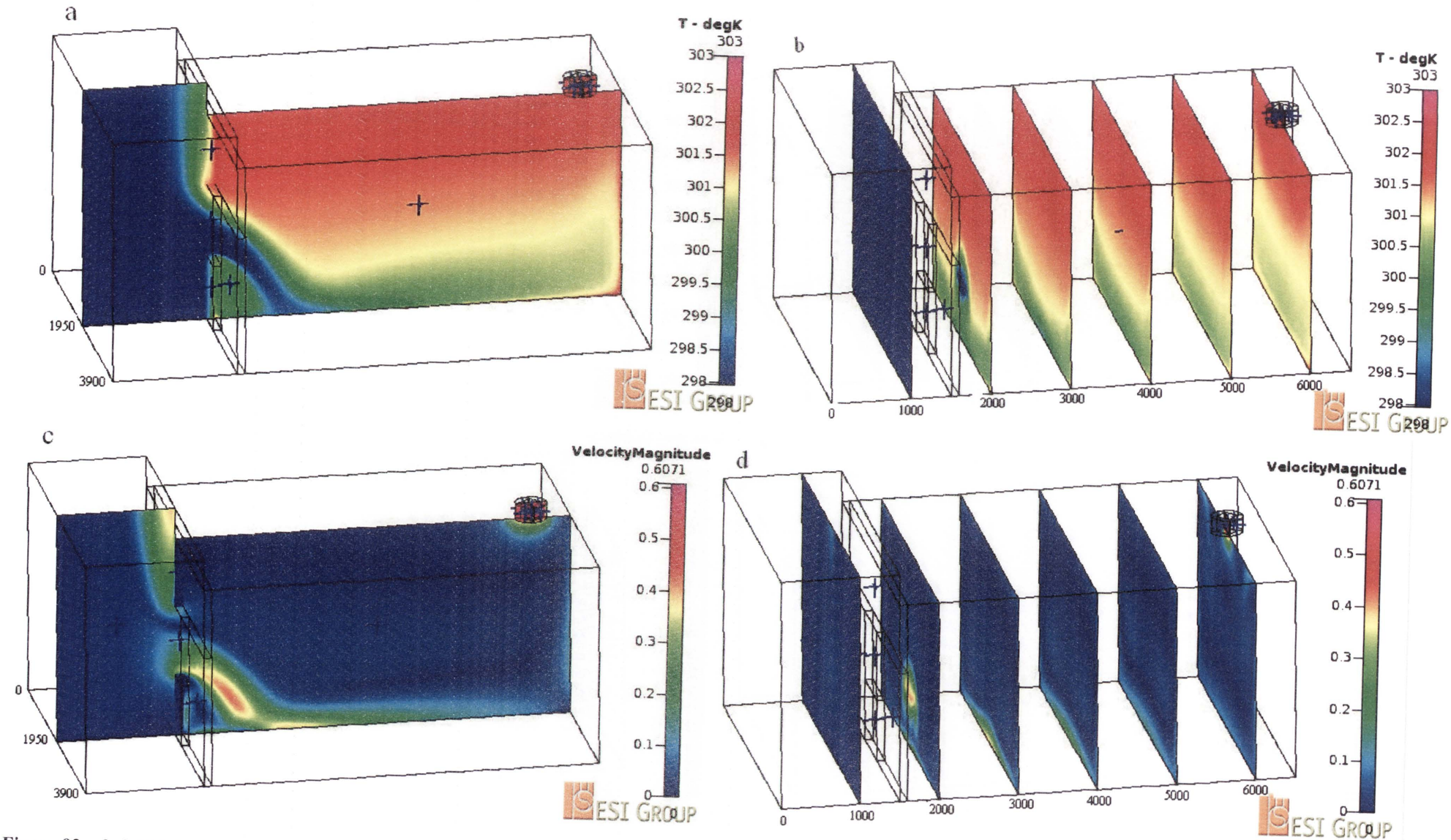

Figure 92 – 3_0.505_303 Temperature and velocity distributions with airflows through fan of 0.505 m/s

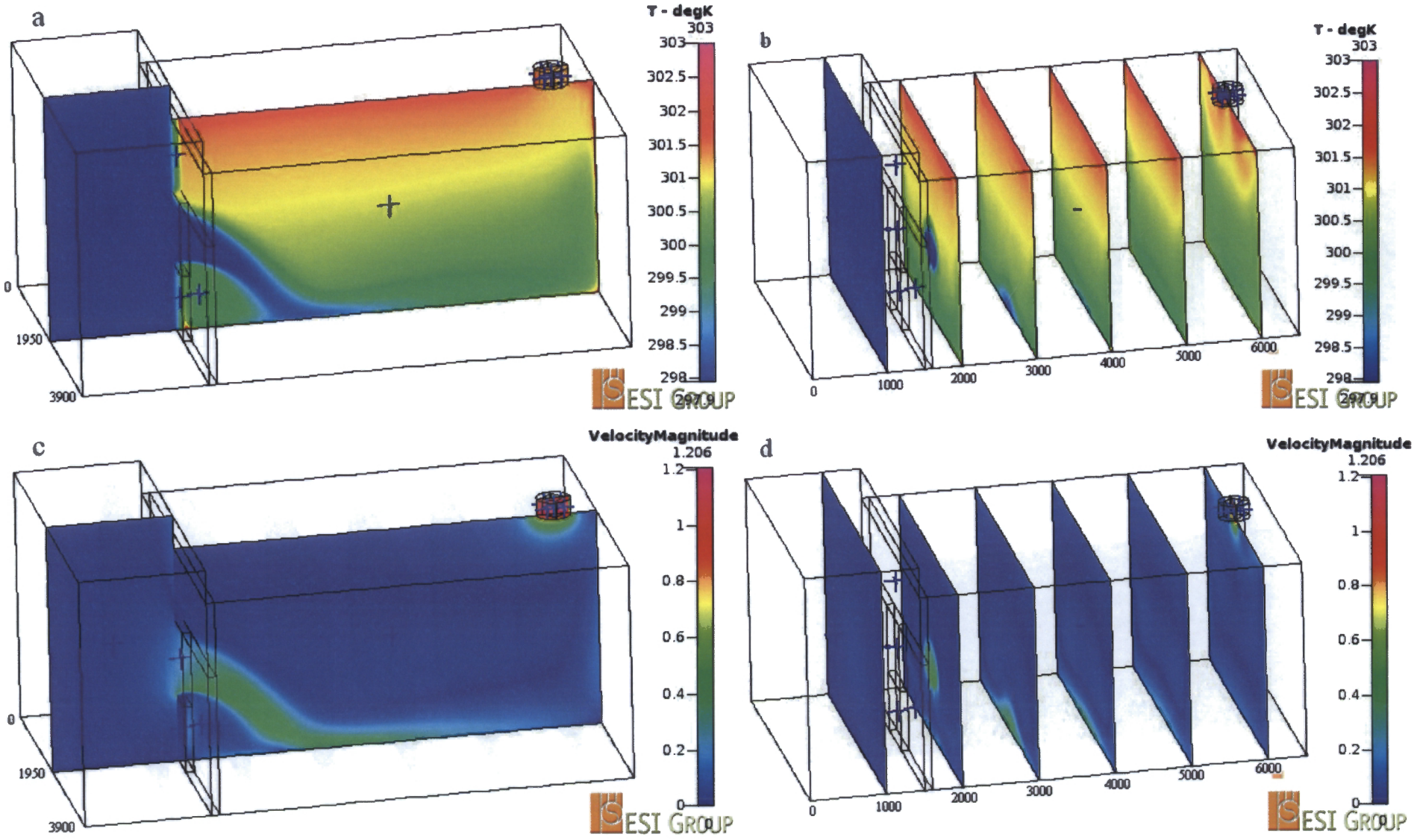

Figure 93 – 3_1_303 Temperature and velocity distributions with airflows through fan of 1 m/s

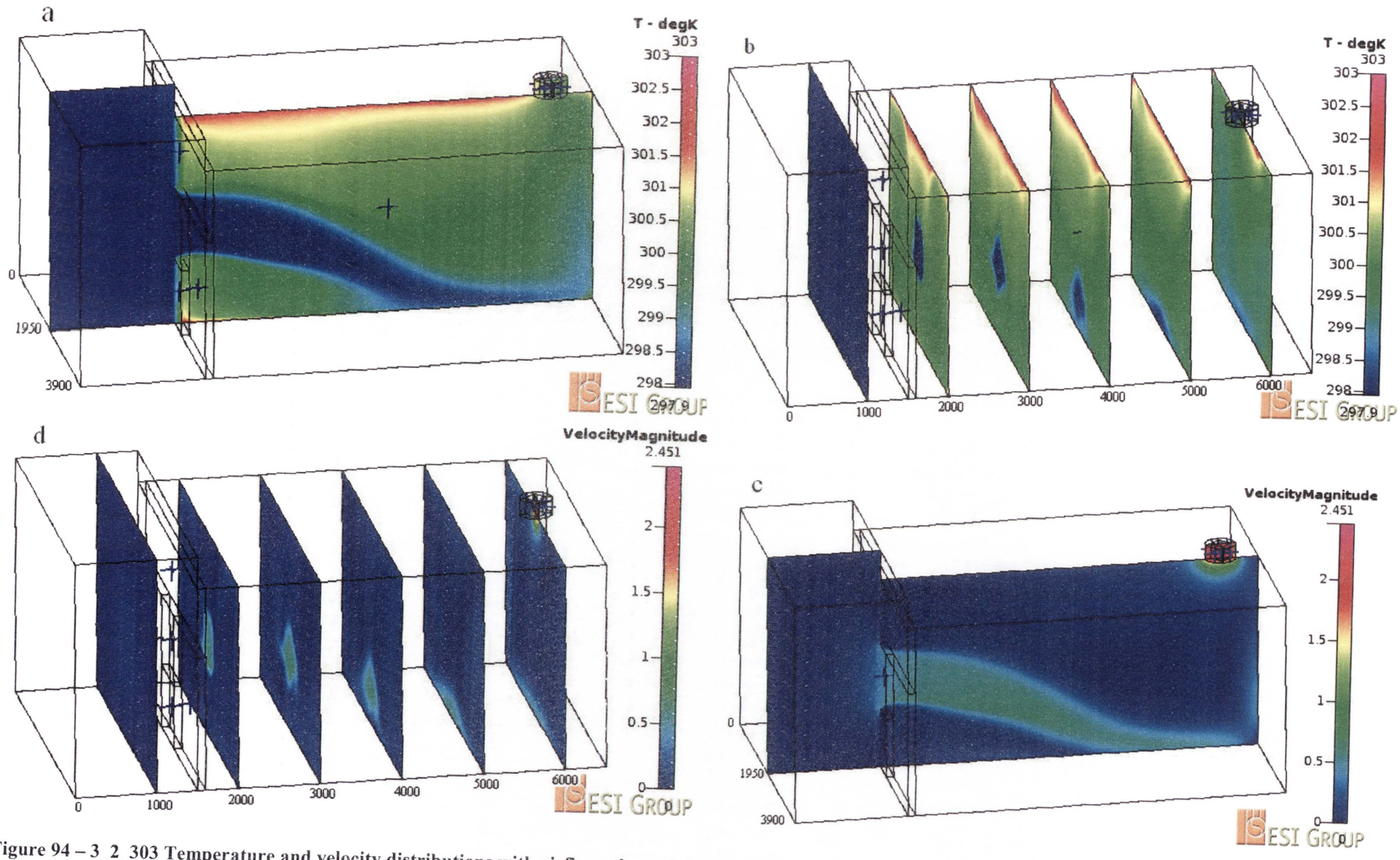

Figure 94 – 3_2_303 Temperature and velocity distributions with airflows through fan of 2 m/s

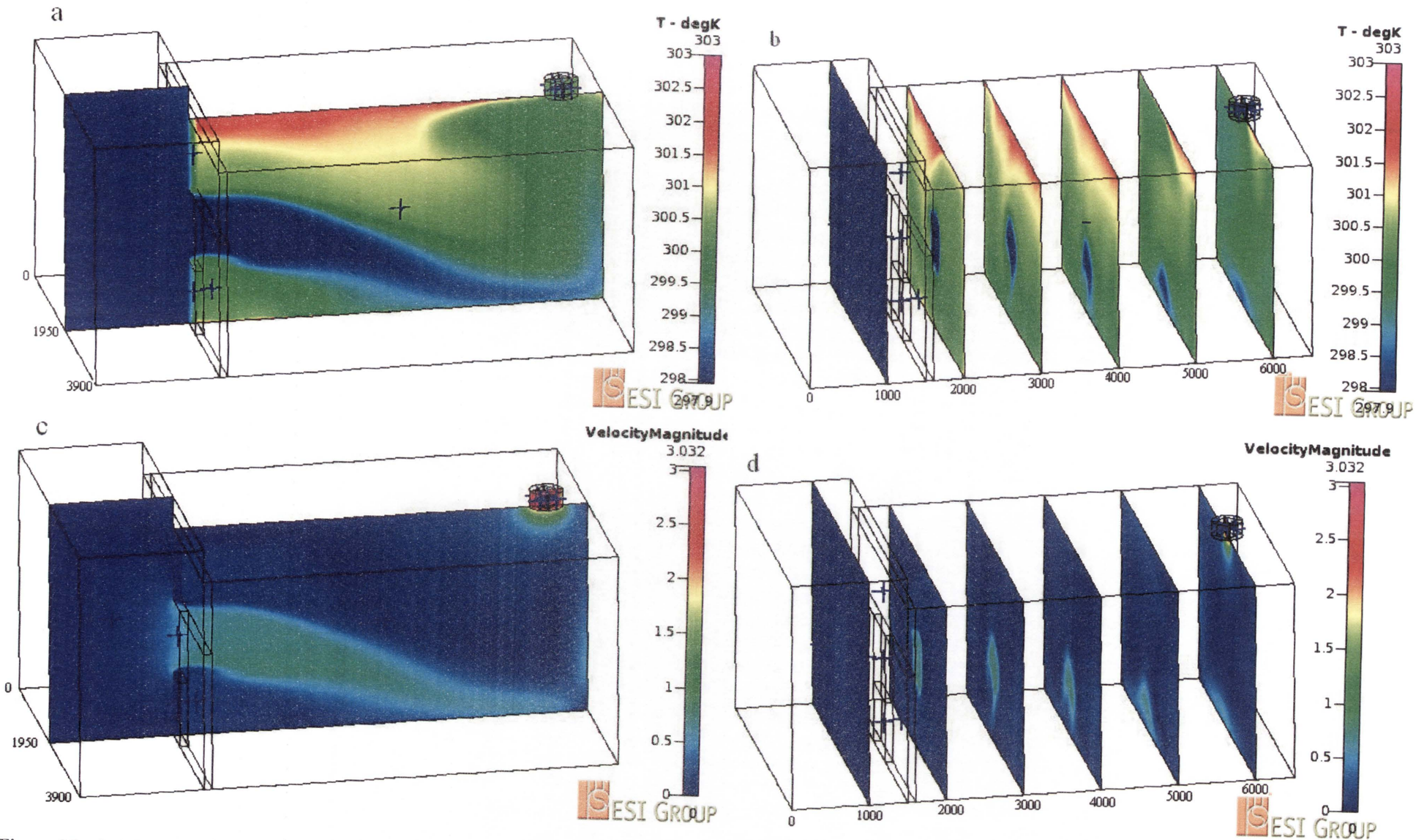

Figure 95 – 3_2.5_303 Temperature and velocity distributions with airflows through fan of 2.5 m/s

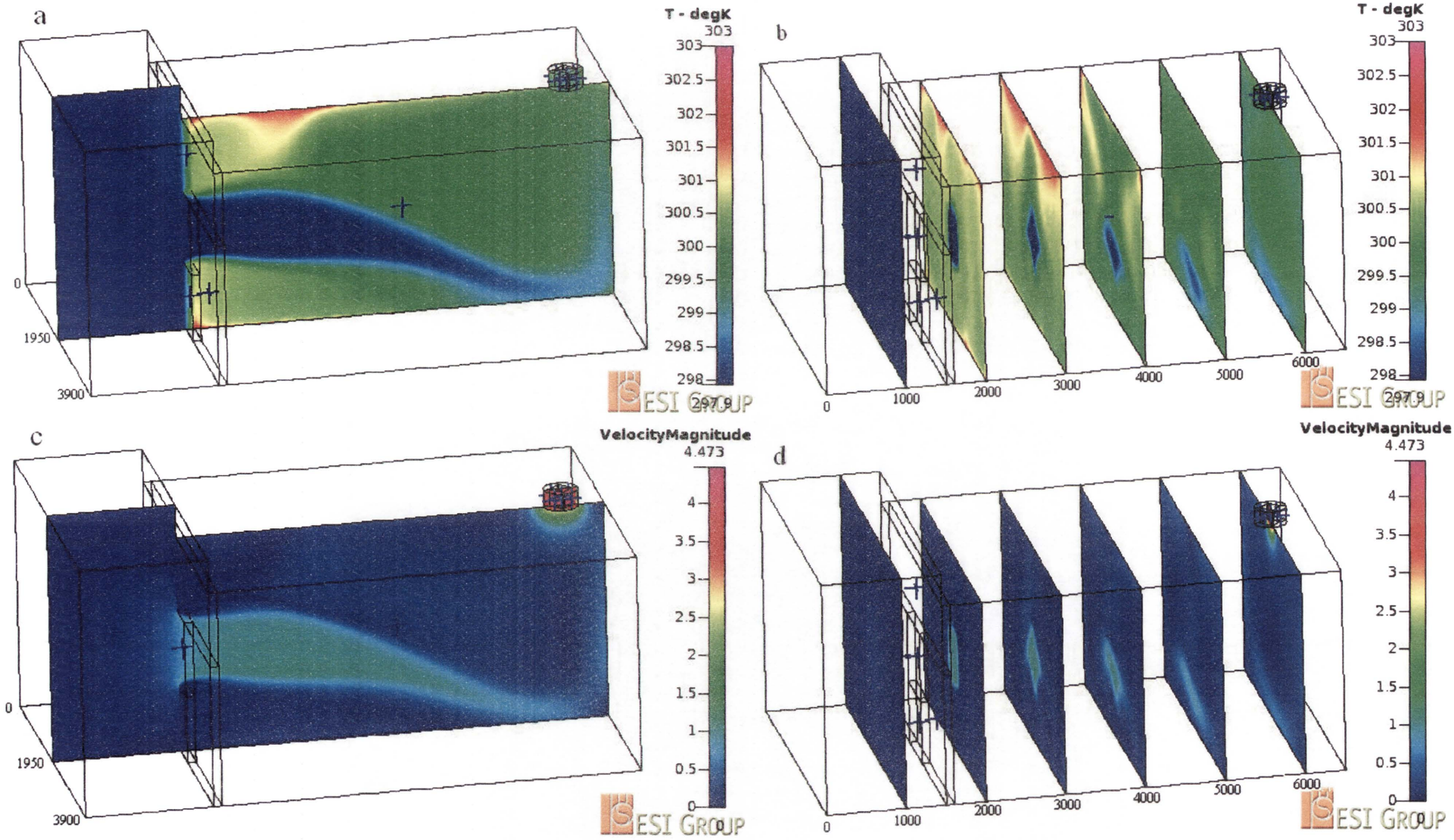

Figure 96 – 3_3.7_303 Temperature and velocity distributions with airflows through fan of 3.7 m/s

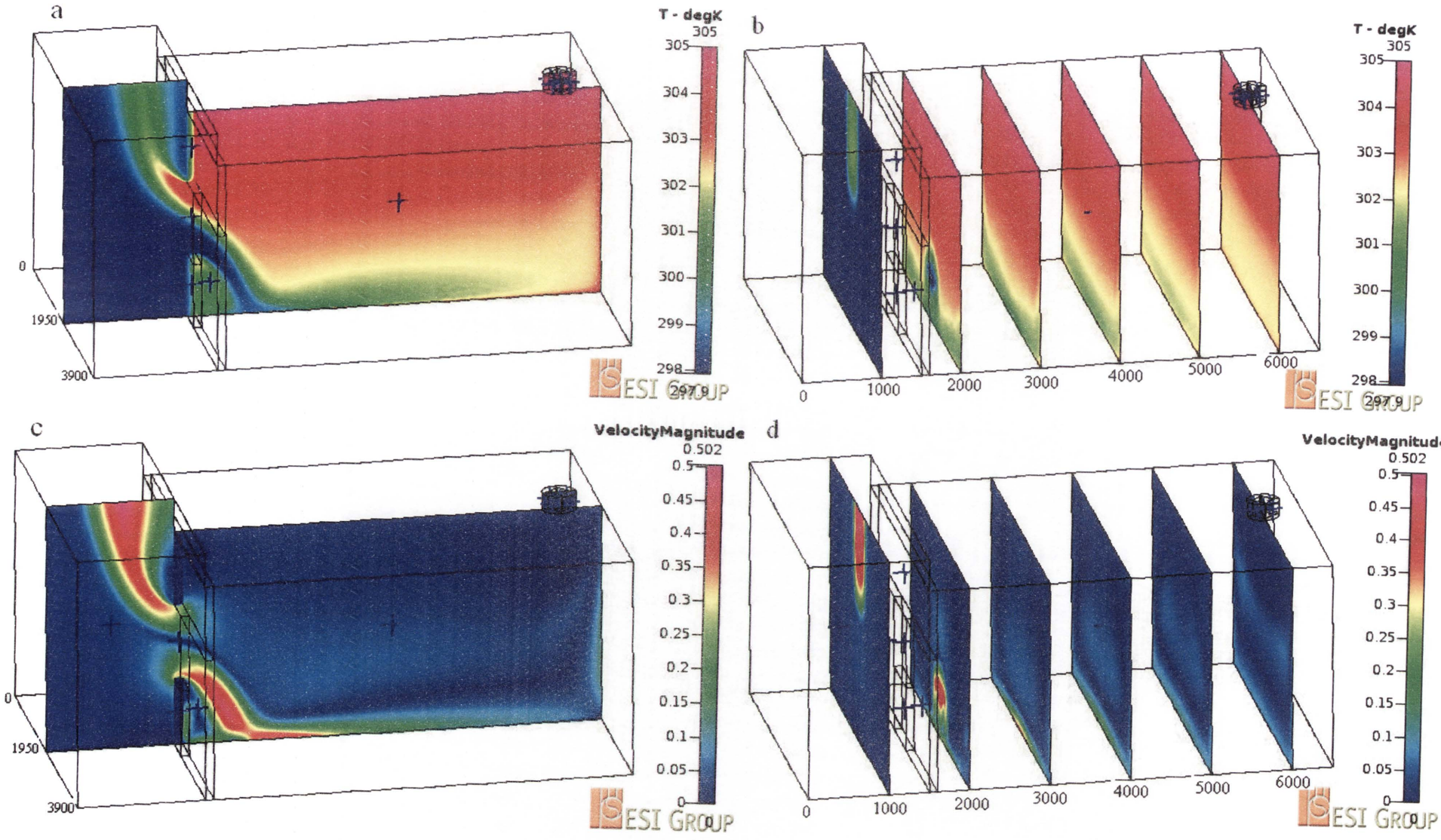

Figure 97 – 3_0.0001_305 Temperature and velocity distributions with airflows through fan of 0.0001 m/s

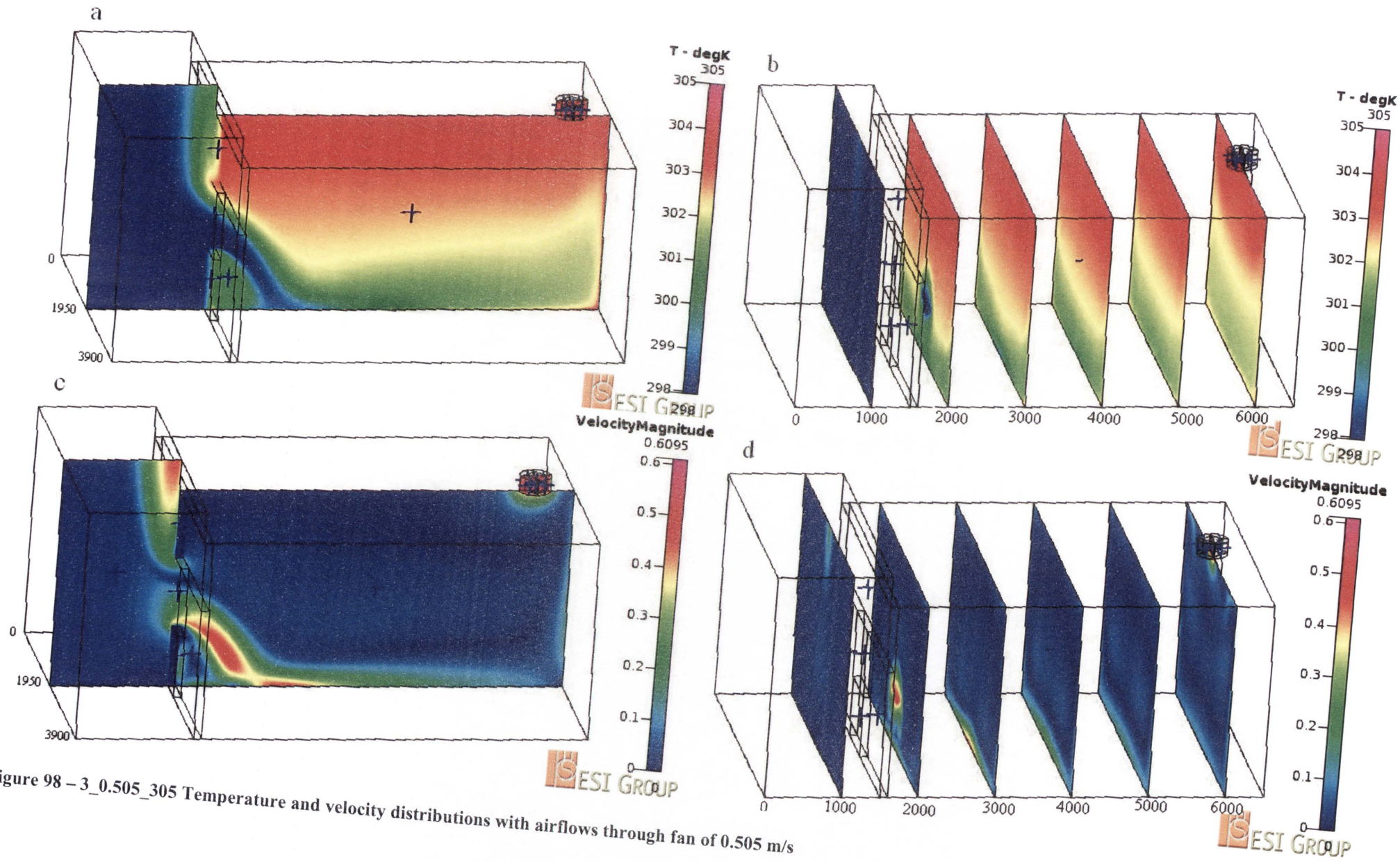

Figure 98 – 3_0.505_305 Temperature and velocity distributions with airflows through fan of 0.505 m/s

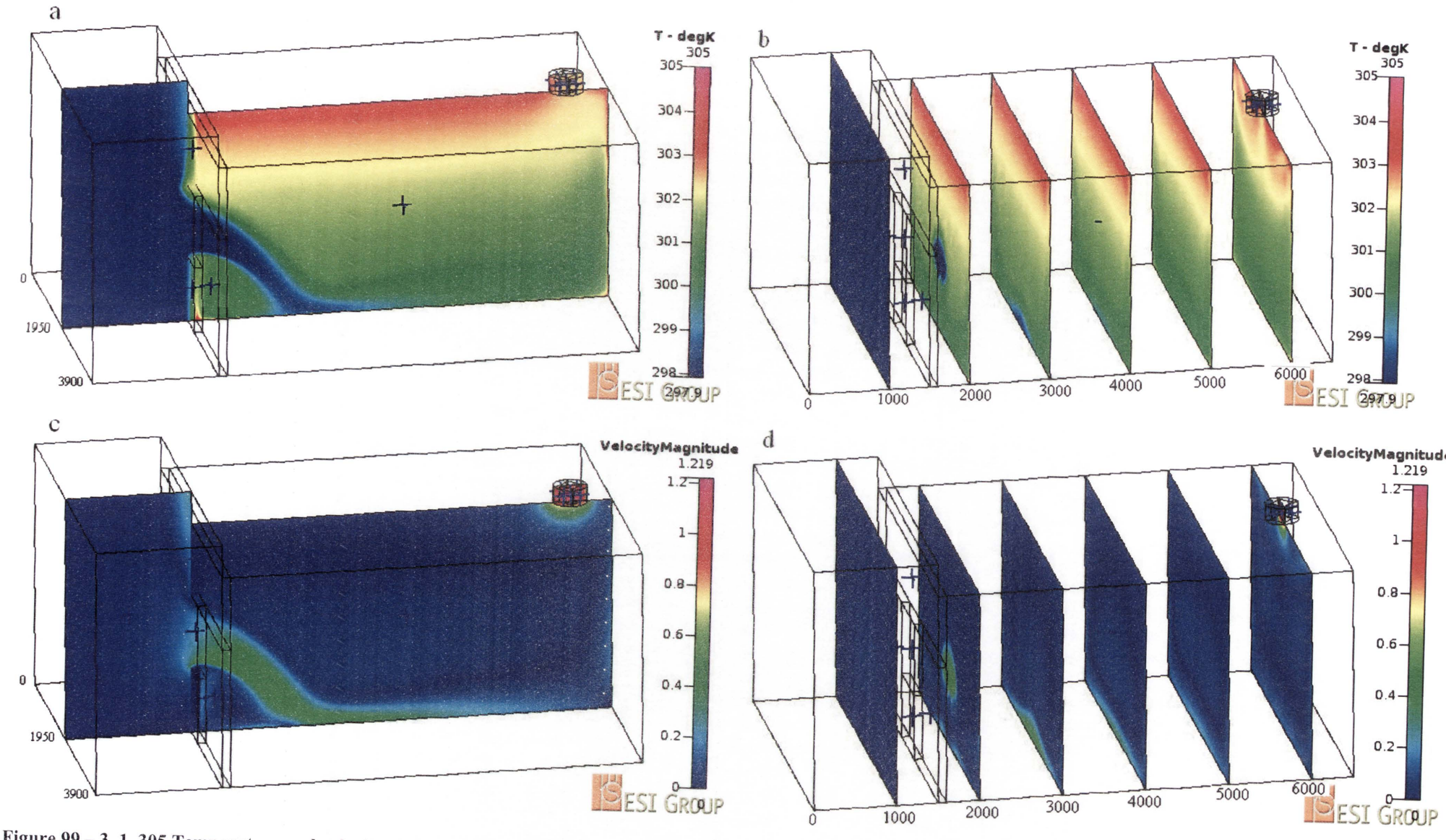

Figure 99 – 3_1_305 Temperature and velocity distributions with airflows through fan of 1 m/s

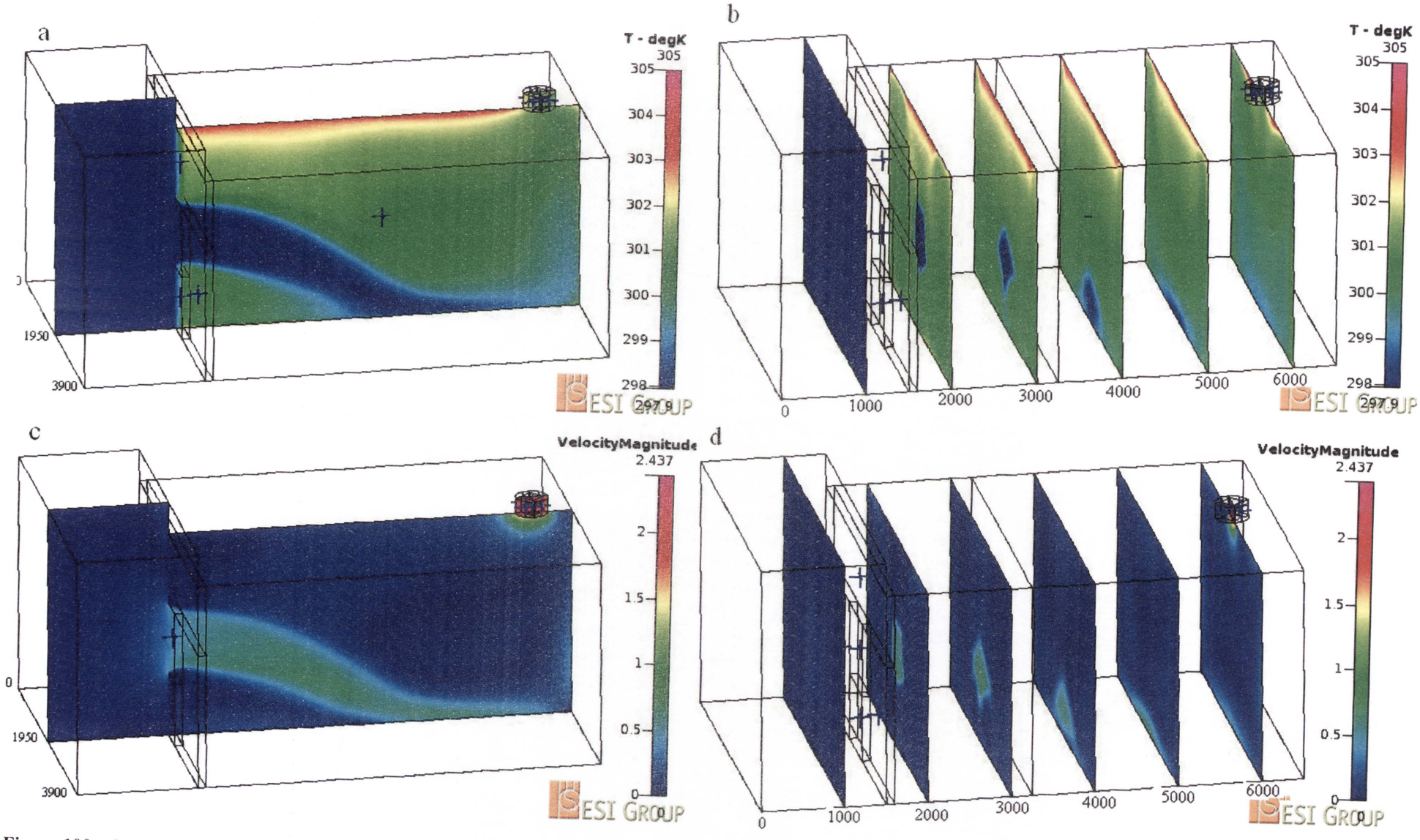

Figure 100 – 3_2_305 Temperature and velocity distributions with airflows through fan of 2 m/s

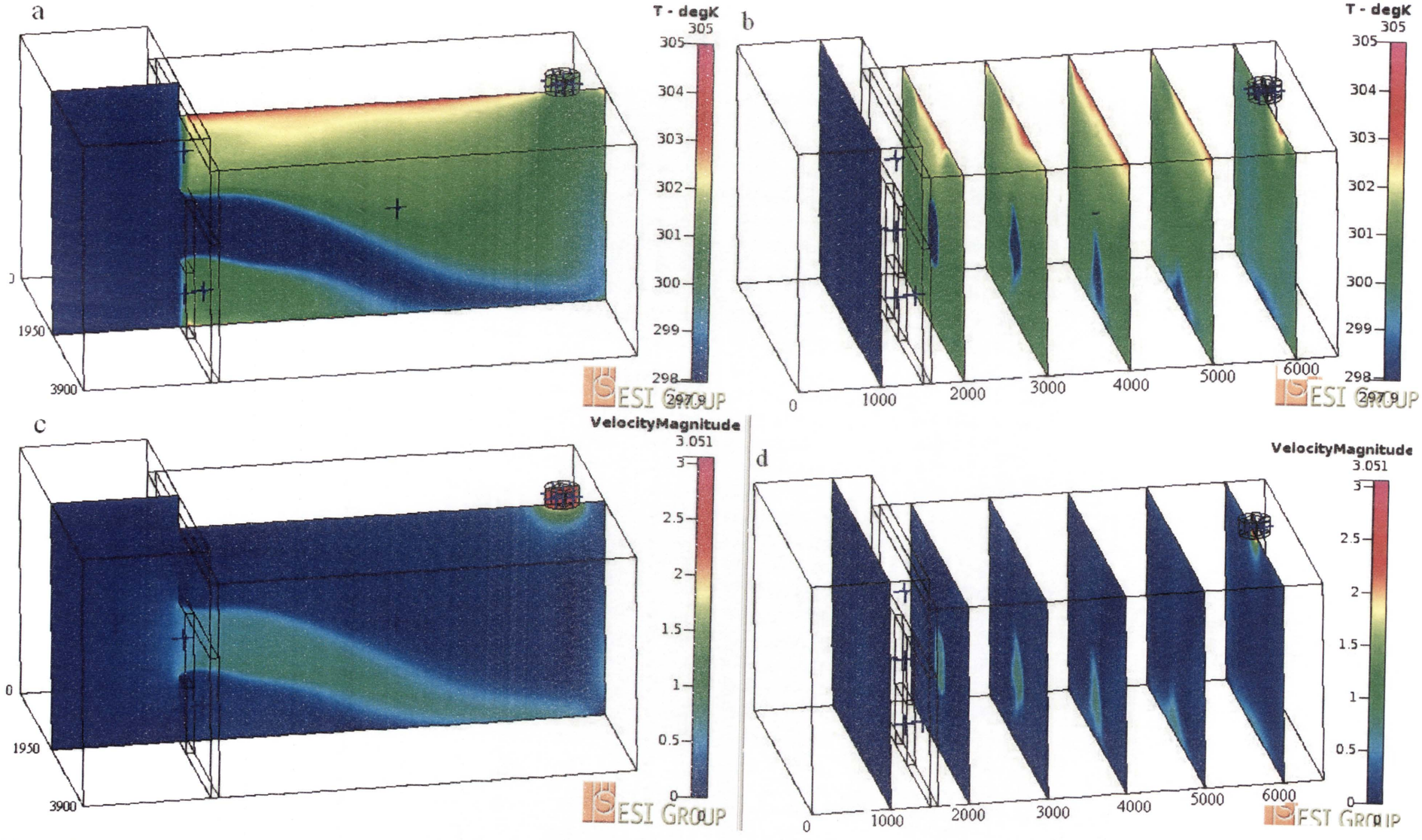

Figure 101 – 3_2.5_305 Temperature and velocity distributions with airflows through fan of 2.5 m/s

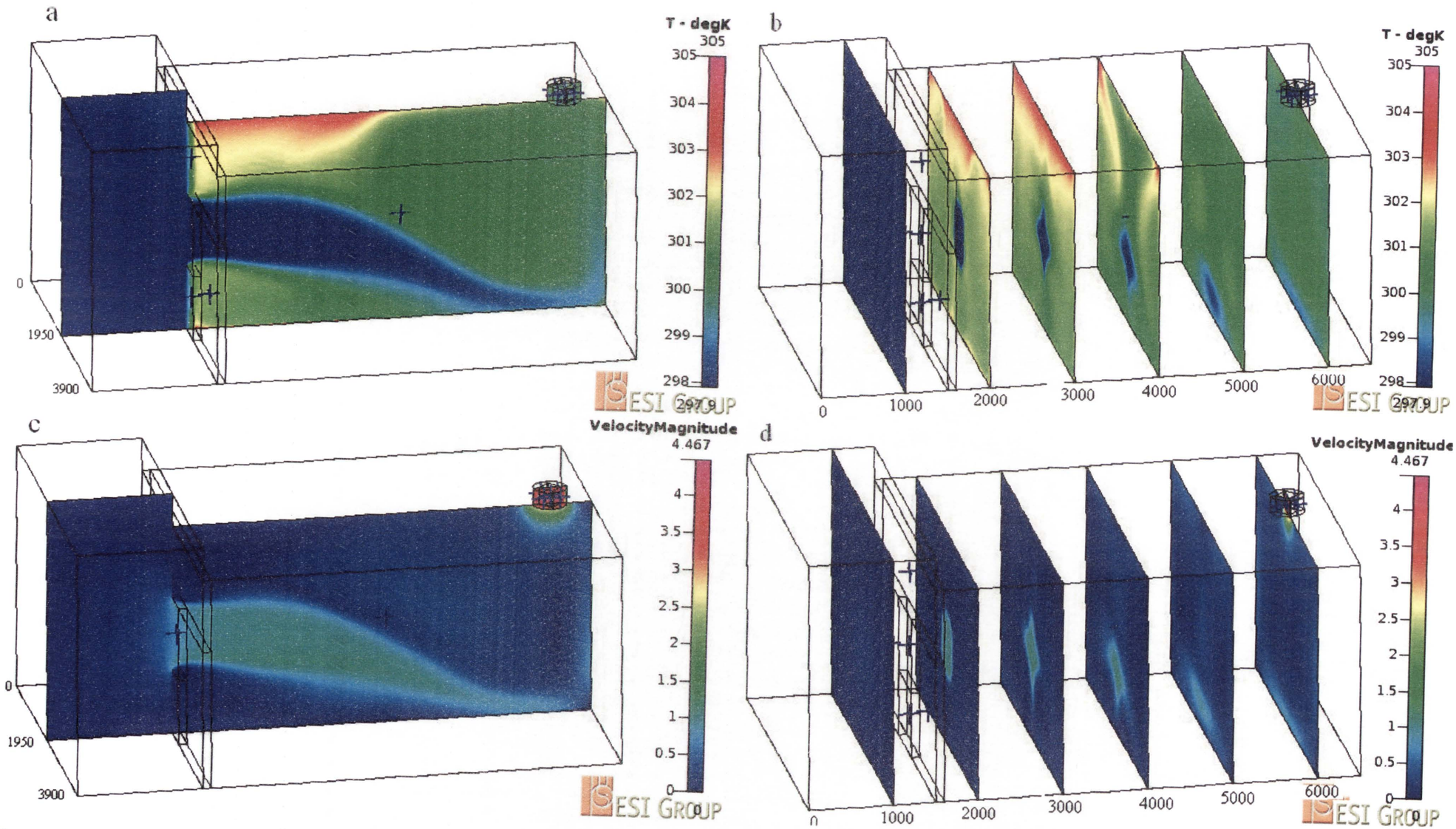

Figure 102 – 3_3.7_305 Temperature and velocity distributions with airflows through fan of 3.7 m/s

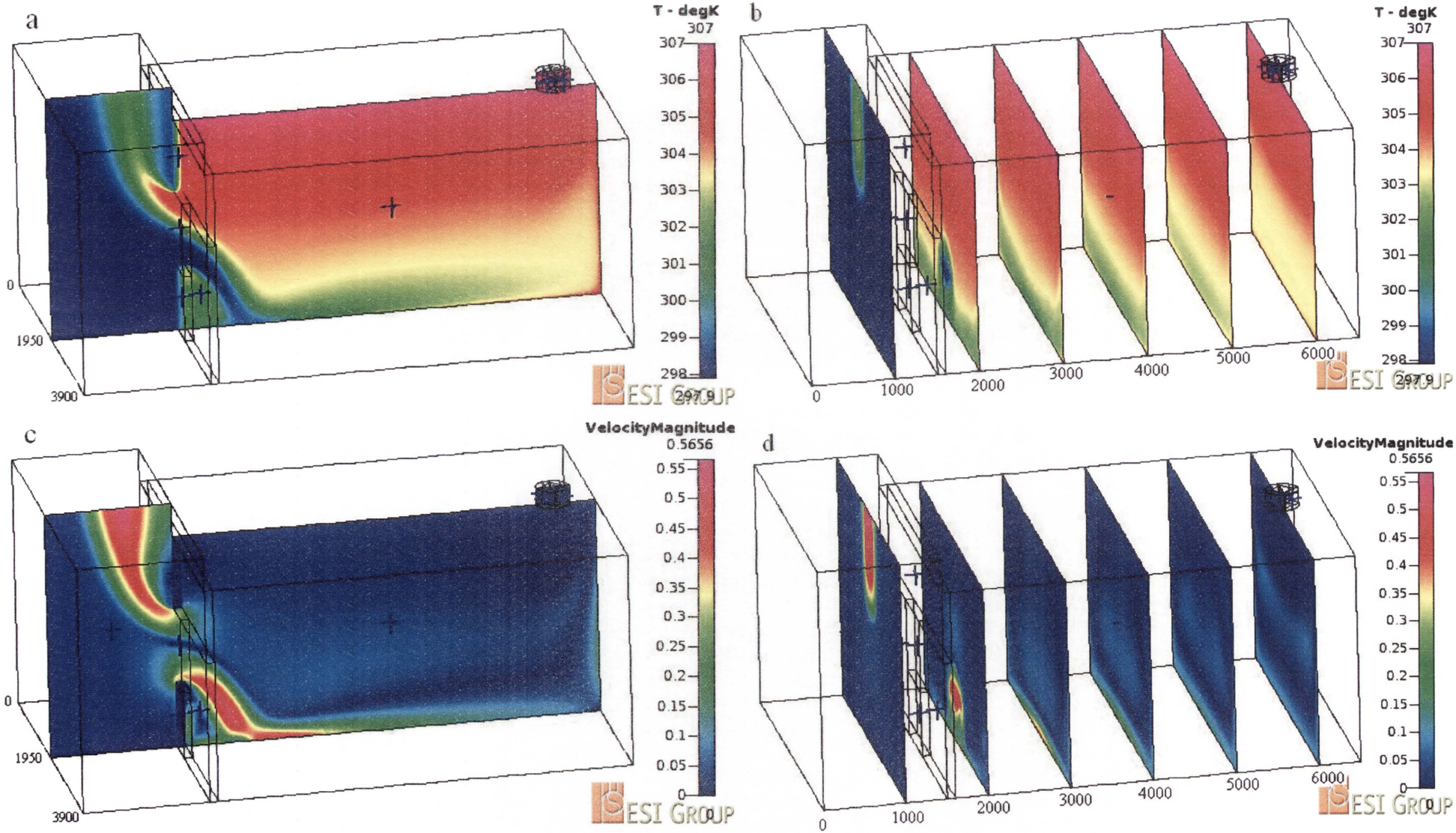

Figure 103 – 3_0.0001_307 Temperature and velocity distributions with airflows through fan of 0.0001 m/s

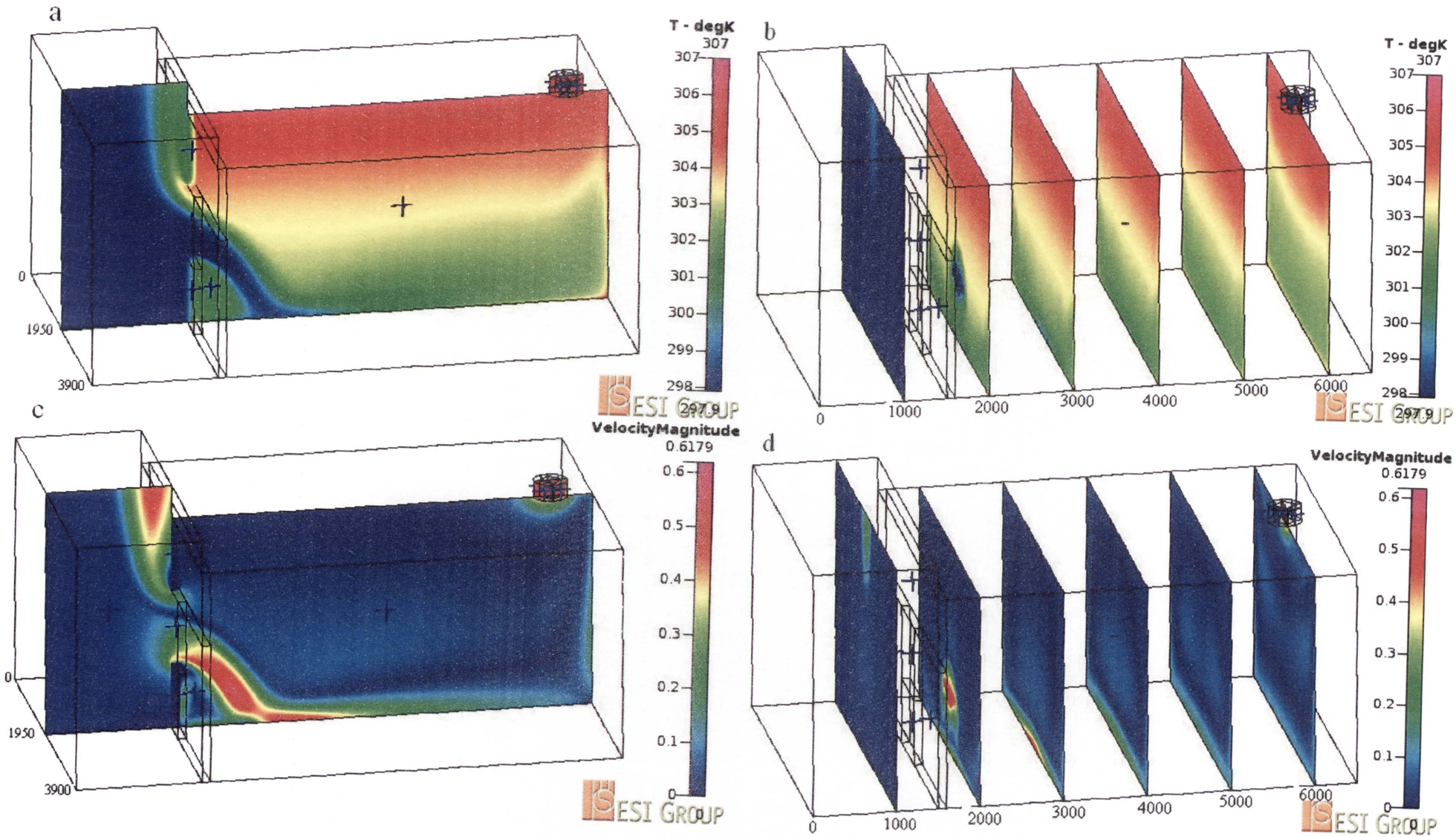

Figure 104 – 3_0.505_307 Temperature and velocity distributions with airflows through fan of 0.505 m/s

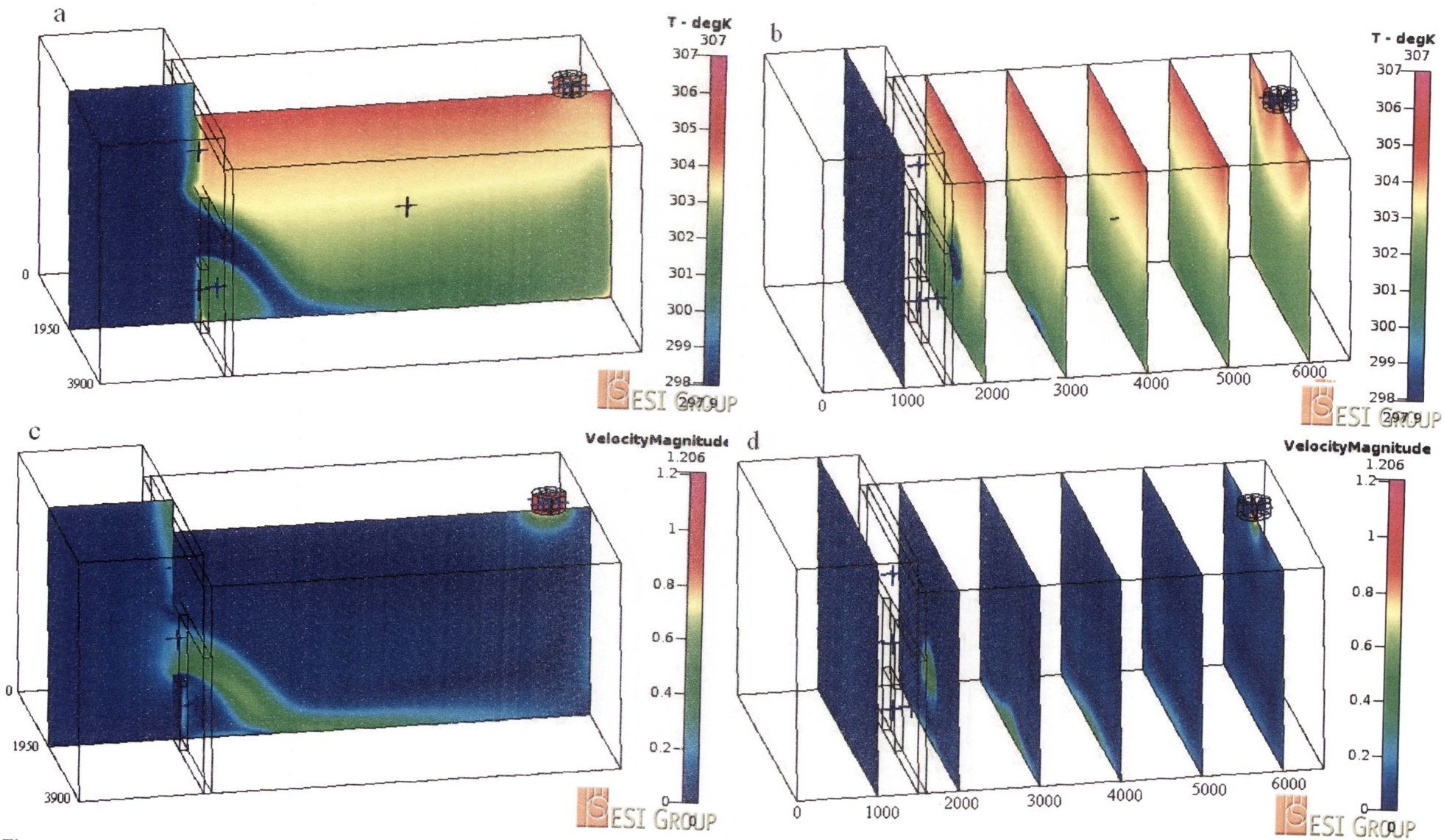

Figure 105 – 3_1_307 Temperature and velocity distributions with airflows through fan of 1 m/s

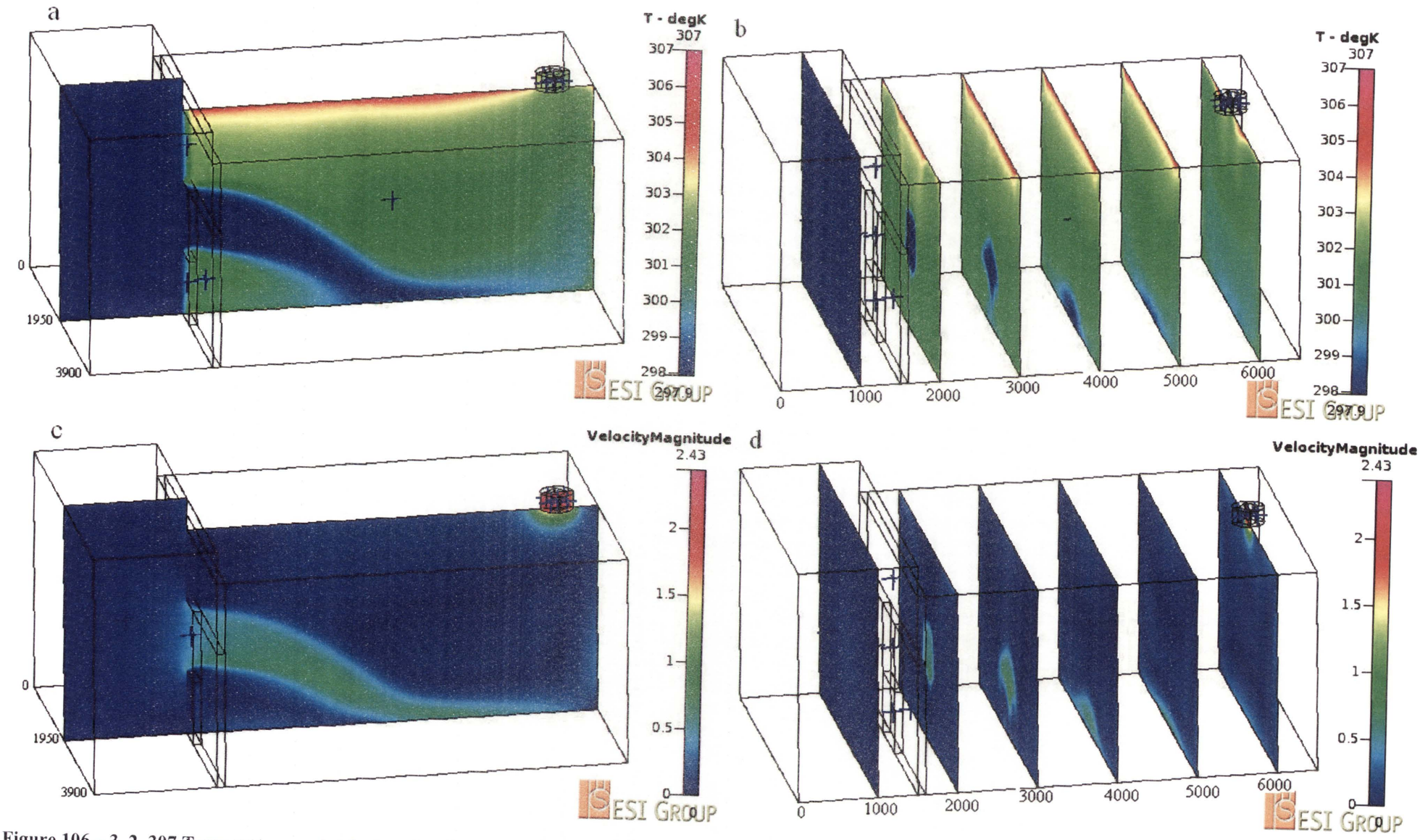

Figure 106 – 3_2_307 Temperature and velocity distributions with airflows through fan of 2 m/s

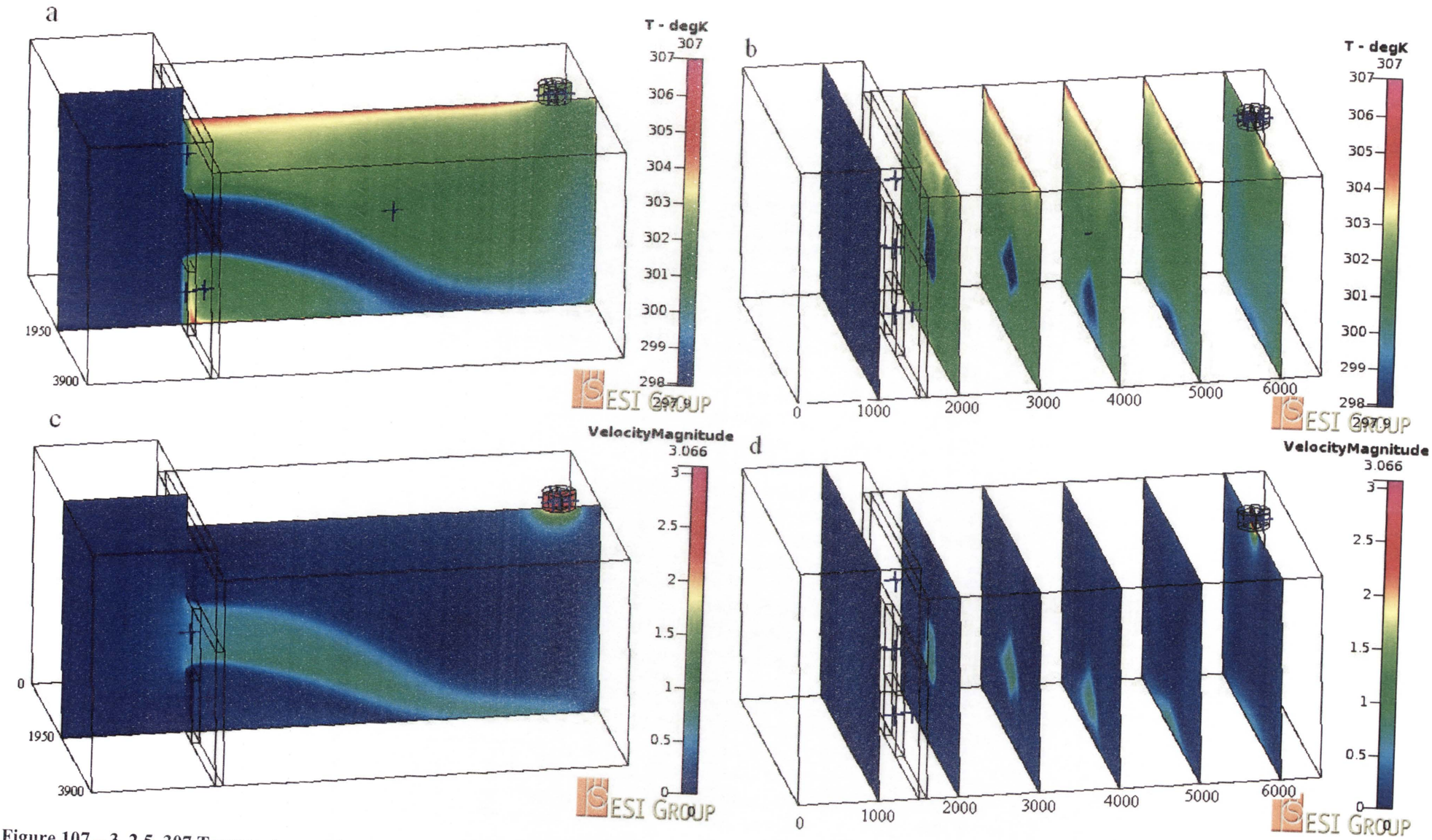

Figure 107 – 3_2.5_307 Temperature and velocity distributions with airflows through fan of 2.5 m/s

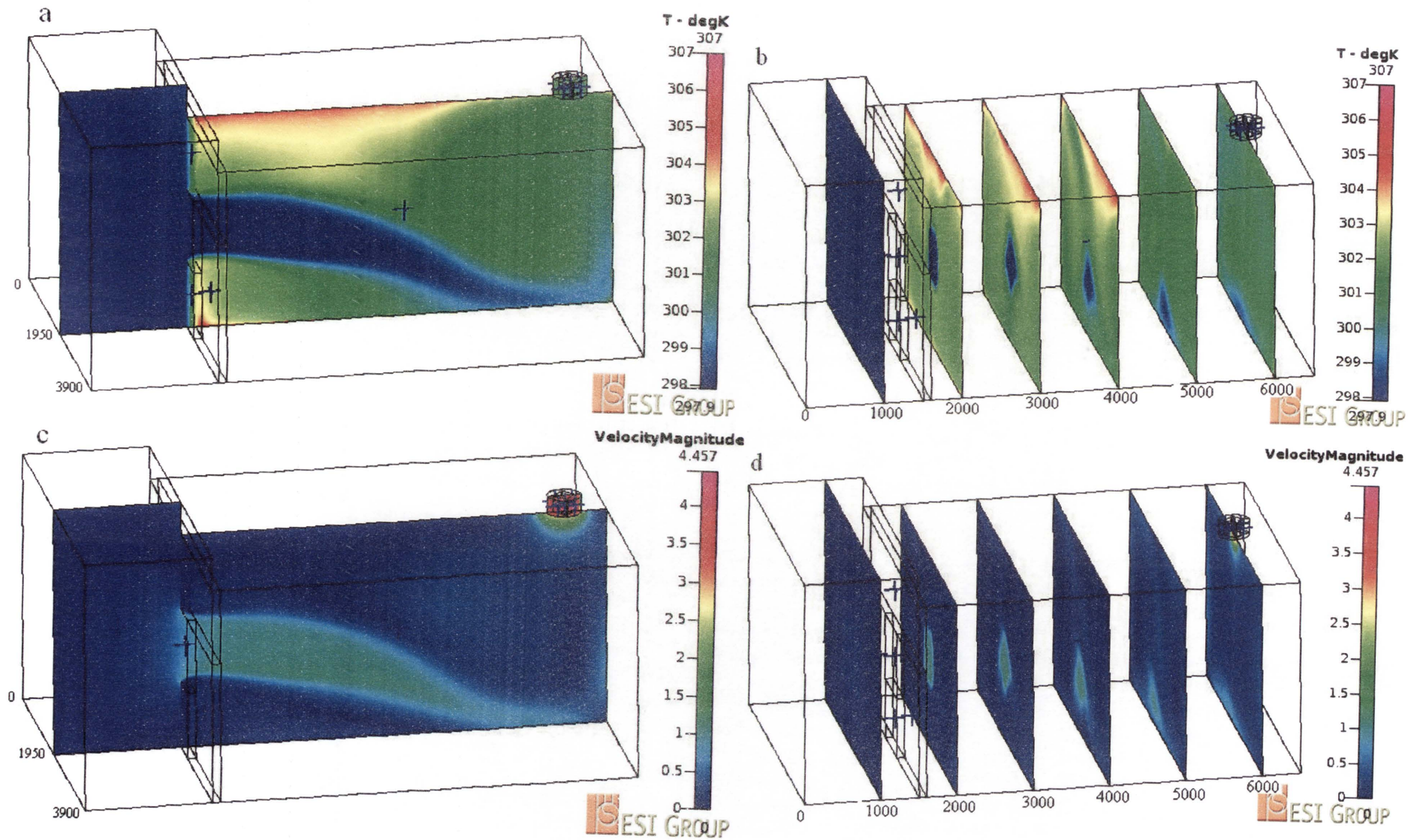

Figure 108 – 3_3.7_307 Temperature and velocity distributions with airflows through fan of 3.7 m/s

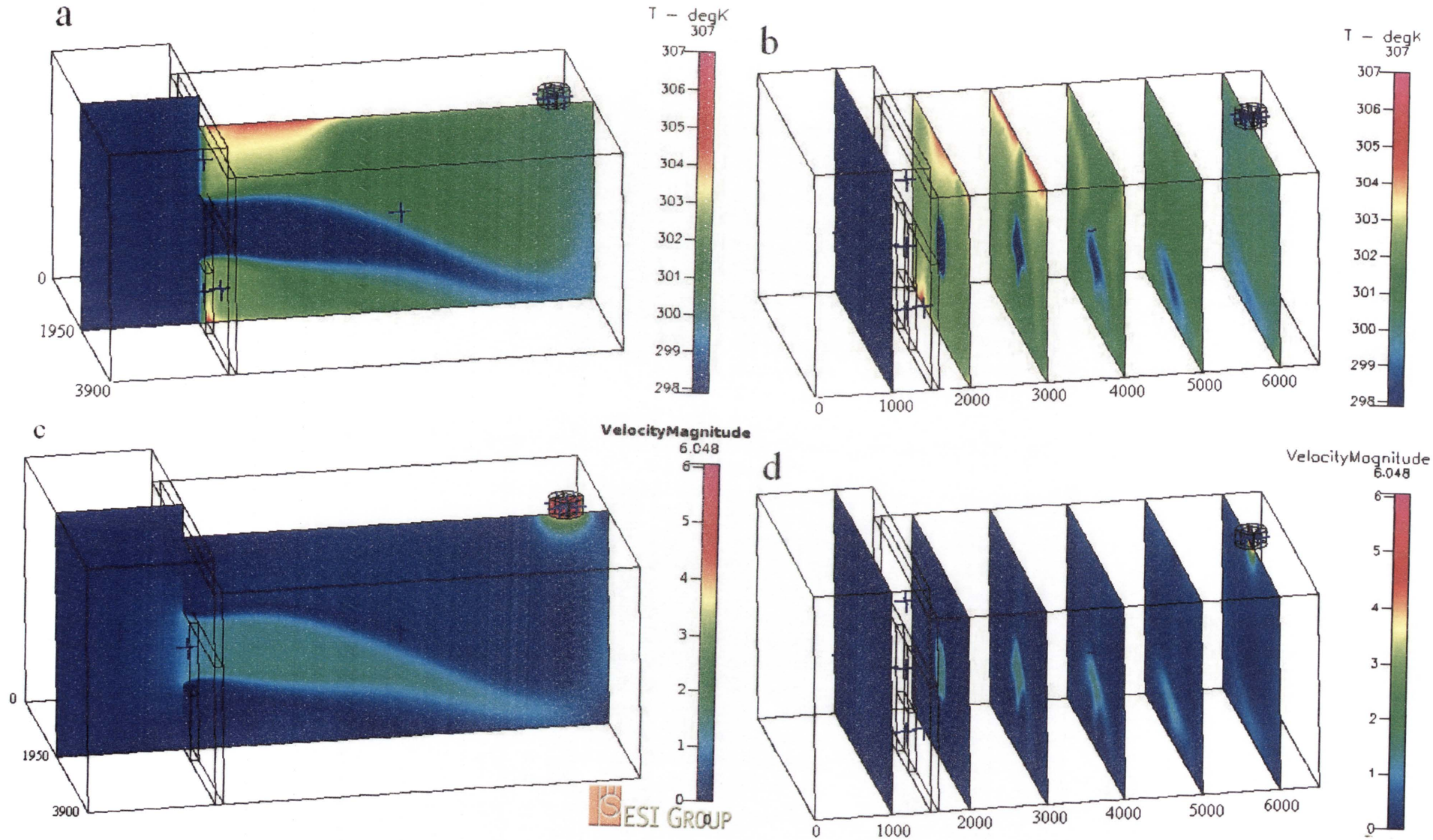

Figure 109 – 3_5_307 Temperature and velocity distributions with airflows through fan of 5 m/s

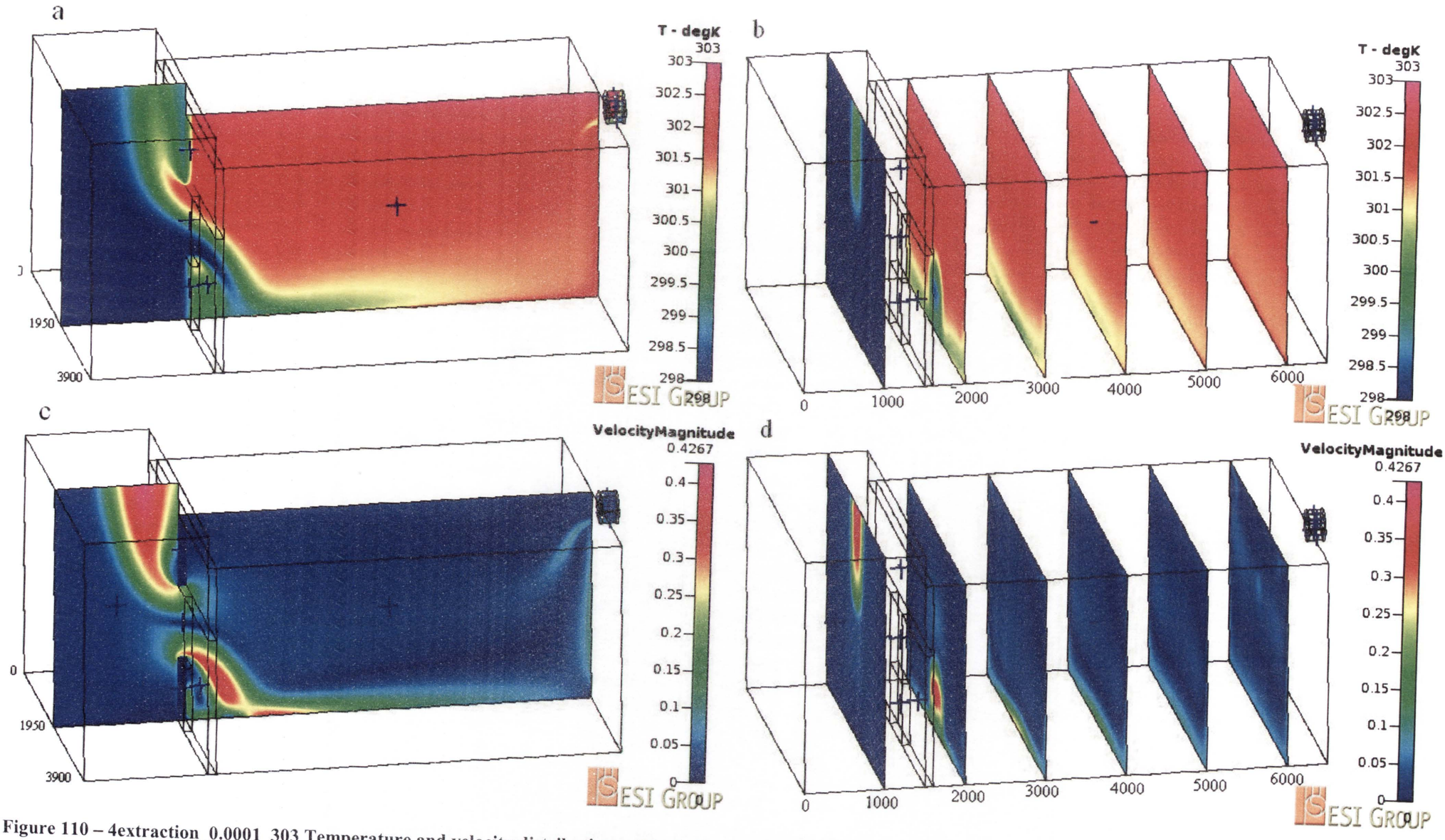

Figure 110 – 4extraction_0.0001_303 Temperature and velocity distributions with airflows through fan of 0.0001 m/s

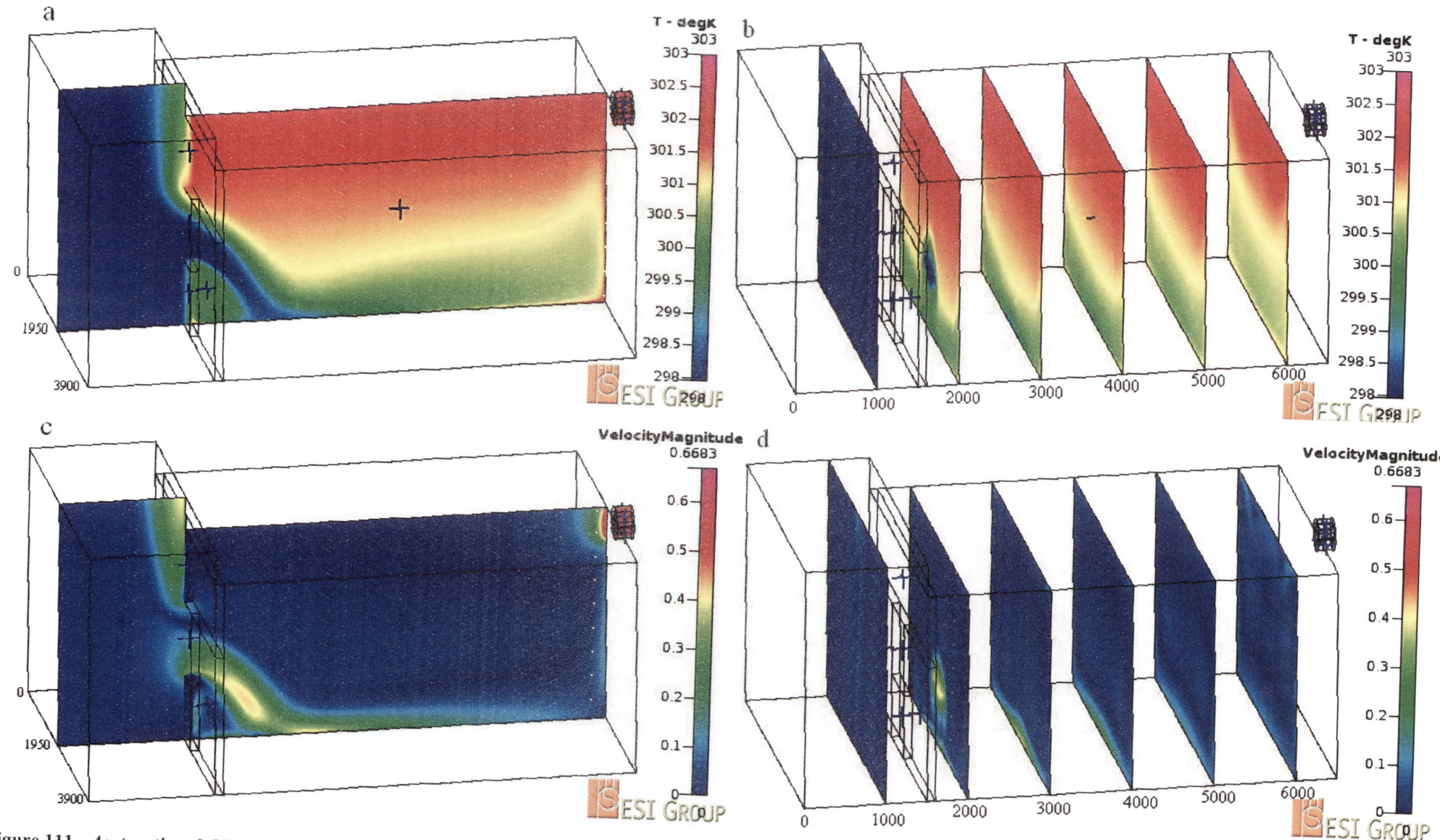

Figure 111 – 4extraction_0.505_303 Temperature and velocity distributions with airflows through fan of 0.505 m/s

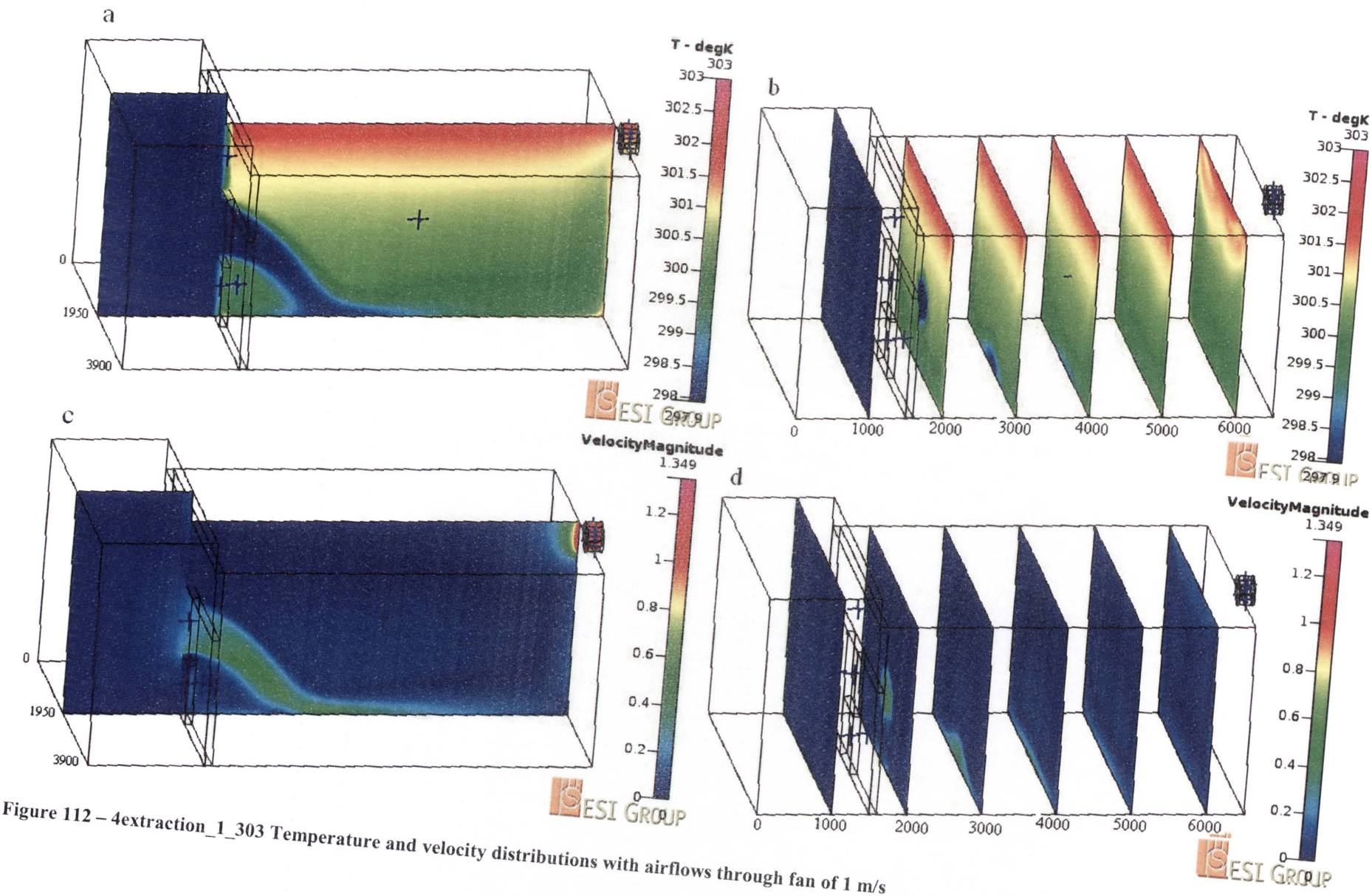

Figure 112 – 4extraction_1_303 Temperature and velocity distributions with airflows through fan of 1 m/s

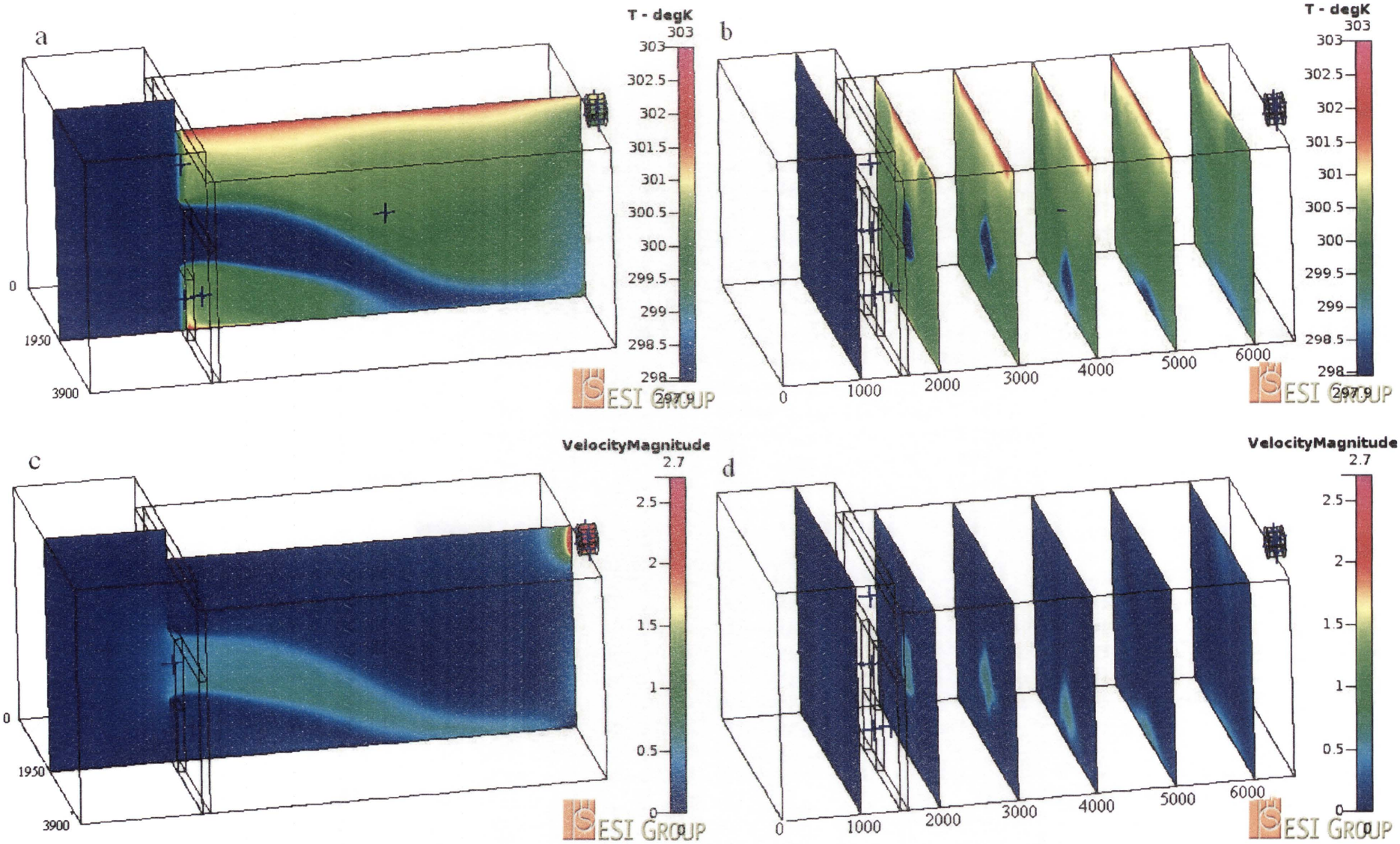

Figure 113 – 4extraction_2_303 Temperature and velocity distributions with airflows through fan of 2m/s

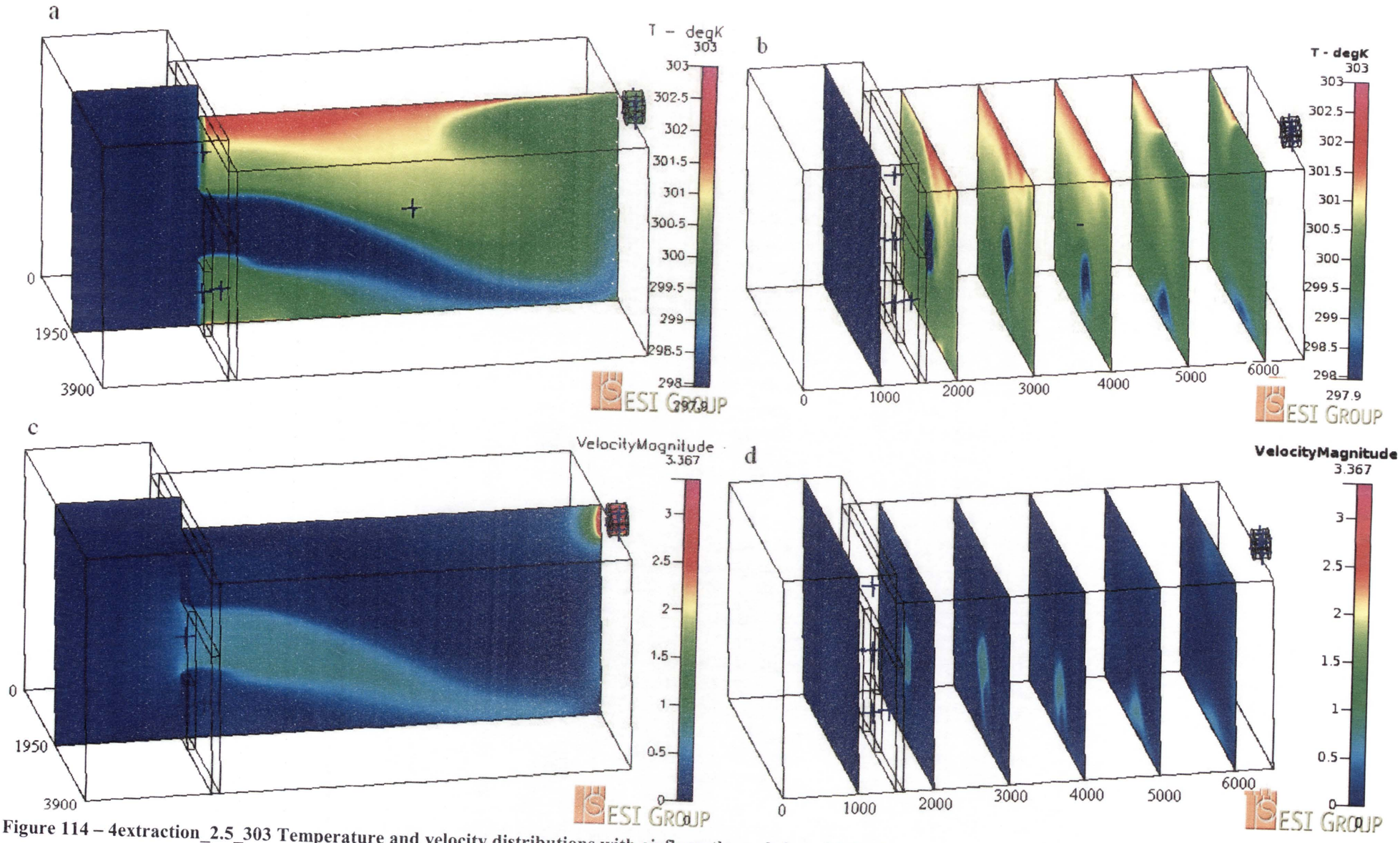

Figure 114 – 4extraction_2.5_303 Temperature and velocity distributions with airflows through fan of 2.5 m/s

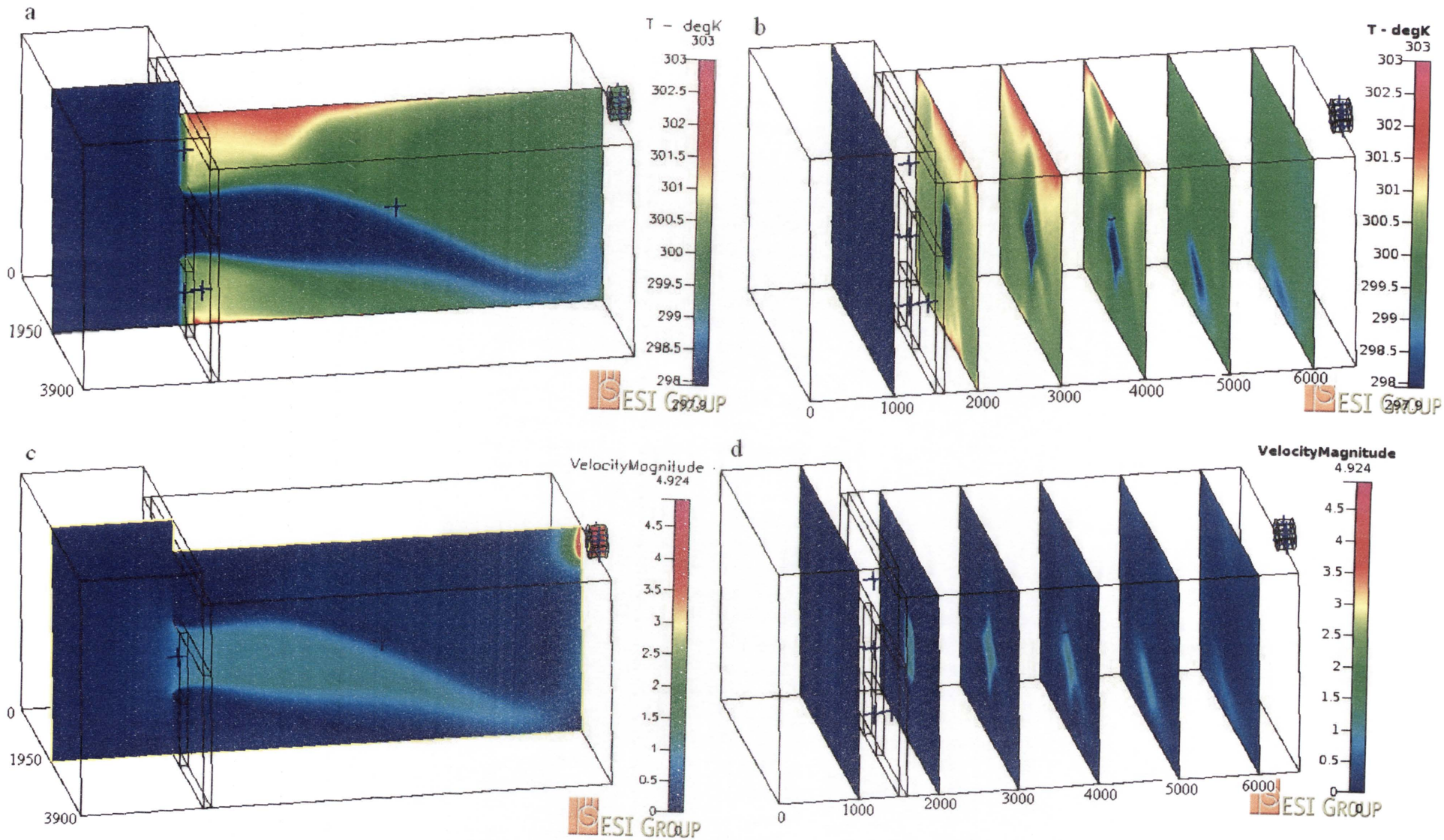

Figure 115 – 4extraction_3.7_303 Temperature and velocity distributions with airflows through fan of 3.7 m/s

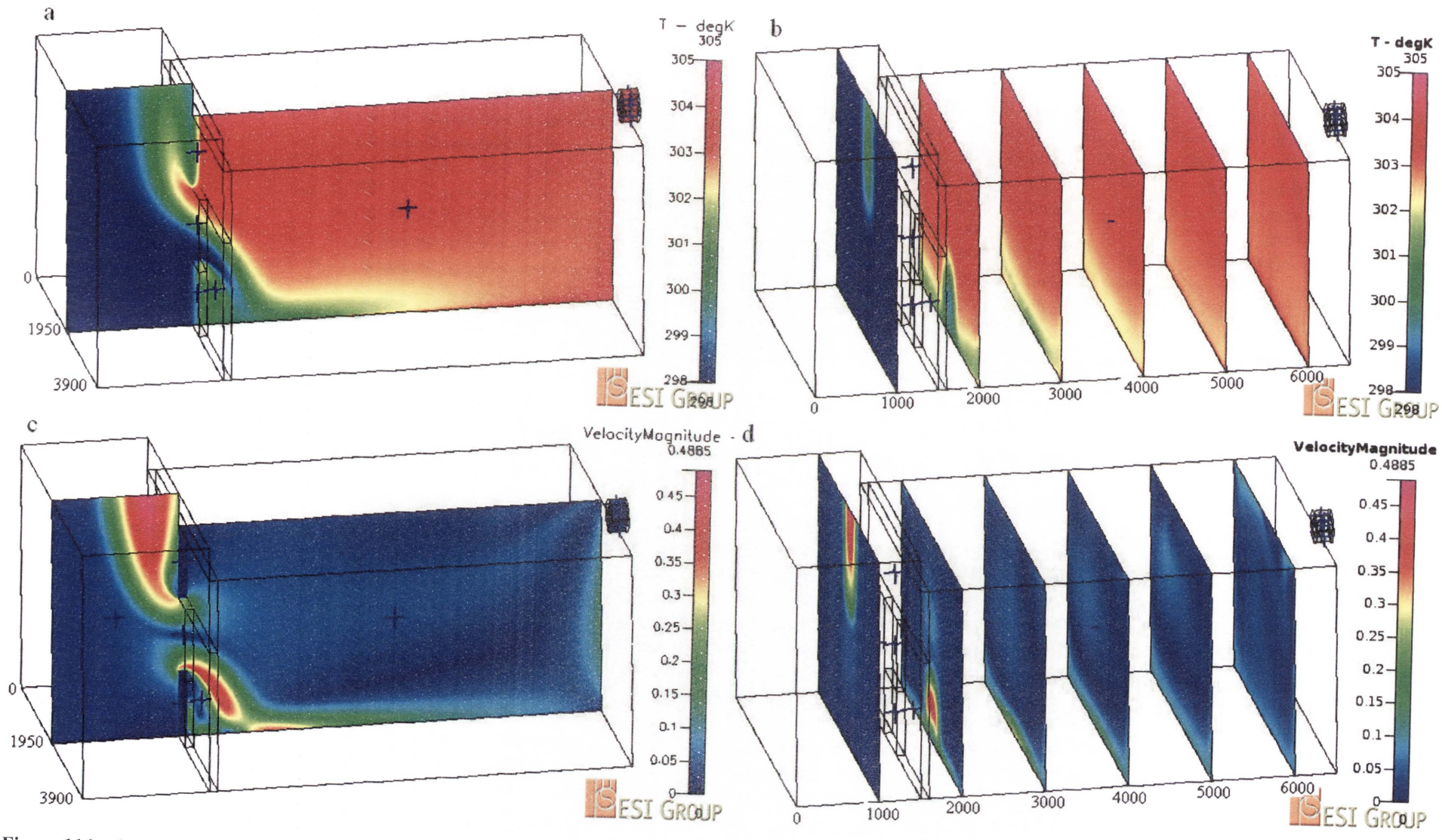

Figure 116 – 4extraction_0.0001_305 Temperature and velocity distributions with airflows through fan of 0.0001 m/s

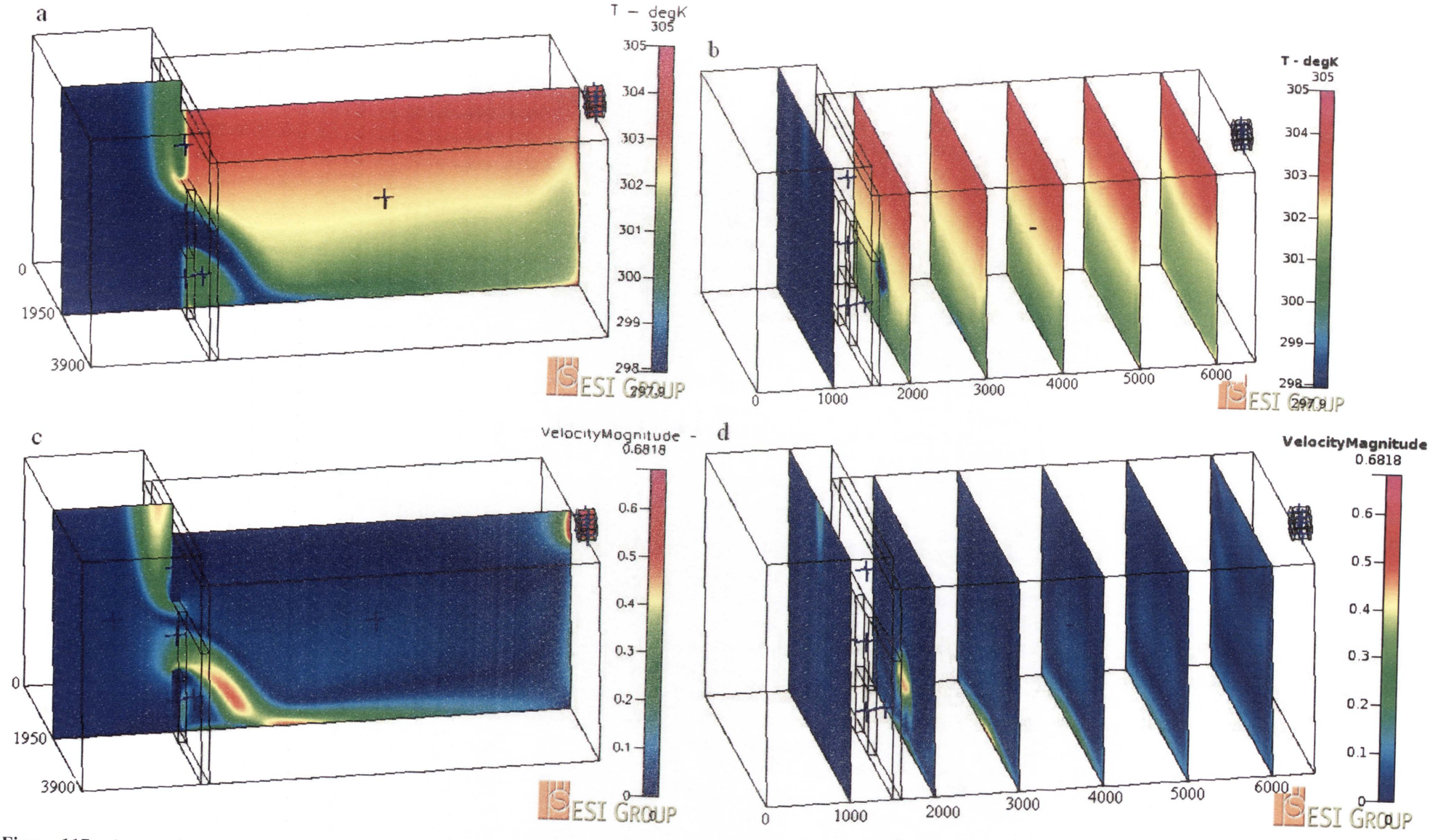

Figure 117 – 4extraction_0.505_305 Temperature and velocity distributions with airflows through fan of 0.505 m/s

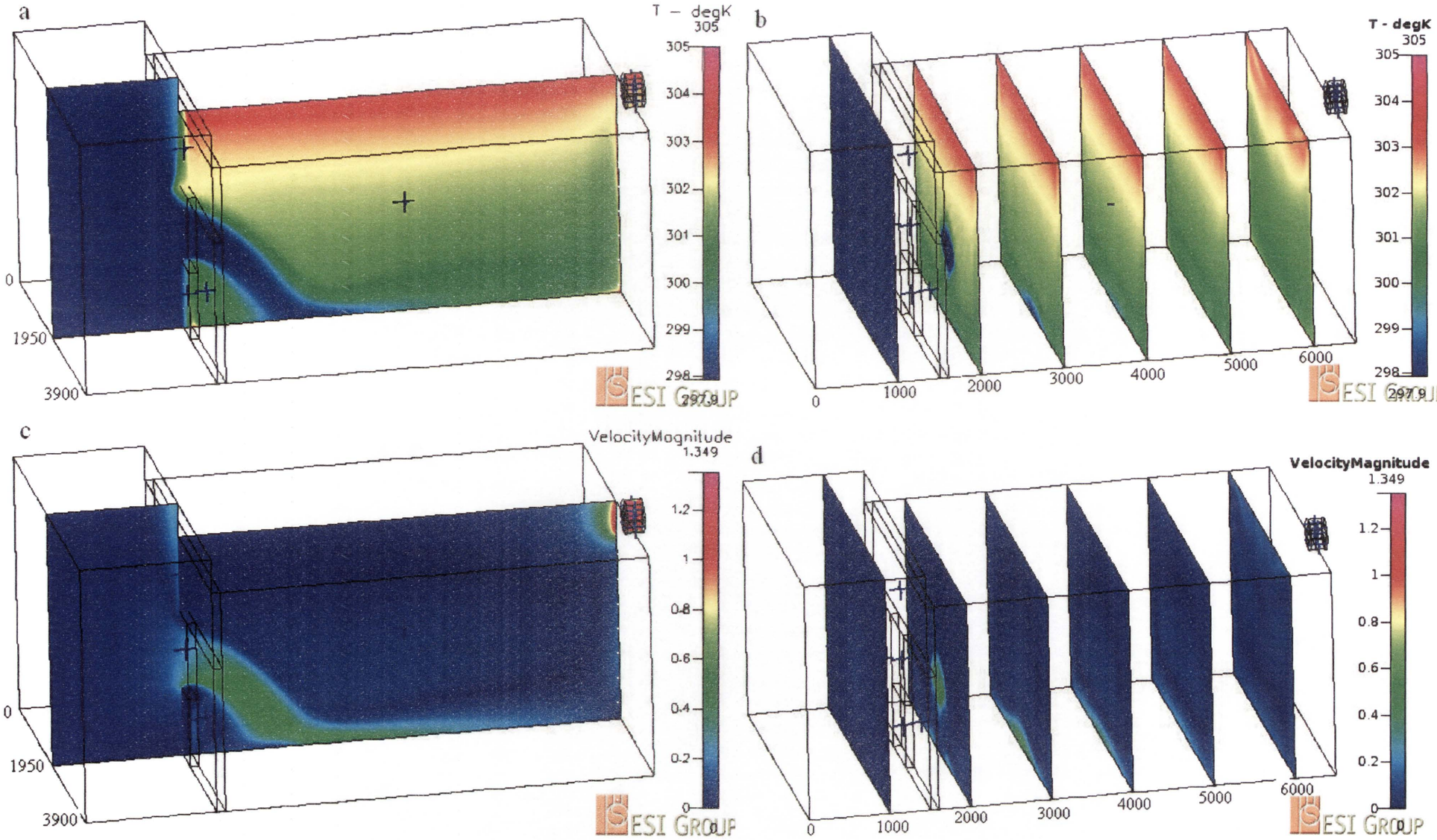

Figure 118 – 4extraction_1_305 Temperature and velocity distributions with airflows through fan of 1 m/s

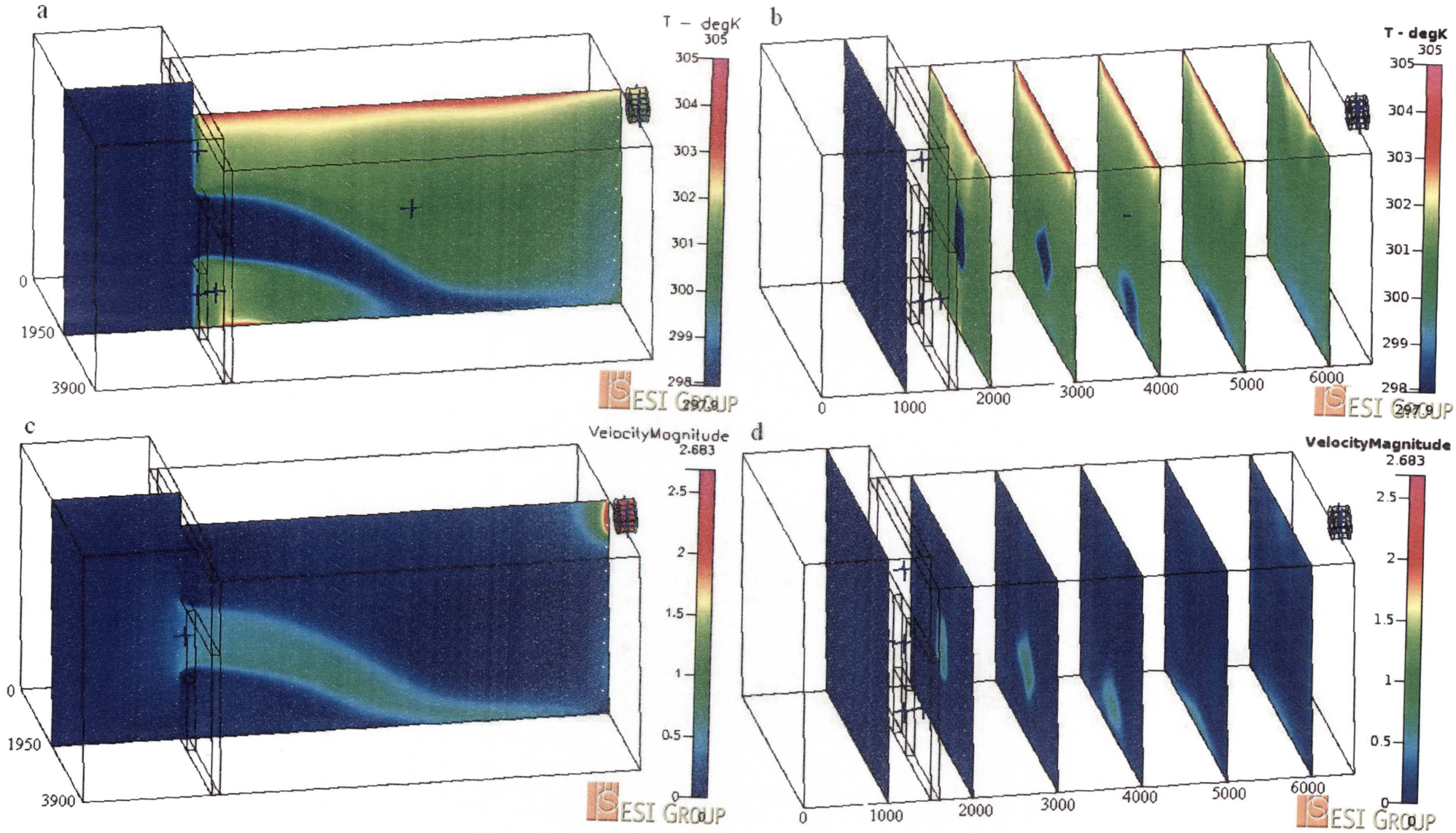

Figure 119 – 4extraction_2_305 Temperature and velocity distributions with airflows through fan of 2m/s

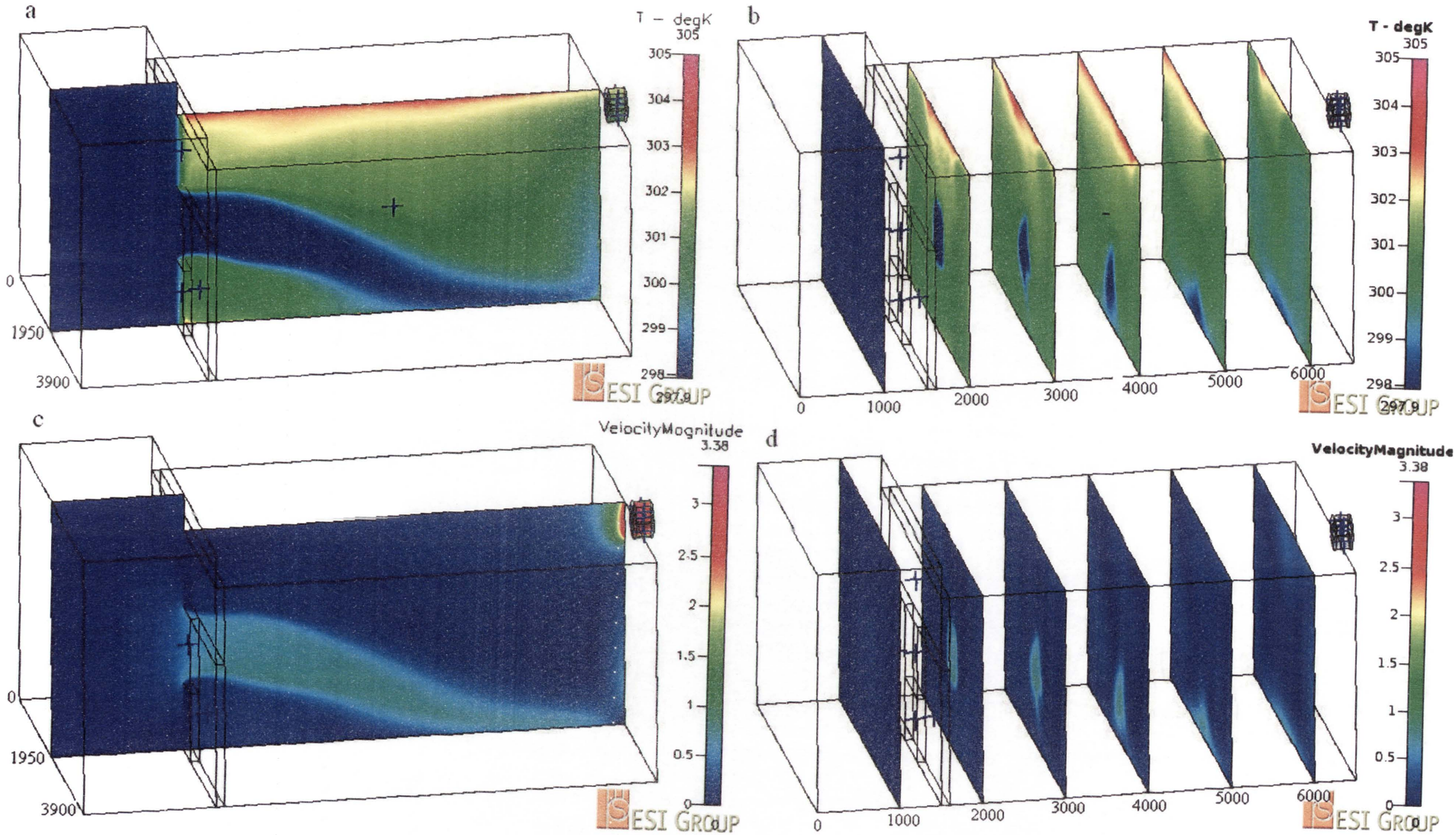

Figure 120 – 4extraction_2.5_305 Temperature and velocity distributions with airflows through fan of 2.5 m/s

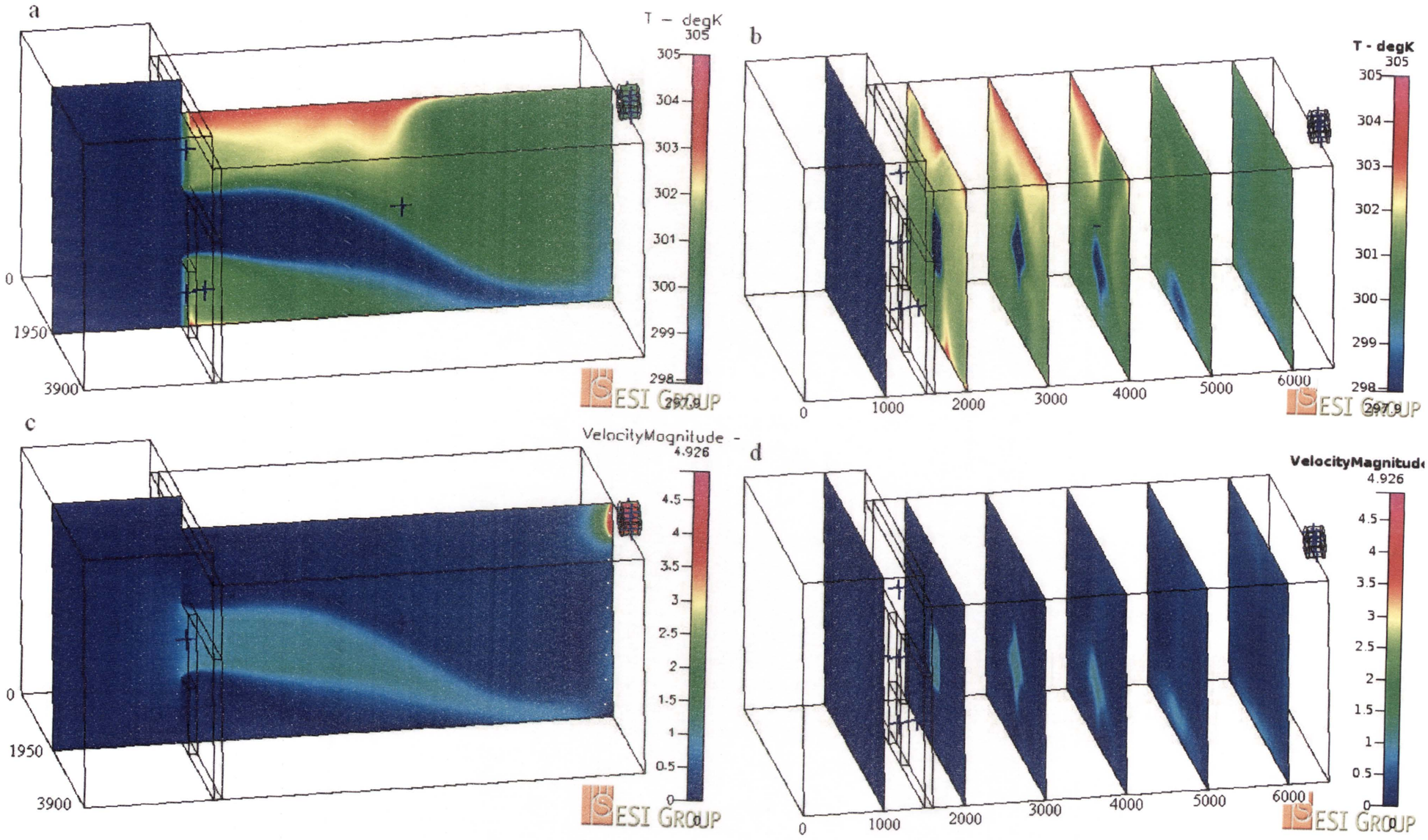

Figure 121 – 4extraction_3.7_305 Temperature and velocity distributions with airflows through fan of 3.7 m/s

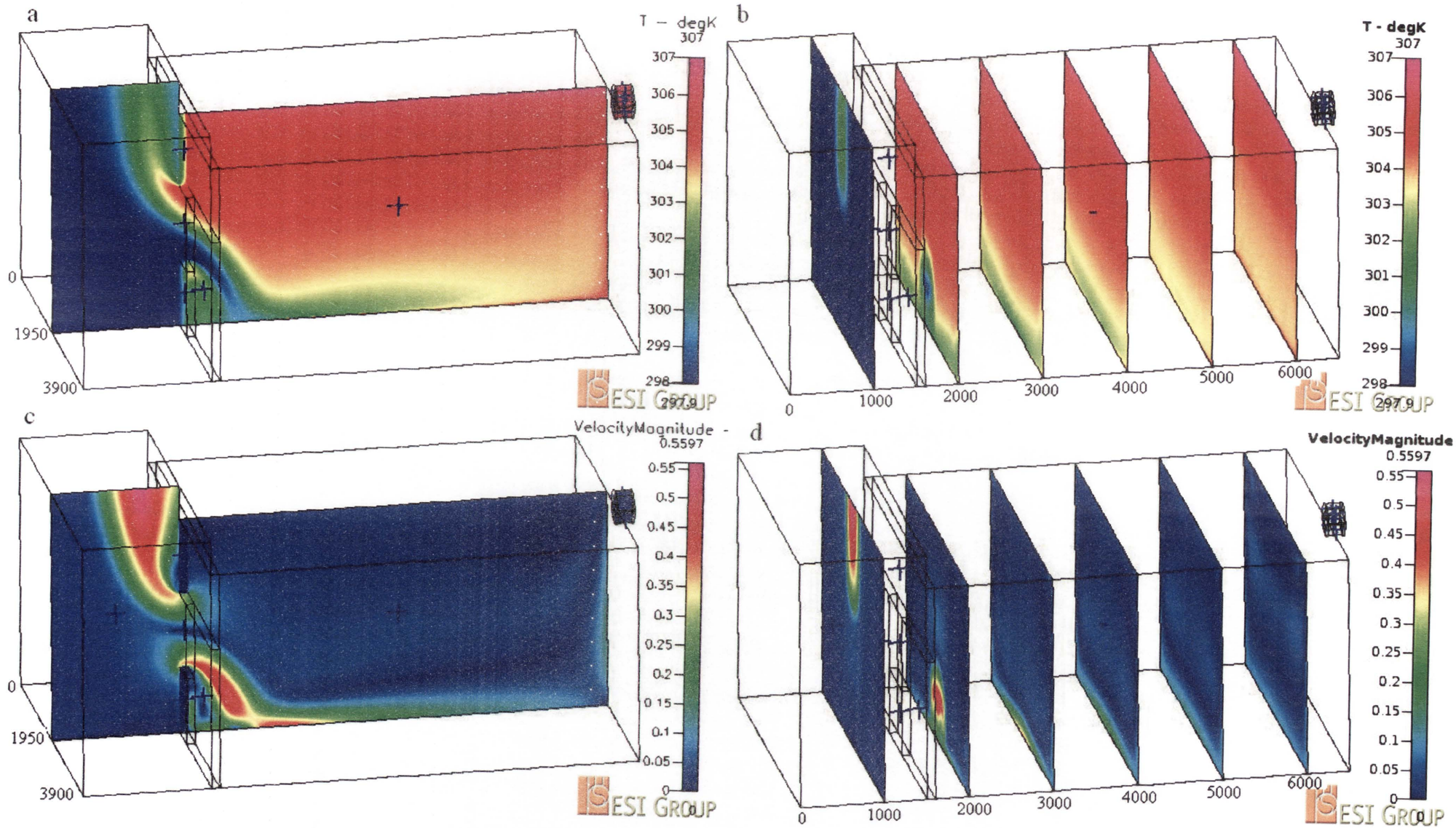

Figure 122 – 4extraction_0.0001_307 Temperature and velocity distributions with airflows through fan of 0.0001 m/s

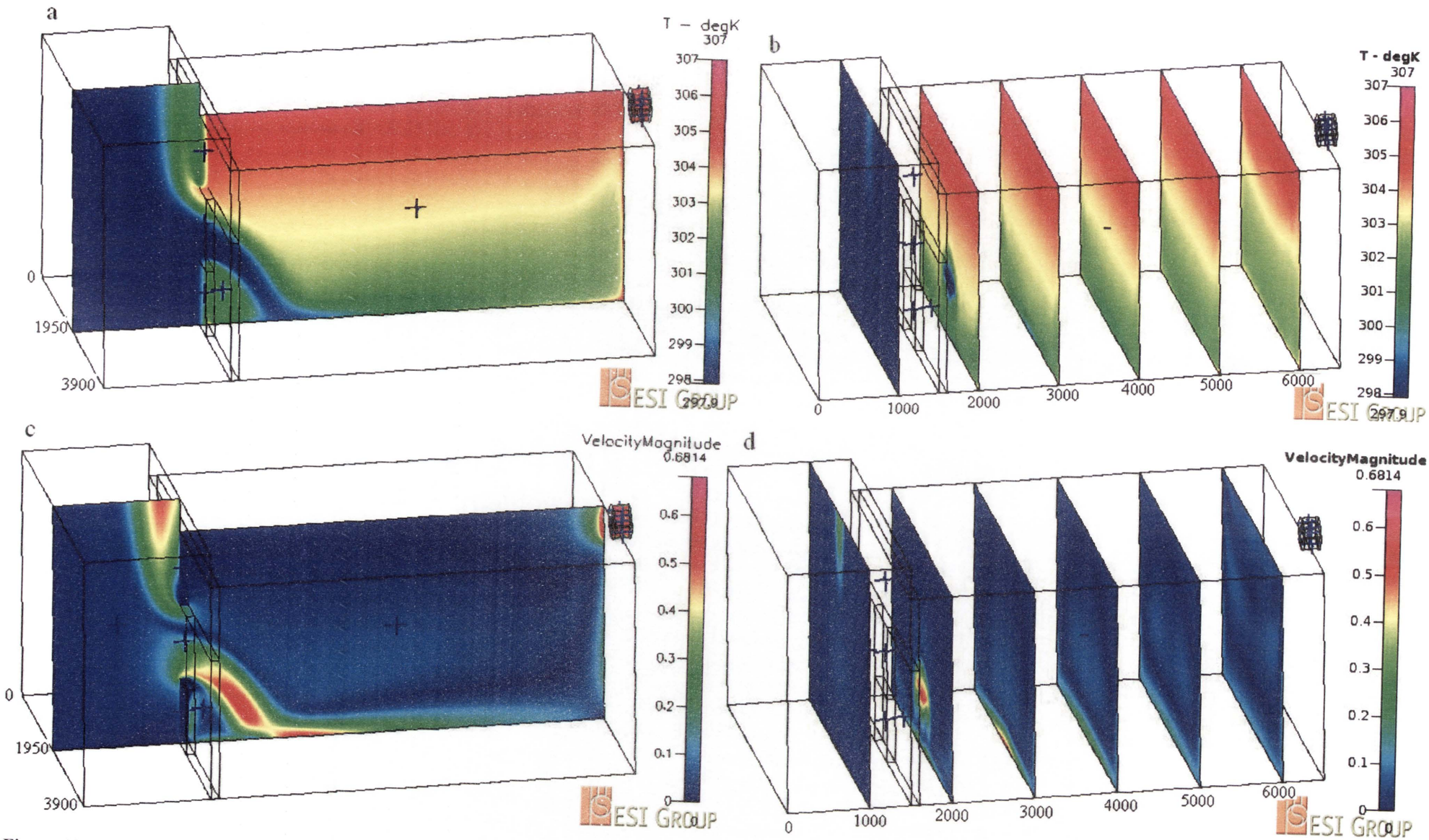

Figure 123 – 4extraction_0.505_307 Temperature and velocity distributions with airflows through fan of 0.505 m/s

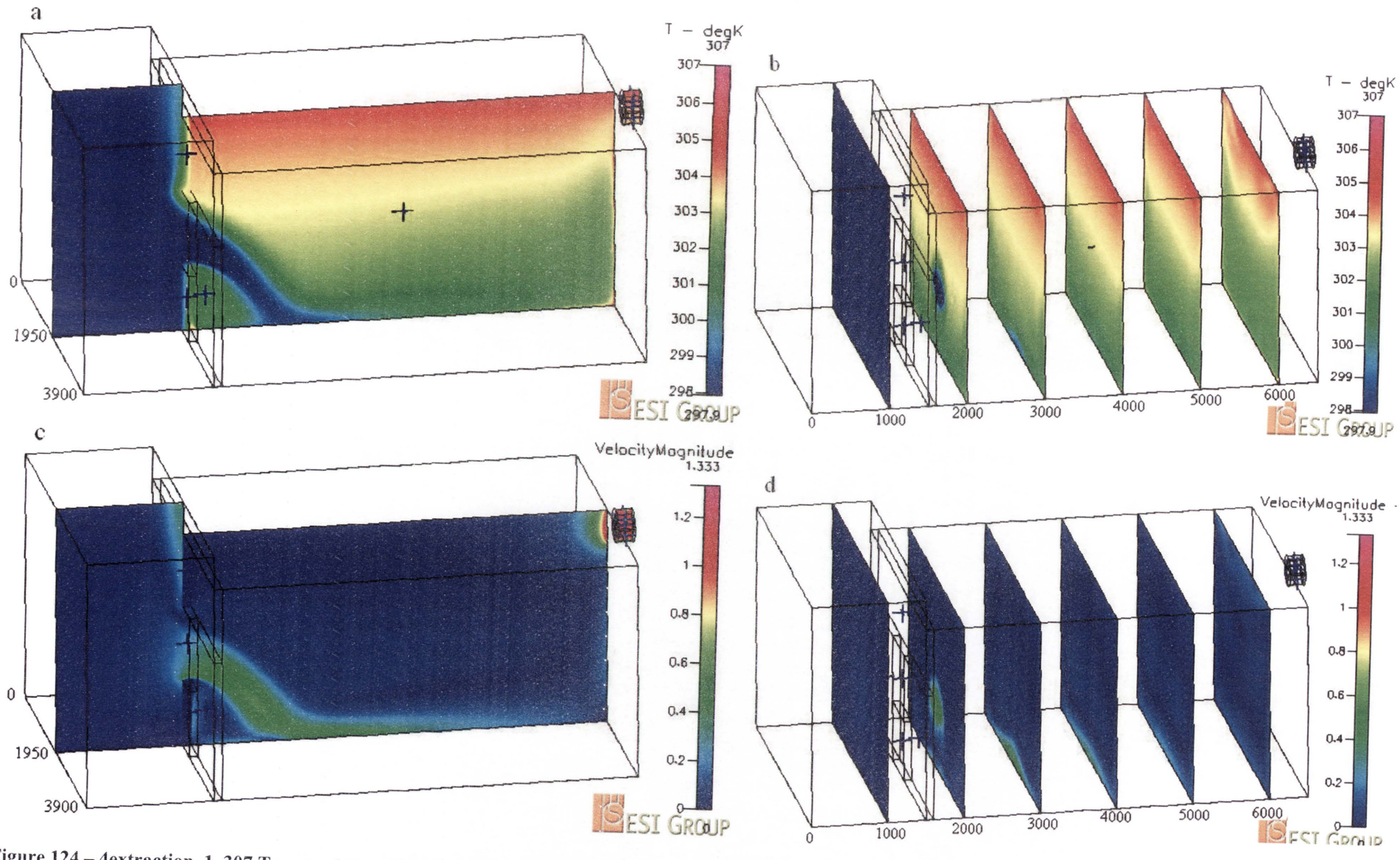

Figure 124 – 4extraction_1_307 Temperature and velocity distributions with airflows through fan of 1 m/s

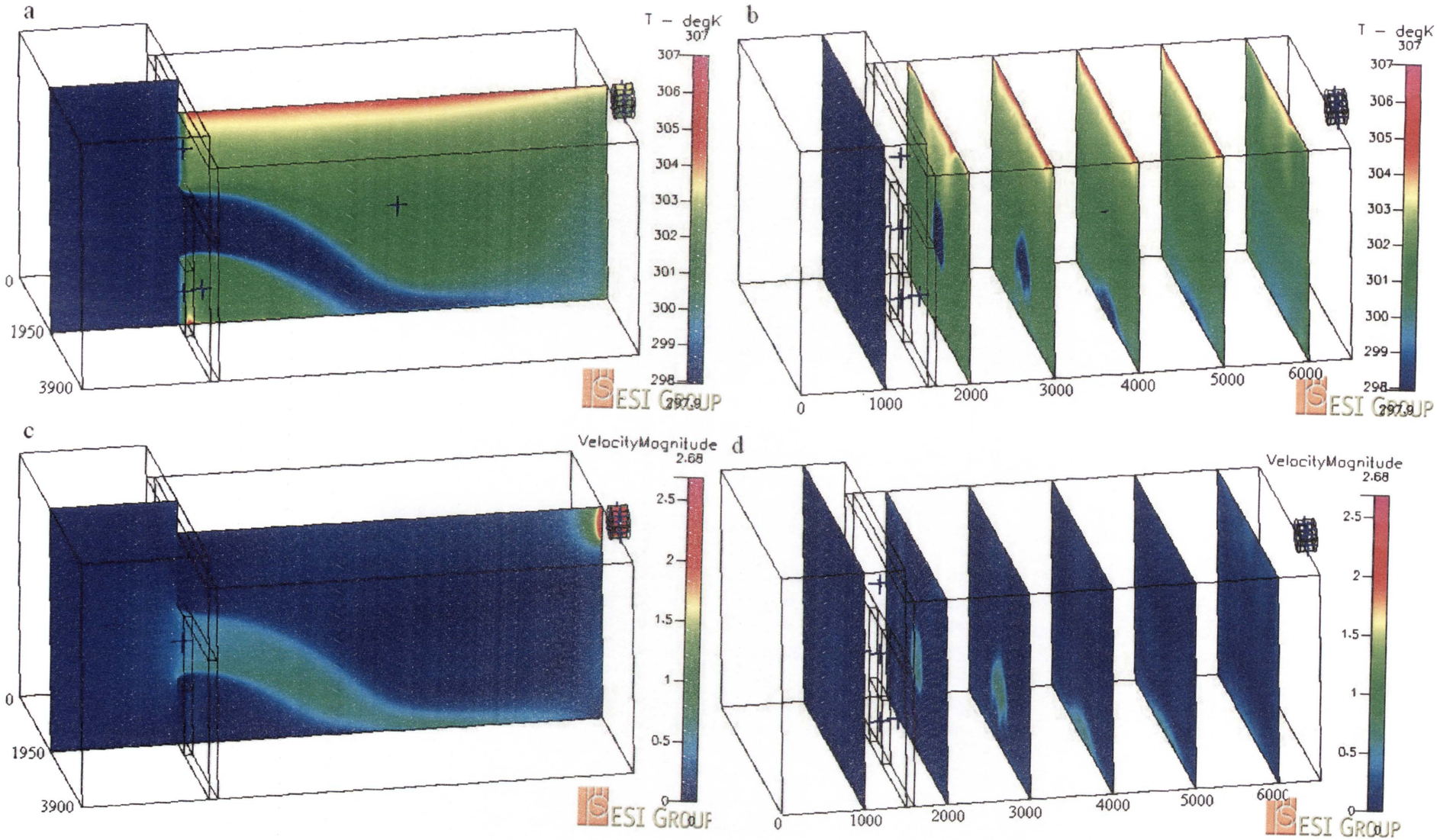

Figure 125 – 4extraction_2_307 Temperature and velocity distributions with airflows through fan of 2m/s

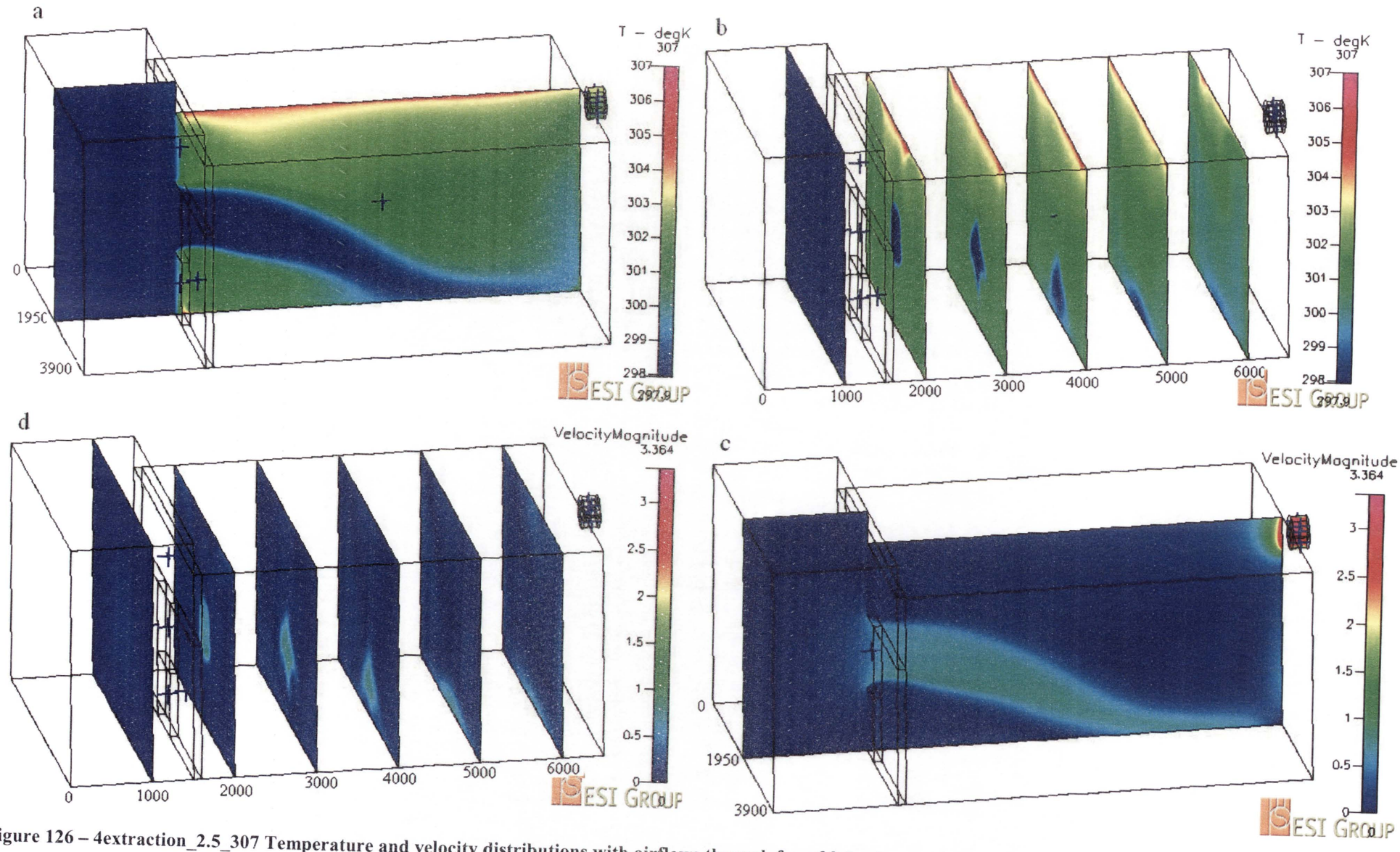

Figure 126 – 4extraction_2.5_307 Temperature and velocity distributions with airflows through fan of 2.5 m/s

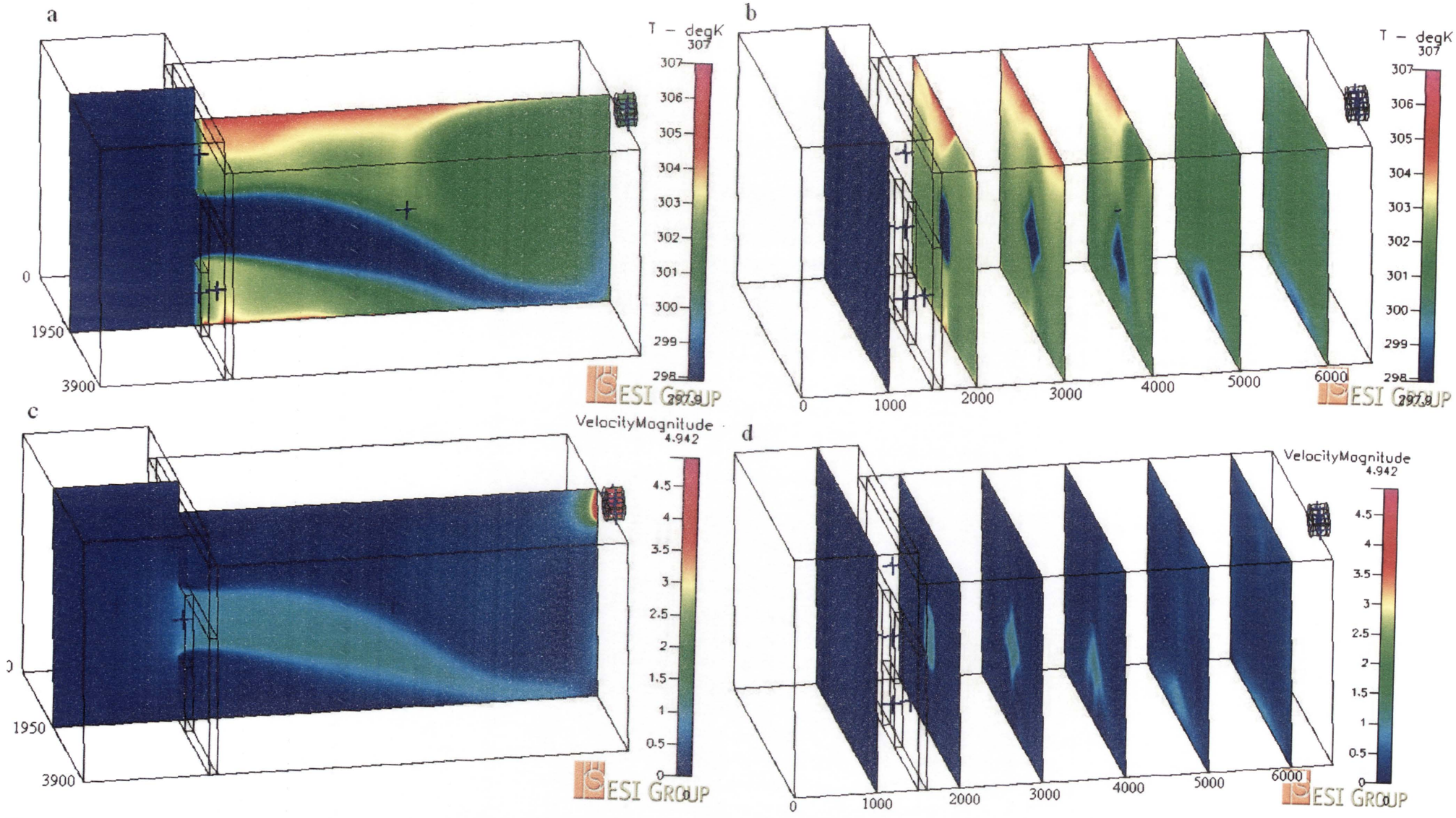

Figure 127 – 4extraction_3.7_307 Temperature and velocity distributions with airflows through fan of 3.7 m/s

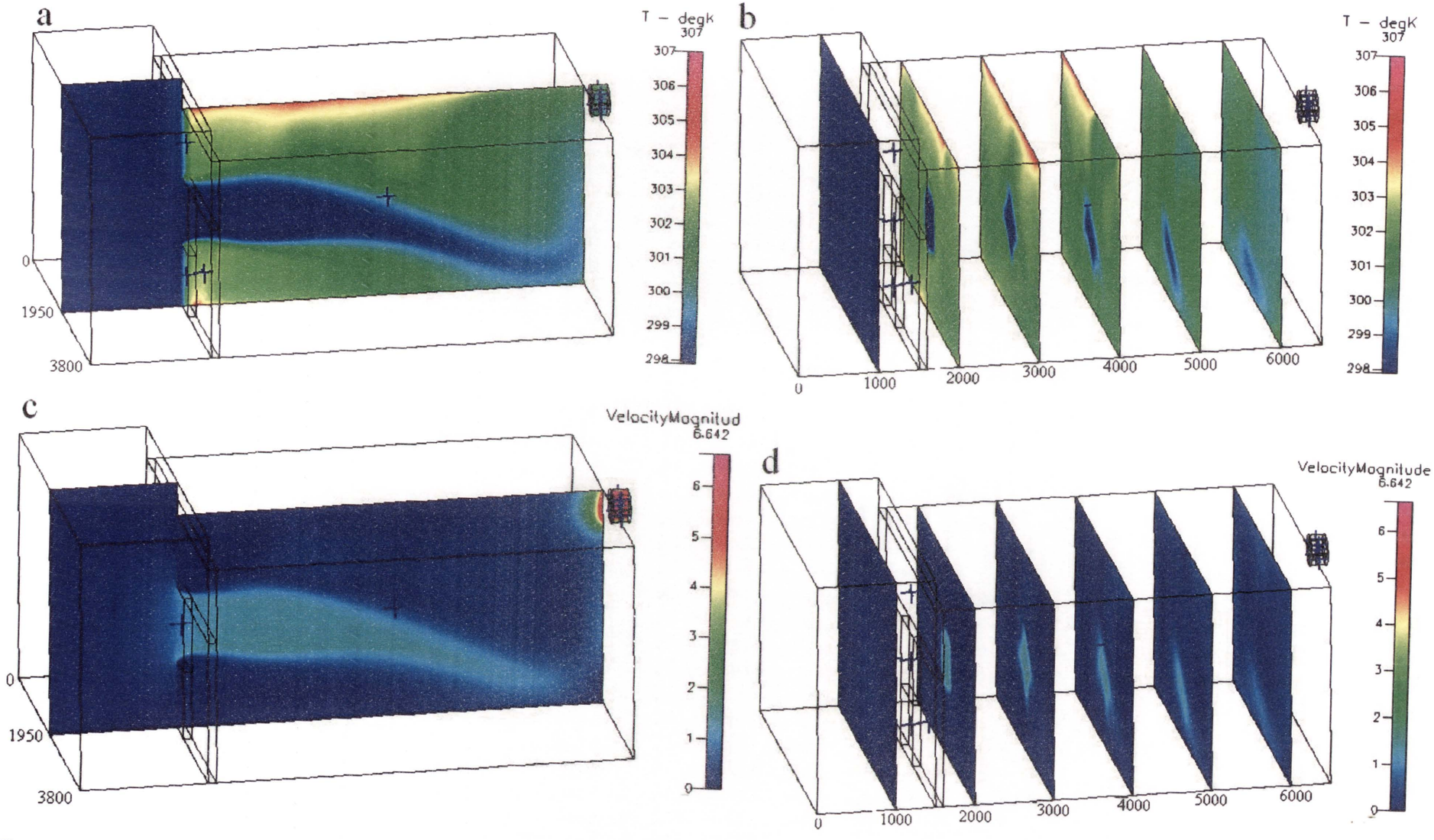

Figure 128 – 4extraction_5_307 Temperature and velocity distributions with airflows through fan of 5 m/s

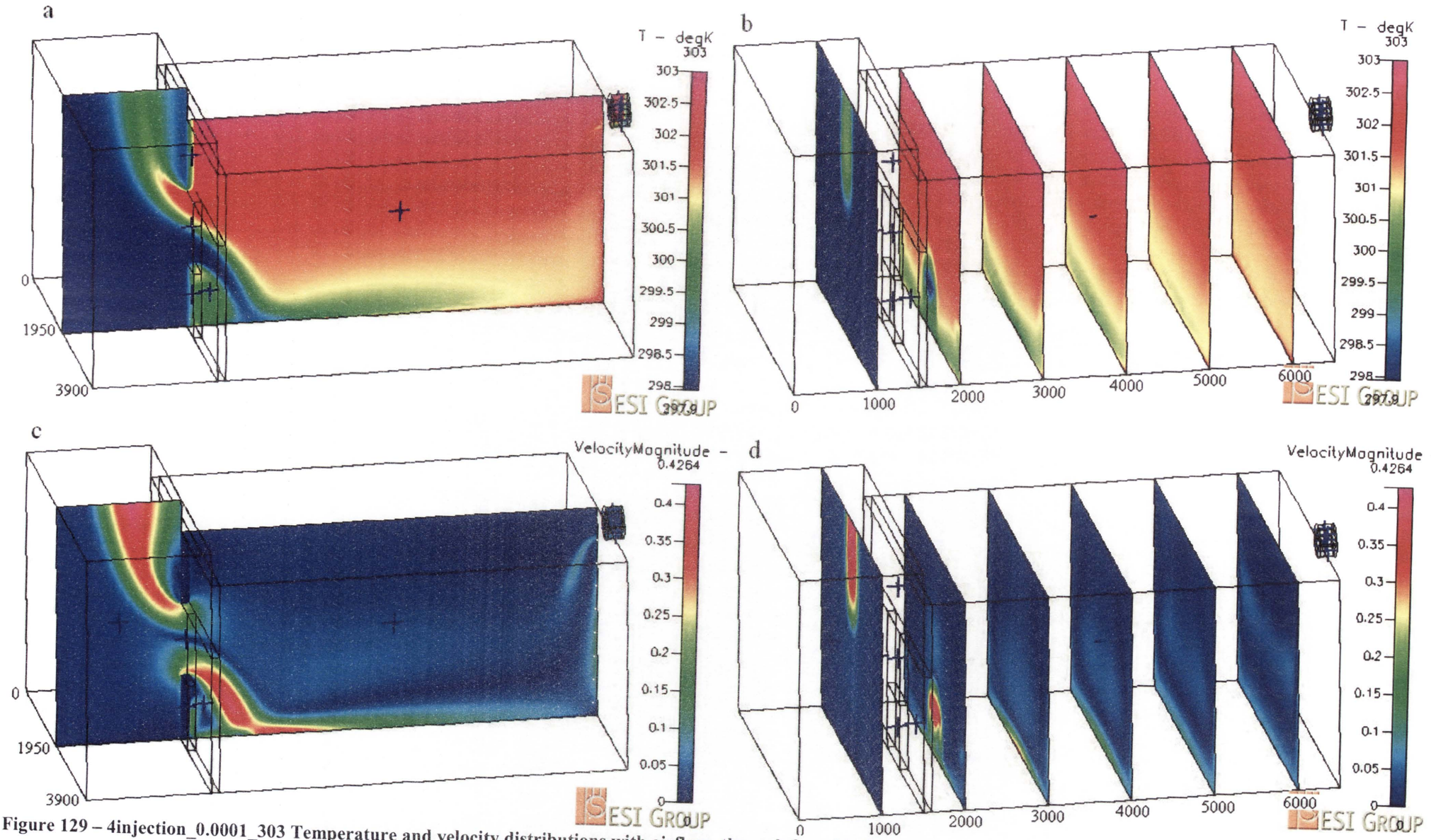

Figure 129 – 4injection_0.0001_303 Temperature and velocity distributions with airflows through fan of 0.0001 m/s

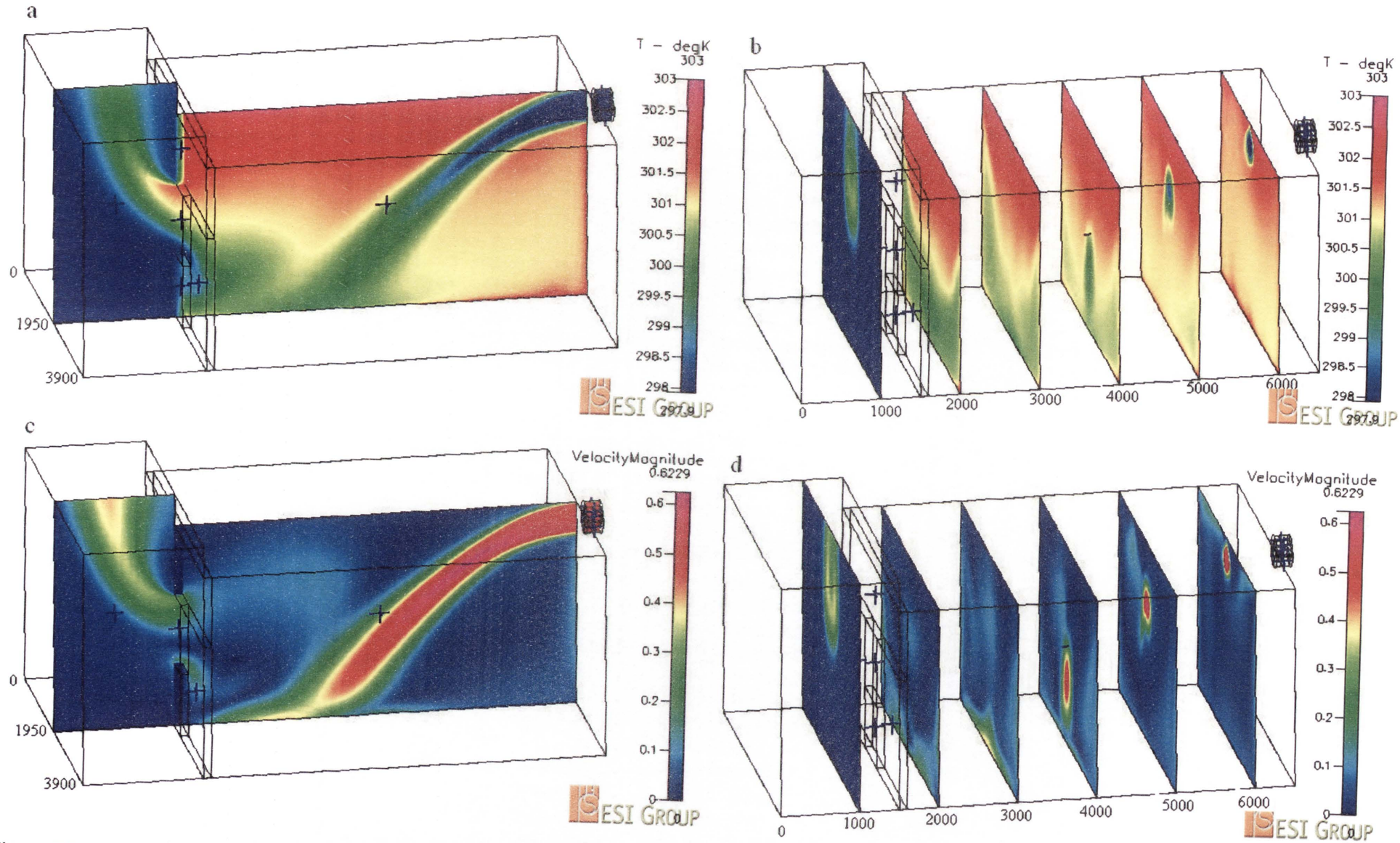

Figure 130 – 4injection_0.505_303 Temperature and velocity distributions with airflows through fan of 0.505 m/s

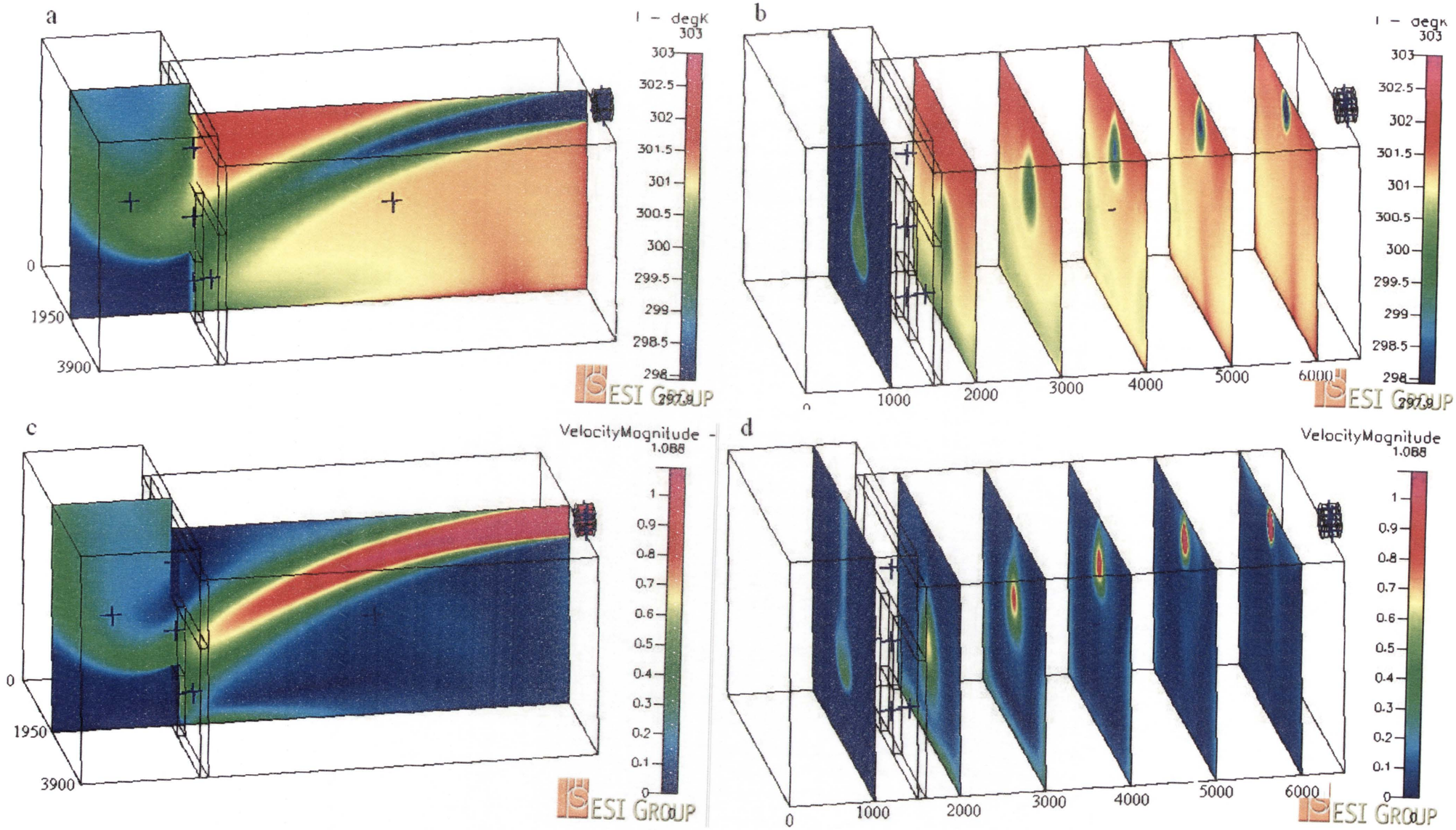

Figure 131 – 4injection_1_303 Temperature and velocity distributions with airflows through fan of 1 m/s

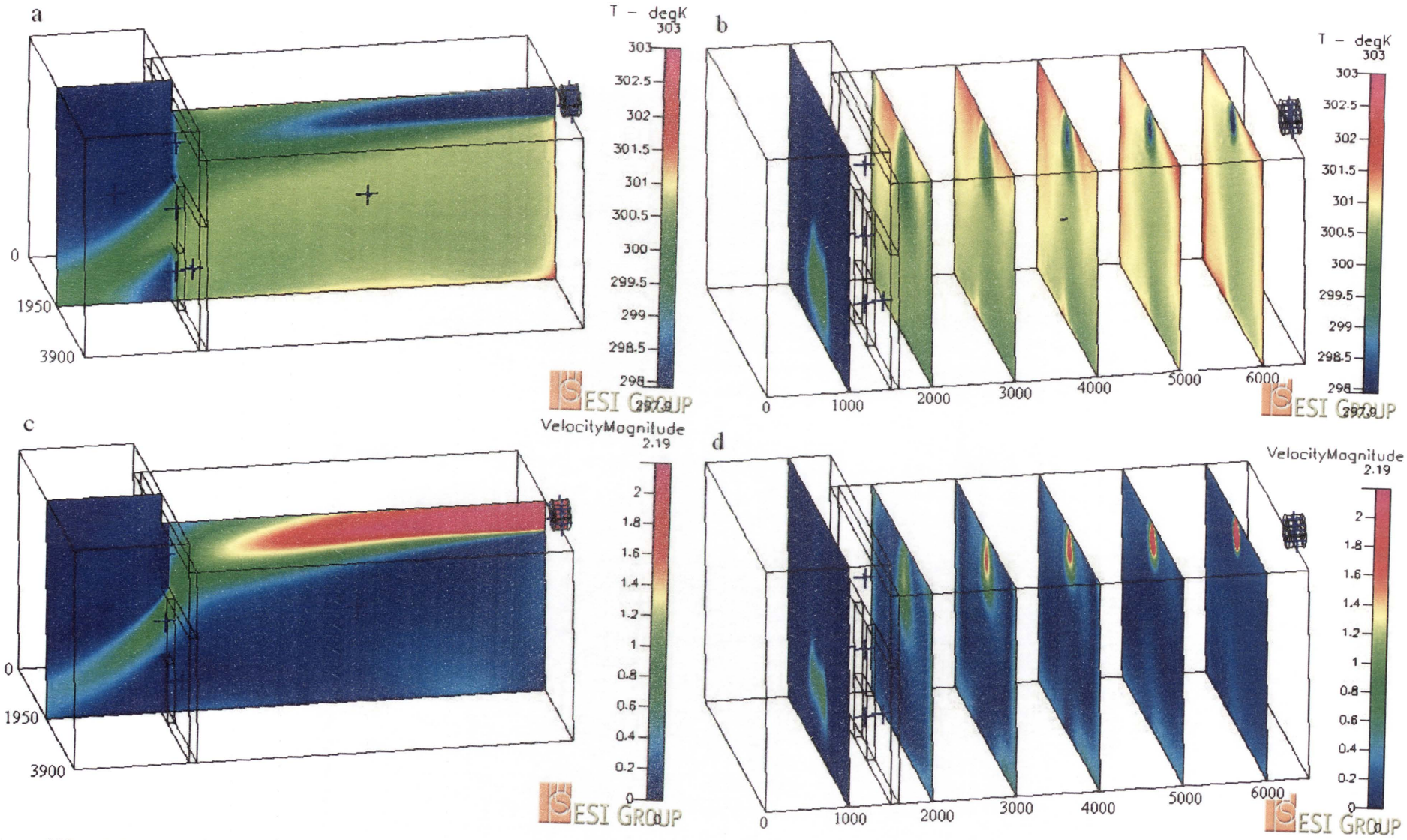

Figure 132 – 4injection_2_303 Temperature and velocity distributions with airflows through fan of 2m/s

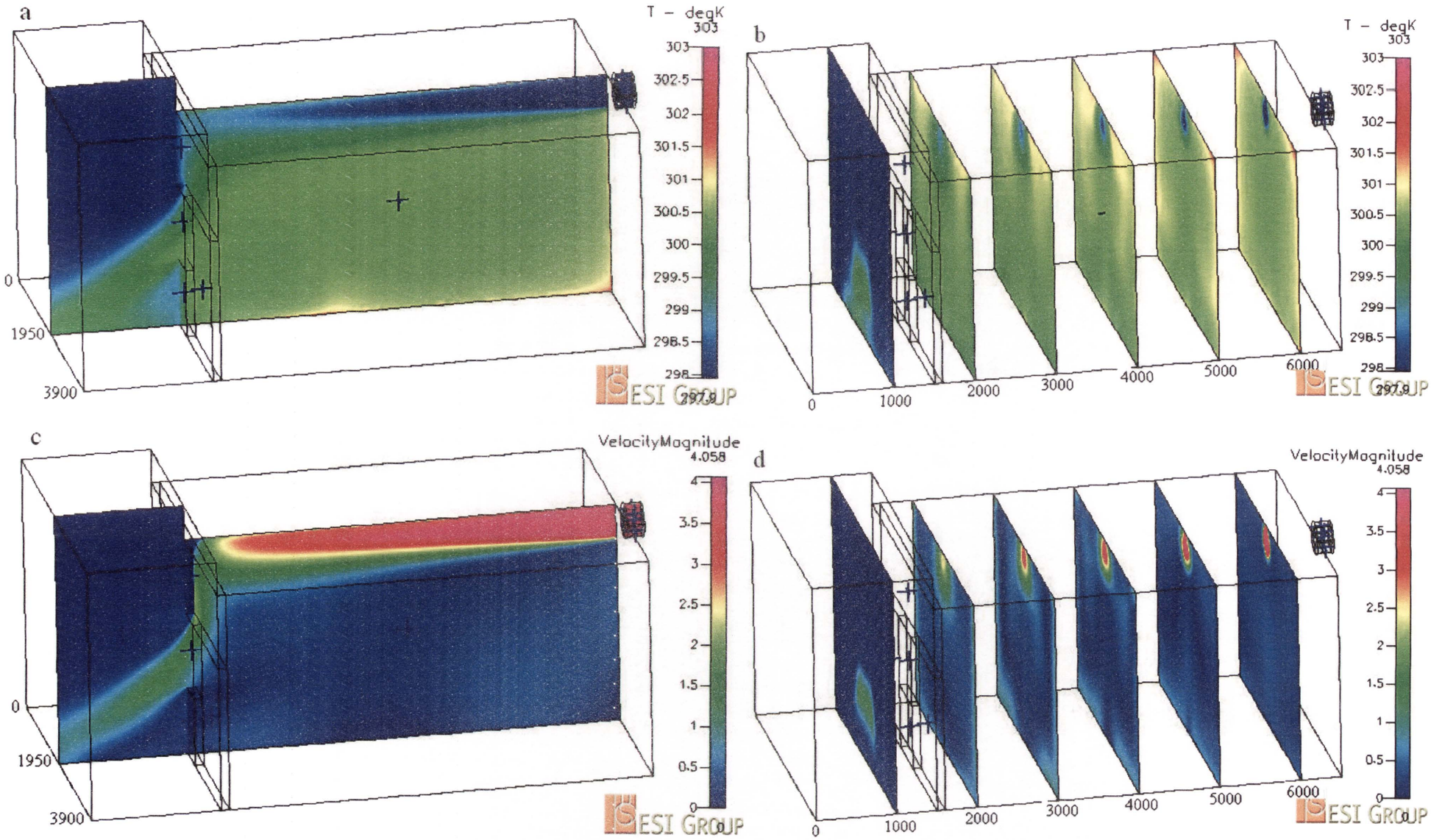

Figure 133 – 4injection_2.5_303 Temperature and velocity distributions with airflows through fan of 2.5 m/s

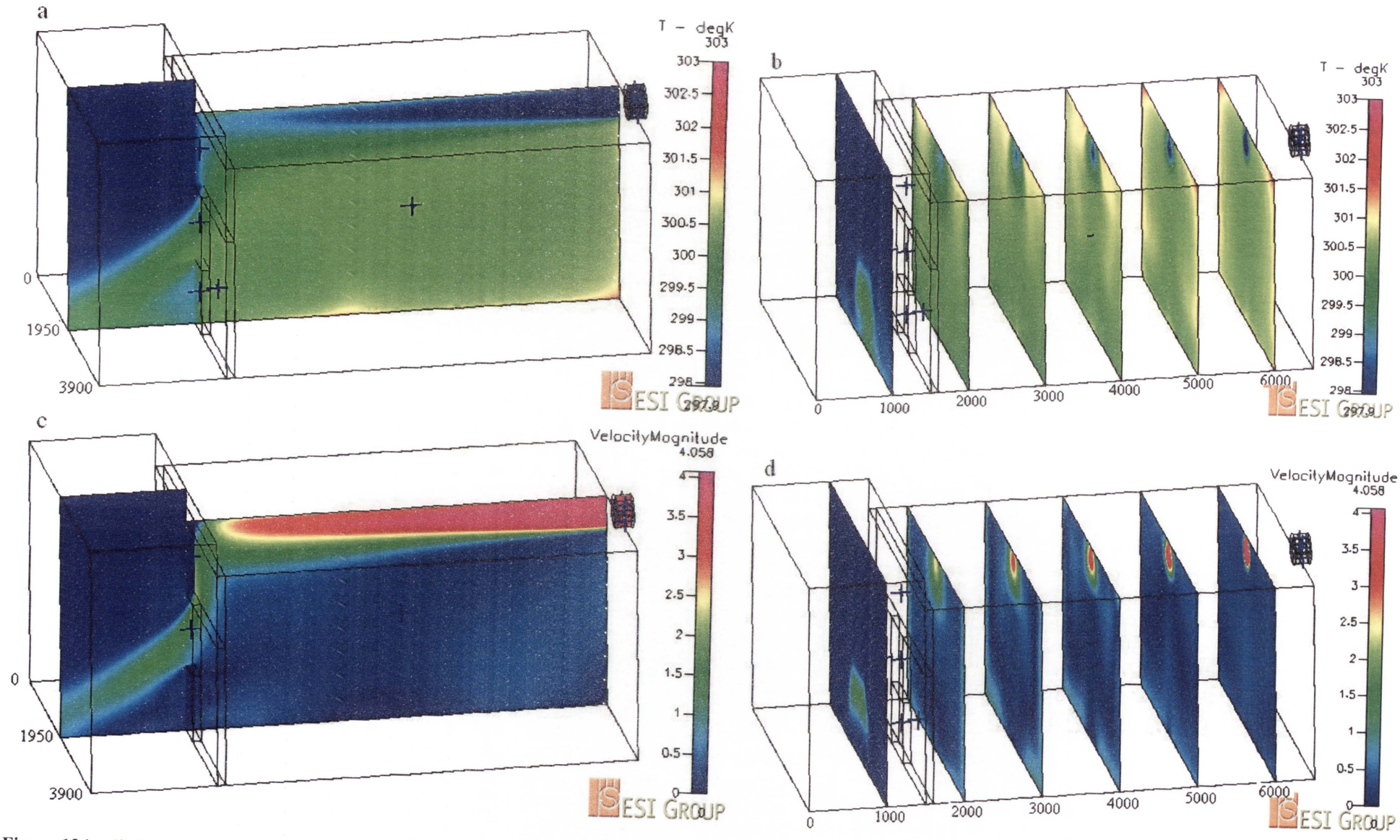

Figure 134 – 4injection_3.7_303 Temperature and velocity distributions with airflows through fan of 3.7 m/s

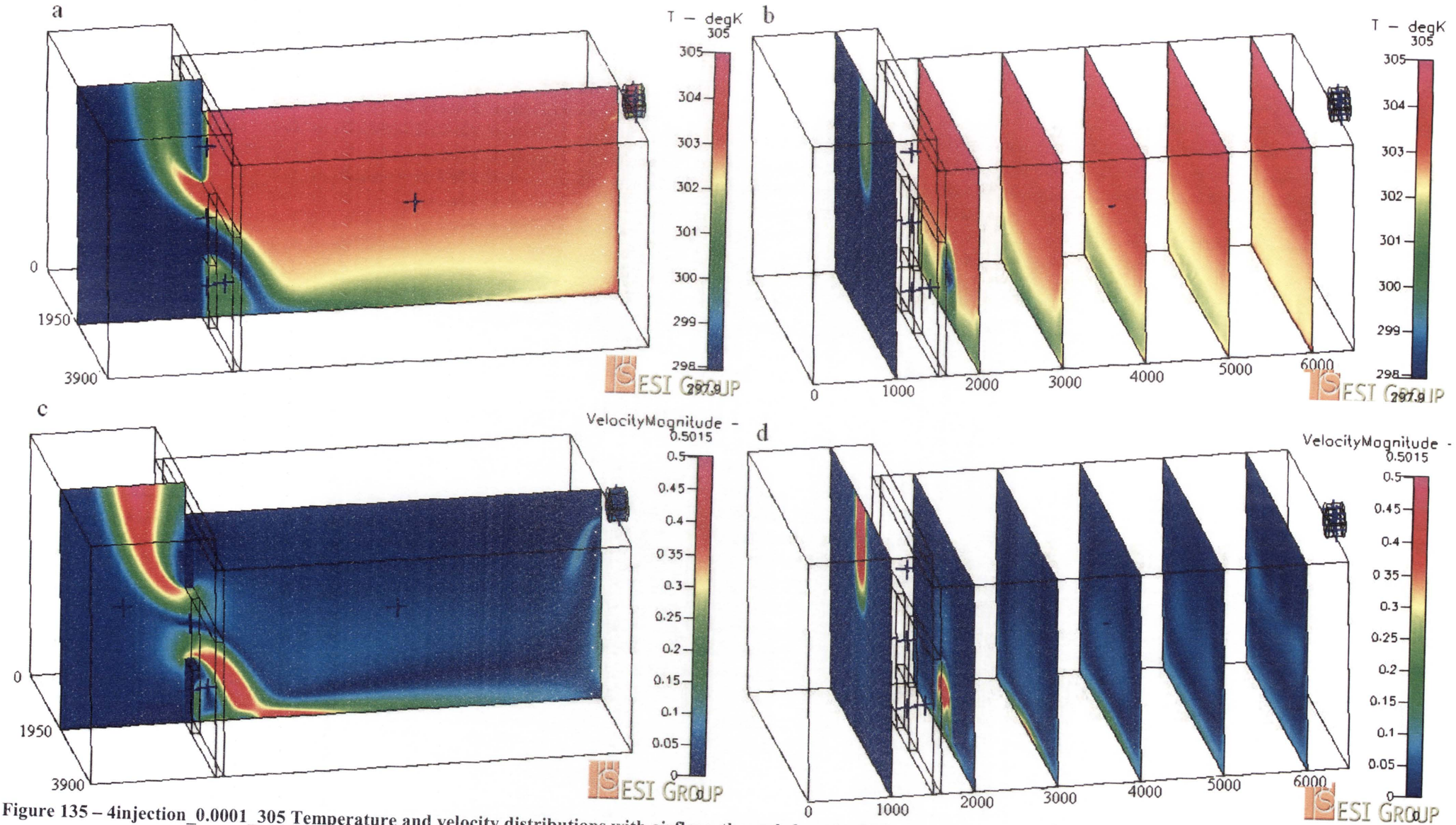

Figure 135 – 4injection_0.0001_305 Temperature and velocity distributions with airflows through fan of 0.0001 m/s

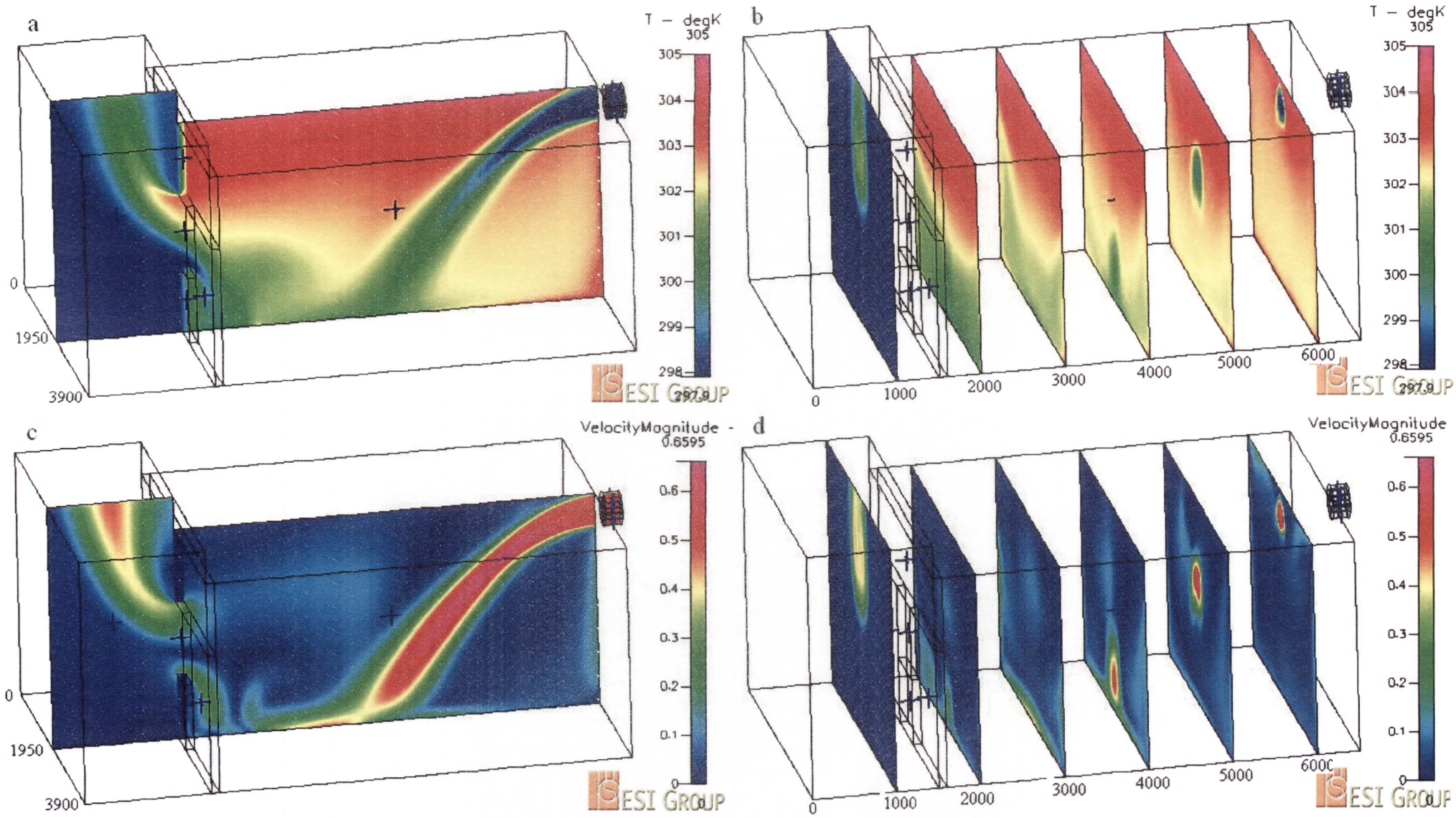

Figure 136 – 4injection_0.505_305 Temperature and velocity distributions with airflows through fan of 0.505 m/s

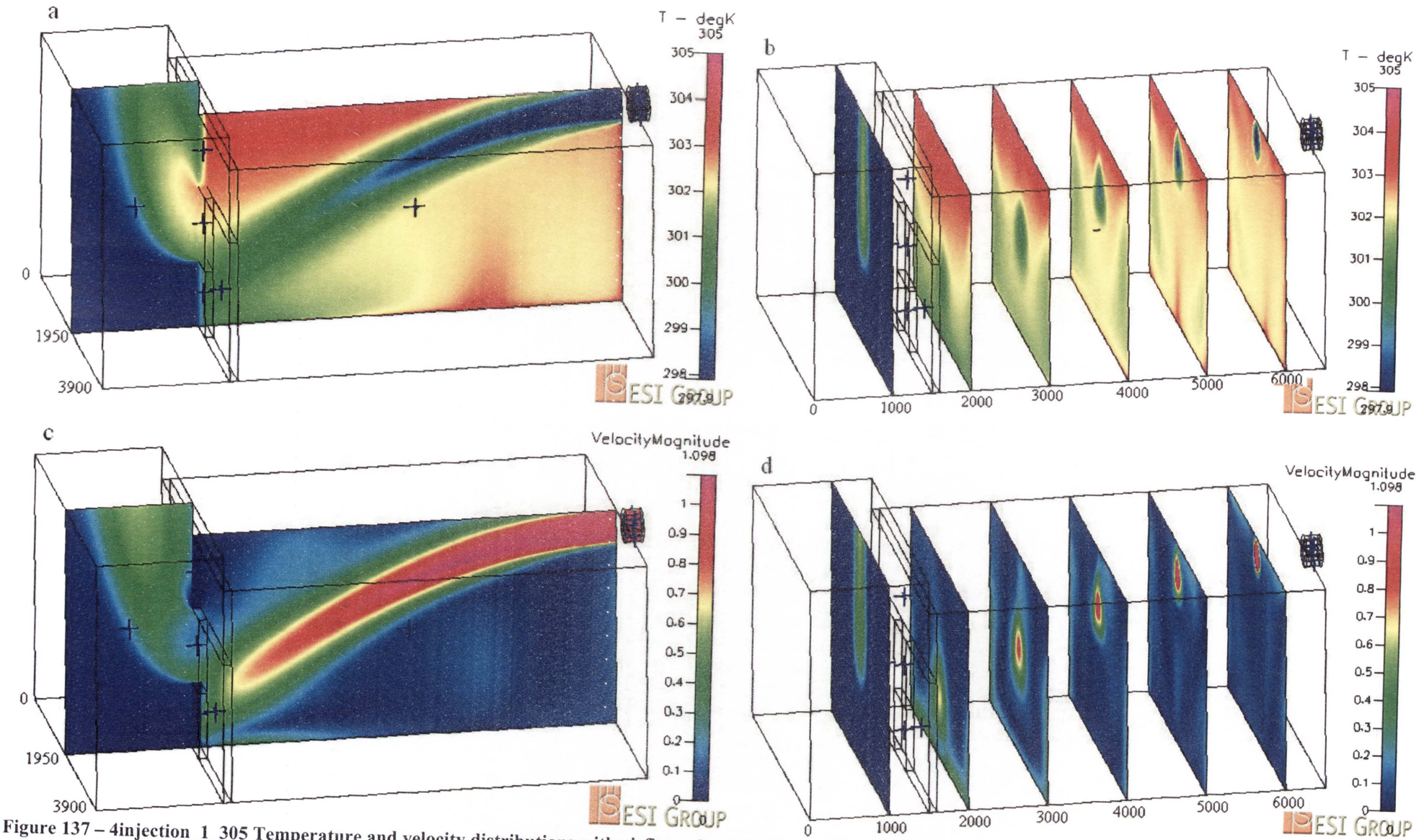

Figure 137 – 4injection_1_305 Temperature and velocity distributions with airflows through fan of 1 m/s

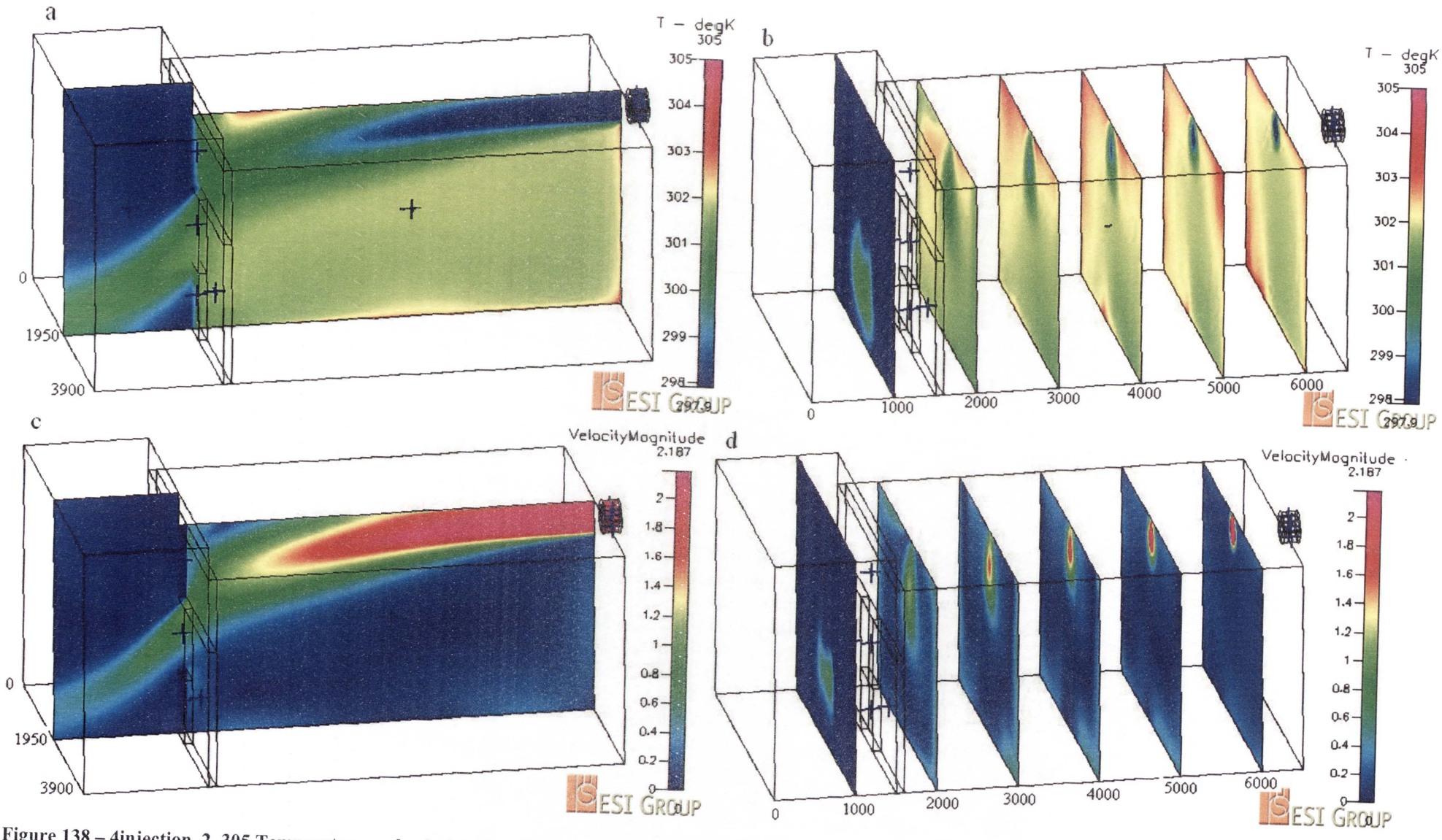

Figure 138 – 4injection_2_305 Temperature and velocity distributions with airflows through fan of 2m/s

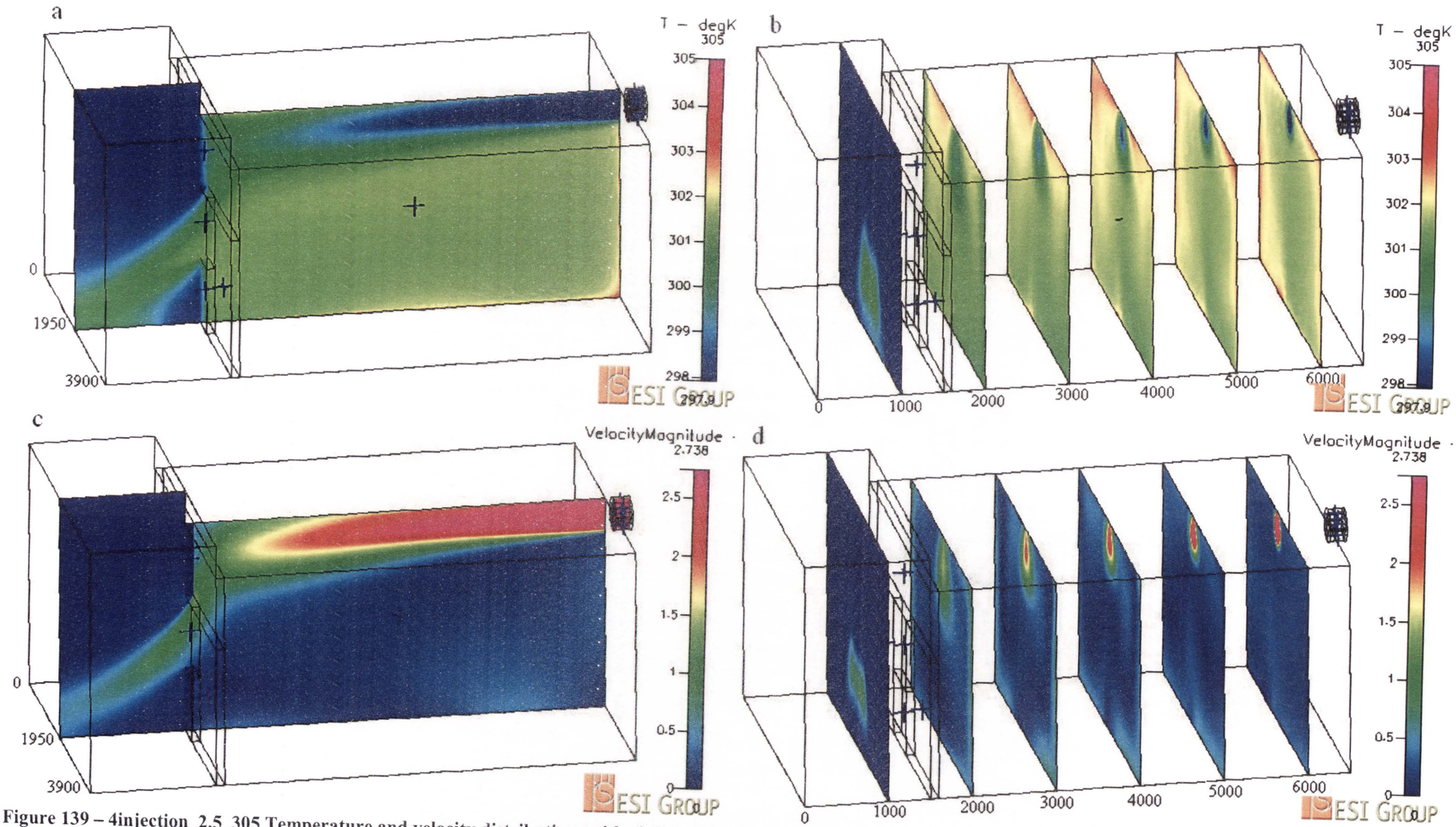

Figure 139 – 4injection_2.5_305 Temperature and velocity distributions with airflows through fan of 2.5 m/s

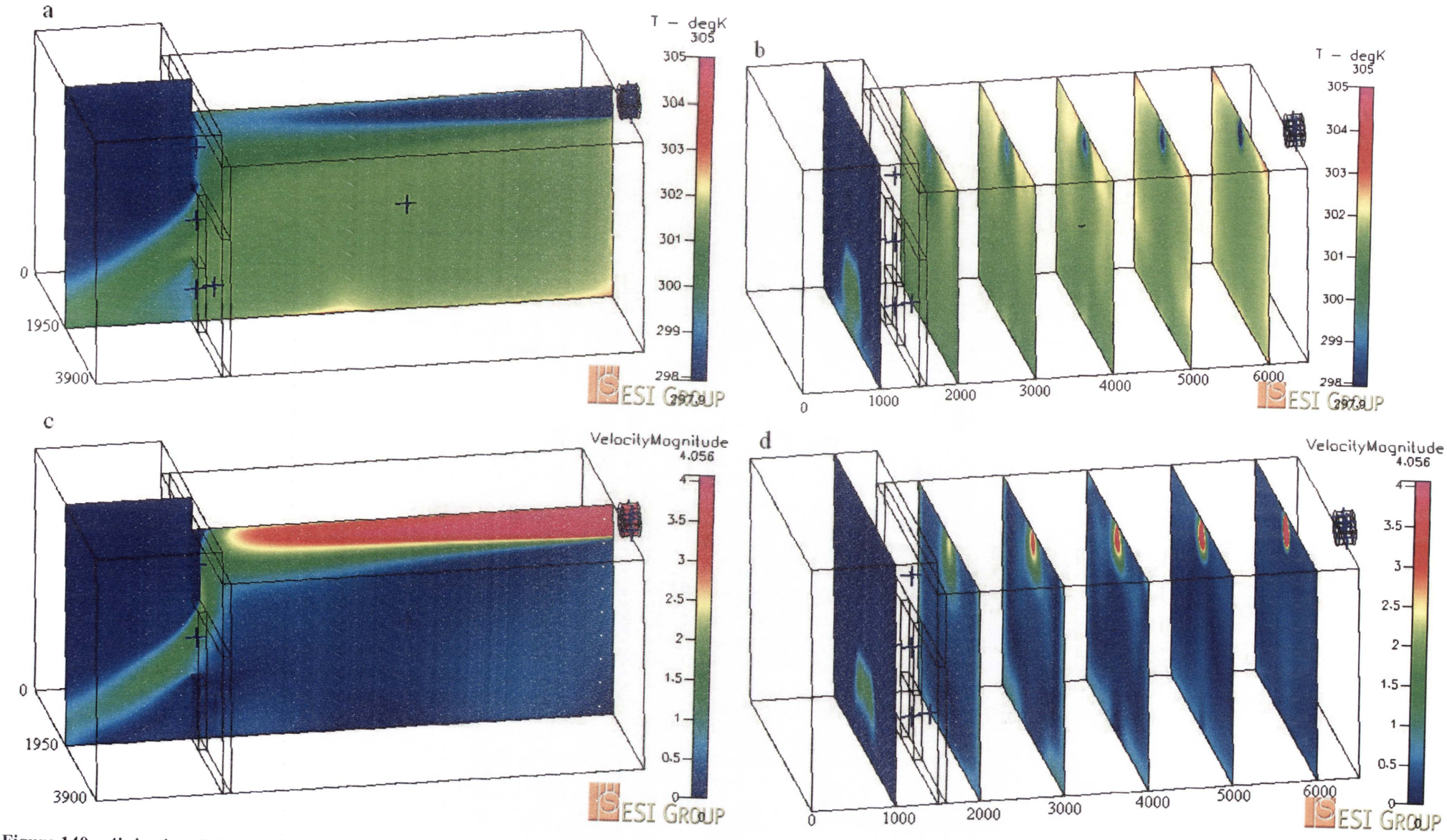

Figure 140 – 4injection_3.7_305 Temperature and velocity distributions with airflows through fan of 3.7 m/s

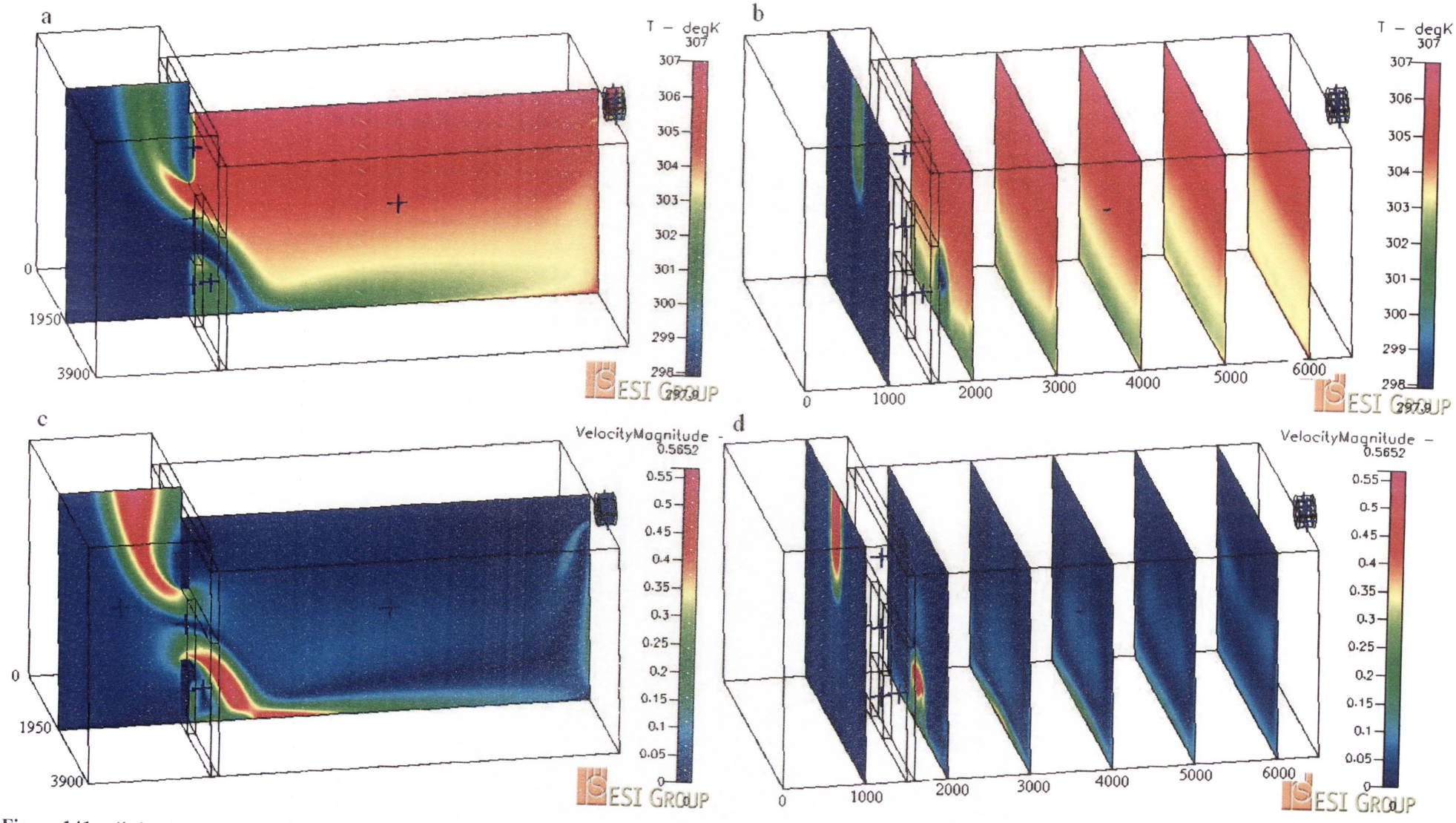

Figure 141 – 4injection_0.0001_307 Temperature and velocity distributions with airflows through fan of 0.0001 m/s

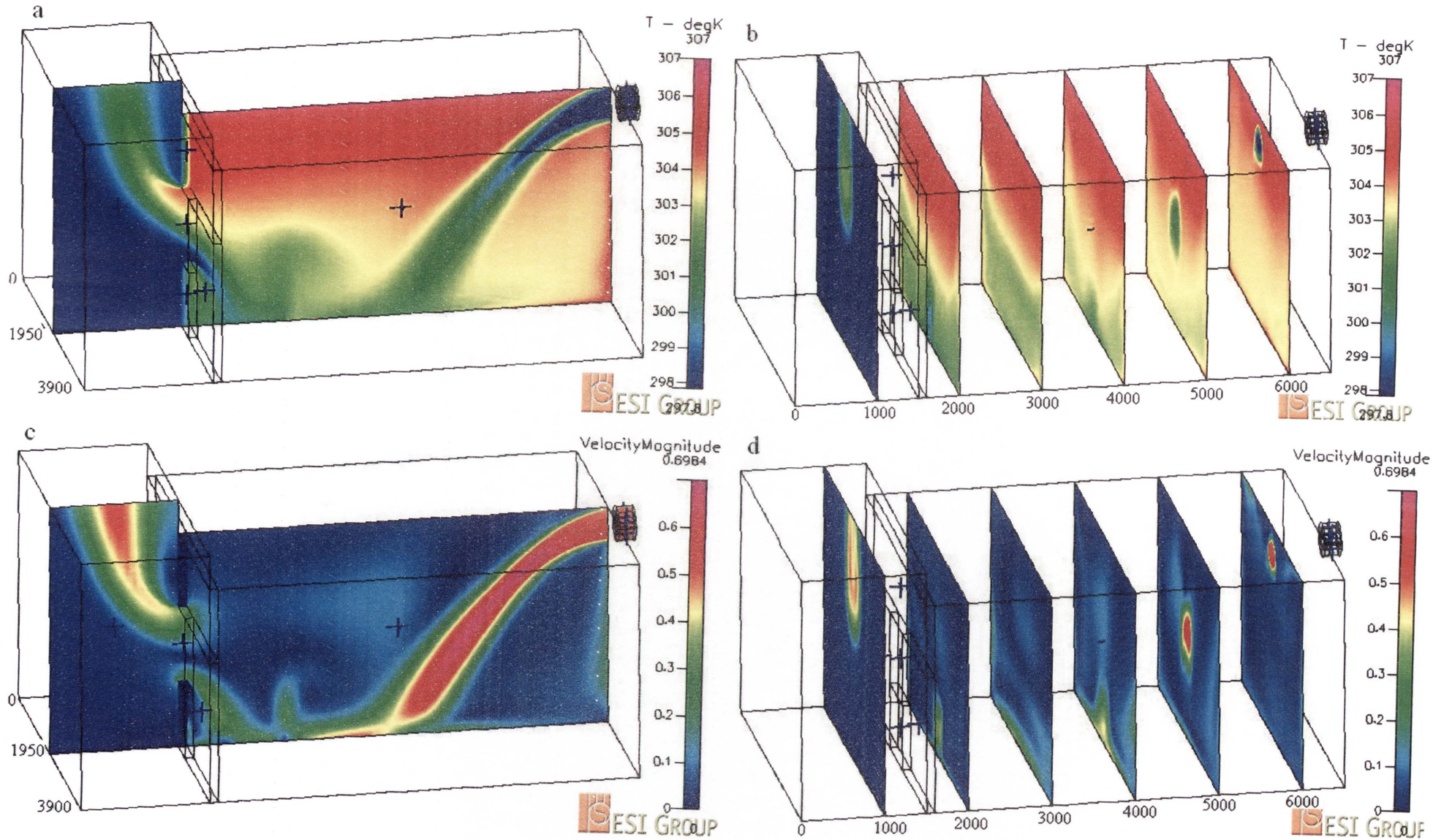

Figure 142 – 4injection_0.505_307 Temperature and velocity distributions with airflows through fan of 0.505 m/s

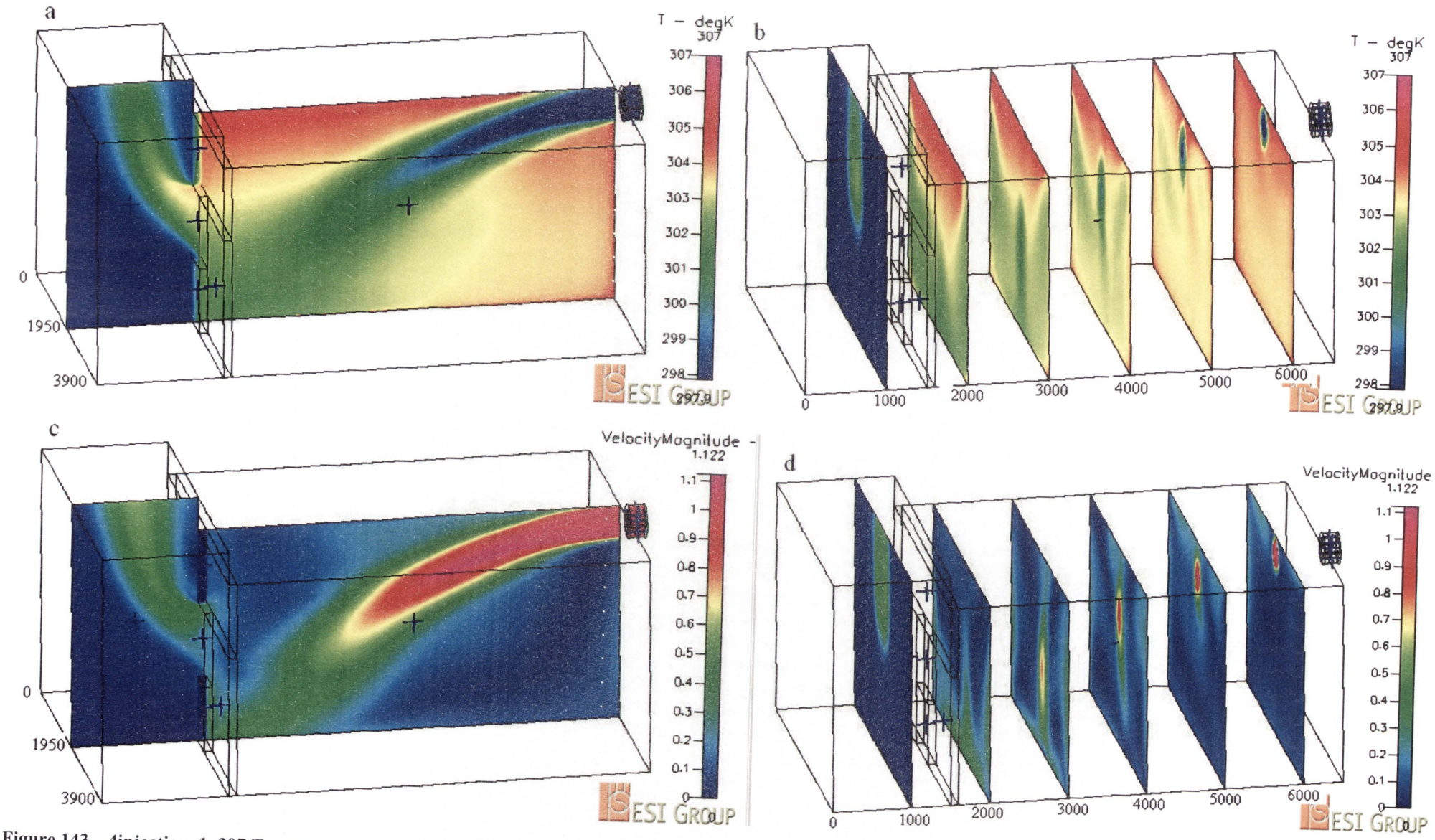

Figure 143 – 4injection_1_307 Temperature and velocity distributions with airflows through fan of 1 m/s

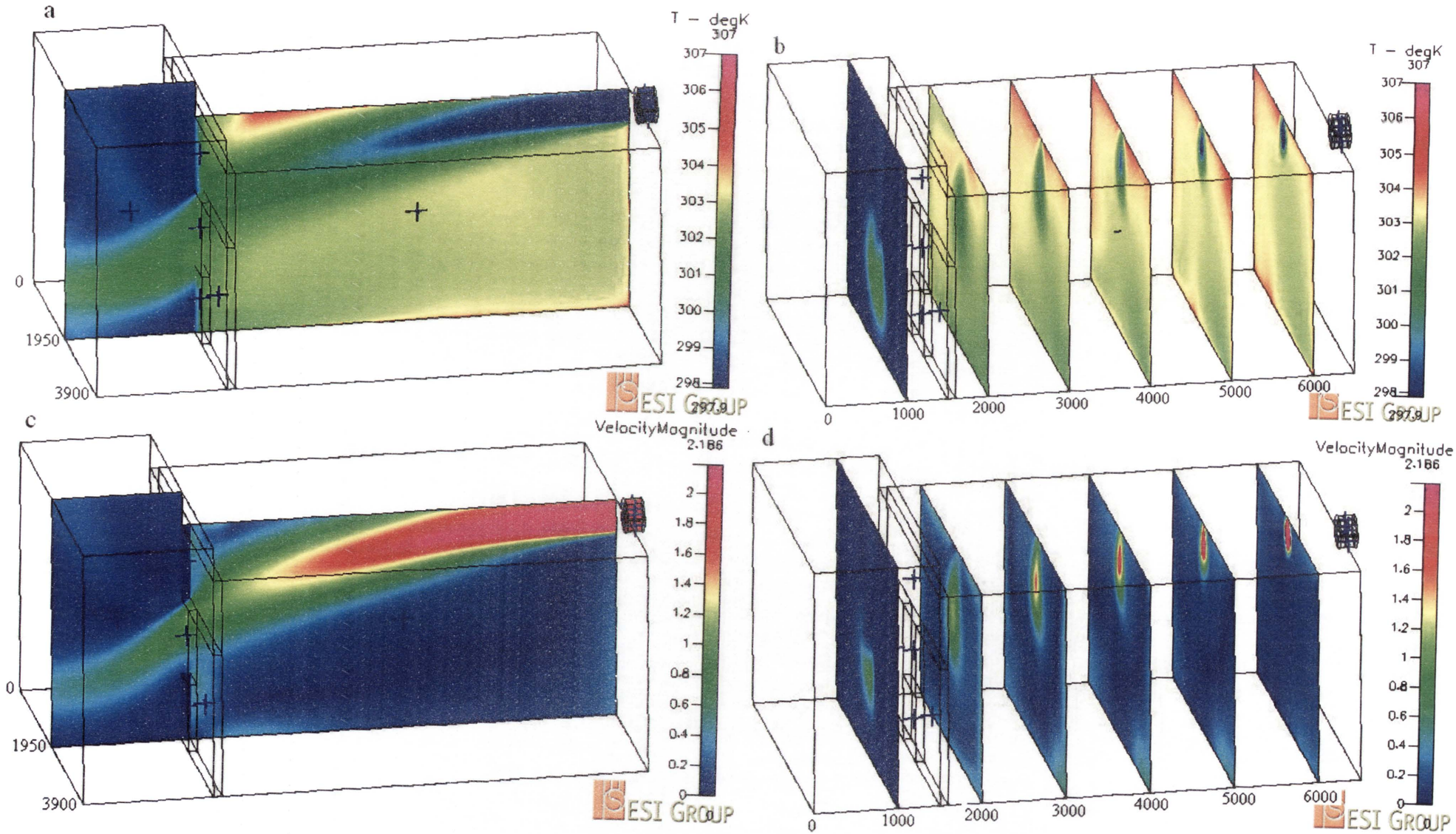

Figure 144 – A 4injection_2_307 Temperature and velocity distributions with airflows through fan of 2m/s

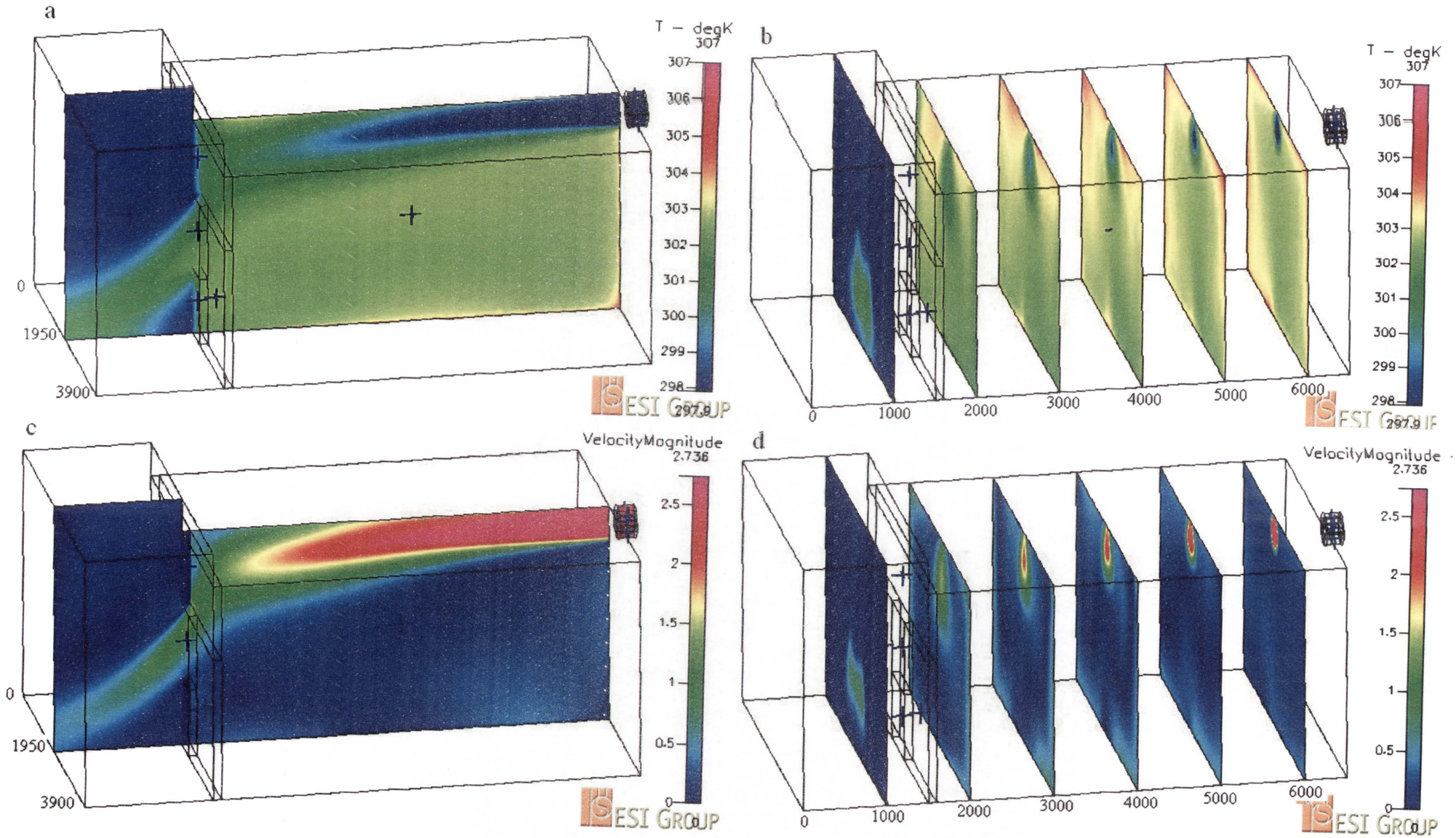

Figure 145 – 4injection_2.5_307 Temperature and velocity distributions with airflows through fan of 2.5 m/s

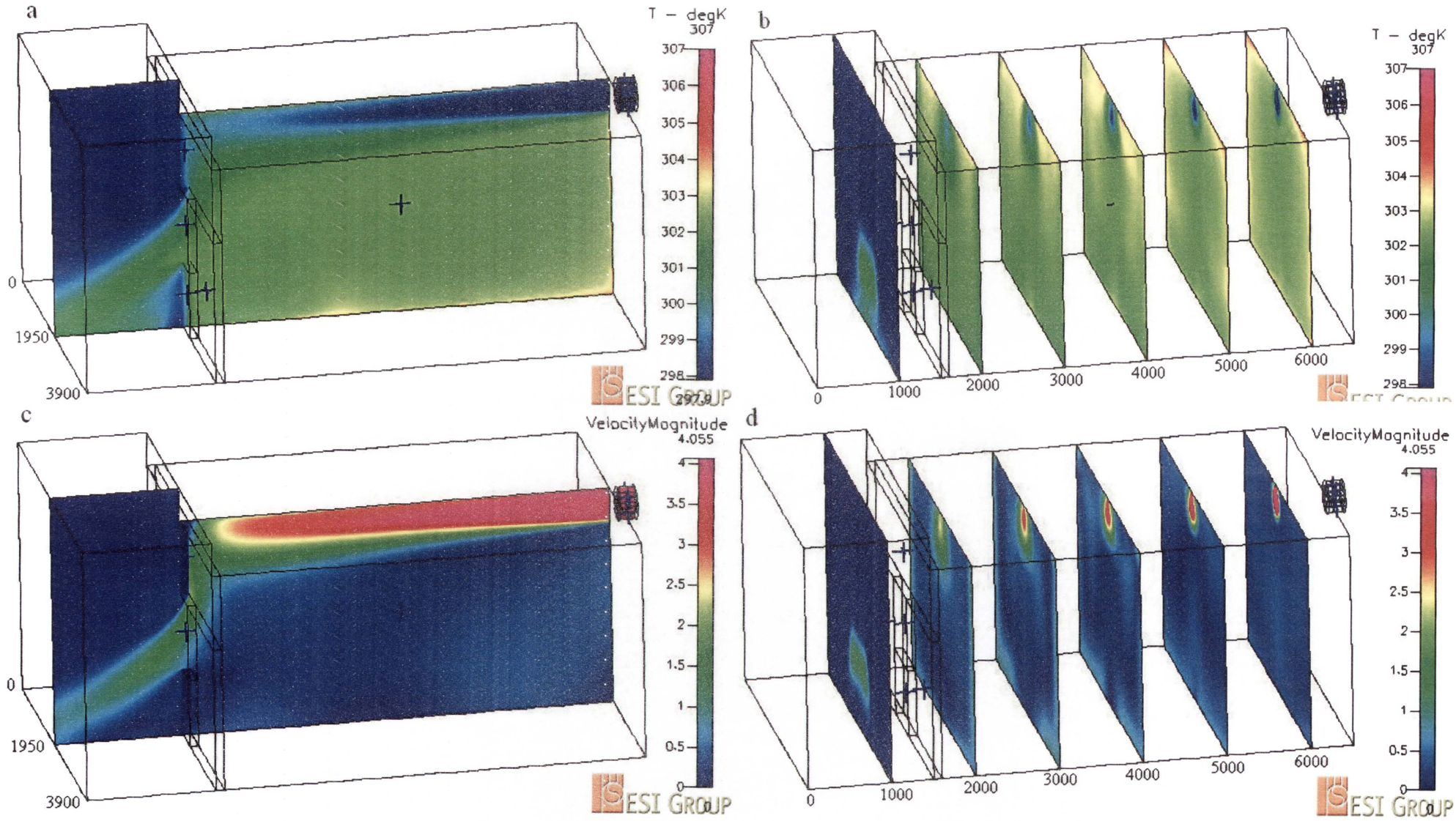

Figure 146 – 4injection_3.7_307 Temperature and velocity distributions with airflows through fan of 3.7 m/s

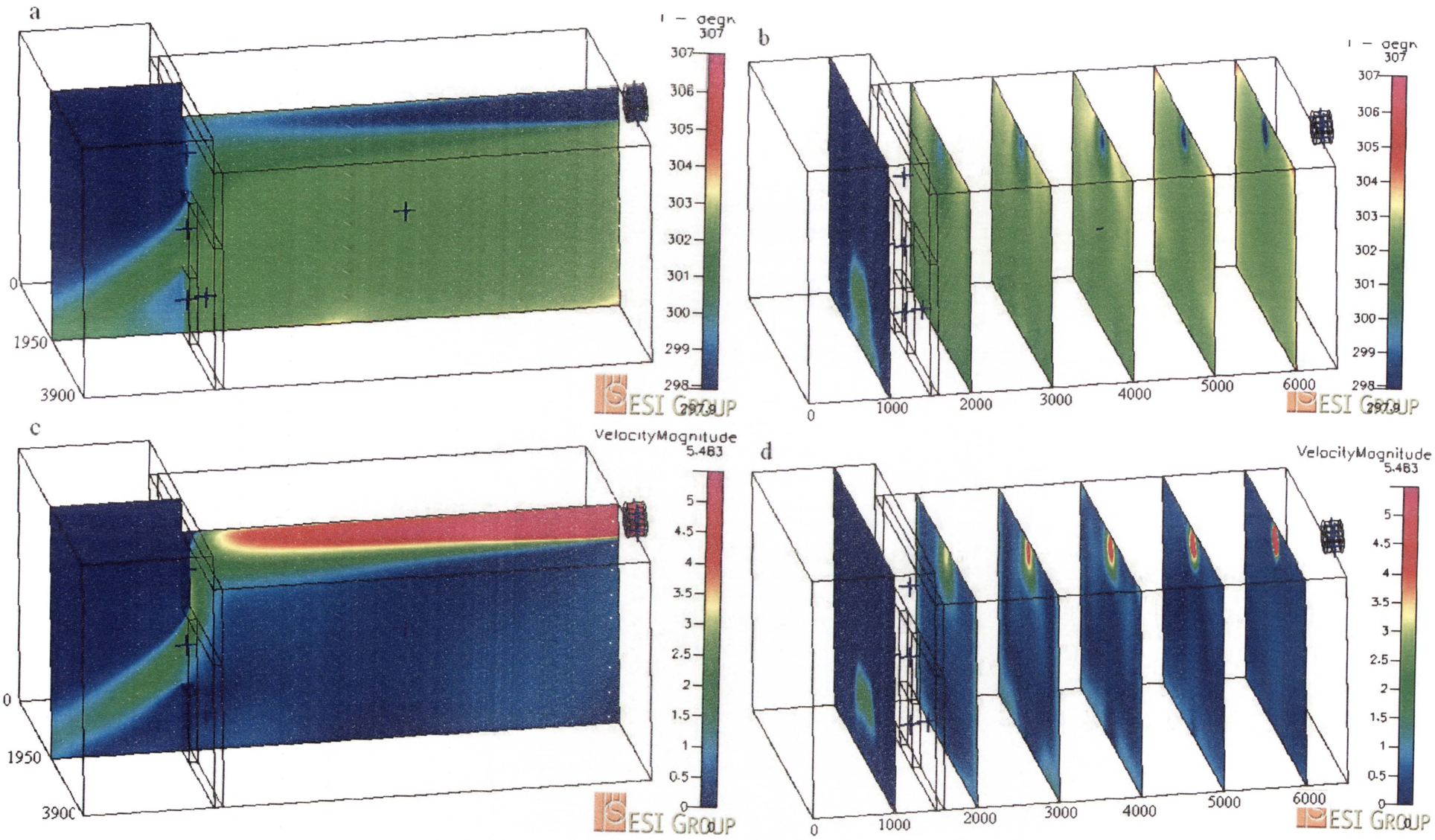

Figure 147 – 4injection_5_307 Temperature and velocity distributions with airflows through fan of 5 m/s

References

Ahmann, D. & Durston L. 2008, 'Hybrid ventilation in the Harm A. Weber academic center: A late-summer case study', *Journal of Green Building,* vol. 3, no. 1, pp 56-73

Allocca, C., Chen, Q. & Glicksman, L. R. 2003, 'Design analysis of single-sided natural ventilation', *Energy and Building,* vol. 35, pp 785-795

Almeida ,M., Maldonado, E., Santamouris, M. & Guarracino, G. 2005, 'The design of optimal openings' in C. Ghiaus & F. Allard (Eds.), *Natural ventilation in the urban environment*, Earthscan, London

Anderson, J. D. 1995, *Computational fluid dynamics: The basics with applications*, McGraw-Hill, New York

ASHRAE.1989, *American standard: ventilation for acceptable indoor air quality,* (ANSI/ASHRAE 62.2-2007), ASHRAE, Atlanta GA

Awbi, H.B. 1989, 'Application of computational fluid dynamics in room ventilation', *Building and Environment*, vol. 24, no. 1, pp 73-84

Awbi, H. B. 2003, *Ventilation of buildings*, 2nd edn, Spon, London

Binggeli, C. 2002, *Building systems for interior designers*, John Wiley, Hoboken, NJ

Binggeli, C. 2007, *Materials for interior environments*, John Wiley, Hoboken, NJ

Blazek, J. 2005, *Computational fluid dynamics: Principles and applications*, Elsevier, Oxford

Blomqvist, C. & Sandberg, M. 2000, 'Measurements and control of air motions within a building'. In

Proceedings of the 18th Annual AIVC Conference, Athens, Greece, vol. 1, pp 427-436

CFD-ACE+ V2007.2 Modules manual (ESI CFD Inc., 2007)

Chattot, J. J. 2002, *Computational aerodynamics and fluid dynamics: An introduction*, Springer, Berlin

Chen, Q.1995, 'Comparison of different k-ε models for indoor airflow computations', *Numerical Heat Transfer*, vol. 28B, pp 353-369

Chen, Q. & Glickman, L. 2003, 'System performance and evaluation of design guidelines for displacement ventilation', *American Society of Heating, Refrigerating and Air Conditioning Engineering,* Atlanta, GA

Chiu, Y. H. & Etheridge, D.W. 2004, 'Experimental technique to determine unsteady flow in natural ventilation stacks at model scale', *Journal of Wind Engineering and Industrial Aerodynamics*, vol. 92, pp 291–313

Cockroft, J.P. & Robertson P. 1976, 'Ventilation of an enclosure through a single opening', *Building and Environment*, vol. 11, pp 29-35

Costola, D. & Etheridge, D.W. 2008, 'Unsteady natural ventilation at model scale-flow reversal and discharge coefficients of a short stack and on orifice', *Building and Environment,* vol. 43, pp 1491-1506

Dascalaki, E., Santamouris, M., Argiriou, A., Helmis, C., Asimakopoulos, D., N., Papadopoulos, K. & Soilemes, A. 1996, 'On the combination of air velocity and flow measurements in single sided natural ventilation configurations', *Energy and Buildings,* vol. 24, pp 155-165

Davidson, P. A. 2004, *Turbulence: An introduction for scientists and engineers*, Oxford University Press

Duell, M., De Boer, F., Enthaler, C., Anda, M., James, G., Zappavigna, L., Bibra, G., Hughes Z. & Boyle G. 2006, 'Scoping study of design and thermal performance in the desert built environment'. Report of a study for the Desert Knowledge Cooperative Research Centre, Alice Springs

Fanger, P. O. 1982, *Thermal comfort,*. Robert E. Krieger, Malabar, FL

Fanger, P.O., Banhidi, L., Olesen, B. W. & Langkilde, G. 1980, 'Comfort limits for heated ceilings', *ASHRAE Transactions*, vol. 86, no. 2, pp 141-156

Favarolo, P.A. & Manz, H. 2005, 'Temperature-driven single-sided ventilation through a large rectangular opening', *Building and Environment*, vol. 40, pp 689-699

Fitzner. K. 1996, 'Displacement ventilation and cooled ceiling, results of laboratory tests and practical installations', In *Proceedings of the Conference on Indoor Air '96,* Nagoya, Japan, pp 41-50

Fox R.W. & McDonald A.T. 1985, *Introduction to fluid mechanics*, 3rd edn., John Wiley, New York

Gan, G. 1995, 'Evaluation of room air distribution systems using computational fluid dynamics', *Energy and Buildings*, vol. 23, pp 83-93

Gao, J., Zhao J. & Gao F. 2006, 'Displacement of natural ventilation in an enclosure with a convective/radiative heat source and nonadiabatic envelopes', *Journal of Solar Energy Engineering,* vol. 128, no. 1, 83 (7 pages)-89

Gatski, T. B., Hussaini M. Y. & Lumley J. L. 1996, '*Simulation and modeling of turbulent flows*, Oxford University Press

Ghiaus, C. & Allard, F. 2005, 'The physics of ventilation', in C. Ghiaus & F. Allard (Eds.)., *Natural ventilation in the urban environment*, Earthscan, London

Godish, T. 1995, S*ick buildings: definition, diagnosis, and mitigation*, CRC Press, Boca Raton, FL

Goodfellow, H. D. & Tähti E. 2001, *Industrial ventilation design guidebook*, Academic Press, San Diego, CA

Gorton, R. L. & Sassi, M. M. 1982, 'Determination of temperature profiles in a thermally stratified air-conditioned system: Part 2. Program description and comparison of computed and measured results.' *ASHRAE Transactions*, vol. 88, no. 2

Hearne Scientific Software. 2008, *Accurate* by CSIRO, viewed March Month 2009, http://www.hearne.com.au/products/accurate/

Heiselberg, P., Jepsen, L.B., Hyldgaard, A., Li, Z.G., Nielsen, P.V. & Perino, M. 2003, 'Short-time airing by single-sided natural ventilation', In *Proceedings of ISHVAC 2003, The 4th International Symposium on Heating, Ventilation and Air-Conditioning*, Beijng, China, vol.1, s 117-124

Heiselberg, P., Svidt, K. & Nielsen, P. 2001, 'Characteristics of airflow from open windows', *Building and Environment*, vol. 36, no. 7, pp 859–869

Hens, H. S. L. C. 2008, *Building physics - heat, air and moisture: fundamentals and engineering methods with examples and exercises*, Ernst & Sohn, Berlin

Horan, J.M. & Finn, D.P. 2005, 'CFD reliability issues in analysis of naturally ventilated building'. Paper presented at the *International Conference on Passive and Low Energy Cooling for the Built Environment'*, 19-21 May 2005, Santorini, Greece

International Organization for Standardization, International standard: ergonomics of the thermal environment - analytical determination and interpretation of thermal comfort using calculation of the PMV and PPD indices and local thermal comfort criteria (ISO 7730 2005), International Organization for Standardization, Geneva, Switzerland

Janna, W. S. 1983, *Introduction to fluid mechanics*, Brooks/Cole Engineering, Monterey, CA

Jambunathan, K., Lai, E., Moss, M.A. & Button, B.L. 1992, 'A review of heat transfer data for single circular jet impingement', *International Journal of Heat and Fluid Flow*, vol. 13, no. 2, pp 106-115

Jiang, Y. & Chen Q. 2003, 'Buoyancy-driven single-sided natural ventilation in buildings with large opening', *International Journal of Heat and Mass Transfer*, vol.46, no. 6, pp 973-988

Jirka, G.H. 1982, 'Turbulent buoyant jets in shallow fluid layers', in W. Rodi (Ed.), *Turbulent Jets and Plumes,* Pergamon Press, Oxford

Kestin, J. 1979. *A course in thermodynamics, Vol. 1.* McGraw-Hill, New York

Kiel, D. E. & Wilson, D. J. 1989, 'Combining door swing pumping with density driven flow', *ASHRAE Transactions*, vol. 95,no. 2, pp 590-599

Kreith, F. & Bohn, M. S. 1986, *Principles of heat transfer*, Harper & Row, New York

Kuhn, S. Z., Kang, H. K. & Peterson P. F. 2002, 'Study of mixing and augmentation of natural convection heat transfer by a forced jet in a large enclosure', *Journal of Heat Transfer*, vol. 124, no. 4, pp 660-666

Kuznik, F., Rusaouen, G. & Brau, J. 2007, 'Experimental and numerical study of a scale ventilated enclose: Comparison of four two equations closure turbulence models',*Building and Environment*, vol. 42, pp 1043-1053

Larsen, T. S. & Heiselberg, P. 2008, 'Single sided natural ventilation driven by wind pressure and temperature difference', *Energy and Building*, vol. 40, pp 1031-1040

Launder, B. E.& Spalding, D. B. 1974, 'The numerical computation of turbulent flows', *Computer Methods in Applied Mechanics and Engineering*, vol. 3, pp. 269-289

Li, K. & Teh, S. L. 1996, 'Two-dimensional numerical study of airflow through large opening', *Indoor Air*, vol. 2, pp 1027-1032

List E. J. 1982, 'Turbulent buoyant jets and plumes' *Annual Review of Fluid Mechanics*', vol. 14, pp 189-212

Maas, J., Roulet, C. A. & Hertig, J. A. 1989, 'Some aspects of gravity driven air flow through large apertures in buildings', *ASHRAE Transactions*, vol. 95, part2, pp 573-583

Mahajan, B. M. & Hill, D. D. 1986, 'Interzonal natural convection for various aperture configurations'. In *Proceedings of the ASME Winter Annual Meeting*, Anaheim CA

Majahan, B. A. 1987, 'Measurement of interzonal heat and mass transfer by natural convection', *Solar Energy*, vol. 38 (b), pp 437-446

Müllejans, H. 1966, 'Simulation between non-isothermal flow and heat transfer in mechanically ventilated rooms', Research report no. 1656, RWTH Aachen University

Munso, B. R., Young, D. F. & Okiishi, T. H. 2006, *Fundamentals of fluid mechanics*, 5th edn., John Wiley and Sons, New York

Murakami, S. & Kato, S. 1989, 'Numerical and experimental study on room airflow: 3-D predictions using k-e turbulence model', *Building and Environment*, vol. 24, pp 85-97

Obha, M., Irie K. & Kurabuchi, T. 2001, 'Study on airflow characteristics inside and outside a cross-ventilated model, and ventilation flow rates using wind tunnel experiments', *Journal of Wind Engineering and Industrial Aerodynamics*, vol. 89, pp 1513-1524

Papakonstantinou, K. A., Kiranoudis, C. T. & Markatos, N. C. 2000, 'Numerical simulation of air flow field in single-sided ventilated buildings', *Building and Environment*, vol. 33, pp 41-48

Perino, M. & Heiselberg, P. 2003, *'Short-time airing by single-sided natural ventilation, Part 2: Comparison of experimental results and model predictions'.* In *Proceedings of the 4th International Symposium on Heating, Ventilating and Air-conditioning*, vol. 1, pp 117-124

Peterson, P. F. 1994, 'Scaling and analysis of mixing in large stratified volumes, *International Journal of Heat Mass Transfer*, vol. 37, pp 97-106

Phaff, J. C., Gids, W. F., Ton, J. A., van der Ree, D. V. & Schijndel, L. L. M. 1980, 'The ventilation of buildings: Investigation of the consequences of opening one window on the internal climate of a room'. Report C 448, TNO Research Institute for Environmental Hygiene, Delft, The Netherlands

Posner, J. D., Buchanan, C. R. & Dunn-Rankin, D. 2003, 'Measurement and prediction of indoor air flow in a model room', *Energy and Building*, vol. 35, pp 515-526

Riffat, S. B. 1988, 'A study of heat and mass transfer through a doorway in a conventional house'. Report, Research in Building Group, Polytechnic of Central London

Roulet, C.A. 2005, 'The role of ventilation', in C. Ghiaus & F. Allard (Eds.), *Natural ventilation in the urban environment*, Earthscan, London

Russell, M., Sherman, M. & Rudd, A. 2005, 'Review of residential ventilation technologies'. Report LBL-57730, Lawrence Berkeley National Laboratory

Shaw, B. H. &,Whyte W. 1974, 'Air movement through doorways – The influence of temperature and its control by forced airflow', *Building Services Engineering,* vol. 42, pp 210-218

Spindler H. C. & Norford, L. K. 2008 'Naturally ventilated and mixed-mode buildings, Part II: Optimal control', *Building and Environment*, vol. 44, issue 4

Standards Australia. Australian/New Zealand Standard: *Natural ventilators - Classification and performance* (AS/NZS 4740:2000), Standards Australia, Sydney

Sun, H., Zhao, L. & Zhang, Y. 2007, 'Evaluating RNG k-ε models using PIV data for airflow in animal buildings at different ventilation rates', *ASHRAE Transactions,* vol. 113, pp 358-365

Tanny, J., Haslavsky, V. & Teitel, M. 2008, 'Airflow and heat flux through the vertical opening of buoyancy-induced naturally ventilated enclosures', *Energy and Buildings,* vol. 40, pp 637-646

Tu, J., Yeoh, G. H. & Liu, C. 2008, *Computational fluid dynamics: A practical approach*, Butterworth-Heinemann, Boston

Versteeg, H. K. & Malalasekera,W. 1995, *An introduction to computational fluid dynamics: The finite volume method*, Addison Wesley Longman, Harlow, UK

Versteeg, H. K. & Malalasekera, W. 2007 *An introduction to computational fluid dynamics: The finite volume method*, 2nd edn., Prentice Hall, Harlow, UK

Voigt, L. K. 2000, 'Comparison of turbulence models for numerical calculation of airflow in an annex 2D room', Report, International Centre for Indoor Environment and Energy Department of Energy Engineering, Technical University of Denmark

Vonk, R. 2004, 'A study of natural ventilation and the effect of rotating, wind driven ventilators', Undergraduate thesis, University of Sydney

Warren, P.R. & Parkins, L.M. 1985 'Single-sided ventilation through open windows'. In *Proceedings of the 1985 ASHRAE Conference on Thermal Performance of the Exterior Envelopes of Buildings,* Florida, CA, *ASHRAE Transactions* vol. 49, pp 209–228

Wilson, D. J. & Kiel, D. E. 1990, 'Gravity driven counterflow through an open door in a sealed room', *Building and Environment,* vol. 25, no. 4, pp 379–388

Xu, H., Hihara, E. & Saito, T. 1994, 'Temperature stratification of heated air flow in a fire tunnel', *JSME International Journal*, Series B, vol. 1, pp 187-194

Xue, H. & Shu, C. 1999, 'Mixing characteristics in a ventilated room with non-isothermal ceiling air supply', *Building and Environment*, vol. 34, pp 245-251

Yakhot, V. & Orszag, S. A. 1986, 'Renormalization group analysis of turbulence: I. Basic theory', *Journal of Scientific Computing*, vol. 1, pp 1-51

Yoshida, A., Tominaga, K. & Watani S. 1990, 'Field measurements on energy balance of an urban canyon in the summer season,' *Energy and Buildings,* vol. 15-16, pp 417-423

Zhang, Y. 2005, *Indoor air quality* , CRC Press, Boca Raton, FL

Zhang, J. S., Wu, G. J. & Christianson L. L. 1993, 'A new similitude modelling technique for studies of non-isothermal room ventilation flows', *ASHRAE Transactions*, vol. 99, pp 129-138

Zhao, L.Y., Zhang, Y., Wang, X., Riskowski G. L. & Christianson L. L. 1999, 'Development of particle image velocimetry techniques to measure room airflow patterns in ventilated airspaces', *ASHRAE Transactions*, vol.105, no. 2, pp 1098-1107

Zhao, L.Y., Zhang, Y., Riskowski, G. L. & Christianson, L. L. 2000, 'A study of jet momentum effects on airflow in ventilated airspaces using particle image velocimetry techniques', ASAE Paper No. 004117, American society of Agricultural Engineers, St Joseph, MI

Zhao, L.Y., Zhang, Y., Wang, X., Riskowski G. L. & Christianson, L. L. 2001, 'Measurement of 2-D air velocity in a full-scale room using a particle image velocimetry system', *ASHRAE Transactions*, vol. 107, pp 434-444